“Granulite facies metamorphism and partial melting processes in the Ivrea Zone, Northern Italy”

Dissertation zur Erlangung des Grades

„Doktor
der Naturwissenschaften“

am Fachbereich Chemie, Pharmazie und Geowissenschaften
der Johannes Gutenberg-Universität Mainz

Charlotte Redler
geb. in Kassel

Mainz, 2011

Dekan:

1. Berichterstatter:
2. Berichterstatter:

Tag der mündlichen Prüfung: 19.01.2012

Declaration/Erklärung

Ich versichere hiermit, die vorliegende Arbeit selbstständig und nur unter Verwendung der angegebenen Hilfsmittel verfasst zu haben. Alle wörtlich oder inhaltlich übernommenen Stellen habe ich als solche gekennzeichnet.

Ich habe die hier als Dissertation vorgelegte Arbeit nicht als Prüfungsarbeit für eine staatliche oder andere wissenschaftliche Prüfung eingereicht.

Ich versichere außerdem, dass ich weder die vorgelegte Arbeit noch Teile davon in einer anderen Fakultät oder einem anderen Fachbereich als Dissertation eingereicht habe und dass diesem Promotionsverfahren keine endgültig gescheiterten Promotionsverfahren vorausgegangen sind.

_____ _____

Ort, Datum Unterschrift

Abstract

The Ivrea Zone in northern Italy has been the focus of numerous petrological, geochemical and structural studies. It is commonly inferred to represent an almost complete section through the mid to lower continental crust, in which metamorphism and partial melting of the abundant metapelites was the result of magmatic underplating by a large volume of mantle-derived magma. This study concerns amphibolite and granulite facies metamorphism in the Ivrea Zone with focus on metapelites and metapsammites/metagreywackes from Val Strona di Omegna and metapelites from Val Sesia and Val Strona di Postua, with the aim to better constrain their metamorphic evolution as well as their pressure and temperature conditions via phase equilibria modelling.

In Val Strona di Omegna, the metapelites show a structural and mineralogical change from mica-schists with the common assemblage bi-mu-sill-pl-q-ilm ± *liq* at the lowest grades, through metatexitic migmatites (g-sill-bi-ksp-pl-q-ilm-*liq*) at intermediate grades, to complex diatexitic migmatites (g-sill-ru-bi-ksp-pl-q-ilm-*liq*) at the highest grades. Within this section several mappable isograds occur, including the first appearance of K-feldspar in the metapelites, the first appearance of orthopyroxene in the metabasites and the disappearance of prograde biotite from the metapelites. The inferred onset of partial melting in the metapelites occurs around Massiola. The prograde suprasolidus evolution of the metapelites is consistent with melting via the breakdown of first muscovite then biotite. Maximum modelled melt fractions of 30–40 % are predicted at the highest grade. The regional metamorphic field gradient in Val Strona di Omegna is constrained to range from conditions of 3.5–6.5 kbar at T = 650–730 °C to P > 9 kbar at T > 900 °C. The peak P–T estimates, particularly for granulite facies conditions, are significantly higher (around 100 °C) than those of most previous studies. In Val Sesia and Val Strona di Postua to the south the exposure is more restricted. P–T estimates for the metapelites are 750–850 °C and 5–6.5 kbar in

Val Sesia and approximately 800–900 °C and 5.5–7 kbar in Val Strona di Postua. These results show similar temperatures but lower pressure than metapelites in Val Strona di Omegna. Metapelites in Val Sesia in contact with the Mafic Complex exhibit a metatexitic structure, while in Val Strona di Postua diatexitic structures occur. Further, metapelites at the contact with the Mafic Complex contain cordierite (± spinel) that overprint the regional metamorphic assemblages and are interpreted to have formed during contact metamorphism related to intrusion of the Mafic Complex. The lower pressures in the high-grade rocks in Val Sesia and Val Strona di Postua are consistent with some decompression from the regional metamorphic peak prior to the intrusion of the Mafic Complex, suggesting the rocks followed a clockwise *P–T* path. In contrast, the metapelites in Val Strona di Omegna, especially in the granulite facies, do not contain any cordierite or any evidence for a contact metamorphic overprint. The extrapolated granulite facies mineral isograds are cut by the rocks of the Mafic Complex to the south. Therefore, the Mafic Complex cannot have caused the regional metamorphism and it is unlikely that the Mafic Complex occurs in Val Strona di Omegna.

Zusammenfassung

Die Ivrea Zone, eine im nördlichen Italien gelegene geologische Einheit, setzt sich aus hochmetamorphen Gesteinen der Amphibolit- und Granulitfazies zusammen. Die Gesteine wurden in der Vergangenheit vielfach petrologisch, geochemisch und strukturgeologisch untersucht, da sie als ein klassisches Profil der mittleren bis unteren kontinentalen Kruste interpretiert werden. Die Ivrea Zone wird, neben einer Einheit die überwiegend aus einer Wechsellagerung von Metasedimenten und Metabasiten besteht (Kinzigit Formation), durch eine ehemals magmatische Einheit, dem sogenannten „Mafischen Komplex“, charakterisiert. Der Mafische Komplex entstand nach gängigen Meinungen durch *magmatic underplating*; er intrudierte in die Gesteine der unteren Kruste und wird somit als Auslöser für die Metamorphose und die Anatexis in der Ivrea Zone interpretiert.

Die vorliegende Dissertation beschäftigt sich hauptsächlich mit amphibolit- und granulitfaziellen Metasedimenten (unterteilt in Metapelite und Metapsammite/Metagrauwacken) des Val Strona di Omegna, des Val Sesia und des Val Strona di Postua, wobei erstgenanntes den Schwerpunkt der Arbeit bildet. Ziel der Arbeit ist es, im Vergleich zu vorherigen Arbeiten, die Druck- und Temperaturbedingungen der Metamorphose und Gesteinsaufschmelzung anhand von Mineral- bzw. Phasengleichgewichtsmodellierung weiter einzugrenzen und Aussagen über den Grad der Teilschmelzenbildung treffen zu können. Des Weiteren soll die Frage geklärt werden, inwiefern der „Mafische Komplex“, speziell im Val Strona di Omegna, tatsächlich als Auslöser für die Metamorphose und die Aufschmelzung der Gesteine in Frage kommen kann.

Die Metapelite im Val Strona di Omegna zeigen, von Südost nach Nordwest, welches dem Übergang von niedrig- zu hochgradigen metamorphen Bedingungen entspricht, eine kontinuierliche Entwicklung von Glimmerschiefern

(generell bi-mu-sill-pl-q-ilm ± *liq*) über metatexitische Migmatite (g-sill-bi-ksp-pl-q-ilm-*liq*) hin zu komplexen diatexitischen Migmatiten (g-sill-ru-bi-ksp-pl-q-ilm-*liq*). Innerhalb der Gesteinsabfolge war es möglich Isograden von Mineralstabilitäten auszukartieren, wie zum Beispiel die Isograde, die das Verschwinden von Muskovit, einhergehend mit dem ersten regulären Auftreten von Alkalifeldspat, abbildet. Weitere Isograden, welche die Granulitfazies kennzeichnen, sind die des ersten Auftretens von Orthopyroxen in Metabasiten und die des Verschwindens von Biotit in den Metapeliten. Die ersten Anzeichen der Schmelzbildung, welche einher geht mit dem Zerfall und dem Verschwinden von zunächst Muskovit und später Biotit aus der *peak* Mineralparagenese, sind im Gelände in der Gegend um Massiola zu beobachten; dadurch werden in den höchstgradigen Metapeliten Schmelzgrade von 30–40 % erreicht, während die Metapsammite/Metagrauwacken Schmelzgrade von weniger als 10 % aufweisen. Die resultieren Druck- und Temperaturwerte im Val Strona di Omegna zeigen einen regionalmetamorphen Trend und eine kontinuierliche Zunahme von 3.5–6.5 kbar mit T = 650–730 °C unter niedriggradigen Bedingungen bis hin zu $P > 12$ kbar und $T > 950$ °C unter höchstgradigen Bedingungen. Die Druck- und Temperaturbedingungen, speziell in der Granulitfazies sind somit deutlich höher (ca. 100 °C) als jene der meisten bisherigen Studien. Die Modellierung von Metapsammiten/Metagrauwacken bestätigt den ermittelten regionalmetamorphen Trend. In den beiden südlicher gelegenen Tälern, Val Sesia und Val Strona di Postua, hingegen zeigen die modellierten Druck- und Temperaturwerte keinen regionalmetamorphen Trend; die Werte reichen im Val Sesia von 750–850 °C und 5–6.5 kbar und von 800–900 °C und 5.5–7 kbar im Val Strona di Postua und spiegeln somit ähnliche Temperaturen, aber niedrigere Drücke als im Val Strona di Omegna wider. Die Metapelite im direkten Kontakt zum „Mafischen Komplex“ zeigen im Val Sesia metatexitische, im Val Strona di Postua diatexitische Strukturen und sind bis in einen Umkreis von 2–3 km rund um den Komplex Cordierit-führend, wobei sie im Val Strona di Postua noch zusätzlich geringe Mengen Spinell enthalten. Beides deutet darauf hin, dass die Gesteine im Val Sesia und Val Strona di Postua durch die Intrusion des „Mafischen Komplexes“ kontaktmetamorph überprägt wurden und es nachträglich zu einer Druckentlastung in Folge der Regionalmetamorphose kam, wodurch in diesem Bereich der Ivrea Zone ein *clockwise P–T* Pfad beschrieben wird. Im Gegensatz

dazu enthalten die Gesteine im Val Strona di Omegna keinen Cordierit und auch sonst sind keinerlei Anzeichen für eine nachträgliche Überprägung der regional metamorphen Mineralparagenesen erkennbar. Des Weiteren werden die zuvor erwähnten Isograden von Orthopyroxen und Biotit im Süden des Val Strona di Omegna durch die Einheit des „Mafischen Komplexes“ abgeschnitten.

Die Frage, ob der „Mafische Komplex“ als Auslöser für Metamorphose und Teilschmelzenbildung verantwortlich ist, kann dahingehend beantwortet werden, dass die Intrusion nachträglich zur Regionalmetamorphose und Teilschmelzenbildung erfolgte und lediglich eine kontaktmetamorphe Überprägung der vorhandenen Paragenesen auslöste, aber nicht generell für die Metamorphose in der Ivrea Zone verantwortlich ist. Zudem is es unwahrscheinlich, dass der „Mafische Komplex“ im Val Strona di Omegna lokalisiert ist; diese Einheit ist wahrscheinlich auf den südlichen Teil der Ivrea Zone begrenzt und die im Val Strona di Omegna bei Campello Monti vorliegenden Metabasite können der Kinzigit Formation zugeordnet werden.

Table of Contents

List of figures

List of tables

Abbreviations

g/grt	garnet
cd	cordierite
sill	sillimanite
and	andalusite
ky	kyanite
ru	rutile
sp	spinel
ilm	ilmenite
mt	magnetite
bi	biotite
mu	muscovite
pa	paragonite
ksp	K-feldspar
pl	plagioclase
q	quartz
hb/hbl	hornblende
ged	gedrite
cc	calcilte
opx	orthopyroxene
cpx	clinopyroxene
di	diopside
st	staurolite
sph	sphene
tur	tourmaline
scap	scapolite
liq	silica melt/*liquid*
H2O	water/fluid phase
ab	albite
an	anorthite
or	orthoclase
alm	almandine
py	pyrop

spess	spessartine
grs	grossular
oct	octahedral
tet	tetrahedral
a.p.f.u.	atoms per formular unit
XRF	X-ray fluorescence
EMPA	electron microprobe analysis
CMB Line/CMBL	Cossato-Mergozzo-Brissago Line
V.S.d.O.	Val Strona di Omegna
M.C.	Mafic Complex
Ma	mega years
sd	standard division
vol%	volume per cent
T	temperature
P	pressure
Cp	heat capacity
V	molar volume
S	entropy
α	thermal expansion
β	isothermal compressibility
H	enthalpy
ΔG^0	standard Gibbs free energy
R	universal gas constante
K	equilibrium constant for balanced reactions
n=10	number of measured minerals per sample

Chapter 1
Introduction

1.1 Introduction to the topic

Regional metamorphic belts that preserve a range of metamorphic grades are ideally suited to the understanding of the development of metamorphic rocks and how they transform in structure, texture and mineral assemblage with increasing metamorphic grade (e.g. Barrow, 1893; Binns, 1964), because they preserve a coherent trend in *P–T* conditions (metamorphic field gradient). Such belts have underpinned much of the understanding of the stability of different mineral assemblages as a function of pressure and temperature and the nature of progressive metamorphism in the crust (e.g. Carmichael, 1970; Spear *et al.,* 2002; White *et al.,* 2003). High-grade metamorphic terranes are best for investigating of processes in the lower crust, especially the formation of melt, its segregation and transfer as important processes for the differentiation of the continental crust.

The Ivrea Zone (also referred as Ivrea-Verbano Zone) is an example that preserves a metamorphic field gradient from amphibolite to granulite facies conditions developed in a variety of rock types. It has been the focus of numerous petrological, geochemical and structural studies (e.g. Bertolani, 1968; Mehnert, 1975; Rivalenti *et al.*, 1975; Boriani *et al.*, 1977; Zingg, 1980; Schmid, 1993; Schnetger, 1994; Sinigoi *et al.*, 1994; Rutter & Brodie, 1996; Henk *et al.*, 1997; Vavra & Schaltegger, 1999; Barboza *et al.*, 1999; Barboza & Bergantz, 2000; Quick *et al.*, 2003; Peressini *et al.*, 2007; Rutter *et al.*, 2007; Luvizotto & Zack, 2009), largely because it is inferred to represent an almost complete section through the mid to lower continental crust. This area offers the potential to study processes in the lower crust, such as partial melting and melt loss. The

Ivrea Zone is also interpreted as one of the best examples of magmatic underplating in which a large volume of mantle-derived magma intruded into rocks at the base of the crust (Rivalenti *et al.*, 1975), resulting in high-grade metamorphism and the resetting of chemical and isotopic systems (Henk *et al.*, 1997). A few studies disagree that the Ivrea Zone is an analogue for the lower continental crust (e.g. Sills, 1984) based on pressure estimates that are too low and the granulite facies metasediments did not derive from deep crustal levels. In addition, Barboza *et al.*, 1999; Barboza & Bergantz, 2000 and Peressini *et al.*, 2007 question whether the intrusion of the Mafic Complex caused the high-grade metamorphism in the Ivrea Zone based on the development of a possible contact aureole around the Mafic Complex, together with appropriate minerals and age determinations. Previous studies on the investigation of pressure and temperature conditions of the amphibolite to granulite facies metamorphism are based largely on the abundant metapelites in the Ivrea Zone (e.g. Henk *et al.*, 1997; Luvizotto & Zack, 2009). Henk *et al.* (1997) used conventional thermobarometry (e.g. Fe–Mg exchange thermometry) to derive *P*–*T* estimates of 600–800 °C and 4–8 kbar in Val Strona di Omegna. Calculations in Luvizotto & Zack (2009) based on Zr-in rutile thermometry suggest higher peak temperatures (850–930 °C) for the granulite facies metamorphism.

1.2 Aim of the study

This work presents new pressure and temperature constraints calculated via phase equilibria modelling using the program THERMOCALC (Powell & Holland, 1988) and the internally consistent dataset of Holland & Powell (1998, ds5, updated 22 November 2003). Detailed field investigations of three main valleys in the Ivrea Zone, Val Strona di Omegna, Val Sesia and Val Strona di Postua were undertaken as well as petrographical and petrological analysis of the appropriate rocks. Within the framework of this study four main questions need to be answered:

- What are the field relations of metapelites, metapsammites/metagreywackes and metabasites in Val Strona di Omegna, Val Sesia and Val Strona di Postua?

- What is the evidence for partial melting and melt loss in the various lithologies?

- What ranges of *P–T* conditions are recorded within the metamorphic field gradient in Val Strona die Omegna and how does this field gradient compare to those in Val Sesia and Val Strona di Postua?

- What is the relationship between the Mafic Complex and the granulite facies metamorphism in Val Strona di Omegna and is the Mafic Complex the source of heat for the high-grade metamorphism in the Ivrea Zone?

1.3 Outline of the thesis

Chapter 2: This Chapter gives an introduction and overview to the geology of the Ivrea Zone as well as a summary of previous work.

Chapter 3: In this Chapter the analytical methods are described with the main focus on the phase equilibria modelling with THERMOCALC. This covers the basics of the program as well as the structure of the internally consistent dataset, the activity-composition models and how to calculate a *P–T* pseudosection.

Chapter 4: The results of field work and petrographic investigation of thin sections are presented in this Chapter, which is sub-divided into three parts corresponding to the three valleys Val Strona di Omegna, Val Sesia and Val Strona di Postua. Detailed field sketches at different scales from Val Strona di Omegna are presented.

Chapter 5: The results of the whole rock and mineral chemistry analysis are presented in this Chapter and are compared between the three valleys.

Chapter 6: In this Chapter the results of the phase equilibria modelling are presented, largely involving calculated *P–T* pseudosections. This Chapter is sub-divided into the three valleys.

Chapter 7: In Chapter 7 the main results are discussed in context of previous work and the main questions of this study outlined above.

Chapter 8: In the last Chapter the conclusions of this study are presented with an outline of possible future researches in the Ivrea Zone.

Chapter 2
Geology of the Ivrea Zone and summary of previous work

2.1 Introduction

The Ivrea Zone (also referred as the Ivrea-Verbano Zone), located in the southern Alps of northwest Italy, is a part of the pre-alpidic basement (e.g. Schmid, 1993; Vavra & Schaltegger, 1999). It extends lengthwise for a distance of 120 km from Locarno to Castellamonte and is up to 14 km wide (northwest-southeast extension). The Ivrea Zone is bounded to the northwest by the Insubric Line (Fig. 2.1.1), a NW-dipping Neogene shear zone (Gansser, 1968) that separates it from mostly greenschist facies rocks of the Alpine units of the Sesia-Lanzo Zone. To the southeast the Cossato-Mergozzo-Brissago (CMB) Line and the Pogallo Line separate the Ivrea Zone from the Strona-Ceneri Zone (also Serie dei Laghi) (Boriani *et al.,* 1977; Rivalenti *et al.,* 1984; Schmid *et al.*, 1987; Barboza & Bergantz, 2000).

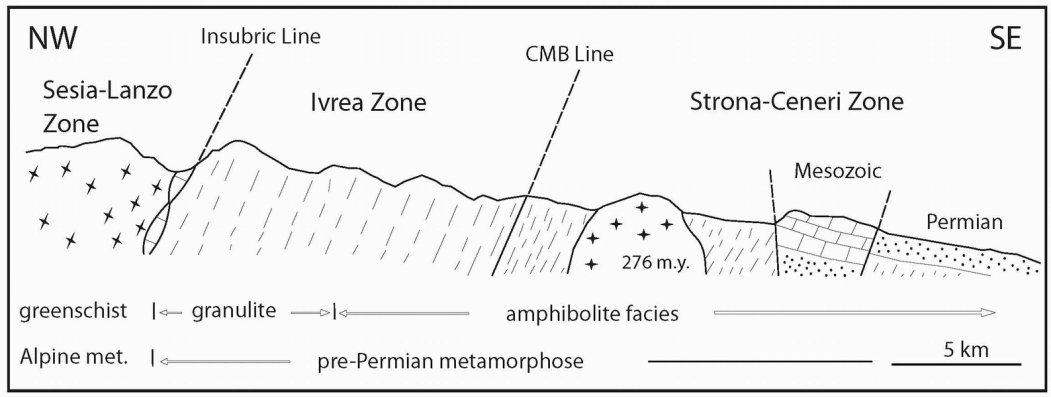

Figure 2.1.1. Schematic composite sketch through the section of the southern Alps (modified after Zingg, 1983 and Schnetger, 1994).

The CMB Line is a major sub-vertical pre-metamorphic tectonic discontinuity of Permian age (Rutter & Brodie, 1996; Boriani & Villa, 1997), which is partly displaced by the Pogallo Line, a younger extensional fault zone (Early Mesozoic) characterized by amphibolite to greenschist facies mylonites (Hodges & Fountain, 1984; Schmid *et al.,* 1987; Rutter & Brodie, 1996; Boriani & Villa, 1997). The Serie dei Laghi comprises amphibolite facies orthogneiss, paragneiss and mica schists that are intruded by Permian granitic plutons (Boriani *et al.,* 1988; Quick *et al.,* 2009). Both the Serie dei Laghi and the Ivrea Zone have been affected by tectonism related to the Alpine orogeny (Schmid, 1993).

2.2 Lithological units, overview

The rocks of the Ivrea Zone have commonly been described in terms of three broad lithological subdivisions: 1) ultramafic rocks, 2) mafic rocks of the Mafic Complex and 3) supracrustal rocks of the Kinzigite Formation (Fig. 2.2.1).

The ultramafic unit consists of different types of mantle peridotites, which are interpreted to represent the deepest levels (Schnetger, 1994) and are best exposed in Val Sesia near Balmuccia (Balmuccia peridotite) and in Val Cannobina near Finero (Finero peridotite) (Fig. 2.2.1). The largest peridotite is the Balmuccia peridotite, whose dominant lithology is spinel lherzolite (Sills, 1984; Boriani & Giobbi, 2004) with less abundant harzburgite and dunite. The peridotites contain dykes and bands rich in green clinopyroxene and lavender aluminium-augite (Quick *et al.*, 2003). Other literature did not refer the peridotites as a single unit but as a part of the lower Mafic Complex (Rivalenti *et al.,* 1975) and interpreted them as residual products (cumulates) of partial melting in the upper mantle (Rivalenti *et al.,* 1975; Sills, 1984). Further, Rivalenti *et al.* (1981) interpreted the eastern contact of the Balmuccia peridotite body as an exposed petrological Moho, which is in contrast to a study of Quick *et al.* (1995). According to Boriani & Giobbi (2004) the peridotite lenses were intercalated with metasedimentary rocks prior to the intrusion of the overlying rocks of the Mafic Complex.

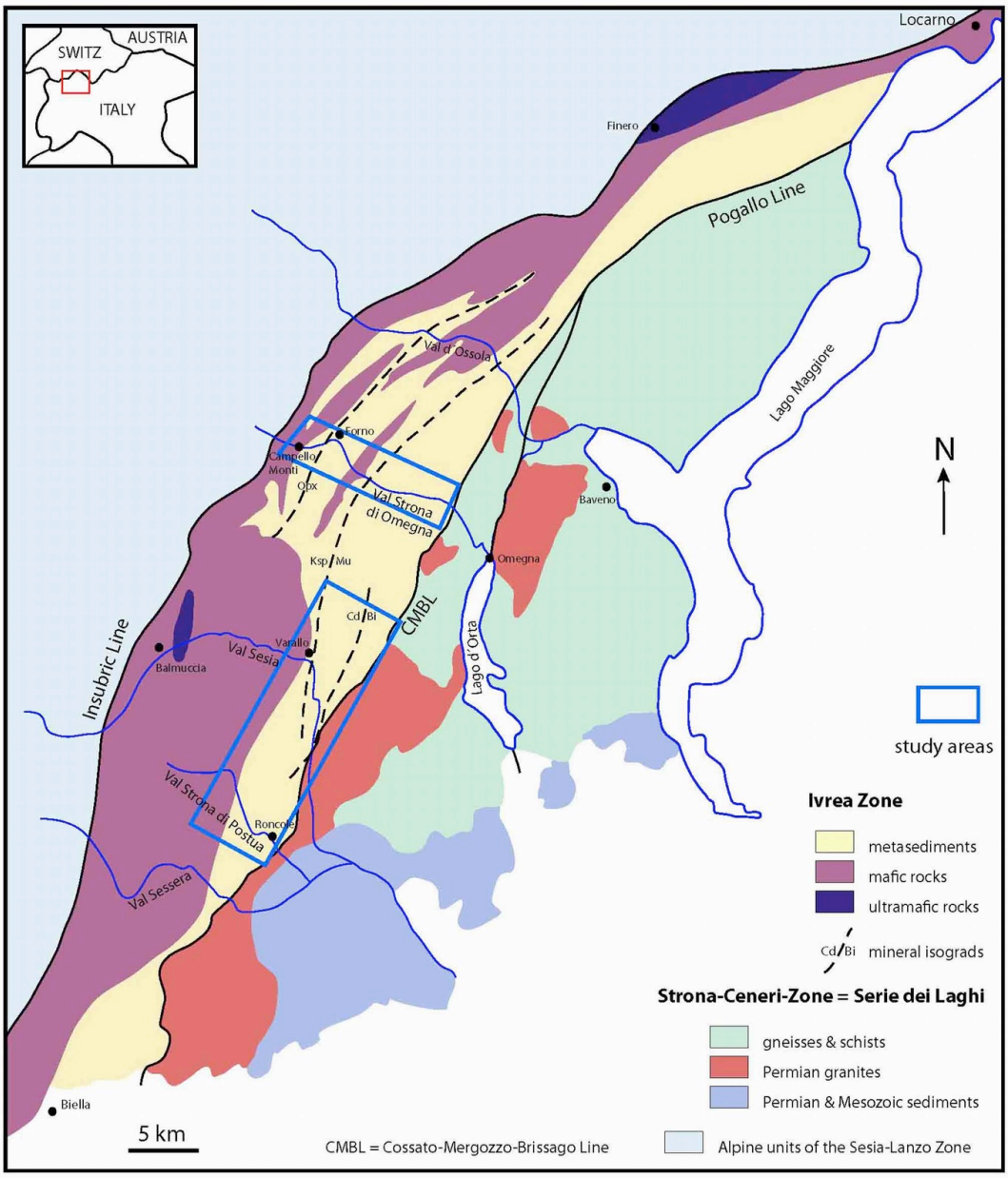

Figure 2.2.1. Schematic geological map of the Ivrea Zone in the southern Alps of northwest Italy, including working areas (modified after Hunziker & Zingg, 1980, Schnetger, 1994 and Siegesmund *et al.,* 2008).

The second unit, which forms the base of the Ivrea Zone in the northwest, is the Mafic Complex (or Mafic Formation) (Sinigoi *et al.,* 1994; Schnetger, 1994; Harlov & Wirth, 2000). It extends for a distance of 80 km in northwest-southeast direction with a maximum thickness of 10 km from east to west (Schnetger, 1994). According to Rivalenti *et al.* (1975), the Mafic Complex consists of granulite facies rocks that, in Val Sesia, can be subdivided into three subunits: the lower layered group (LLG), the upper layered group (ULG) and the main gabbro (MG).

The lower layered group extends for around 900 m in thickness and consists of pyroxenite and pyroxene-rich gabbro with minor peridotite (Rivalenti *et al.,* 1975; Sills, 1984). The upper layered group comprises plagioclase-rich gabbro with minor anorthosite and pyroxenite layers (ultramafic cumulates). This subunit is around 500 m wide. The main gabbro extends for around 5 km and grades towards the southeast into diorite (Rivalenti *et al.,* 1975; Sills, 1984). This subdivision is published by Rivalenti *et al.* (1975). Sinigoi *et al.* (1994) and Harlov & Wirth (2000) do not classify the Mafic Complex directly into subunits, but describe it as consisting of mafic and ultramafic cumulate rocks at the base, followed by massive layered gabbro-noritic rocks, which change towards the roof of the Complex into K-feldspar and quartz-bearing diorites. Quick *et al.* (2003) use another classification for the Mafic Complex describing the subunits from west to east in the southern part of the Ivrea Zone (predominant around Val Sesia) based on the lithological characteristics and mineral assemblages of the rocks. In Quick *et al.* (2003) the first subunit is an amphibole gabbro with a granoblastic texture, containing black-weathered amphiboles and is bordered to the west by the Insubric Line. The second unit is called “gabbro and norite” with a higher abundance of pyroxene. This is the area Rivalenti *et al.* (1975) and Sills (1984) characterized as the “Main Gabbro and upper layered unit” (Quick *et al.,* 2003). The third unit is the “diorite” of Val Sesia and corresponds to the diorites of Rivalenti *et al.* (1975) and Sills (1984). Other described rock types are pegmatitic clinopyroxenites, cumulate ultramafic rocks, charnockitic rocks, dioritic and gabbroic rocks, which all appear locally in the three subunits, additionally with granodiorites and leucotonalites in Val Strona di Postua (Quick *et al.,* 2003).

Best exposed in Val Strona di Omegna the Kinzigite Formation (third unit of the Ivrea Zone) consists of a sequence of interlayered metapelites, metapsammites/metagreywackes and metabasites plus minor calcsilicates and marbles. The Kinzigite Formation forms the highest structural level of the Ivrea Zone and overlies the Mafic Complex. The rocks range in metamorphic grade from amphibolite facies to granulite facies (Zingg, 1980; Schmid, 1993; Harlov & Wirth, 2000). It is not certain that the amphibolite and granulite facies assemblages represent a continuous metamorphic sequence in their present position (Schmid & Wood, 1976).

2.3 Kinzigite Formation

The Kinzigite Formation has been subdivided into three main units based on the grade of metamorphism. These are, from southeast to northwest, a Kinzigite Zone (amphibolite facies), a transition zone (transitional amphibolite to granulite facies rocks) and a Stronalite Zone (granulites facies rocks) (Bea & Montero, 1999) (Fig. 2.3.1).

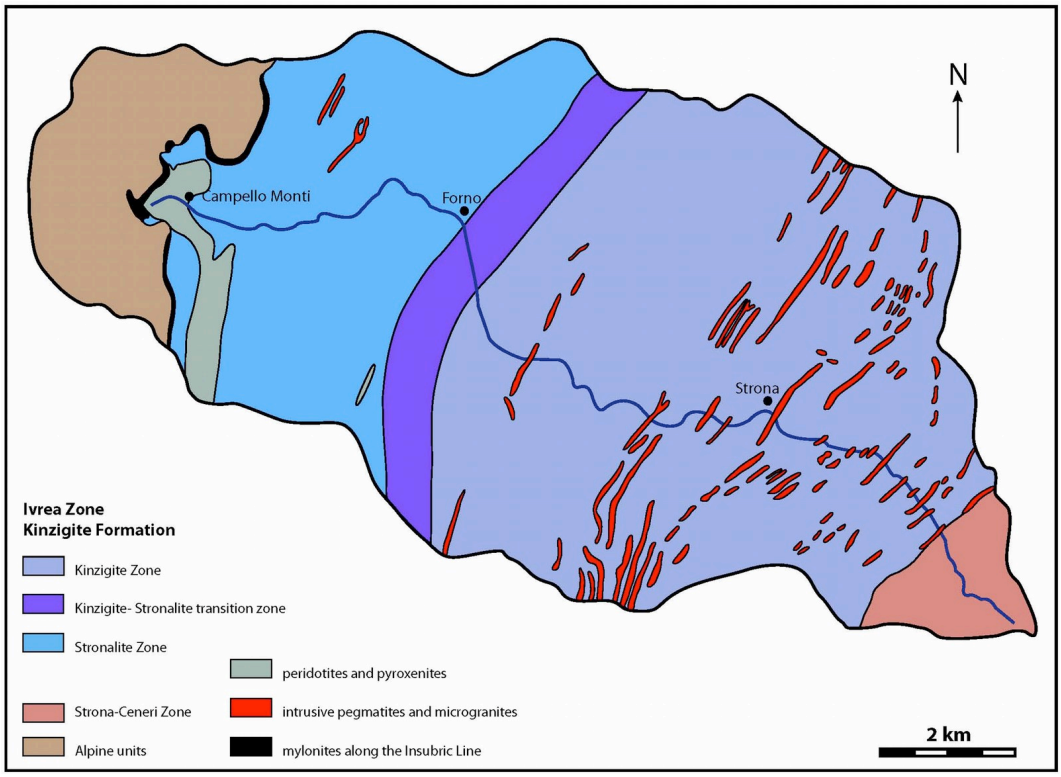

Figure 2.3.1. Simplified geological map of Val Strona di Omegna area (see blue boxes in Fig. 2.2.1) (modified after Bea & Montero, 1999).

In the older literature, the terms Kinzigite and Stronalite are used for amphibolite facies rocks and upper amphibolite to granulites facies rocks respectively (Schmid, 1968). However, more recent literature uses Kinzigite for amphibolite facies rocks and Stronalite only for rocks preserving granulite facies assemblages (Schnetger, 1994). Both terms are used exclusively for the metasediments, although these are everywhere interlayered with metabasites, calcsilicates and marbles.

In general, the supracrustal rocks of the Kinzigite Formation are aluminous metapelites (Barboza & Bergantz, 2000). According to Schmid & Wood (1976) the amphibolite facies rocks are granoblastic while the granulite facies rocks have mylonitic textures. Other authors reported that with increasing metamorphic grade the rocks evolve from schists to banded migmatitic gneisses as a result of an up-grade decrease in the mode of muscovite and biotite and increase in the mode of K-feldspar and garnet (Schmid & Wood, 1976; Zingg, 1980; Schnetger, 1994; Sinigoi *et al.,* 1994; Barboza *et al.,* 1999; Rutter *et al.*, 2007). This increase in garnet and decrease in biotite has been described by the reaction: biotite + sillimanite + quartz = garnet + K-feldspar + H_2O (Schmid & Wood, 1976). Sillimanite changes from fibrolitic to prismatic with increasing metamorphic grade (Schmid & Wood, 1976). In the whole Kinzigite Formation the rocks change in detail from sillimanite-almandine-muscovite subfacies (amphibolite facies) to pyroxene-granulite subfacies (granulite facies) (Bertolani, 1968). According to Quick *et al.* (2003) the peak metamorphic grade for the Kinzigite Formation in Val Sesia and Val Strona di Postua was amphibolite facies, based on the absence of prograde muscovite in the metapelites and the absence of orthopyroxene in the metabasites.

In lower Val Strona di Omegna (Kinzigite Zone) the metapelites contain biotite + plagioclase + quartz ± garnet ± sillimanite ± muscovite ± K-feldspar. Rare cordierite is reported (Zingg, 1980). The peak metamorphic muscovite is limited to these low-grade rocks. The metabasites of the Kinzigite Zone contain amphibole + plagioclase ± clinopyroxene (Barboza & Bergantz, 2000). In the upper Kinzigite Zone discordant leucosome-like veins with modal quartz up to 95 % are widespread. They are reported to be hydrothermal mobilizates instead of partial melting (Bea & Montero, 1999). According to Schnetger (1994) the Kinzigites of the amphibolite facies are migmatitic with melanosomes enriched in biotite and garnet, while the leucosomes are enriched in quartz, plagioclase and K-feldspar. Bea & Montero (1999) characterized the Kinzigite Zone by a modal value of biotite/garnet > 2.

Beyond the transition zone, the metabasites grade smoothly into amphibolite-clinopyroxene-sphene-bearing amphibolite facies gneisses interlayerd with

biotite-bearing metapelitic gneisses (Harlov & Wirth, 2000). An area of migmatites also occurs (Mehnert, 1975). Orthopyroxene appears at the onset of the granulite facies in granoblastic amphibole- and plagioclase-bearing metabasites. According to Sills (1984), assemblage blebs of myrmekite, which replaces K-feldspar, are quite common. A possibly tectonic boundary between amphibolite and granulite facies rocks is suggested by the presence of ultramylonites and a slightly increase in metamorphic grade across this boundary (Schmid & Wood, 1976). According to Bea & Montero (1999) the transition zone is defined by a modal value of biotite/garnet between 0.5 and 2.

The Stronalites represent a 4–5 km wide unit comprising migmatitic garnet-sillimanite-K-feldspar-rich gneisses with subordinate garnet-orthopyroxene-bearing metabasites and calcsilicates. The Stronalites are interpreted to represent the residuum following extraction of melt from partial melting of the metapelites during granulite facies conditions (Schnetger, 1988; Voshage *et al.,* 1990; Harlov & Wirth, 2000). Small patches and concordant veins of quartz + plagioclase + K-feldspar ± garnet leucosomes are intermingled with the garnet + sillimanite + biotite ± orthopyroxene melanosomes. The bulk composition of the Stronalites or granulite facies rocks can be explained by extraction of 20–40 % anatectic melt from a protolith that is similar to the unmelted amphibolite facies rocks of the Kinzigite Formation (e.g. Schnetger, 1994; Harlov & Förster, 2002; Peressini *et al*., 2007). According to Sills (1984) Mg-rich and Al-poor metapelites with orthopyroxene, garnet and plagioclase were found. Near to the contact with the Mafic Complex, cordierite and hercynitic spinel may occur in the metapelites in the Val Strona di Omegna (Zingg, 1980). The garnetiferous metagabbros (Sills, 1984) can be related to the cumulate layers in Val Sesia. The Stronalite Zone is characterized by modal value of biotite/garnet < 0.5 (Bea & Montero, 1999).

Granulite facies rocks are not reported from Val Sesia or Val Strona di Postua (Quick *et al.,* 2003), except for a few septa of paragneiss within the Mafic Complex. These septa are within a ‘paragneiss-bearing belt’ that is located between the upper and the lower Mafic Complex (Sinigoi *et al.*, 2011).

2.4 Existing pressure and temperature estimates

Quantitative constraints on pressure *(P)* and temperature *(T)* conditions of metamorphism have typically used conventional exchange and net transfer thermobarometry. Existing estimates for *P–T* conditions in the Ivrea Zone, especially in Val Strona di Omegna vary widely and are summarised in Table 2.4.1.

Schmid & Wood (1976) published *P–T* conditions of 660 ± 70 °C and 7 ± 2 kbar for Val Strona di Omegna. Hunziker & Zingg (1980) calculated *P–T* conditions of 540–820 °C and 4.7–10 kbar for Val Strona di Omegna, both increasing towards the Insubric Line. Schnetger (1988) suggested slightly higher temperatures but similar pressures (750 ± 50 °C, 6 ± 1 kbar). Thermobarometric investigations by Henk *et al.* (1997) give values for the three parts of the Kinzigite Formation in Val Strona di Omegna as 631–647 ± 40 °C and 4.3–5.2 kbar for amphibolite facies rocks of the Kinzigite Zone, 672–690 ± 30 °C and 6 ± 0.5 kbar for the transition zone and 716–762 ± 30 °C and 6.3–7.6 ± 1 kbar for the Stronalite Zone at the highest metamorphic grade. Towards the CMB Line in the southeast, a decrease in peak metamorphic conditions to amphibolite facies conditions of 615 ± 30 °C and 4.1 ± 1 kbar are inferred (Sills, 1984; Franz & Harlov, 1998). Bea & Montero (1999) reported pressure intervals of 4–5 kbar (Kinzigite Zone), 5–6 kbar (transition zone) and 6–8 kbar (Stronalite Zone). Based on Zr-in-rutile thermometry Luvizotto & Zack (2009) suggested significantly higher peak temperatures (850–930 °C) for granulite facies metapelites in Val Strona di Omegna than those of previous studies.

Rock Type	Minerals	*T*	sd *T*	*P*	sd *P*	Methods (thermometry/barometry)		Reference
metagabbro	g-cpx-pl-hbl ± opx, bi, ru, ilm	**810**	**50**	**8**	**2**	TWEEQ (1)	calcite-carbon isotop	Henk *et al.*(1997)
gneiss	g-opx-pl-q ± ksp, bi, ru, ilm	**762**	**30**	**8**	**1**	g-opx (2)	g-opx-pl-q (2)	Henk *et al.* (1997)
gneiss	g-opx-pl-q ± ksp, bi, ru, ilm	**728**	**30**	**7**	**1**	g-opx (2)	g-opx-pl-q (2)	Henk *et al.* (1997)
gneiss	g-opx-pl-q ± ksp, bi, ru, ilm	**716**	**30**	**6**	**1**	g-opx (2)	g-opx-pl-q (2)	Henk *et al.* (1997)
migmatite	g-sill-bi-pl-ksp-q ± ilm	**690**	**30**	**6**	**0.5**	g-opx (3)	GASP (4)	Henk *et al.* (1997)
gneiss	g-sill-bi-pl-ksp-q ± ilm	**657**	**30**	**6**	**0.5**	g-opx (3)	GASP (4)	Henk *et al.* (1997)
amphibolite	g-hbl-pl-bi ± ilm, sp	**631**	**30**	**5**	**0.5**	g-hbl (5)	g-hbl-pl-q (6)	Henk *et al.* (1997)
calcsilicate schist	g-cpx-hbl-pl-cc-q ± bi, ilm, sp	**647**	**50**	**4**	**2**	g-cpx (7)	g-cpx-pl-q (8)	Henk *et al.* (1997)
mica-schist (CMBL)	g-bi-mu-pl-q ± ilm	**615**	**30**	**4**	**1**	g-bi (9)	g-pl-bi-mu (10)	Sills (1984)
gneiss (Omegna)	and-sill-bi-mu-pl-ksp-q ± cd, ilm	**580**	**30**	**2**	**1**	feldspar (11)	mu (12)	Henk *et al.* (1997)
metapelite in granulite facies	g-bi; opx-g-pl-q; g-sill-pl-q;	**750**	**50**	**6**	**1**			Sills (1984)
		615	**30**	**4**	**1**	g-bi (3)	g-pl-bi-mu (10)	Lal (1993) in Henk *et al.* (1997)
granulite facies conditions		**720–760**		**6–8**		g-opx-pl-q	g-opx-pl-q	Lal (1993) in Henk *et al.* (1997)

Table 2.4.1. Summary of some pressure and temperature ranges investigated in Val Strona di Omegna. Sources for *P–T* estimates are Henk *et al.* (1997): (1) Berman, 1991; (2) Lal, 1993; (3) Zhu & Sverjensky, 1992; (4) Koziol & Newton, 1988; (5) Graham & Powell, 1986; (6) Kohn & Spear, 1990; (7) Ellis & Green, 1979; (8) Newton & Perkins, 1986; (9) Williams & Grambling, 1992; (10) Hoisch, 1990; (11) Fuhrman & Lindsley, 1988; (12) Massonne, 1990.

2.5 Age determinations

A range of different ages for the metamorphism of the Ivrea Zone have been reported, many of which were constrained using rocks from the Mafic Complex (Table 2.5.1). According to Hunziker & Zingg (1980) the Rb-Sr whole rock ages give a Caledonian age (around 400 Ma) for metamorphism. This is consistent with Schmid & Wood (1976) who also give a Caledonian age for the main metamorphic event. In contrast, the monazites from the same rocks analysed by Rb-Sr whole rock give Permian ages (Köppel, 1974), while ages from hornblende and micas, analysed by K-Ar are lower Mesozoic (Hunziker, 1974; Zingg, 1980). The age of the high-grade metamorphism of the Kinzigite Formation has been determined at approximately 280 Ma using U-Pb dating on monazites (Teufel & Schärer, 1989). For the intrusion of the Mafic Complex, numerous and widely ranging ages between 250 and 290 Ma have been suggested (Hunziker & Zingg, 1980; Pin & Sills, 1986; Voshage *et al.,* 1987; Voshage *et al.,* 1990; Gebauer*,* 1993; Schnetger, 1994). According to Voshage *et al.* (1987) the age for magmatic underplating, which is responsible for the formation of the Mafic Complex, is around 270 Ma. Peressini *et al.* (2007) give ages ranging between 286 ± 6 Ma and 292 ± 4 Ma for the massive growth of the upper Mafic Complex. Barboza & Bergantz (2000) give a Late Carboniferous-Early Permian age for the crystallization of the upper Mafic Complex. Different cooling ages are reported for the granulite facies portion of the Ivrea Zone. Köppel (1974), Bürgi & Klötzli (1990) and Henk *et al.* (1997) reported ages of 275 ± 2 Ma for U-Pb in monazites and 274 ± 17 Ma for Rb-Sr in whole rock. Lu *et al.* (1997) published ages of 215 ± 15 Ma for Sm-Nd in garnets. K-Ar dating in hornblendes gives ages of 210 ± 5 Ma (Brodie *et al.,* 1989) and for biotite, McDowell & Schmid (1968) calculated cooling ages of 175 ± 5 Ma. According to Peressini *et al.* (2007) ages range from > 600 Ma (Hunziker & Zingg, 1980; Voshage *et al.,* 1987) to around 30 Ma. However, ages older than of 400 Ma, based on Rb-Sr and Sm-Nd whole rock data are interpreted to be the slopes of mixing lines with no age significance (Voshage *et al.,* 1990). Ages of around 30 Ma can reflect resetting during the Alpine event. Peressini *et al.* (2007) reported that the high-grade metamorphism in the Kinzigite Formation started at about 310 Ma.

Locality/ Unit	rock type / event	**age (Ma)**	**sd age (Ma)**	method and mineral	References
Kinzigite Formation		**287**	**3**	SHRIMP on zircon	Quick *et al.* (2009)
Kinzigite Formation		**310**	**3**	SHRIMP on zircon	Peressini *et al.* (2007)
lower M.C.		**299**	**5**	U-Pb on zircon	Vavra *et al.* (1999)
lower M.C.	amphibole gabbro	**279**	**5**	SHRIMP on zircon	Peressini *et al.* (2007)
upper M.C.	Gabbronorit	**258–318**		SHRIMP on zircon	Peressini *et al.* (2007)
upper M.C.	emplacement of the M.C.	**254–355**		SHRIMP on zircon	Vavra *et al.* (1999) in Quick *et al.* (2009)
upper M.C.	gabbronorit	**292**	**4**	Pb-Pb evaporation	Garuti *et al.* (2001)
upper M.C.	Gabbronorit	**289**	**3**	SHRIMP on zircon	Peressini *et al.* (2007)
upper M.C.	diorit	**285–295**	**7**	conventionell U-Pb	Pin (1986)
Val Strona di Omegna	g-opx-gneiss	**285**		U-Pb on monazite	Henk *et al.* (1997)
V.S.d.O./ M.C.	metagabbro	**276**		U-Pb on monazite	Henk *et al.* (1997) in Franz & Harlov (1998)
V.S.d.O.	amphibolite	**265**		U-Pb on monazite	Henk *et al.* (1997)
V.S.d.O.	migmatite	**258**		U-Pb on monazite	Henk *et al.* (1997)
near Omegna	sill-and-gneiss	**288**		U-Pb on monazite	Henk *et al.* (1997)
	intrusion of the M.C.	**250–290**		U-Pb on monazite + zircon	Voshage *et al.* (1990)
Val Sesia (Balmuccia)	event of crust formation	**600**		Sm-Nd	Voshage *et al.* (1987)
	granulite facies metamorphism	**285**	**10**	zircon	Köppel (1974) in Henk *et al.* (1997)
	metasediments	**280**		U-Pb on monazite	Teufel & Schärer (1989) in Schnetger (1994)

Table 2.5.1. Summary of some age determinations mostly measured on rocks from the upper Mafic Complex (M.C.).

2.6 Emplacement of the Mafic Complex and history of the Ivrea Zone

There are many different views relating to the development of the Mafic Complex and its relationship to the metamorphism of the metasediments of the Kinzigite Formation.

The Mafic Complex is commonly interpreted to be the source of heat for the regional metamorphism in the Ivrea Zone (Schmid, 1967; Schmid & Wood, 1976; Sinigoi *et al.,* 1994; Quick *et al.,* 1994; Snoke *et al.,* 1999). Furthermore, the thermal input of this magmatic underplating is also inferred to have induced granulite facies metamorphism in the metabasites (Quick *et al.,* 1994; Schnetger, 1994; Harlov & Wirth, 2000). However, according to Rivalenti *et al.* (1984) and Barboza & Bergantz (2000) the Mafic Complex could also have been intruded during or after regional metamorphism and cooled slowly thereafter under granulite facies conditions (Voshage *et al.,* 1990), explaining why the Mafic Complex itself is metamorphosed at granulite facies conditions (Sinigoi *et al.*, 1994; Bea & Montero, 1999).

According to Franz & Harlov (1998), it is commonly postulated that the thermal input during the magmatic underplating of the Mafic Complex induced granulite facies metamorphism in the overlying rocks (Sinigoi *et al.,* 1994; Henk *et al.,* 1997) and allowed partial melting of the lower crustal rocks. The magmatic underplating is inferred to have occurred at or near the Moho during the late Palaeozoic (Voshage *et al.,* 1990; Schnetger, 1994). This is identical to the interpretation of Rutter *et al.* (1993) and Rutter & Brodie (1996) who reported that the Mafic Complex intruded into the originally flat-lying but migmatized lower crustal country rocks, immediately above the Moho.

A reconstruction of the pre-Alpine geological setting (Variscan and/or Caledonian) is very difficult, because the Ivrea Zone represents a lower crustal level during Palaeozoic orogeny (Schmid, 1993). For Sills and Tarny (1984) the metasediments with their intercalations of MORB-type basic rocks originated and

became strongly deformed in an accretionary prism. It is unknown when and by which processes the rocks became buried to a depth of around 30 km (Vavra *et al.,* 1999). At this depth the rocks, now the Kinzigite Formation, were intruded by large volumes of mantle-derived magma (magmatic underplating) during the Late Carboniferous and Early Permian (Gebauer, 1993; Henk *et al.,* 1997; Vavra *et al.,* 1999; Abart *et al.,* 2001).

Brodie & Rutter (1987) and Rutter *et al.* (1993) suggested that some high temperature shear zones (in combination with radiometric cooling ages) indicated that the exhumination of the Ivrea Zone had already started in Permian. Tectonic and volcanic evidence in the upper crust and sedimentary cover of the southern Alps indicate that continental rifting started in Late Triassic, giving rise to further exhumation (Vavra *et al.,* 1999). The most obvious expression of the Late Triassic to Early Jurassic events is the formation of pegmatitic oligoclasite dykes, found in the ultramafic and mafic granulite facies rocks (Vavra *et al.,* 1999). Temperatures of more than 500 °C during or after the formation of the pegmatite dykes have be suggested. Based on this the granulite facies rocks were still or again at high temperature at this time (Vavra *et al.,* 1999).

The final exhumination occurred during the Alpine orogeny (Vavra *et al.*, 1999; Vavra & Schaltegger, 1999; Abart *et al.,* 2001). The Ivrea Zone cooled below 300 °C at around 180 Ma (Zingg, 1983; Bürgi & Klötzli, 1990). In the Late Oligocene to Early Miocene the Ivrea Zone was affected by brittle to semi-brittle faulting and folding under greenschist to subgreenschist facies conditions ($T < 300$ °C). This can be observed near the Insubric Line (Brodie & Rutter, 1987; Schmid *et al.,* 1987; Handy & Zingg, 1991; Harlov & Wirth, 2000).

Barboza *et al.* (1999), Barboza & Bergantz (2000) and Peressini *et al.* (2007) questioned whether the Mafic Complex was the source of heat for the granulite facies metamorphism. Barboza *et al.* (1999) reported that in the southern Ivrea Zone the granulite facies metamorphism predates the emplacement of the Mafic Complex. The thermal effect of the intrusion was relatively small with a conspicuous contact metamorphism event only within one kilometre to the roof of the Mafic Complex (Barboza *et al.*, 1999; Barboza & Bergantz, 2000).

Furthermore Peressini *et al.* (2007) suggested that according to stable isotope investigations of Ahrendt *et al*. (1989), a direct correlation between the Mafic Complex and the granulite facies metamorphism of the crust is unlikely.

Chapter 3
Methods

3.1 Introduction

In this chapter the various analytical methods used in the project are described, with particular focus on the mineral equilibrium modelling.

3.2 Field work and sample preparation

Three main periods of field work (altogether around 10 weeks) were undertaken. During this time approximately 250 samples were collected. The majority were metapelites from Val Strona di Omegna together with representative samples of metabasites, metapsammites/metagreywackes, calcsilicates and marbles. Samples of all these rock types from Val Sesia and Val Strona di Postua were also collected for comparison with those from Val Strona di Omegna. Where appropriate, detailed field relationships were recorded in areas of good exposure in order to examine the partial melting of the metapelites, the morphology and distribution of former melt networks, the difference between unmelted and migmatized metapelites and the relationship between the metapelites and other rock types. Detailed field sketches at varying scales from Val Strona di Omegna illustrating these relationships are presented in Chapter 4.2.

From all collected samples polished thin sections with an average thickness of 30–50 μm were prepared for petrographic analysis using standard polarisation microscopy. From these, 37 samples were chosen for further mineral chemical analysis by electron microprobe (EMPA; Chapter 5 and Appendix B). Powders

were prepared from 46 metapelite samples for analysis by X-ray fluorescence (XRF; Appendix A).

3.3 Bulk rock analysis

Major element bulk rock analyses were performed using an 'MagiXPRO Phillips 2002' X-ray fluorescence spectrometer at the Johannes-Gutenberg University of Mainz. Glass beads of samples were prepared using 0.4 mg of sample powder and 5.2 mg $LiBO_4$ as a flux. The following oxides were analysed (with a relative error): SiO_2 (0.4 %), TiO_2 (1.0 %), Al_2O_3 (0.7 %), Fe_2O_3 (total) (0.8 %), MnO (1.8 %), MgO (0.3 %), CaO (0.5 %), Na_2O (1.3 %), K_2O (0.8 %), P_2O_5 (1.1 %), Cr_2O_3 (2.0 %), NiO (0.8 %) and SO_3 (4.0 %). With measuring loss on ignition (LOI) the combined content of volatile phases (H_2O, CO_2, CH_4) for each sample were determined. The amount of total Fe_2O_3 as measured was converted to values for FeO calculated with a factor of 0.899. In addition the FeO : Fe_2O_3 ratio was measured by iron titration, the latter to underline and verify the calculated results. From both calculation and titration almost the same values resulted. Results of the XRF analysis are presented in Appendix A.

3.4 Mineral chemical analysis

Investigations of the mineral chemistry were made using the 'Jeol JXA 8900 RL' electron probe microanalyser (EMPA) at the Johannes-Gutenberg University of Mainz using the analytical program 'SilUMainz', which is an universal program for most silicate phases (Tab. 3.4.1). The analysis used an accelerating voltage of 15 kV, a beam current of 12 nA with a beam diameter of 2 μm (5 μm for feldspars). Analysed minerals are: plagioclase, K-feldspar, garnet, biotite, muscovite, cordierite, orthopyroxene and oxide minerals. Results are presented in Appendix B.

Spectrometer (channel)	analyser crystal	Element (standard)
1	TAP	Na (Albite), Al (Corundum)
2	TAP	Si (Wollastonite), Mg (Periclase)
3	PET	K (Orthoclase), Ca (Wollastonite)
4	PET	Ti (MnTi), Cr (Chromite)
5	LIFH	Fe (Hematite), Mn (MnTi)

Table 3.4.1. Analysed elements, standards and their position on the five spectrometers.

3.5 Phase equilibria modelling

3.5.1 Introduction

During the last 15 years or so, thermodynamic phase equilibria modelling has become a widely used method for quantitative investigations of metamorphism. The method can be used to understand complex metamorphic processes, including mineral assemblage development and the formation of reaction textures. The principal use is to calculate the stability of specified mineral assemblages that are inferred to have been in equilibrium in a metamorphic rock as a function of pressure and temperature.

The thermodynamic calculations use an internally consistent thermodynamic dataset for mineral end-members (e.g. Holland & Powell, 1985; Holland & Powell, 1990; Holland & Powell, 1998), as well as activity-composition (*a-x*) models for solid solution phases (e.g. Powell & Holland, 1993; Holland & Powell, 1996 a and b; Holland & Powell, 2003). Calculations were performed using the software THERMOCALC (e.g. Powell *et al.*, 1998; Powell & Holland, 1988). This chapter gives an introduction to the approach; further details are available at the following url: http://www.metamorph.geo.uni-mainz.de/thermocalc/.

3.5.2 Basic principles of the dataset

Powell & Holland (1985) first reported the techniques and methods required to create an internally consistent thermodynamic dataset of mineral end-members with which it should be possible to calculate any equilibria between these end-members. The required thermodynamic data are heat capacities (C_p), molar volumes (V), entropies (S), thermal expansion (α), isothermal compressibilities (β) and enthalpies (H) for the mineral end-members. Most of these data are taken directly from values in the literature (measured by calorimetry and other experiments). By contrast, the values for ΔH are determined via least squares analysis from the available experimental and calorimetric data (Powell & Holland, 1985; Powell & Holland, 1993). For every element in the dataset a so-called "anchor" phase is needed (Holland & Powell, 1985) for which good calorimetric data exists (e.g. Si: quartz, Ti: rutile, Al: corundum, Fe: iron, Mg: periclase).

The calculation method uses sets of simultaneous non-linear equations involving the equilibrium relation for a balanced chemical reaction between mineral end-members whereby:

$$0 = \Delta G^0 + R T \ln K$$

where ΔG^0 is the standard-state Gibbs free energy of reaction (calculated from the Gibbs energy of end-members that are part of the reaction), R is the universal gas constant, T is temperature (in degrees Kelvin) and K is the equilibrium constant for a balanced reaction calculated from the activities of the mineral end-members (Powell & Holland, 1988).

The version of the dataset of Holland & Powell (1998) used here has undergone numerous updates. The latest version ds55 (November 2003, updated) contains 190 end-members and 319 reaction equilibria. The dataset has only information on end-members, but not on solid solution phases. For the way end-members mix in a solid solution phase activity-composition models are needed (Chapter 3.5.4).

3.5.3 End-members

The internally consistent thermodynamic dataset contains predominantly naturally occurring end-members but also includes some fictive end-members for minerals. Natural end-members exist in their pure form and can be calibrated from experiments of end-member reactions, while fictive end-members are not stable in nature and cannot be synthesised in their pure form. Examples for natural end-members are Fe-cordierite ($Fe_2Al_4Si_5O_{18}$) and Mg-cordierite ($Mg_2Al_4Si_5O_{18}$), while Mn-cordierite ($Mn_2Al_4Si_5O_{18}$) is a fictive end-member. Most of the Mn-bearing phases in the dataset, except the end-member for garnet, are fictive end-members and derived from exchange of Mg–Mn from natural end-members (Maher *et al.,* 1997; Holland & Powell; 1998).

Some fictive-end-members are also created in the activity-composition *(a-x)* coding (Chapter 3.5.4). They resulted from reactions, e.g. the Fe^{3+} end-member mots for orthopyroxene (Tab. 3.5.1), which can be calibrated from the reaction (White *et al.,* 2002):

1 mgts + ½ hem = mots + ½ cor

Depending on the chosen system for thermodynamic calculations (e.g. KFMASH, NCKFMASH, NCKFMASHTO) different minerals (and their end-members) are involved in the calculation. The following list shows the minerals and their real and fictive end-members used in the NCKFMASHTO system (Appendix C) in this work.

Phase	Symbol	End-member	Formula (abbreviation)
quartz (q)	q	quartz	SiO_2
kyanite (ky)	ky	kyanite	Al_2SiO_5
sillimanite (sill)	sil	sillimanite	Al_2SiO_5
andalusite (and)	and	andalusite	Al_2SiO_5
rutile (ru)	ru	rutile	TiO_2
water (H_2O)	h2o	H_2O	H_2O

Phase	Symbol	End-member	Formula (abbreviation)
melt (liq)	qL	silica liquid	SiO_2
	abL	albite liquid	$NaAlSi_3O_8$
	kspL	K-feldspar liquid	$KAlSi_3O_8$
	anL	anorthite liquid	$CaAl_2Si_2O_8$
	silL	sillimanite liquid	Al_2SiO_5
	foL	forsterite liquid	Mg_2SiO_4
	faL	fayalite liquid	Fe_2SiO_4
	h2oL	H_2O liquid	H_2O
biotite (bi)	phl	phlogopite	$KMg_3AlSi_3O_{10}(OH)_2$
	ann	annite	$KFe_3AlSi_3O_{10}(OH)_2$
	obi	ordered biotite *	$KFeMg_2AlSi_3O_{10}(OH)_2$
	east	eastonite	$KMg_2Al_3Si_2O_{10}(OH)_2$
	tbi	Ti-biotite *	$KMgTiAlSi_3O_{10}(OH)_2$
	fbi	Fe^{3+}-biotite *	$KMg_2Fe^{3+}Al_2Si_2O_{10}(OH)_2$
cordierite (cd)	crd	cordierite	$Mg_2Al_4Si_5O_{18}$
	fcrd	Fe-cordierite	$Fe_2Al_4Si_5O_{18}$
	hcrd	hydrous cordierite	$Mg_2Al_4Si_5O_{18} * H_2O$
staurolite (st)	mst	Mg-staurolite	$Mg_4Al_{18}Si7_{.5}O_{48}H_4$
	fst	Fe-staurolite	$Fe_4Al_{18}Si7_{.5}O_{48}H_4$
garnet (g)	alm	almandine	$Fe_3Al_2Si_3O_{12}$
	py	pyrope	$Mg_3Al_2Si_3O_{12}$
	gr	grossular	$Ca_3Al_2Si_3O_{12}$
	andr	andradite	$Ca_3Fe_2Si_3O_{12}$
orthopyroxene (opx)	en	enstatite	$Mg_2Si_2O_6$
	fs	ferrosilite	$Fe_2Si_2O_6$
	mgts	Mg-Tschermak pyroxene	$MgAl_2SiO_6$
	fm	Fe-Mg ordered pyroxene *	$FeMgSi_2O_6$
	mots	Fe^{3+}-orthopyroxene *	$MgFe^{3+}AlSiO_6$
muscovite (mu)	mu	muscovite	$KAl_3Si_3O_{10}(OH)_2$
	pa	paragonite	$NaAl_3Si_3O_{10}(OH)_2$
	cel	celadonite	$MgAlSi_4O_{10}(OH)_2$
	fcel	Fe- celadonite	$KFeAlSi_4O_{10}(OH)_2$
paragonite (pa)	mu	muscovite	$KAl_3Si_3O_{10}(OH)_2$
	pa	paragonite	$NaAl_3Si_3O_{10}(OH)_2$
	cel	celadonite	$MgAlSi_4O_{10}(OH)_2$
	fcel	Fe- celadonite	$KFeAlSi_4O_{10}(OH)_2$

Phase	Symbol	End-member	Formula (abbreviation)
K-feldspar (ksp)	san	sanidine	$KAlSi_3O_8$
	abh	high albite	$NaAlSi_3O_8$
	an	anorthite	$CaAl_2Si_2O_8$
plagioclase (pl)	san	sanidine	$KAlSi_3O_8$
	abh	high albite	$NaAlSi_3O_8$
	an	anorthite	$CaAl_2Si_2O_8$
spinel (sp)	herc	hercynite	$FeAl_2O_4$
	sp	spinel	$MgAl_2O_4$
	mt	magnetite	Fe_3O_4
	usp	ulvospinel	Fe_2TiO_4
ilmenite (ilm)	ilm	ilmenite	$FeTiO_3$
	dilm	disordered-ilmenite *	
	hem	hematite	Fe_2O_3

Table 3.5.1. List of mineral end-members in the system NCKFMASHTO used in this study for calculation pseudosections of metapelite samples. Symbol, name of the end-member and their formula are taken from e.g. Holland & Powell, 1998. With * the fictive end-members are denoted.

3.5.4 Activity-composition (*a-x*) models

The internally consistent dataset only contains the thermodynamic information for end-members but not for solid solution phases. Activity-composition (*a-x*) models (e.g. Powell & Holland, 1993; Holland & Powell, 1996 a and b; Holland & Powell 2003; Holland & Powell, 2006) are required for minerals that exhibit solid solutions. Such models describe the distribution of elements on the appropriate sites in a mineral along with their interaction energies (W´s).

In general, the *a-x* relationships have to be calibrated using both natural data and experimental results. These relationships relate to the distribution of elements in a mineral end-member (site distribution) and also the ideal/non-ideal nature of mixing between end-members (interaction energies) (Powell & Holland, 1993).

The two site distribution models used are the equipartition model (e.g. Holland & Powell, 2006) and the order-disorder model (Holland & Powell, 1996 a and b). The equipartition model describes that the distribution of two or more end-

members are the same on every site (e.g. xMgM1 = xMgM2) or that the proportion of two elements is kept constant e.g. xFeM1 = xFeM2, where xFe = $Fe^{2+}/(Fe^{2+} + Mg)$. However, this kind of model does not consider the mixing of other elements on the appropriate site (Holland & Powell, 2006) and is not appropriate for complex minerals that have many sites (e.g. pyroxenes and amphiboles). The order-disorder model considers that the distribution of the elements is different on each site (xMgM1 ≠ xMgM2 or xFeM1 ≠ xFeM2). Some elements are equally distributed to both sites, so it is possible that an *a-x* model for a mineral can involve the order-disorder model for one element and the equipartition model for another (Holland & Powell, 1996 a and b).

For the mixing of the end-members, three mixing models are used – the ideal mixing (ideal), the symmetric formalism (sf) and the asymmetric formalism (asf). Ideal mixing means that there is only ideal (and no non-ideal) interaction between the end-members and no interaction parameters (W(ij) = W(ji) = 0) are needed. The symmetric formalism relates to the interaction of two or more end-members that are non-ideal but symmetric (W(ij) = W(ji) ≠ 0) (Powell & Holland, 1993; Holland & Powell, 1996 a and b). This is the most common type of model used, but it has the disadvantage that it cannot deal with asymmetric mixtures (Holland & Powell, 2003). The asymmetric formalism relates to the interaction of two or more end-members that are both non-ideal and asymmetric (W(ij) ≠ W(ji) ≠ 0). It uses a macroscopic 'van Laar' formalism for non-ideality (Holland & Powell, 2003) in which a symmetric interaction parameter is modified via an asymmetry factor (alpha).

Altogether, an *a-x* model has to describe the defining variables, the end-member properties, the mixing parameters, the site distributions and the ideal activities. Therefore, every model is build up by a combination of the site distribution models and the mixing models (e.g. equipartition model and ideal mixing for very simple *a-x* models and order-disorder model and asymmetric formalism for very complex *a-x* models).

An example: an *a-x* model for orthopyroxene

In this simplest model orthopyroxene consists of a mix between the end-members enstatite (en, $Mg_2Si_2O_6$) and ferrosilite (fs, $Fe_2Si_2O_6$). A general formula can be formulated as [(M2)(M1)(T_2O_6)]. As described in White *et al.* (2002) and later in Holland & Powell (2006), orthopyroxene is a two-octahedral site mineral, where Mg and Fe can be distributed between M1 and M2 sites, additionally with Al and Fe^{3+} on the M1 site with charge balance accommodated by Si $\rightleftarrows$ Al substitution on the tetrahedral site (Fig. 3.5.1), where the amount of Al in most natural minerals is limited to ~ 0.5. To fully describe the distribution of the elements, more end-members (fictive and natural) are needed: Fe-Mg ordered pyroxene (fm, $FeMgSi_2O_6$, fictive end-member) for an ordering of Mg on M1 and Fe on M2, Mg-Tschermak´s pyroxene (mgts, $MgAl_2SiO_6$) for Al on the M1 site and Fe^{3+}-orthopyroxene (mots, $MgFe^{3+}AlSiO_6$, fictive end-member) for Fe^{3+} on the M1 site. The relationships for orthopyroxene were modelled in the FMASO system and use natural and experimental data of orthopyroxene-garnet pairs to define the Fe-Mg exchange reactions (White *et al.*, 2002).

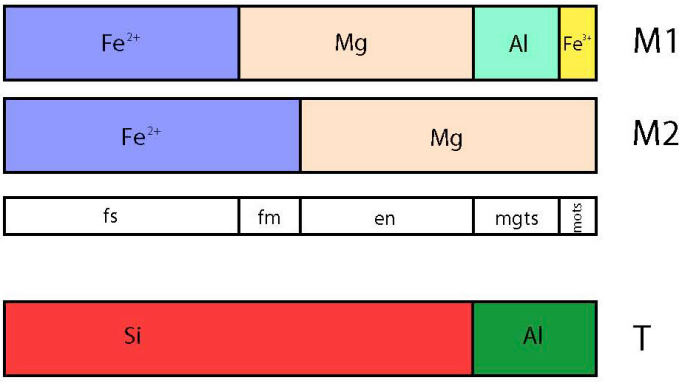

Figure 3.5.1. Site distributions and end-members for the model of orthopyroxene.

Coding

In general the *a-x* file consists of five sections divided from each other by " % ----------" (Appendix C). The first section contains the name of the mineral, the chemical system in which it was calibrated, the references for the model, the definition of the variables used for the mineral end-members (depending on the formulation in the program also the abbreviations of the end-members), the

number of independent end-members and their starting guesses. The *a-x* model for orthopyroxene contains 5 end-members. Therefore 4 variables are defined with one of them (Q) as an order-disorder parameter (White *et al.*, 2002).

```
% Orthopyroxene: FMASO
% White RW, Powell R, Clarke GL (2002) The interpretation of reaction textures
% in Fe-rich metapelitic granulites of the Musgrave Block, central Australia:
% constraints from mineral equilibria calculations in the system
% K2O-FeO-MgO-Al2O3-SiO2-H2O-TiO2-Fe2O3. Journal of Metamorphic Geology 20, 41-55.
%
%       x(opx) = Fe2/(Fe2 + Mg)
%       y(opx) = x(Al,M1)
%       Q(opx) = 2(x(Fe,M2) - x)
%       f(opx) = x(Fe3+,m1)

opx 5  %

x(opx)          0.5156
y(opx)          0.1519
Q(opx)          0.3927
f(opx)          0.006407
```

The second section contains the proportions of the end-members. In this section fm is the ordered end-member. Each term follows some blocks of numbers. Block 1 and, if present, block 3 contain one or two numbers. These numbers are related to the number of lines and the number of terms on that line. Block 2, 4 and 5 are defined as block of the functions for the end-members. The first numbers (e.g. 1 4 for p(en)) are a constant and the number of mixing variables in a term on a line, followed by the mixing variables and their multiplier.

```
Term          Block 1      Block 2
              Block 3      Block 4      Block 5

p(en)         1  1         1  4 -1  x -1  y -1/2 Q  -1  f

p(fs)         2  1         0  1  -1/2  Q
                 2         0  1  1  x    1  2  -1  y -1  f

p(mgts)       1  1         0  1  1  y

p(fm)         2  1         0  1  1  Q
                 2         0  1  1  x    0  2  1  y  1  f

p(mots)       1  1         0  1  1  f
```

The proportions of the end-members are read as follow:

p(en) = 1- x - y - 1/2Q - f

p(fs) = - 1/2Q + x (-y - f)

p(mgts) = y

p(fm) = Q + x (y + f)

p(mots) = f

The third section in the *a-x* model contains the information of the type of mixing model (sf = symmetric formalism) followed by macroscopic interaction energies (W(ij) for i-j binaries) (Powell & Holland, 1993; Holland & Powell, 1996 a and b). For other *a-x* models this block also include asymmetric parameters (α´s). The terms for the W(ij)´s are linearised in *P* and *T* as a + b*T* + c*P*.

```
sf

W(en,fs)              6.8  0  0
W(en,mgts)              0  0  0
W(en,fm)              4.5  0  0
W(en,mots)            -14  0  0

W(fs,mgts)             -1  0  0
W(fs,fm)              4.5  0  0
W(fs,mots)              6  0  0

W(mgts,fm)            1.2  0  0
W(mgts,mots)            0  0  0

W(fm,mots)              6  0  0
```

In the fourth section the numbers of site terms and the site distributions for each element on the site where it can be positioned in the mineral are present.

```
6

x(Al,M1)      1 1   0  1  1  y

x(Fe3,M1)     1 1   0  1  1  f

x(Mg,M1)      2 1   1  3  -1  y     -1  f  1/2 Q
                2   0  1  -1  x     1  2  -1  y  -1  f

x(Fe,M1)      2 1   0  1           -1/2 Q
                2   0  1  1  x     1  2 -1  y -1  f

x(Mg,M2)      1 1   1  2 -1  x -1/2 Q

x(Fe,M2)      1 1   0  2  1  x  1/2 Q
```

The fifth section contains the ideal mixing activities and any thermodynamic adjustment (DQF = Darken's Quadratic Formalism; e.g. Powell 1987) for an end-member. Any fictive end-members (e.g. fm, mots) that are not included in the dataset are made here.

```
en      1  2          x(Mg,M1)  1   x(Mg,M2) 1
     check 0 0 0 0

fs      1  2          x(Fe,M1) 1   x(Fe,M2) 1
     check 1 0 0 0

mgts    1  2          x(Al,M1) 1   x(Mg,M2) 1
     check 0 1 0 0

fm      1  2          x(Mg,M1)  1   x(Fe,M2) 1
     check 1/2 0 1 0
     make       2       en 1/2    fs 1/2
     DQF    -6.95  0  0

mots    1  2          x(Fe3,M1)  1   x(Mg,M2) 1
     check 0 0 0 1
     make       3       mgts 1    cor -1/2   hem 1/2
     DQF    22  0  0
```

3.5.5 Melt model

Due to the fact that partial melting commonly occurs in high-grade metamorphic rocks, a thermodynamic model for the melt is required.

Holland & Powell (2001) created a melt model for haplogranitic systems in the NCKASH (Na_2O–CaO–K_2O–Al_2O_3–SiO_2–H_2O) system. The model involves units for the end-members albite liquid (abL, $NaAlSi_3O_8$), anorthite liquid (anL, $CaAl_2Si_2O_8$), K-feldspar liquid (kspL, $KAlSi_3O_8$), quartz liquid (qL, $4SiO_2$), sillimanite liquid (silL, 8/5 Al_2SiO_5) and H_2O liquid (h2oL, H_2O). Their properties were calibrated on melting experiments in subsystems of NCKASH. White *et al.* (2001) extended this melt model by the addition of FeO and MgO to allow the calculation of mineral-melt equilibria in the NCKFMASH system. The additional end-members are forsterite liquid (foL, $Mg_4Si_2O_8$) and fayalite liquid (faL, $Fe_4Si_2O_8$) to add magnesium and iron to the granitic system.

The most current version of the melt model is published by White *et al.* (2007) using the approach of Holland & Powell (2001) with each melt end-member having eight oxygen atoms, except for H_2O. Some of these eight oxygen end-members (e.g. foL, $Mg_4Si_2O_8$; qL, SiO_8) are shown by Holland & Powell (2003), developing an asymmetric formalism model for forsterite-enstatite-silica melting. The melt model is given in Appendix C included in the NCKFMASHTO system.

3.5.6 THERMOCALC

The computer program, THERMOCALC, written in *Pascal*, was used for the calculations and used the internally consistent thermodynamic dataset of Powell & Holland (1988). The calculations on rocks usually involve the definition of temperature, pressure and, if its necessary, the fluid composition. With the advancement of the dataset and also the software (Holland & Powell, 1998) it is possible to calculate mineral equilibria involving solid solutions in complex systems that are close to natural systems. It allows the construction of phase diagrams showing equilibrium phase relationships in a rock (Powell & Holland, 1998). Many different diagrams, such as *P–T* projections, compatibility diagrams, *T–x* and *P–x* pseudosections and, most commonly, *P–T* pseudosections can be calculated directly (Powell & Holland, 1998).

THERMOCALC calculates mineral equilibria for an input pressure and temperature and composition of the phases that are involved in the reaction. This equilibria calculation is based on the variance or degree of freedom. The expression for the variance:

$$V = n - p + 2$$

contains the number of components in the chosen system (n), the number of phases in equilibrium (p) and the number of variables (2 = pressure + temperature) (Powell *et al.*, 1998).

Before starting the calculation of a pseudosection the user has to decide the model system in which the calculation should be done. This system is a chemical system and specifies which phases should be included in the calculation (Powell & Holland, 1998). For metapelites typical systems are KFMASH (K_2O–FeO–MgO–Al_2O_3–SiO_2–H_2O), NCKFMASH (Na_2O–CaO–K_2O–FeO–MgO–Al_2O_3–SiO_2–H_2O) and NCKFMASHTO (Na_2O–CaO–K_2O–FeO–MgO–Al_2O_3–SiO_2–H_2O–TiO_2–O). In this work the system NCKFMASHTO was chosen to get the most reliable results of the calculation in comparison with the natural relationships of the rocks (White *et al.*, 2007).

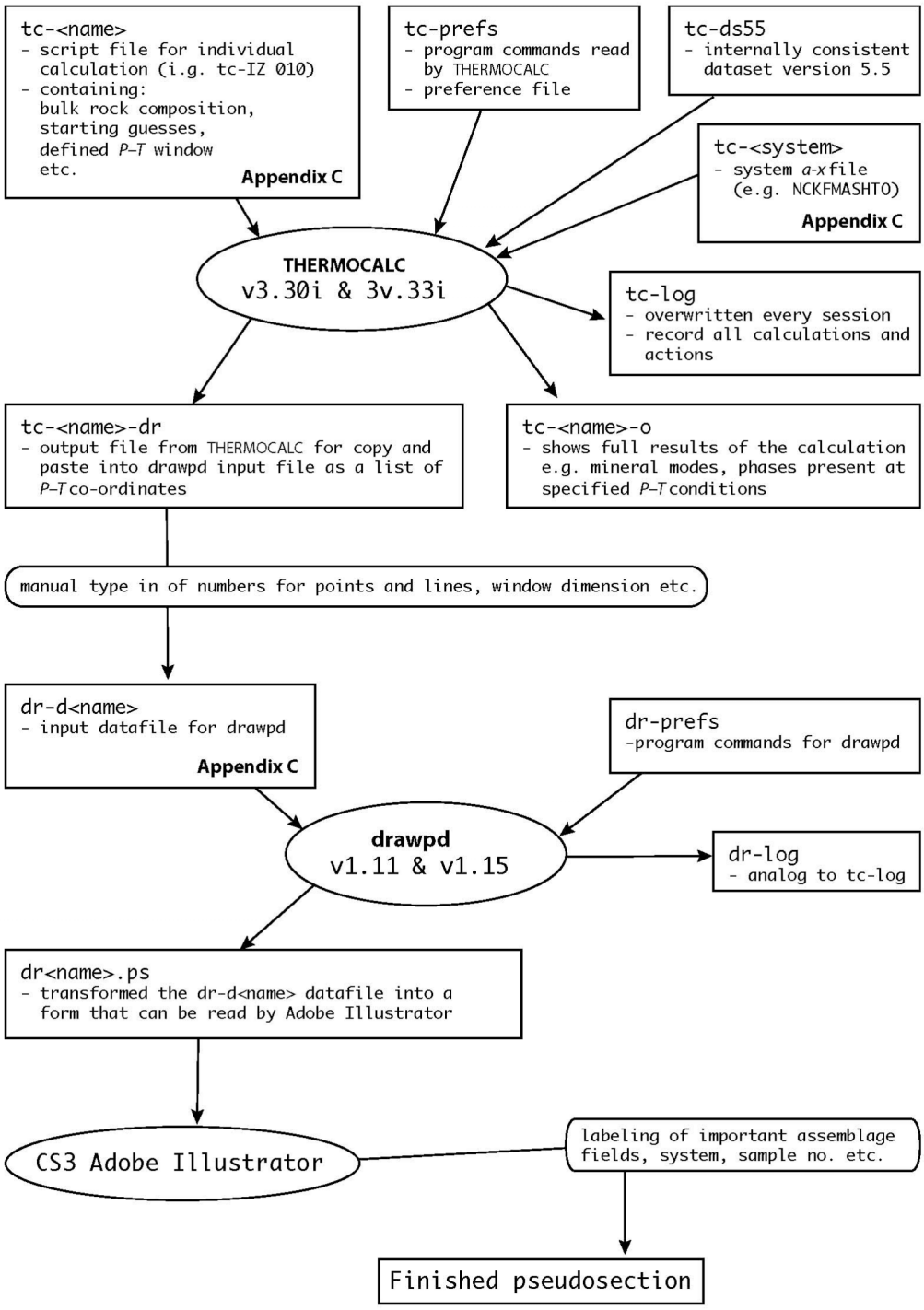

Figure 3.5.2. Flow chart of datafiles and steps used for a construction of *P–T*, *P–x* and *T–x* pseudosections.

3.5.7 Calculation of *P–T* and *T–x* pseudosections

P–T pseudosection

A *P–T* pseudosection is a multivariant phase diagram and is constructed for a fixed bulk rock composition. It consists of several effective invariant points and univariant lines (phase boundaries). These are lines where a mineral (mode) goes to zero. Across these phase boundaries the variance changes by one e.g. from 3 to 4 and through points by two e.g. from 3 to 5 or by zero (Fig. 3.5.3; Powell *et al.,* 1998). For starting the calculation of a *P–T* pseudosection it is the best to know an assemblage with many minerals and of low variance (depending on the used system). An example for calculating with THERMOCALC is given below.

In this example for the calculation of a *P–T* pseudosection sample IZ 010 is chosen with a known assemblage field containing g-cd-sill-bi-ksp-pl-q-ilm-*liq* (variance v = 3, trivariant). The complete *P–T* pseudosection for this sample is given in Chapter 6.2. The specified bulk rock composition of this sample in mol% is needed and is entered in the 'tc-IZ 010' file (Appendix C). THERMOCALC normalises this composition to 100 % during the calculation to in this case to almost the same values as input. The proportion of "O" represents the extra oxygen in the system that converts FeO to Fe_2O_3.

```
% --------------------------------
% Bulk rock from IZ 010 (CaO adjustment for P2O5 -0.23 apatite)
% --------------------------------
%               H2O    SiO2   Al2O3   CaO   MgO   FeO   K2O   Na2O   TiO2   O
setbulk yes    4.33   74.25   9.37   0.38  2.53  4.54  2.00   1.57   0.65  0.1
composition
(from script)  4.34   74.46   9.40   0.38  2.54  4.55  2.01   1.57   0.65  0.1
```

Here the first calculated phase boundary (line 1; Fig. 3.5.3) is the g = 0 line along with the mode of cd trends to zero in the direction to the effective invariant point with (in this case [g, cd]). As shown below THERMOCALC asks 'which phases' and the user has to type in all stable minerals for this assemblage field minus any that have been set to in-excess in the script file (nothing in excess in this example). THERMOCALC then asks for the variance and which mineral should be zero at this line ('which to set'). The user can then decide either to type in a pressure range

or a temperature range in which THERMOCALC should search for the phase boundary or use the defaults. For this example a pressure range from 5 to 7.5 kbar was chosen.

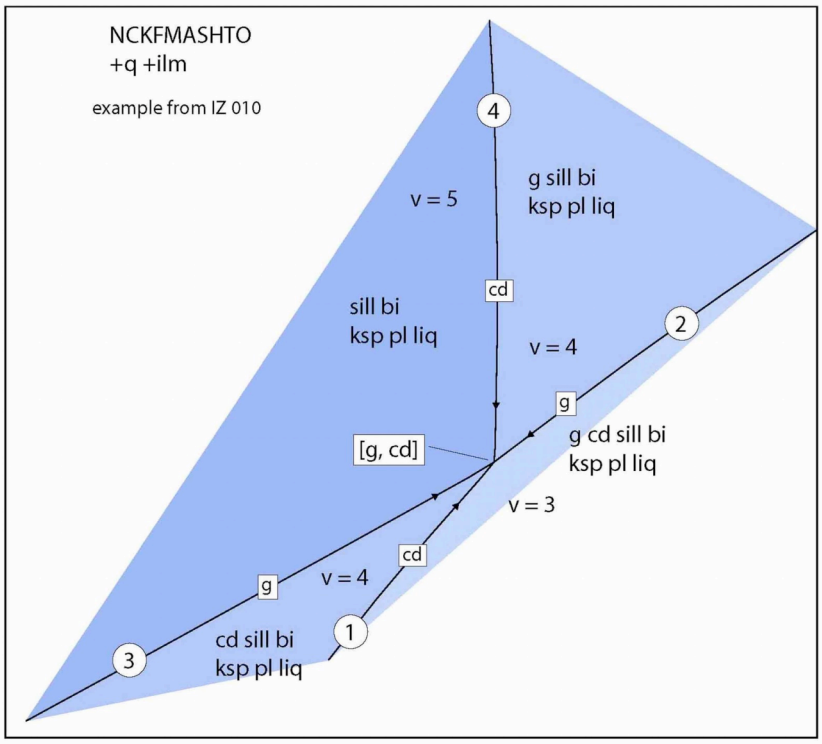

Figure 3.5.3. Geometry of field boundaries and phase relations for a part of *P–T* pseudosection IZ 010.

The user has to type in a pressure interval (here 0.2) and the program calculates pressure and temperature coordinates for this line. This calculation runs on until another mode goes to zero and an effective invariant point can be assumed. It is also possible at this stage that THERMOCALC not only calculate the stable part of a line but also the metastable part and the user has to cut this line at the effective invariant point. The calculation of lines 2, 3 and 4 occur in a similar way with changing the assemblages and the variance (Fig. 3.5.3). To calculate line 2 the assemblage and the variance have to be the same as for line 1 by setting g to zero. For line 3 the user has to calculate with the assemblage cd-sill-bi-ksp-pl-q-ilm-*liq* (variance v = 4, quadrivariant) by setting g to zero (line 2). The assemblage for the calculation of line 4 is given with g-sill-bi-ksp-pl-q-ilm-*liq* (variance v = 4, quadrivariant) by setting cd to zero.

```
THERMOCALC 3.30 (Free Pascal version)
the main output is in the file, "tc-neu-o.txt"
other (eg drawpd) output is in the file, "tc-neu-dr.txt"
calcs use:
reading a-x datafile, "tc-NCKFMASHTOp.txt"...
 ged  anth  liq  bi  cd  ep  st  g  opx  chl  ctd  mu  pa  ksp  pl  osm
sp  mt  ilm  hem  and  sill  ru  ky  q  H2O
choose from: ged  anth  liq  bi  cd  ep  st  g  opx  chl  ctd  mu  pa  ksp  pl
osm  sp  mt  ilm  hem  and  sill  ru  ky  q  H2O
which phases : g cd sill bi pl q ilm liq ksp
no phases in excess (from script)

variance of required equilibria :
     0 = invariant
     1 = univariant
     2 = divariant
     ...
     n = n-variant
variance : 3
you may set zero modal proportions, from:liq bi cd g ksp pl ilm sill q
which to set : cd
calculate T at  P (rather than P at T) ?

specification of PT window:
P range over which T of reactions to be calculated
P window: P low,high : 5 7.5
T window within which reactions expected to lie
T window: T low,high :
P window :4 <-> 8 kbar :P interval : 0.2
composition (from script)
   H2O  SiO2 Al2O3   CaO   MgO   FeO   K2O  Na2O  TiO2     O
  4.34 74.46  9.40  0.38  2.54  4.55  2.01  1.57  0.65  0.10


7 ------------------------------------------------------------------
P(kbar)  T(?C)   q(L)   fsp(L)   na(L)   an(L)    ol(L)    x(L)     h2o(L)   x(bi)
5.20    773.5  0.1687  0.3412  0.5569 0.005344  0.004547  0.8095   0.4595   0.6020
               y(bi)   f(bi)    t(bi)    Q(bi)    x(cd)   h(cd)      x(g)    z(g)
             0.4597  0.02174  0.1178   0.1330   0.4368  0.5455    0.8203  0.01069
               f(g)  na(ksp)   ca(ksp)  ca(pl)    k(pl)   x(ilm)   Q(ilm)
           0.002034   0.4131  0.01598  0.1308   0.1131  0.8279   0.7059

mode     liq       bi      cd       g      ksp       pl      ilm     sill       q
       0.1168   0.1927     0    0.005452  0.03114  0.1047 0.009077  0.07981 0.4604
------------------------------------------------------------------
P(kbar)  T(?C)   q(L)  fsp(L)   na(L)   an(L)    ol(L)     x(L)     h2o(L)   x(bi)
5.40   780.6  0.1687  0.3432  0.5530 0.006011  0.004850   0.7980   0.4561   0.5700
               y(bi)   f(bi)    t(bi)    Q(bi)    x(cd)   h(cd)      x(g)    z(g)
             0.4456 0.02257  0.1234   0.1444   0.4126   0.5486   0.8025   0.01134
               f(g)  na(ksp)   ca(ksp)  ca(pl)    k(pl)   x(ilm)   Q(ilm)
           0.002127  0.4040  0.01668  0.1443   0.1077   0.8350   0.7128

mode    liq      bi       cd        g      ksp       pl      ilm     sill        q
      0.1372   0.1659     0   0.02443  0.05113  0.08770 0.009755  0.07804   0.4458
------------------------------------------------------------------
P(kbar)  T(?C)   q(L)  fsp(L)   na(L)   an(L)    ol(L)     x(L)     h2o(L)   x(bi)
5.60   787.9  0.1690  0.3453  0.5488 0.006739 0.005169   0.7863     0.4521  0.5383
               y(bi)   f(bi)    t(bi)    Q(bi)    x(cd)   h(cd)      x(g)    z(g)
             0.4318 0.02341  0.1294   0.1550   0.3894   0.5509   0.7836   0.01195
               f(g)  na(ksp)   ca(ksp)  ca(pl)    k(pl)   x(ilm)   Q(ilm)
           0.002233  0.3959  0.01742   0.1578   0.1030   0.8408   0.7177
```

```
mode    liq      bi       cd        g      ksp       pl      ilm     sill        q
      0.1560   0.1424     0   0.04111  0.06717  0.07373  0.01038  0.07634   0.4329
-----------------------------------------------------------------
etc etc
```

The most common reason why THERMOCALC fails to calculate a point or a line is due to the starting guesses and the user need to change them. This depends on the system chosen for the calculation as well as on the *P–T* window and the minerals involved in the calculation. To change the starting guesses the user can copy the best available starting guesses from the 'tc-log' file to the 'tc-IZ 010' file, for example the starting guesses from the last calculated point. An example how starting guesses can look like (using THERMOCALC 3.30) is given below.

```
% calculated at P =   6.0; T =  804
readxyz q(L)          0.1702
readxyz fsp(L)        0.3502
readxyz na(L)         0.5392
readxyz an(L)       0.008420
readxyz ol(L)       0.005843
readxyz x(L)          0.7619
readxyz h2o(L)        0.4425
readxyz x(bi)         0.4765
readxyz y(bi)         0.4063
readxyz f(bi)        0.02503
readxyz t(bi)         0.1423
readxyz Q(bi)         0.1724
readxyz x(cd)         0.3453
readxyz h(cd)         0.5531
readxyz x(g)          0.7422
readxyz z(g)         0.01300
readxyz f(g)        0.002483
readxyz na(ksp)       0.3813
readxyz ca(ksp)      0.01899
readxyz ca(pl)        0.1849
readxyz k(pl)        0.09548
readxyz x(ilm)        0.8500
readxyz Q(ilm)        0.7237  range -0.920 0.920
```

The calculation of an effective invariant point is very similar to the calculation of field boundaries. At the stage when THERMOCALC asks 'which to set' the user has to type in two phases for the invariant point (here cd & g) as illustrated below. The user can give the program a pressure and temperature range but in most cases it is not necessary. THERMOCALC calculates a pressure-temperature pair for this point.

```
THERMOCALC 3.30 (Free Pascal version)
the main output is in the file, "tc-neu-o.txt"
other (eg drawpd) output is in the file, "tc-neu-dr.txt"
```

```
calcs use:
reading a-x datafile, "tc-NCKFMASHTOp.txt"...
ged anth liq bi cd ep st g opx chl ctd mu pa ksp pl osm
sp mt ilm hem and sill ru ky q H2O
choose from: ged anth liq bi cd ep st g opx chl ctd mu pa ksp pl
osm sp mt ilm hem and sill ru ky q H2O
which phases : g cd sill bi pl q ilm liq ksp
no phases in excess (from script)

variance of required equilibria :
     0 = invariant
     1 = univariant
     2 = divariant
     ...
     n = n-variant
variance : 3
you may set zero modal proportions, from:liq bi cd g ksp pl ilm sill q
which to set : cd g

specification of PT window:
PT window within which invariant points expected to lie
T low,high, P low,high :
composition (from script)
   H2O  SiO2 Al2O3   CaO   MgO   FeO   K2O  Na2O  TiO2     O
  4.34 74.46  9.40  0.38  2.54  4.55  2.01  1.57  0.65  0.10
<=================================================>
phases : liq, bi, cd, g, ksp, pl, ilm, sill, q

-----------------------------------------------------------------------
P(kbar)  T(?C)   q(L)   fsp(L)   na(L)   an(L)    ol(L)    x(L)     h2o(L)   x(bi)
5.15   771.7  0.1688  0.3407  0.5578  0.005178  0.004469  0.8125    0.4603  0.6104
               y(bi)   f(bi)    t(bi)    Q(bi)    x(cd)   h(cd)      x(g)    z(g)
             0.4635 0.02153  0.1164   0.1299   0.4433   0.5445   0.8248   0.01050
                f(g)  na(ksp)   ca(ksp)  ca(pl)    k(pl)   x(ilm)   Q(ilm)
           0.002011  0.4156   0.01580  0.1272   0.1147   0.8258   0.7036

mode     liq       bi      cd     g      ksp       pl      ilm     sill       q
        0.1110   0.2003    0      0   0.02507   0.1098 0.008888  0.08029   0.4646
```

T–x and *P–x* pseudosections

In general a *T–x* or *P–x* pseudosection shows the phase relations over a linear range of compositions at fixed *P* (for a *T–x*) or fixed *T* (for a *P–x*). The calculation of the *T–x* pseudosection is very useful to get starting guesses and assemblage phase boundaries to start a new *P–T* pseudosection. For this the chosen chemical system has to be the same for both the *P–T* and the *T–x* pseudosections, and the bulk rock compositions of both chosen samples for the calculation must be known. The x-axis of the diagram ranges from x = 0 to x = 1, which is from 100 % of the first composition to 100 % of the other composition. On the y-axis the temperature/pressure range is given.

An example for a *T–x* pseudosection from sample IZ 010 to IZ 005 in the NCKFMASHTO system is shown in Fig. 3.5.5.

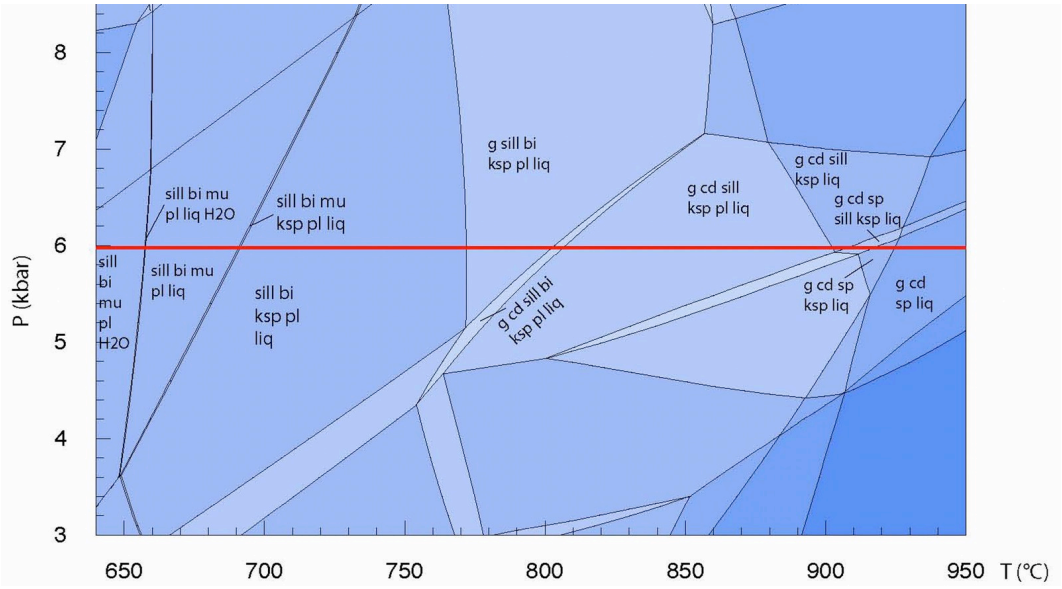

Figure 3.5.4. Section of *P–T* pseudosection IZ 010 (the whole pseudosection is to find in Chapter 6.2). The red line at 6 kbar marked the area for which the *T–x* pseudosection is calculated (Fig. 3.5.5).

```
% --------------------------------
% Bulk rock from IZ 010 (CaO adjustment for P2O5 -0.23 apatite)
% Bulk rock from IZ 005 (CaO adjustment for P2O5 -0.17 apatite)
% --------------------------------
%             H2O    SiO2   Al2O3   CaO   MgO   FeO   K2O   Na2O   TiO2   O
setbulk yes  4.33   74.25   9.37   0.38  2.53  4.54  2.00   1.57   0.65  0.1
setbulk yes  1.96   67.68  12.18   0.75  5.60  8.29  1.39   0.87   0.86  0.1
% ----------------------------
```

For both samples the user has to type in the bulk rock compositions in the 'tc-IZ 010 to 005' script file as well as the pressure and temperature range, which is, in this example, from 640 °C to 950 °C with a fixed pressure of 6 kbar (Fig. 3.5.4)

Similar to the calculation of the *P–T* pseudosection THERMOCALC asks 'which phases' and the user has to type in all stable minerals (in this example the calculation starts with the assemblage sill-bi-mu-pl-q-ilm-liq-H_2O) for the first phase boundary. As the next step THERMOCALC ask for a variance (4) and which phase the user wants to set to zero (*liq*). Afterwards the user is asked to specify the pressure and temperature window that can be given for this calculation with a fixed *P* = 6 kbar and *T* = 600 to 800 °C. The next question of the program is

about the bulk rock composition range for this line that can be answered with 0 to 1. The user also can choose a smaller range depending on the assumed range of the line. The questions how many increments THERMOCALC should calculate can be answered here with 50. An example for a part of the whole run of THERMOCALC is given below.

```
THERMOCALC 3.33 (Free Pascal version)
the main output is in the file, "tc-neu-o.txt"
other (eg drawpd) output is in the file, "tc-neu-dr.txt"
 calcs use:
reading a-x datafile, "tc-NCKFMASHTOp.txt"...
ged  anth  liq  bi  cd  ep  st  g  opx  chl  ctd  mu  pa  ksp  pl  osm
sp  mt  ilm  hem  and  sill  ru  ky  q  H2O
choose from: ged  anth  liq  bi  cd  ep  st  g  opx  chl  ctd  mu  pa  ksp  pl
osm  sp  mt  ilm  hem  and  sill  ru  ky  q  H2O
which phases : sill bi mu pl q ilm liq H2O
no phases in excess (from script)
variance of required equilibrium (4?) : 4
you may set zero modal proportions, from:liq bi mu pl ilm sill q H2O
which to set : liq

specification of PT window:
P range over which T of reactions to be calculated
P window: P low,high : 6 6
T window within which reactions expected to lie
T window: T low,high : 600 800
making a bulk composition range within the range specified,
start and finish proportions across bulk composition range : 0 1
how many increments (max = 100) : 50

composition
   H2O  SiO2 Al2O3   CaO   MgO   FeO   K2O  Na2O  TiO2     O
  4.34 74.46  9.40  0.38  2.54  4.55  2.01  1.57  0.65  0.10
  1.97 67.90 12.22  0.75  5.62  8.32  1.39  0.87  0.86  0.10       (50 increments
across 0 to 1.000 of original range)
<================================================>
phases : liq, bi, mu, pl, ilm, sill, q, H2O


-------------------------------------------------------------------
P(kbar)   T(?C)   q(L)  fsp(L)    na(L)   an(L)    ol(L)     x(L)   h2o(L)   x(bi)
6.00     657.3  0.1071  0.2294  0.7503 0.001946 0.0003426   0.7790  0.6554  0.6082
               y(bi)   f(bi)    t(bi)   Q(bi)   fe(mu)   y(mu)   na(mu)   ca(pl)
             0.5087  0.01950  0.08365   0.1351  0.5178   0.9614  0.1663   0.1127
               k(pl)   x(ilm)   Q(ilm)
             0.02851   0.8522   0.7826

    mode      liq       bi       mu       pl      ilm     sill        q      H2O
       0        0   0.1987  0.08930   0.1352  0.01077  0.05246   0.5095 0.004058
-------------------------------------------------------------------
P(kbar)   T(?C)   q(L)  fsp(L)    na(L)   an(L)    ol(L)     x(L)   h2o(L)   x(bi)
6.00     657.5  0.1072  0.2293  0.7493 0.001983  0.0003416  0.7784  0.6553  0.6070
               y(bi)   f(bi)    t(bi)   Q(bi)   fe(mu)   y(mu)   na(mu)   ca(pl)
             0.5084  0.01951  0.08383  0.1355   0.5169  0.9612  0.1653  0.1150
               k(pl)   x(ilm)   Q(ilm)
             0.02837   0.8529   0.7834

    mode      liq       bi       mu       pl      ilm     sill        q      H2O
```

```
 0.02000        0   0.2031  0.08319   0.1351  0.01073  0.05532   0.5086 0.004058
-----------------------------------------------------------------------
P(kbar)   T(?C)   q(L)  fsp(L)    na(L)   an(L)    ol(L)     x(L)   h2o(L)   x(bi)
6.00     657.6  0.1074  0.2292  0.7482 0.002019  0.0003407  0.7780  0.6552  0.6058
               y(bi)   f(bi)    t(bi)   Q(bi)   fe(mu)   y(mu)   na(mu)   ca(pl)
              0.5081  0.01952  0.08401  0.1358  0.5160   0.9611  0.1643   0.1173
               k(pl)   x(ilm)   Q(ilm)
             0.02823   0.8535   0.7842

    mode      liq       bi       mu       pl      ilm     sill        q      H2O
 0.04000        0   0.2075  0.07708   0.1350  0.01069  0.05818   0.5076 0.004055
-----------------------------------------------------------------------
etc etc
```

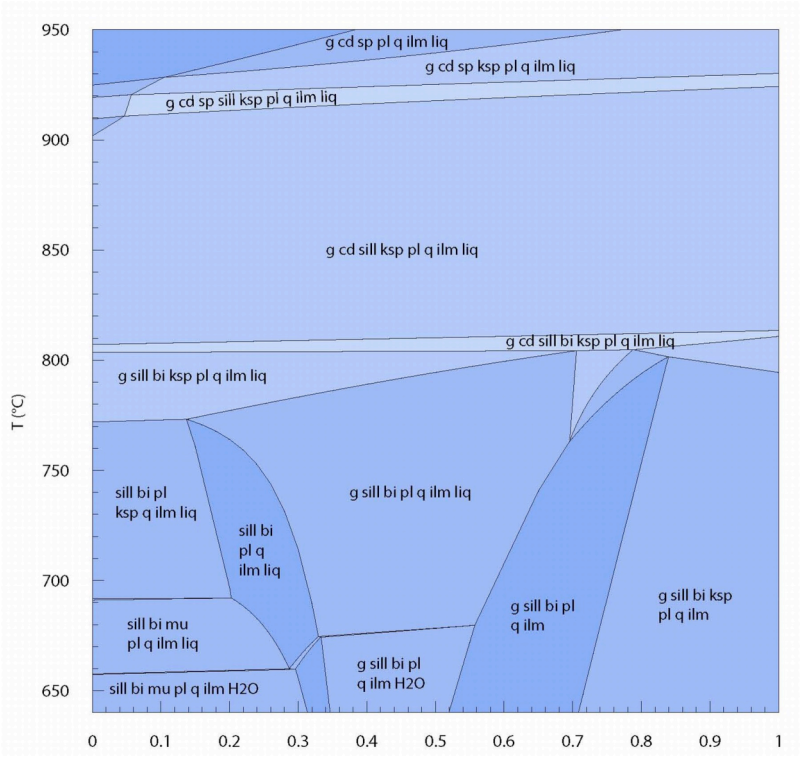

Figure 3.5.5. *T–x* pseudosection from bulk rock composition of sample IZ 010 (x = 0) to the bulk rock composition of sample IZ 005 (x = 1).

Chapter 4
Field relationships and petrography

4.1 Introduction

This chapter outlines field and petrographical relationships of the working areas (Chapter 2, Fig. 2.2.1). These are Val Strona di Omegna, Val Sesia and Val Strona di Postua, with the main focus is on Val Strona di Omegna. In the following sub-chapters, the rocks will be described in detail by their appearance in the field and in thin sections. The main focus is on the metapelites, although metapsammites/metagreywackes, metabasites, calcsilicates and marbles will also be described. For the scale on the field photos, a hand-lense (5 cm), a geological hammer or small sledgehammer (both with a length of 28 cm), a chisel (30 cm) or a large sledgehammer (length of 70 cm) is used unless otherwise stated.

4.2 Val Strona di Omegna

Val Strona di Omegna represents, from southeast to northwest, a 20 km long road/river section through amphibolite to granulite facies rocks, although only 14 km are part of the Ivrea Zone. Val Strona di Omegna is a narrow valley with steep hillsides and ranges from 200 m above sea level at Omegna to 1300 m at Campello Monti. The mountains around range up to over 2000 m above sea level. The river Strona flows through the valley and cuts deeply into the rocks. Where the riversides are not too steep, numerous fresh outcrops can be sampled. The section of the valley is roughly perpendicular to the strike direction of the main lithologies (Fig. 4.2.1). The Val Strona di Omegna section can be

divided into five zones based on mineral isograds and mineral assemblages (Fig. 4.2.2). These zones will be described in the following sub-chapters.

The majority of the rocks in Val Strona di Omegna are metapelites and metabasites with minor calcsilicates, marbles and metapsammites and/or metagreywackes. In most studies (e.g. Zingg, 1980; Schnetger, 1994; Barboza & Bergantz, 2000) a boundary between the Kinzigite Formation and the Mafic Complex is delineated, generally occurring approximately 0.5 km east/southeast of Campello Monti (Chapter 2, Fig. 2.2.1). However, this distinction is not made in the map of Bertolani (1968), and the different rock types in this valley will here be described as a single unit (Fig. 4.2.1 and 4.2.2).

For rocks in zones 2–5 field sketches from different localities are presented. In the schematic map of the valley (Fig. 4.2.2) these localities are marked with numbers in the order they are described. The sketches show the different structures within the metapelites, metapsammites/metagreywackes and metabasites related to their grade of metamorphism and degree of partial melting as well as their relation to each other. According to Sawyer (2008), migmatites are rocks composed of different parts. The first division subdivides the component parts of a migmatite into paleosome, the non-melted part, and neosome, the part that underwent partial melting. The neosome may then be subdivided into leucosome and residuum or in special cases melanosome. The leucosome is the light-coloured part of a migmatite that is enriched in felsic minerals such as quartz and feldspars and derived from segregated partial melt. In contrast, the residuum or melanosome is darker-coloured, contains more mafic minerals such as biotite, cordierite and garnet and represents the material remaining after the melt fraction has been extracted. In this study, special focus is placed on the different types of leucosomes, which can be subdivided into three types. The first, *in situ* leucosome, represents melt that segregated from its residuum but remained at the place where it was formed. The second type, in-source leucosome, migrated from the place where it formed but it is still limited to its source layer. The third type of leucosome comprises veins, which have migrated from their source layer and injected into their current host rock. Other parts of the migmatites, like schollen or selvedges will be described within the appropriate figure captions.

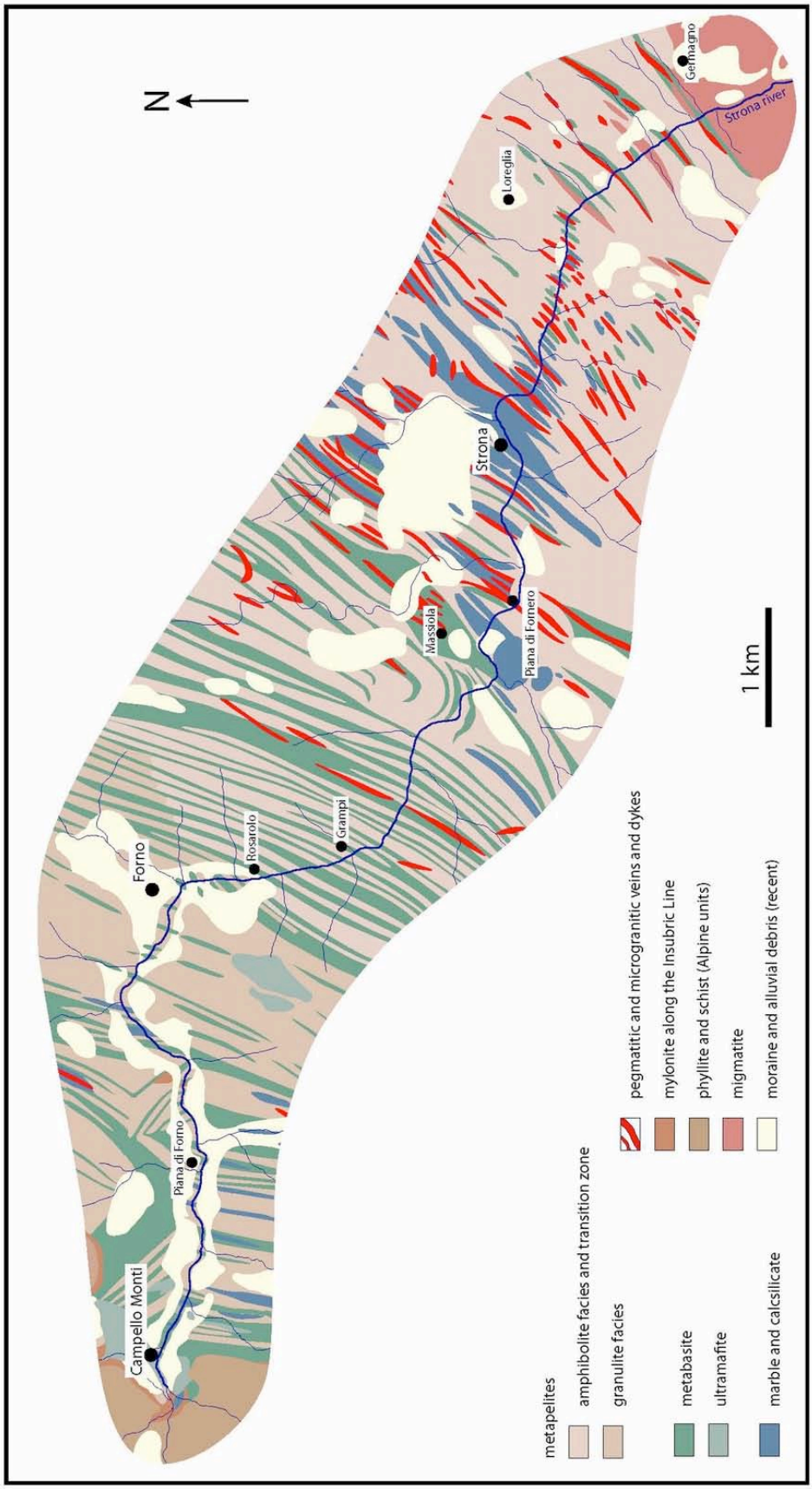

Figure 4.2.1. Lithological map of Val Strona di Omegna (modified after Bertolani, 1968).

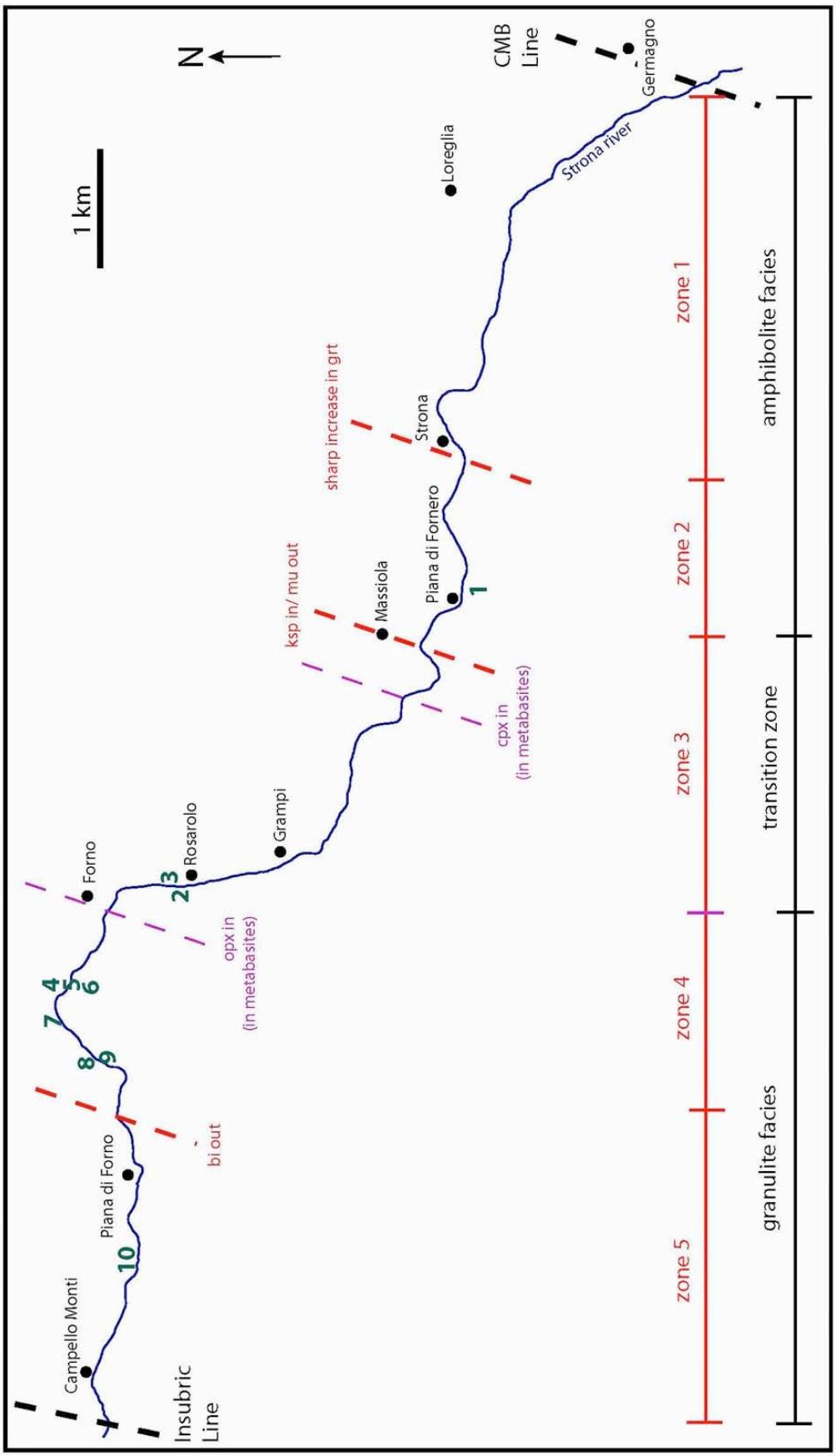

Figure 4.2.2. Schematic map of Val Strona di Omegna with extrapolated mineral isograds, the localities of the field sketches in the descriptive order (numbers) and subdivision into the five zones. The five zones as well as the field sketches will be discussed in the text.

4.2.1 Zone 1 – CMB Line to Strona

The first zone occurs between the villages of Germagno and Strona (Fig. 4.2.3). The CMB Line is located near Germagno, separating the Ivrea Zone from the Strona-Ceneri Zone. It is not possible to define the exact position of the CMB Line due to a lack of outcrop, although it is constrained to lie close to the positions as shown in Fig. 4.2.1 and Fig. 4.2.2, such that the first outcrop north of Germagno (Fig. 4.2.4 a) lies within the Ivrea Zone. From Strona to the northwest, there is a sharp increase in the abundance of garnet in the metapelites, which, while not strictly a mineral isograd, represents a clear mappable feature.

Zone 1 contains metapelites with intercalated metabasites, calcsilicates, marbles and minor metapsammites/ metagreywackes (Fig. 4.2.3). The metapelites are mica-schists, comprising muscovite, biotite, plagioclase, sillimanite and quartz (Fig. 4.2.4 b–d), along with apatite, ilmenite, pyrite, magnetite, hematite, tourmaline, zircon and monazite as accessory minerals.

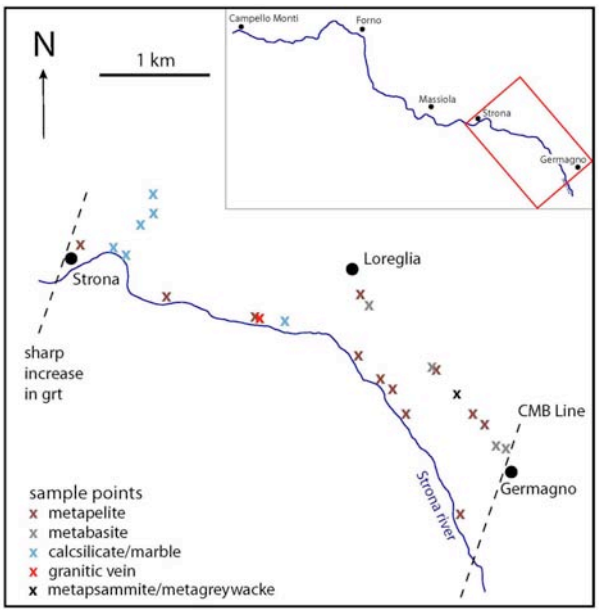

Figure 4.2.3. Overview of zone 1 in Val Strona di Omegna, including sample locations.

In some samples K-feldspar, cordierite and rare garnet are present. These samples are located next to pegmatitic and microgranitic veins and dykes, which were not investigated in detail. South of Strona, one of the granitic veins contains quartz, large crystals of muscovite, plagioclase, minor garnet and tourmaline (Fig. 4.2.4 e). In addition to the granitic dykes, abundant quartz veins are common within the metapelites. Furthermore, in three other samples rutile is present. The

metapelites are strongly deformed (Fig. 4.2.4 c and d) and contain different types of folds, e.g. kink folds, flexural folds and crenulation folds.

The rare metabasites layers (Fig. 4.2.4 a) consist of green hornblende and plagioclase with biotite and sphene and accessory ilmenite, pyrite and hematite. The compositional layering of the metabasites is defined by varying concentrations of hornblende and plagioclase.

The exposed metapsammites/metagreywackes are dominated by quartz, biotite, plagioclase and garnet, along with ilmenite as an accessory mineral. Calcsilicate lenses east of Strona contain combinations of calcite, sphene, plagioclase, biotite, muscovite, sillimanite, clinopyroxene and tremolite. Next to the bridge, approximately 700 m east of Strona, calcsilicates with a mylonitic structure crop out (Fig. 4.2.4 f).

As mentioned above, the metapelites contain plagioclase, biotite, muscovite, sillimanite and quartz as major minerals along with rare garnet, K-feldspar and cordierite. Plagioclase and quartz are the most common minerals in the metapelites. Plagioclase exhibits multiple twinning and grains are mostly subhedral to anhedral. The grain size of plagioclase varies from 0.1 to 0.3 mm. Biotite is very common in this zone and has a brownish to light brown/yellow/orange pleochroism, an average grain size of 0.4 x 0.5 mm and shows a perfect cleavage (e.g. Fig. 4.2.5 a and b). Biotite is texturally similar to muscovite that has a lepidoblastic texture and is present in the same layers and with same preferred orientation as biotite. Sillimanite is present in almost every sample and has a fibrous acicular habit (fibrolite). In places fibrolite appears in clots intergrown with biotite and muscovite (Fig. 4.2.5 c and d). Where present, garnet occurs as small rounded grains with an average grain size of 0.1 to 0.2 mm. K-feldspar and cordierite are rare and are commonly sericitized or pinitized, have a grain size of approximately 0.5 to 1 mm and have an anhedral shape. Cordierite appears in general next to sillimanite, biotite and K-feldspar and is only visible in thin sections.

Figure 4.2.4. Field photographs illustrating the rock types of zone 1 between Germagno and Strona: **a)** First outcrop in the Ivrea Zone, north of Germagno. The exposed metabasites are strongly folded and contain quartz veins. **b)** Typical appearance of mica-schists between Germagno and Strona. **c)** Kink folds in a mica-schist south of Loreglia (the hammer is 17 cm long). **d)** Flexural folds in mica-schist south of Loreglia (the hammer head is 17 cm long). **e)** Pegmatitic quartz vein with large tourmaline crystals (black) and abundant muscovite south of Strona (the pencil is 11 cm long). **f)** Mylonitic calcsilicate next to a bridge south of Strona (the hammer head is 12 cm long).

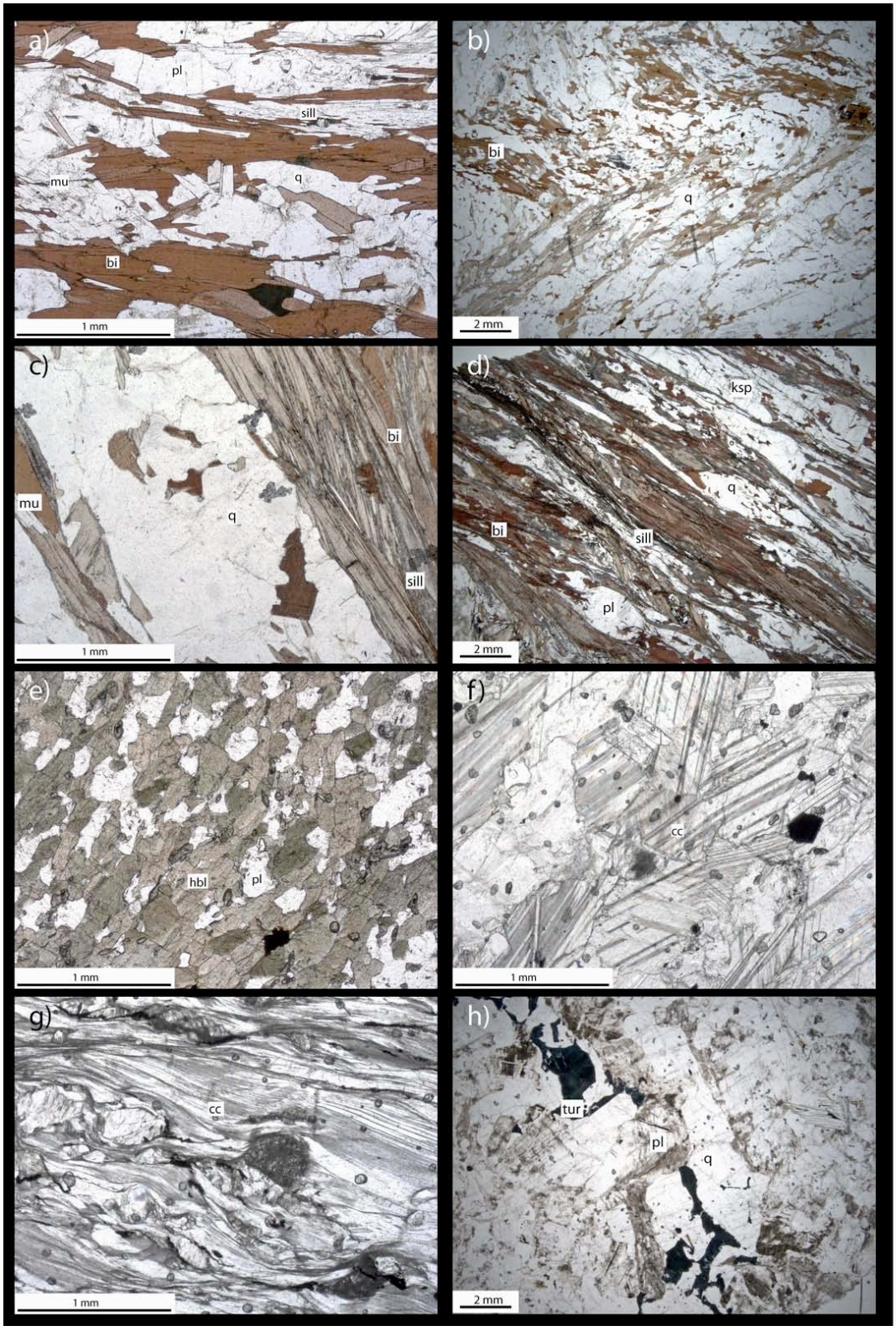

Figure 4.2.5. Photomicrographs illustrating the textures of rocks in zone 1 between Germagno and Strona: **a)** Fine-grained mica-schist from the lowest grade part of the valley next to Germagno (sample IZ 008). The sample has a typical mineral assemblage of biotite, muscovite, quartz and plagioclase, containing small areas with fibrolitic sillimanite, which is always next to the mica and intergrown with it. **b)** Folded fine-grained mica-schist (IZ 013) next to Loreglia with a similar assemblage as a). The mica (mostly biotite) and sillimanite are orientated in the foliation and exhibit

a kink fold. **c)** Quartz-rich vein in a schist dominated by biotite and sillimanite (IV 059) 1 km east of Strona. **d)** Foliation with a mylonitic texture (upper left to lower right, small band) in sample IZ 152 northeast of Strona. This sample contains a few larger plagioclase grains (bottom). **e)** Typical appearance of a metabasite (IZ 007) in the lower grade part of the valley near Germagno. It is fine grained and contains inequigranular grains of green hornblende and plagioclase. **f)** A typical marble (IZ 109) located northeast of Strona. The calcite grains have an inequigranular shape. Additionally some oxides are present. **g)** Crenulation cleavage in a proto-mylonitic calcsilicate/marble 1 km east of Strona (IZ 082). **h)** Example of a tourmaline-bearing quartz vein 1.5 km east of Strona (IZ 020). The vein also contains plagioclase and garnet, but the latter is not visible in this picture.

4.2.2 Zone 2 – Strona to Massiola

Zone 2 extends from Strona to Massiola (Fig. 4.2.6). The southeastern boundary to this zone, near Strona, is defined by a sharp modal increase in garnet within the metapelites. The higher grade boundary to the northwest is defined by the disappearance of peak muscovite and the appearance of K-feldspar. Further to the northwest muscovite is only present as a retrograde mineral (Chapter 5.3.). This boundary is therefore defined as the muscovite-out/K-feldspar-in isograd. Zone 2 comprises the same rock types as zone 1, although the calcsilicates and marbles are more abundant.

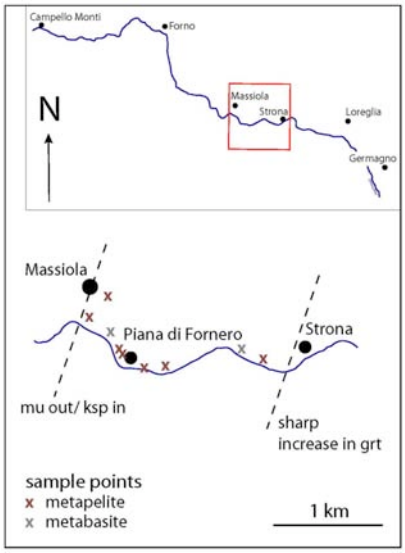

Figure 4.2.6. Overview of zone 2 in Val Strona di Omegna, including sample locations

The major and accessory phase assemblages within the metapelites are similar (muscovite, biotite, plagioclase, quartz, sillimanite with accessory apatite, ilmenite, pyrite, magnetite and hematite) to those within zone 1, but here biotite is the dominant mica (Fig. 4.2.7) and the rocks contain abundant garnet. Some samples also contain K-feldspar that occurs in samples located next to granitic intrusions, similar to its appearance in zone 1.

At the bridge at Piana di Fornero the rocks contain abundant quartz veins (Fig. 4.2.7 c, lower left; Fig. 4.2.8), which is also illustrated in a field sketch. Further,

the field sketch (Fig. 4.2.8) illustrates folded mica-schists of the upper amphibolite facies that do not show evidence for partial melting.

The metabasites in this zone contain similar assemblages as those from zone 1. In one sample northwest of Piana di Fornero garnet is present within hornblende-rich layers, although these rocks are very rare in this part of the valley.

Figure 4.2.7. Field photographs illustrating the metapelites of zone 2 between Strona and Massiola: **a)** Typical mica-schist between Strona and Massiola. Biotite is the dominant mica, while muscovite is rare or absent (the field book is 19 cm long). **b)** Chevron folds in a mica-schist with abundant quartz veins, located in a river section at Piana di Fornero. **c)** Folded (pygmatic folds) schist with abundant quartz veins of different sizes. The quartz veins are within the foliation.

In thin sections of the metapelites from zone 2, garnet occurs mostly as rounded 0.5 to 2 mm diameter poikiloblastic grains with abundant inclusions of quartz, apatite and minor oxide minerals (Fig. 4.2.9 a and b). Sillimanite occurrence is similar to that in zone 1 being fibrolitic and intergrown with the mica. Plagioclase, biotite and muscovite are also similar in appearance to that in zone 1.

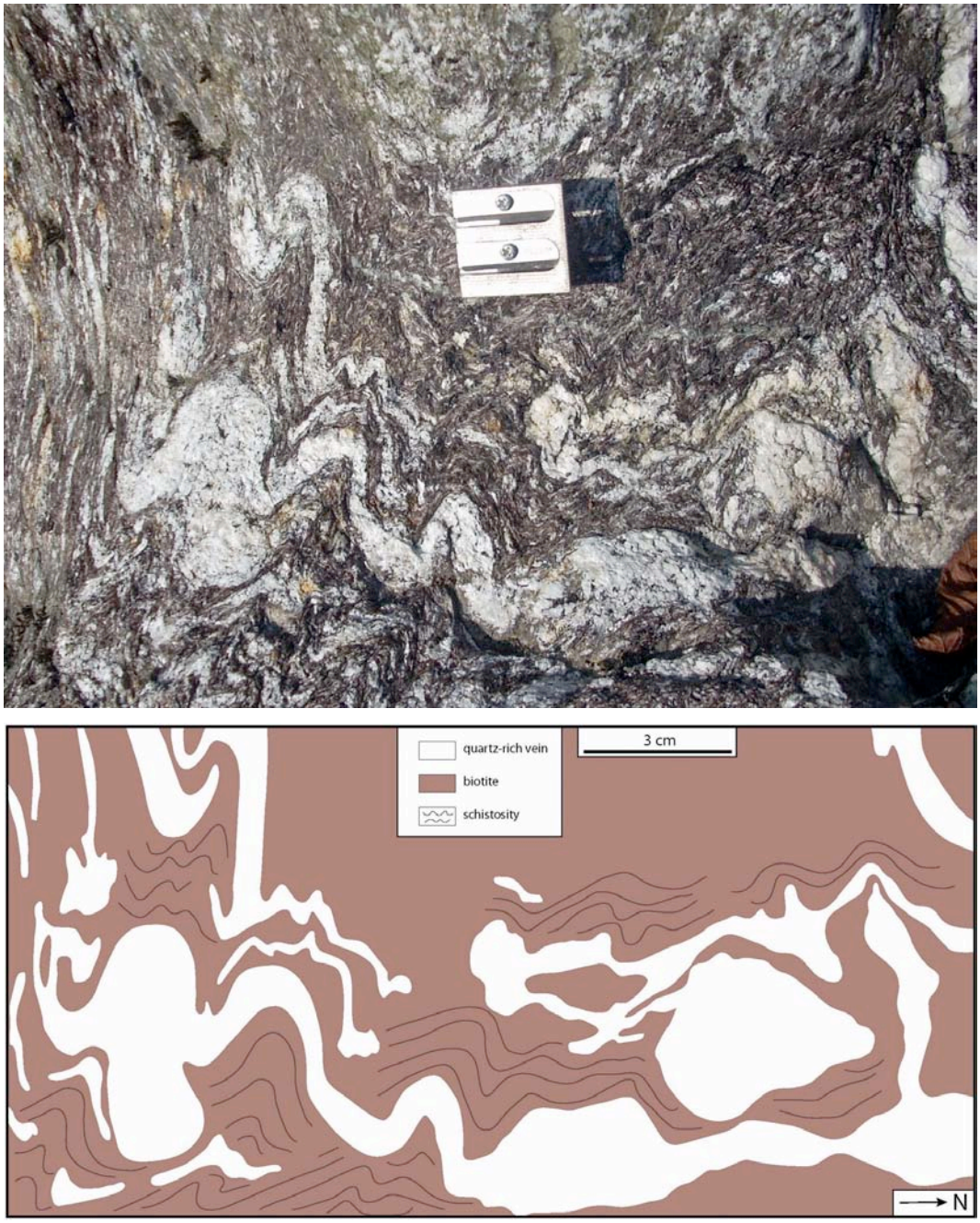

Figure 4.2.8. Field photograph and sketch (1) illustrating folded mica-schists in the upper amphibolite facies, located next to the bridge at Piana di Fornero (Fig. 4.2.2). The schists are dominated by biotite and contain additionally quartz, plagioclase, sillimanite and rarely muscovite. Different quartz veins are observable. In the upper part around the pencil sharpener many smaller quartz veins are present within the foliation. The lower part is dominated by larger patches of quartz. On the left side these patches are parallel or within the foliation, while on the right side they also cross cut the foliation. The schists do not show evidence of partial melting. *Scale on the photo*: the pencil sharpener is 2.5 cm long.

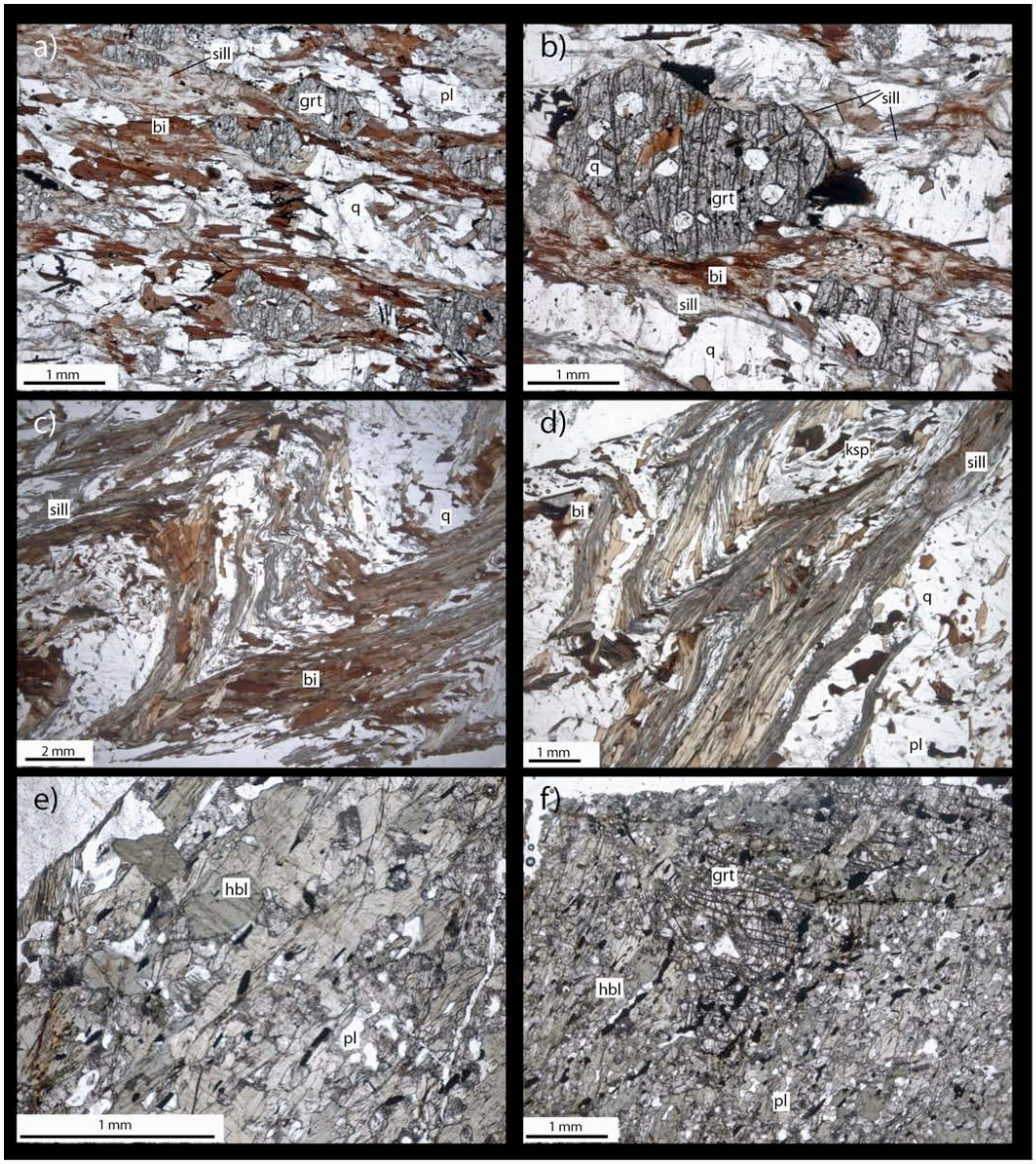

Figure 4.2.9. Photomicrographs illustrating the textures of rocks in zone 2 between Strona and Massiola: **a)** Mica-schist with garnet porphyroblasts 500 m west of Strona (IZ 022). It contains less muscovite then the samples from zone 1 and is much more biotite-rich. Fibrolitic sillimanite is intergrown with the mica. The garnet is poikiloblastic and contains inclusions of mostly quartz and some oxides. Felsic minerals in this sample are quartz and plagioclase. **b)** Poikiloblastic garnet porphyroblast in the same biotite-rich schist (IZ 022) as a). It contains inclusions of quartz, oxides and minor biotite. This garnet is surrounded by fibrolitic sillimanite and biotite. In the lower left part of this picture, a quartz vein with a width of less than 1 mm is visible**. c) and d)** These pictures illustrate kink folds in a biotite-rich mica-schist (IZ 002) located 1.5 km west of Strona. The foliation is defined by biotite and fibrolitic sillimanite. In the middle of c) small sub-folds are visible. Sample d) contains K-feldspar. **e) and f)** A very rare sample of a metabasite (IZ 027) located 500 m southeast of Massiola. It contains green hornblende, garnet and minor plagioclase (f). The garnet is skeletal, containing inclusions of oxides, and is completely surrounded by the green hornblende and minor plagioclase.

4.2.3 Zone 3 – Massiola to Forno

Zone 3 extends from the village of Massiola to the north of Forno (Fig. 4.2.10) and represents a transition zone between amphibolite and granulite facies rocks (Fig. 4.2.2). Zone 3 starts at the point where peak muscovite disappears and K-feldspar appears (i.e. muscovite-out/K-feldspar-in isograd) in the peak metamorphic assemblage. The upper boundary to the north/northwest demarcates the beginning of the granulite facies defined by the first appearance of orthopyroxene in metabasites (Fig. 4.2.10). This boundary is similar to that suggested by Zingg (1980), who defined this isograd as occurring to the northwest of Forno. Orthopyroxene becomes stable in the metapsammites/metagreywackes a short distance south of Forno.

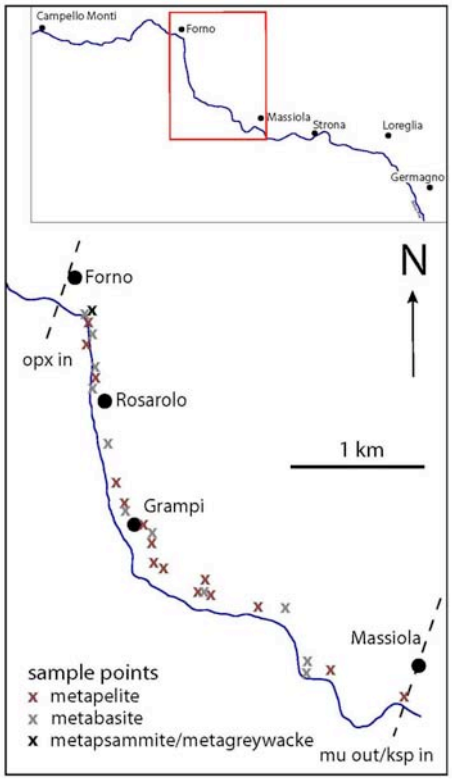

Figure 4.2.10. Overview of zone 3 in Val Strona di Omegna, including sample locations.

The metapelites contain garnet, plagioclase, biotite, sillimanite, quartz and K-feldspar, with accessory zircon, monazite, apatite, ilmenite and pyrite. An increase in the abundance of garnet and a decrease in the abundance of biotite occur towards the northwest. A marked change in the structure of the rocks occurs around Grampi and further to the north/northwest. The schistosity is not longer the predominant structure and the rocks begin to exhibit a migmatitic structure. The rocks are metatexitic and represent the first microscopically-visible signs of partial melting in the field (Fig. 4.2.11 a). Biotite is deflected around larger garnet grains and small leucosomes are observable. These small leucosomes consist mostly of quartz and feldspars, while the ferromagnesian minerals garnet and biotite occur within the melanosome, the darker part of the rock. The boundary between leucosome and melanosome is commonly diffuse. From Rosarolo to the north,

the difference between leucosome and melanosome becomes more distinct (Fig. 4.2.11 d). The leucosomes (around 20 mm wide) become more abundant and coarser grained, developing a distinct stromatic layering (Fig. 4.2.11 d). These structures are shown in detail in Fig. 4.2.12.

In the metabasites, the onset of partial melting is also recorded in this zone, in which the first visible leucosomes are present from Rosarolo north. The metabasites (Fig. 4.2.11 b) contain green and brown hornblende, plagioclase, clinopyroxene and minor garnet. The brown hornblende becomes more abundant to the north, while the proportion of green hornblende decreases until it disappears. In places both green and brown hornblende are present in the rocks and in others only green or brown hornblende is present. Biotite, sphene, ilmenite and rarely calcite are present as accessory minerals. The first appearance of clinopyroxene occurs approximately 0.5 km west of Massiola (Fig. 4.2.11 c). Clinopyroxene and minor garnet may be present in the leucosomes as well as in some hornblende-rich layers in the compositional layering, which is defined by varying amounts of hornblende and plagioclase. The abundance of both garnet and clinopyroxene increase towards north/northwest and both become coarser in grain size in both the hornblende-rich layers and the leucosomes. The leucosomes north from Rosarolo are volumetrically dominated by plagioclase with minor quartz, clinopyroxene and garnet and generally occur as thin layers (approximate 10–30 mm wide) surrounded by small hornblende-rich selvedges (Fig. 4.2.13). 1 km west of Massiola some calcite-rich veins in the metabasites are present. Between Rosarolo and Forno the metabasites are also abundant and in places strongly mylonitised (Fig. 4.2.11 f and g). Next to the first dam in the river north of Rosarolo, the rocks occur as pseudotachylite. In the metapsammites/metagreywackes no visible leucosomes were observed. These rocks contain garnet, biotite, plagioclase and quartz.

Next page:

Figure 4.2.11. Field photographs illustrating the rocks of zone 3 between Massiola and Forno: **a)** Metapelite near Grampi. The rock has a gneissosity and shows the first evidence for partial melting. The garnets are surrounded by biotite and sillimanite. Small leucosomes can be seen in the upper right of the photo (the hammer head is 17 cm long). **b)** Metabasite between Massiola and Forno. The white patches in the upper part consist of plagioclase and are the first visible evidence for partial melting in this rock type (section of the hammer is around 5 cm long). **c)** Small garnet (red) and clinopyroxene (green) crystals in a plagioclase-rich leucosome. **d)** Migmatitic metapelite

between Rosarolo and Forno. The leucosomes becomes larger in comparison to a). **e)** Migmatitic metapelite with interlayered metabasite (green grey) north of Rosarolo. The metapelite contain much more leucosome than the metabasites. **f)** This photo shows different stages of partial melting, north of Rosarolo. In the upper part, boudains of metabasite are observable within the more melted metapelites. The metapelites are very finely layered. In the lower part, the metabasites is a proto-mylonite. **g)** Mylonitic structure in a metabasite, south of Forno (the pencil is approximate 14 cm long).

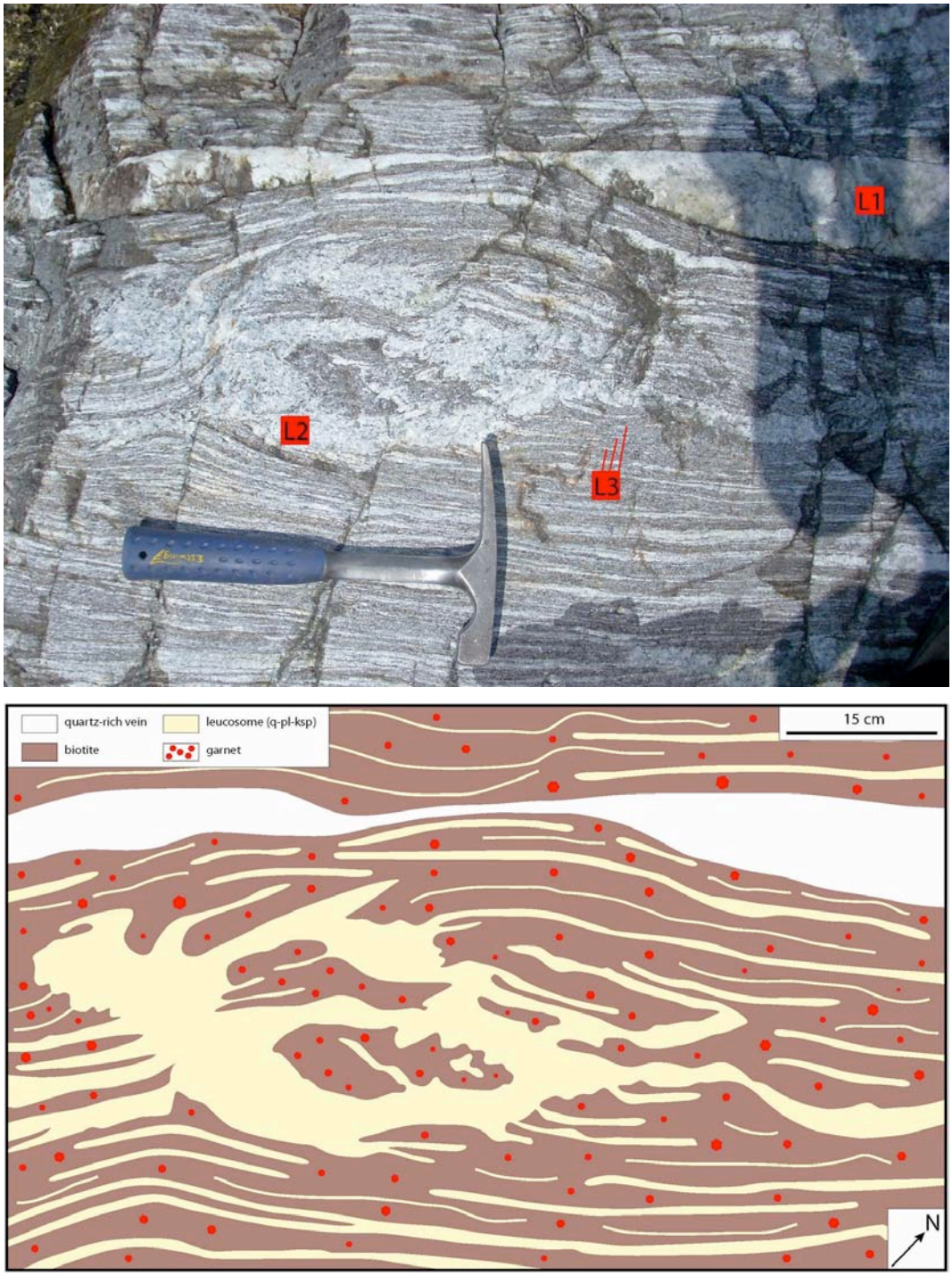

Figure 4.2.12. Field photograph and sketch (2) illustrating a stromatic metatexitic metapelite with a leucocratic patch, located between Rosarolo and Forno. The rock contains three types of leucosomes: *in situ* (L3), in-source (L2) and a leucocratic vein (L1). The quartz dominated leucocratic vein is within the layering of the metapelite. The leucocratic patch is likely represents a dilatant site and can be identified as an in-source leucosome. Thin *in situ* leucosomes can be observed next to the patch at the middle right side of the picture. These leucosomes show petrographic continuity with the larger patch and may represent the melt source for the in-source leucosome. The areas between the leucosomes are difficult to differentiate into melanosome and/or paleosome. However, given on the proportion of *in situ* leucosome it is likely that most of the rocks has undergone some partial melting and that paleosome, if present at all, is minor. The leucosomes are parallel to the gneissc layering in the metapelite, so this rock has a stromatic structure. *Scale on the photo*: the hammer is 28 cm long.

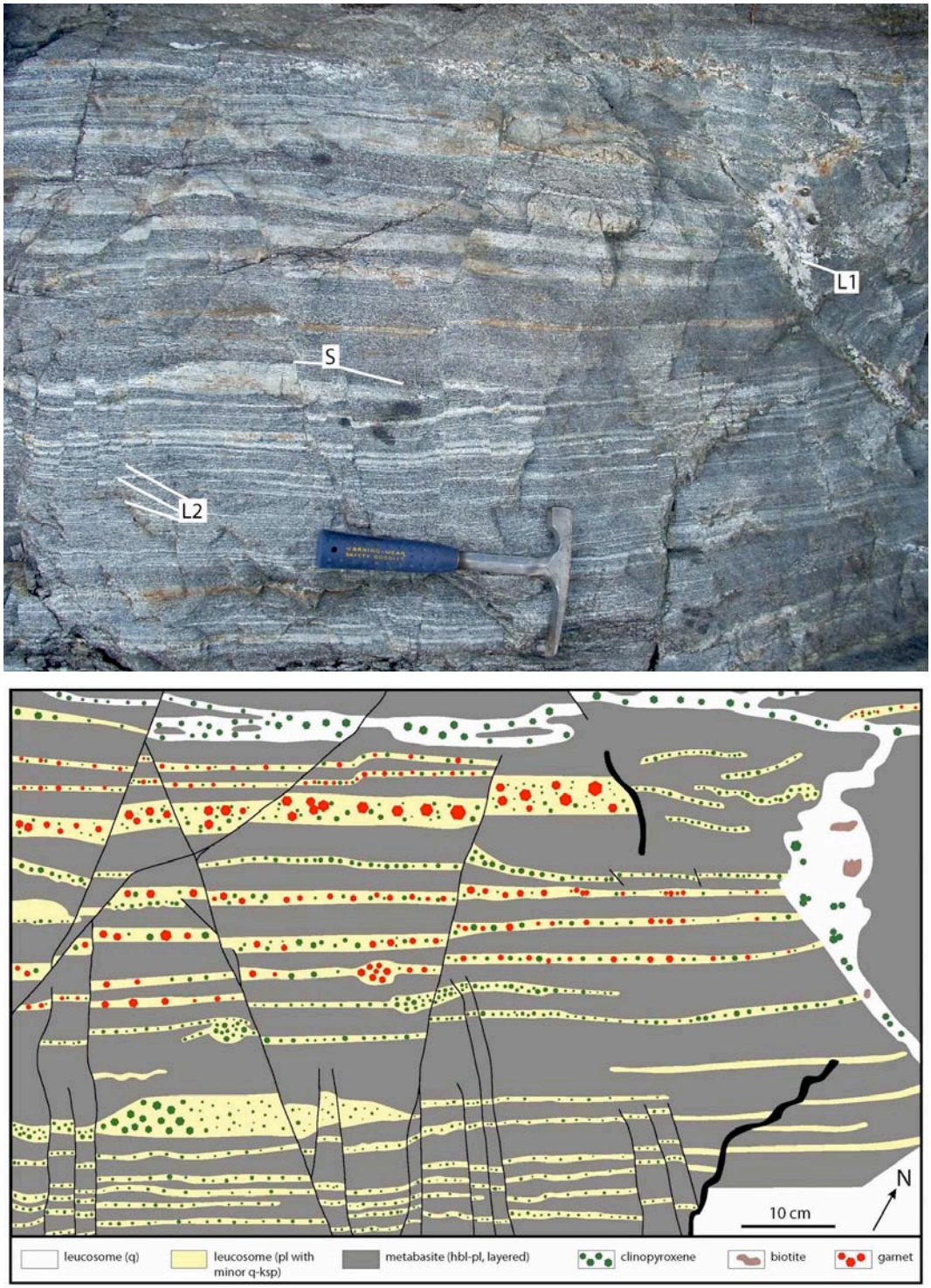

Figure 4.2.13. Field photograph and sketch (3) illustrating a stromatic metabasite between Rosarolo and Forno, located next to the previous sketch. A quartz-rich vein (L1 in the photo) crosses the layering of the rock on the right side of the picture and sketch but becomes broadly layer parallel in the upper part of them. This vein contains minor biotite and clinopyroxene (10–15 mm in diameter). Most of the leucosomes in the picture are plagioclase-rich with lesser, variable amounts of K-feldspar and quartz. In the upper part the metabasite is compositionally layered, consisting of darker hornblende rich layers and lighter plagioclase rich layers. These parts are not affected by partial melting yet. They can be distinguished from the *in situ* leucosomes (L2) in the lower part by the presence of small selvedges (S) around these *in situ* leucosomes. Another way to distinguish the compositionally layered parts from the partially melted parts is the appearance of garnet. Garnet

(grain size 5–15 mm) is only observable in the compositionally layered part (in addition to clinopyroxene) and not in the leucosomes. Based on their small size the selvedges are not drawn in the sketch and only marked in the picture (S). It consists of black weathered hornblende. The neosome of this rock shows a stromatic structure. Neosome and paleosome are affected by small shear zones with a maximum displacement of 1 cm. *Scale on the photo*: the hammer is 28 cm long.

Garnet in thin sections of metapelites from zone 3 form larger poikiloblasts (10–30 mm) with inclusions of mostly quartz and oxide minerals, which are coarser grained than those from lower grades (Fig. 4.2.14 a–d). In places the grains are somewhat elongated. At the lower grade end of this zone, sillimanite is dominantly fibrolitic and is concentrated together with biotite around the margins of garnet porphyroblasts (Fig. 4.2.14 b). Towards the higher grade part of this zone sillimanite becomes prismatic. Biotite has a brownish to light brown/yellow pleochroism and an average grain size of 0.2 x 0.3 mm (e.g. Fig. 4.2.14 a and b). Plagioclase, K-feldspar and quartz occur as larger grains (10–30 mm) within the leucosomes in the higher grade parts of this zone.

Next page:

Figure 4.2.14. Photomicrographs illustrating the textures of rocks in zone 3 between Massiola and Forno: **a)** This sample is located approximately 1.5 km west/northwest of Massiola (IV 020). It shows garnet porphyroblasts in a biotite-sillimanite-schist. The garnets are in places elongate with many inclusions of quartz. Sillimanite is fibrolitic. The lower part of this picture illustrates a plagioclase rich leucosome. **b)** A more detailed look to a biotite-sillimanite-schist with garnet porphyroblasts (IZ 030) located near to a). Sillimanite is fibrolitic to prismatic and intergrown with the biotite (middle left). K-feldspar is also part of the assemblage. **c)** Sample IZ 085 is located 500 m south of Forno and has a more residual composition. It contains mostly garnet and sillimanite. The proportion of biotite and felsic minerals is very low. Biotite is only present as inclusions in the garnets. Sillimanite has a prismatic shape. Minor quartz and K-feldspar are discernible. **d)** This sample (IV 048) of a metapelite is located a few meters southwest from c). It shows a proto-mylonite with skeletal garnet poyphyroblasts. The garnets have abundant inclusions of quartz. Biotite is present between garnets (lower part). **e)** A mylonitic to ultramylonitic metabasite located near c) and d) between Rosarolo and Forno in a river section (IZ 084). On the left hand side a very fine grained quartz vein is present. **f)** This picture illustrates a more detailed view of a garnet grain in d). It shows the mylonitic texture. On the left side of the garnet grain biotite occurs in the strain shadow. **g)** A detailed view of a clinopyroxene porphyroclast of the mylonite shown in e). The clinopyroxene is wrapped by the ultramylonitic material, and shows no internal deformation. **h)** This picture shows a metabasite (IV 051) from approximately 1.2 km south of Forno. It contains green hornblende, plagioclase and clinopyroxene. This rock has a granoblastic texture and shows no evidence for the onset of partial melting, but leucosomes are present in the outcrop (compare Fig. 4.2.10 c)). **i)** Another sample of a metabasite (IZ 143), located 170 m north of Rosarolo. The hornblende here is brown and also the clinopyroxene has a larger grain size in comparison to h).

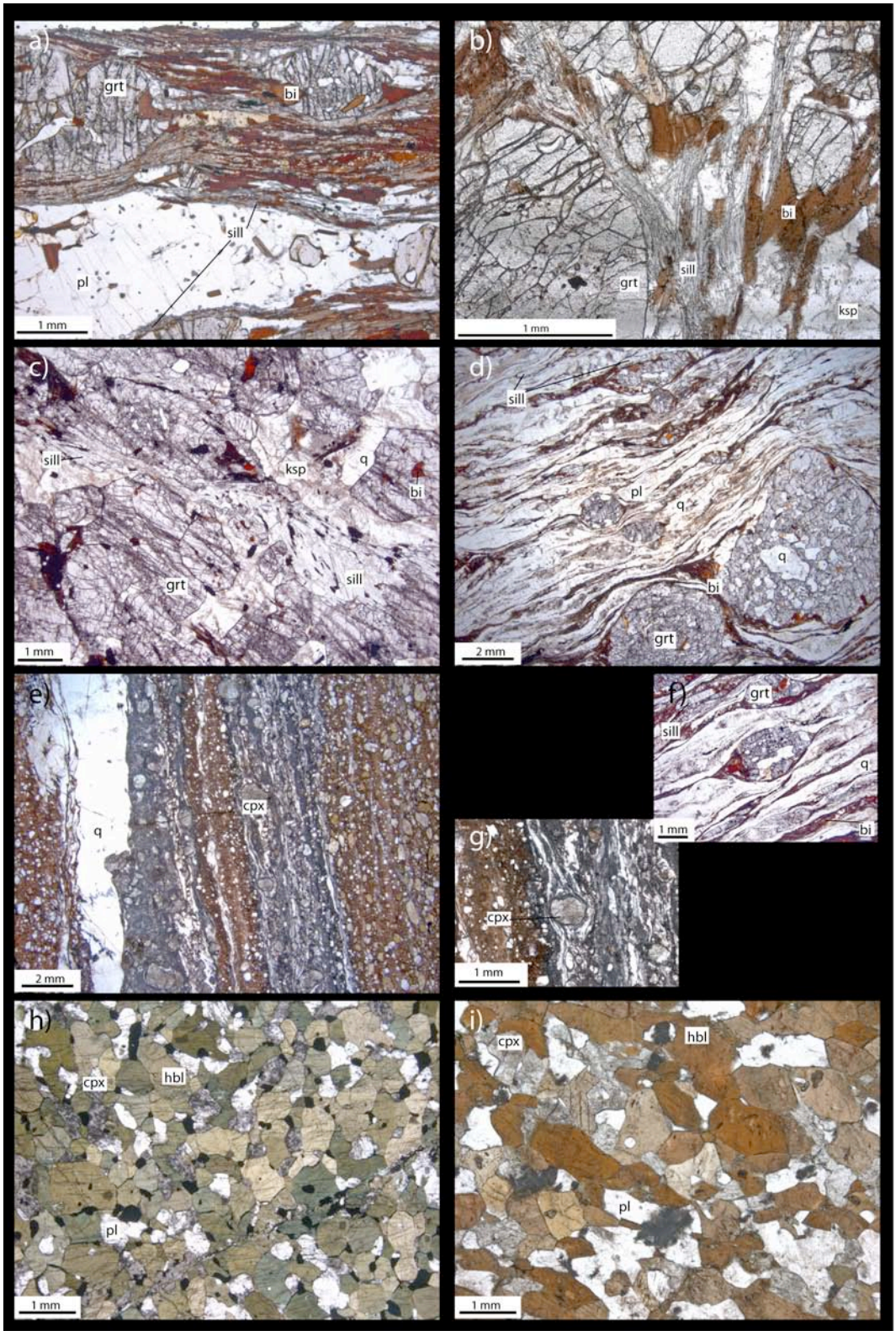
a)
grt
bi
sill
pl
1 mm
b)
bi
grt
sill
ksp
1 mm
c)
sill
ksp
q
bi
grt
sill
1 mm
d)
sill
pl
q
q
bi
grt
2 mm
e)
q
cpx
2 mm
f)
grt
sill
q
1 mm
bi
g)
cpx
1 mm
h)
cpx
hbl
pl
1 mm
i)
cpx
hbl
pl
1 mm

4.2.4 Zone 4 – Forno to Piana di Forno

Zone 4 begins close Forno with the appearance of orthopyroxene in the metabasites and in the metapsammites/metagreywackes (i.e. the orthopyroxene-in isograd), and ranges upgrade to the village of Piana di Forno, where prograde biotite disappears from the metapelites (i.e. the biotite-out isograd) (Fig. 4.2.15).

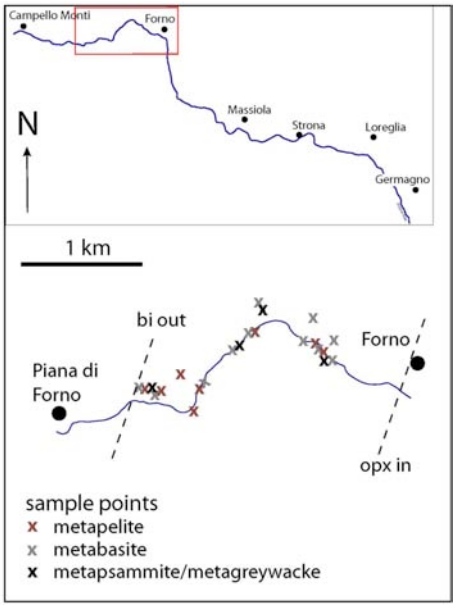

Figure 4.2.15. Overview of zone 4 in Val Strona di Omegna, including sample locations.

The metapelites comprise garnet, sillimanite, plagioclase, quartz and K-feldspar with accessory rutile, ilmenite, zircon, and monazite. The modal increase in garnet and decrease in biotite continue upgrade until the latter is exhausted. The rocks display metatexitic to diatexitic migmatitic structures (Fig. 4.2.16 a), with more complex leucosome networks than migmatites in zone 3. The leucosomes become more abundant and coarser grained towards the north/northwest and a second type of larger (up to 50–80 cm wide) leucosome/leucocratic dyke occurs (Fig. 4.2.16 b), which contains abundant garnet. Around both types of leucosomes small selvedges rich in biotite with variable sized garnet crystals are present.

The metabasites consist of brown hornblende, plagioclase, clinopyroxene and biotite together with orthopyroxene and/or garnet in some samples. Biotite is in places interpreted as a retrograde mineral because it partially replaces orthopyroxene, brown hornblende and clinopyroxene. The proportion of *in situ* leucosome, and hence the inferred degree of partial melting increases in comparison to metabasites from zone 3 and plagioclase-rich leucosomes also contain large clinopyroxene grains (20–30 mm in diameter) and in places garnet (Fig. 4.2.16 f and g). Layered corona textures comprising an inner rim of plagioclase and an outer rim of hornblende commonly surround garnet, visible for

the first time next to the bridge at Forno (Fig. 4.2.16 e). In some samples about 900 m northwest of Forno, the garnet forms porphyroblasts 20–30 mm in diameter. The garnet porphyroblasts are more abundant in the leucosomes but also occur in the melanosome. Garnet also occurs in both leucosome and melanosome with a similar grain size to all the other minerals. The metapsammites/metagreywackes contain orthopyroxene, garnet, plagioclase and biotite. They differ in appearance from those at lower grades due to a greater proportion of leucosomes, which occurs as narrow veins (5–20 mm wide) (Fig. 4.2.16 d). All the mentioned structures are illustrated and described in detail in Figs. 4.2.17–4.2.24.

Small layers of hornblendites, calcsilicates and peridotites are intercalated with the metapelites and metabasites. A hornblendite layer is exposed next to the bridge at Forno and contains brown hornblende with minor clinopyroxene and orthopyroxene. A calcsilicate layer, located in a river section 1 km north of Forno, contains garnet, clinopyroxene and wollastonite. One pyroxenite layer, located around 1.2 km west of Forno, contains minor spinel. At the bridge at Forno and further to the north/northwest, small areas of mylonite are present. One is a one metre thick layer of ultramylonite with a calcsilicate composition containing clinopyroxene, garnet, sphene and scapolite (Fig. 4.2.25 f).

Next page:

Figure 4.2.16. Field photographs illustrating the rock types of zone 4 between Forno and Piana di Forno: **a)** Diatexite with schollen of metapsammite/metagreywacke (grey parts) near Forno. The rocks contain two types of leucosome, one with only felsic minerals and another one additionally with garnet and biotite. The metapsammites/metagreywackes show minor evidence for partial melting. **b)** Outcrop south of Piana di Forno. The light red parts are leucosomes containing abundant garnet and biotite. The grey areas are schollen of metapsammite/metagreywacke, which contain many small orthopyroxene-bearing leucosomes. **c)** Boudinaged layer of metabasite between two layers of metapelite near Forno. The metapelites have been extensively partially melted, while the metabasites appear less effected by partial melting (the camera case is 12 cm long). **d)** Leucosome in a metapsammite/metagreywacke. It contains orthopyroxene and is surrounded by small garnet grains and copious biotite. **e)** Garnet porphyroblasts with an inner rim of plagioclase (white) and an outer rim of hornblende (black). These porphyroblasts occur in the compositional layering of the metabasite as well as in the leucosome. **f)** Sample of a metabasite with clinopyroxene-bearing leucosome, near Forno. The dark grey parts are enriched in hornblende, while the lighter grey schollen are rich in hornblende, plagioclase and clinopyroxene. **g)** Partial melted metabasite in the riverbed. The leucosomes and also the compositional layered parts contain garnet grains.

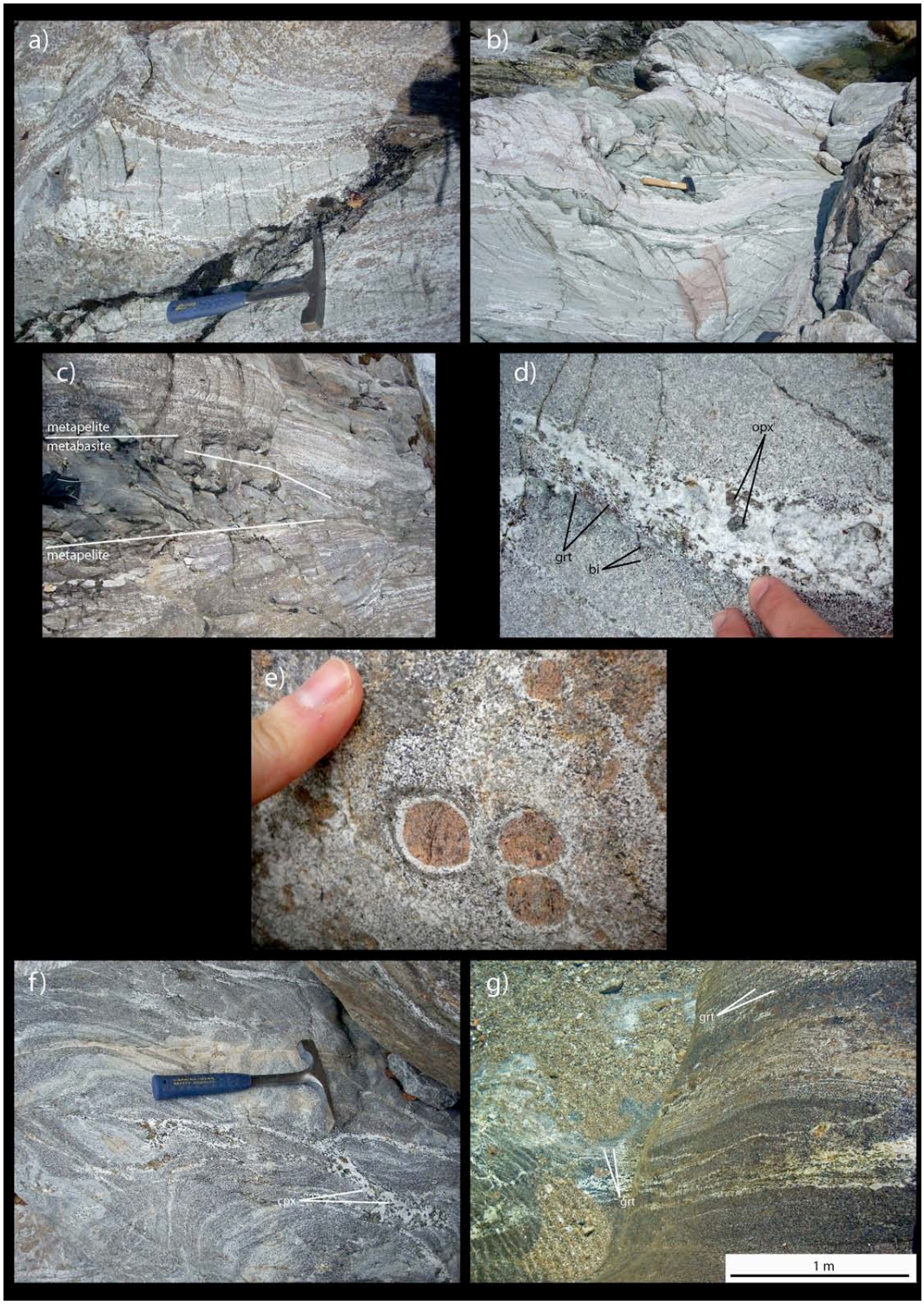
a)
b)
c)
metapelite
metabasite
metapelite
d)
opx
grt
bi
e)
f)
cpx
g)
grt
grt
1 m

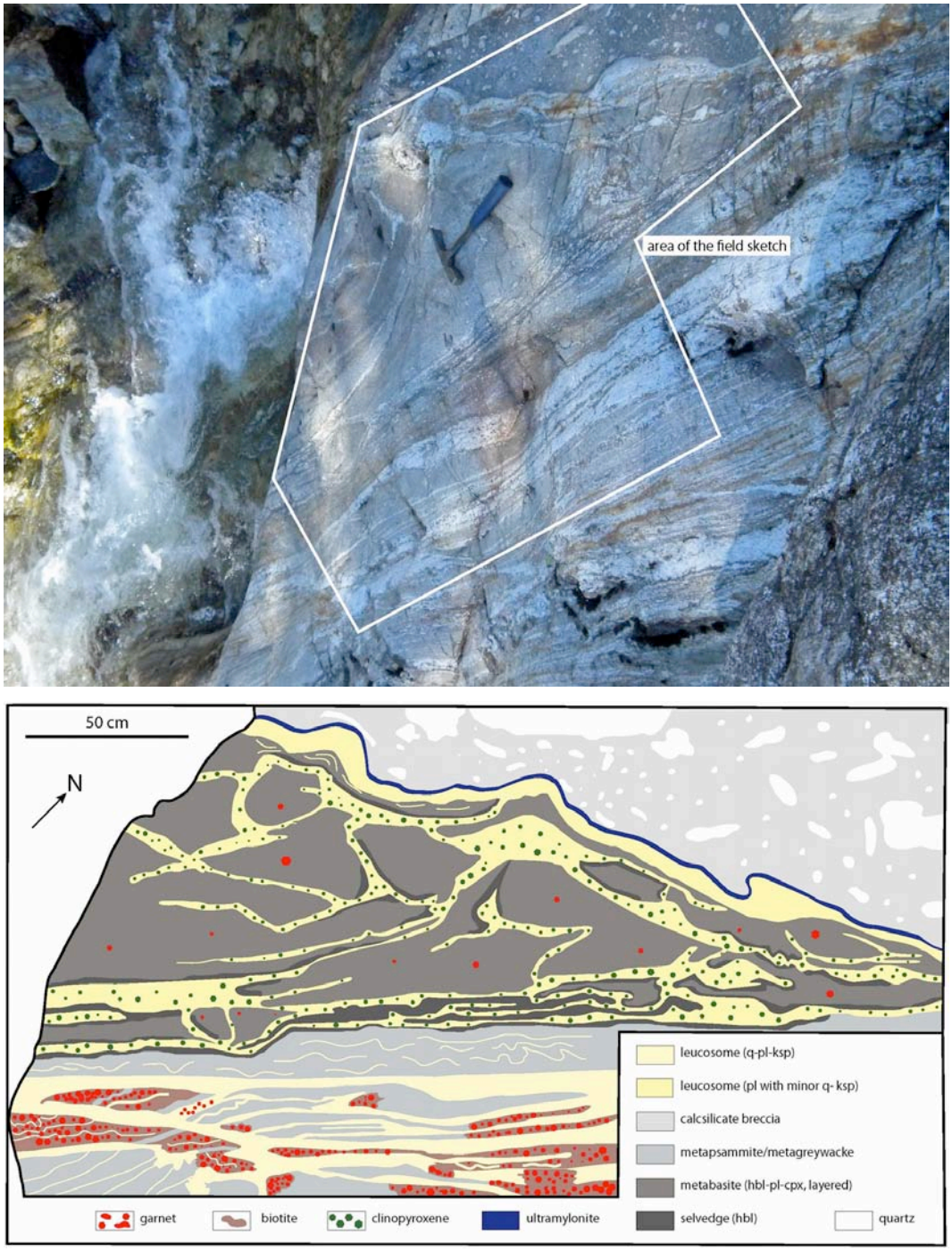

Figure 4.2.17. Field photograph and sketch (4) illustrating the relationships between metapelite, metabasite and metapsammite/metagreywacke next to the bridge of Forno. It shows the connections and interactions of the different rock types additionally to their degree of partial melting at the beginning of the granulite facies. In the upper right part of the sketch an mylonitic to ultramylonitic calcsilicate vein (light grey) is illustrated. This vein contains large porphyroclasts of quartz giving it a brecciated appearance. Clinopyroxene, scapolite and sphene are also observable as smaller porphyroclasts in the matrix (in thin section). The vein is separated from a plagioclase-rich leucosome (yellow) by a small ultramylonitic band (dark blue) of unknown composition. The middle of the sketch contains metatexitic metabasite (dark grey). It is compositional layered, contains hornblende, clinopyroxene, plagioclase and minor garnet and is defined as a paleosome of this rock. The neosome consists of different types of leucosomes (yellow), which are surrounded by an enrichment of hornblende (darkest grey) that forms a selvedge. Due to their small size not all selvedges are illustrated in the sketch. The smallest leucosomes are *in situ* leucosomes and

consists of only plagioclase. The larger leucosomes also contain clinopyroxene and from a interconnected network of in-source leucosomes. The lower part of the sketch illustrates metasediments. Schollen of metapsammites/metagreywackes occur within a diatexitic metapelite (outside the sketch). The metapsammites/metagreywackes show only minor evidence for partial melting with and show small evenly distributed *in situ* leucosomes. In the metapelite no paleosome occurs, the whole rock consists of neosome. The leucosome can be defined as quartz- and feldspar rich in-source leucosome, while the melanosome comprises biotite, garnet and sillimanite (brown with red in the sketch), though much of the biotite here could be retrograde. The melanosome rarely contains *in situ* leucosomes that have not migrated out of this layer. Small selvedges of biotite are present between some leucosomes and metapsammite/metagreywacke but based on the scale of the sketch they are not illustrated. *Scale on the photo:* the hammer is 28 cm long.

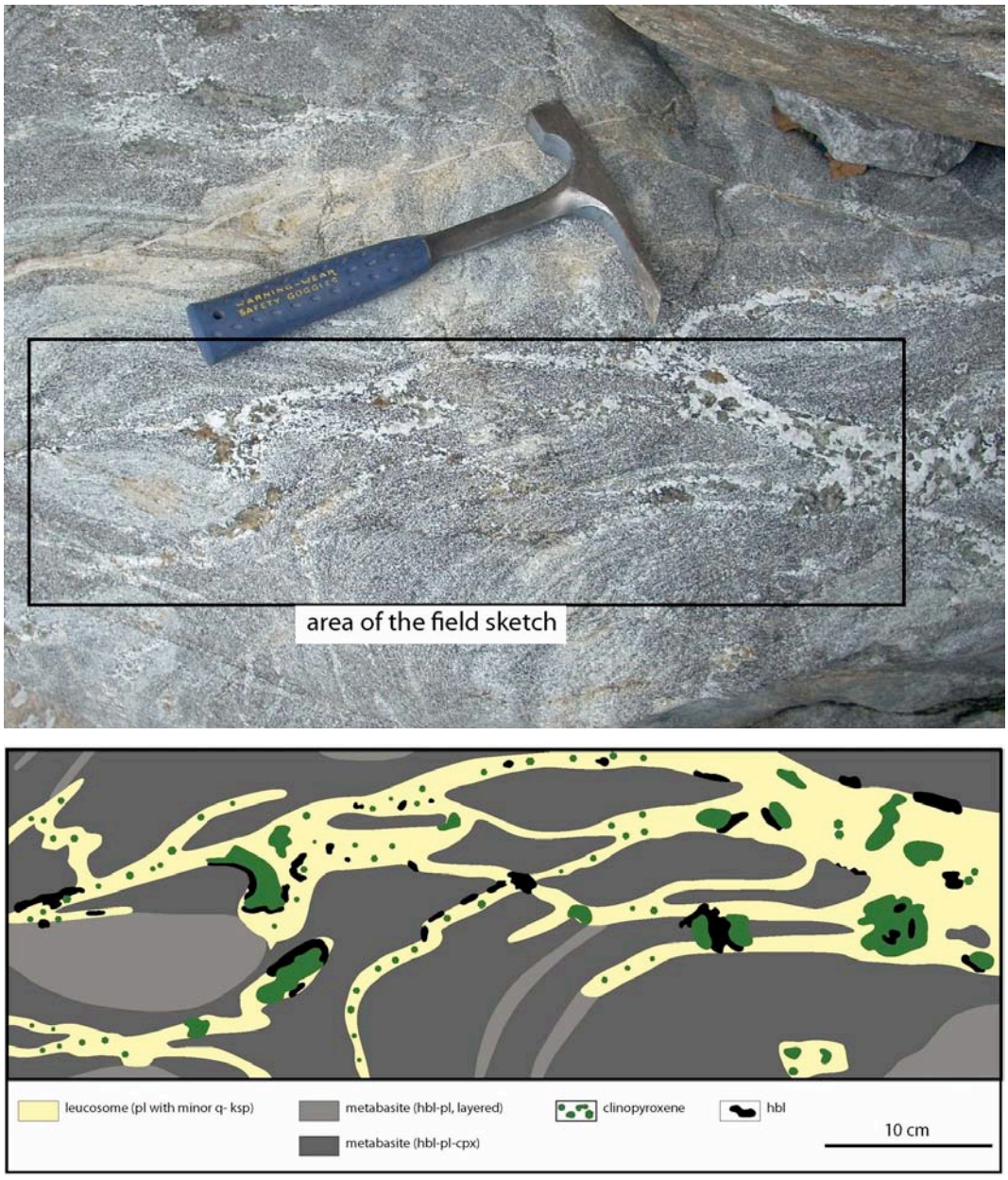

Figure 4.2.18. Field photograph and sketch (5) illustrating metatexitic structures in a boulder of a metabasite from a higher grade part of the granulite facies. It is difficult to name the different parts of the metabasite because it is not clear, which part is paleosome and which is residuum. The light grey schollen in the sketch consist of hornblende, plagioclase and rarely clinopyroxene (not

illustrated in the sketch) and are compositionally layered. The areas illustrated with the dark grey colour in the sketch are composed mostly of hornblende with minor of plagioclase and commonly clinopyroxene. The leucosomes are much coarser grained than the grey areas and appear in places as patches of irregular shape (lower right part). It can be defined as an in-source leucosome and consists of mostly plagioclase and quartz. It contains big crystals of green weathered clinopyroxene and black weathered hornblende. The big clinopyroxenes are limited to the leucosome, while the hornblende is mostly at the rim between leucosome and the dark grey part. *Scale on the photo*: the hammer is 28 cm long.

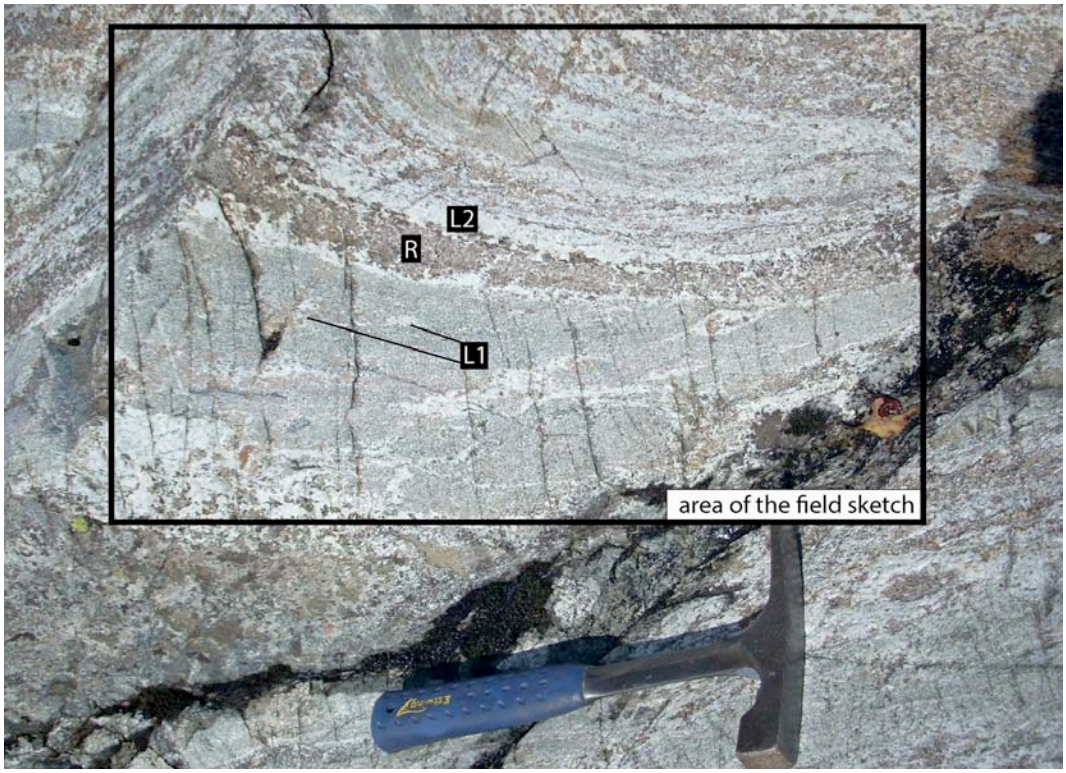

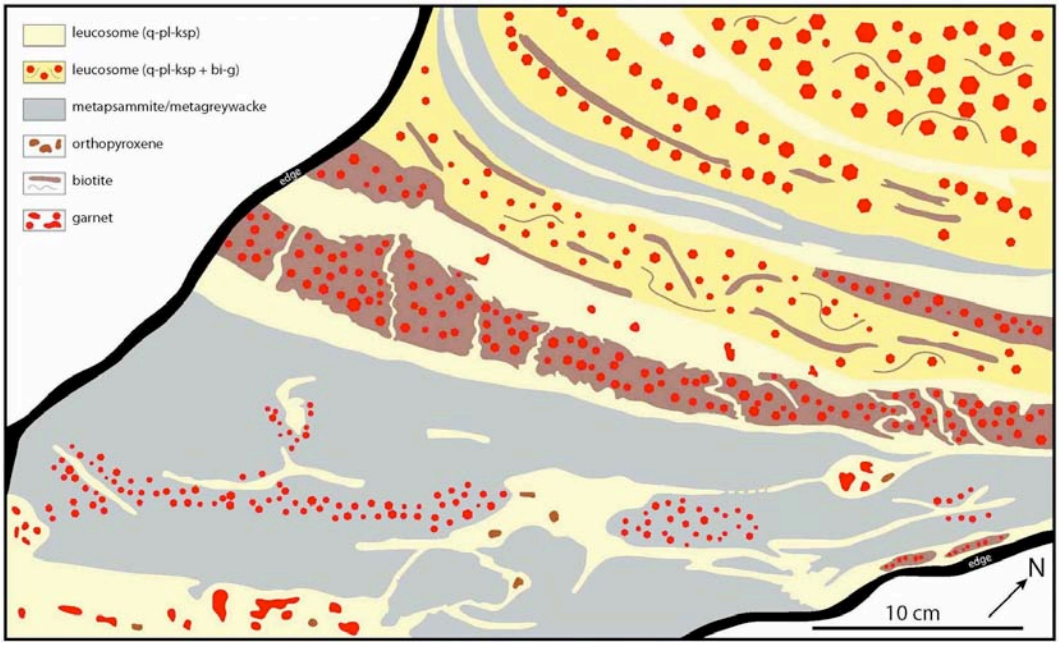

Previous page:

Figure 4.2.19. Field photograph and sketch (6) illustrating a metatexitic to diatexitic metapelite with schollen of metapsammite/metagreywacke. The metapsammites/metagreywackes (grey) consists as schollen (lower part) and schlieren (upper part) in the metapelite. They show evidence for partial melting and contain *in situ* leucosomes (L1), predominantly consisting of plagioclase and quartz. Within the leucosomes minor garnet and orthopyroxene can be observed. Garnet is also observed in the weakly to unmelted parts of the metapsammite/metagreywacke. The metapelites are more complex. In the middle of the photo/sketch a garnet-biotite-sillimanite-bearing melanosome (R) is displayed. Small *in situ* leucosomes are within the melanosome (not illustrated in the sketch). These leucosomes cross over to in-source leucosomes (L2) that surrounded the melanosome (light yellow in the middle of the sketch). The areas that labelled with darker yellow in the field sketch, especially in the upper right part, are leucosomes that contain abundant biotite and garnet. *Scale on the photo*: the hammer is 28 cm long.

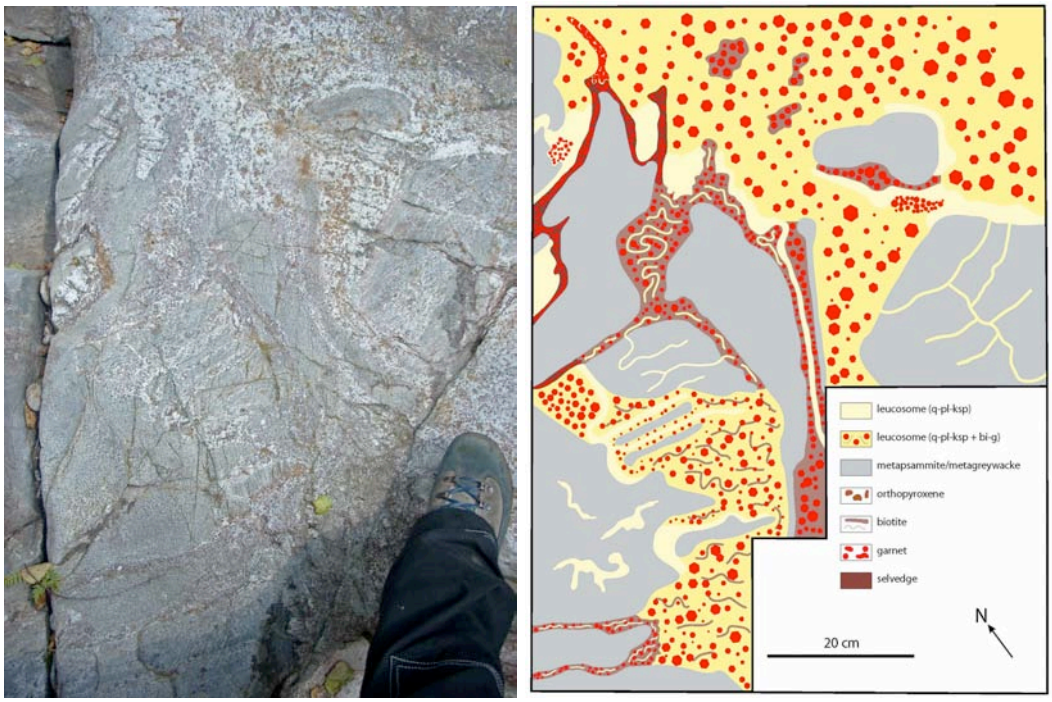

Figure 4.2.20. Field photograph and sketch (7) illustrating a diatexitic metapelite with schollen of metapsammite/metagreywacke. The schollen of metapsammite/metagreywacke contains small *in situ* leucosomes. Some of these leucosomes have a connection to also small leucosomes in the residual part (brown; middle left) of the metapelite. The metapsammites/metagreywackes are less strongly affected by partial melting than the metapelites. The in-source leucosomes (light yellow parts in the sketch) of the metapelite consist of quartz and feldspar and are commonly surrounded by selvedges (dark brown) of mostly biotite and variable proportions of garnet. Almost in the middle of the sketch some melanosome is located. It contains biotite, sillimanite and garnet and minor small veins of leucosome. The majority of the rock consists of leucosomes, which are very rich in garnet and also contain minor biotite. In the upper left part of the sketch an area with enriched in garnet is present. *Scale on the photo*: the shoe is approximate 14 cm long.

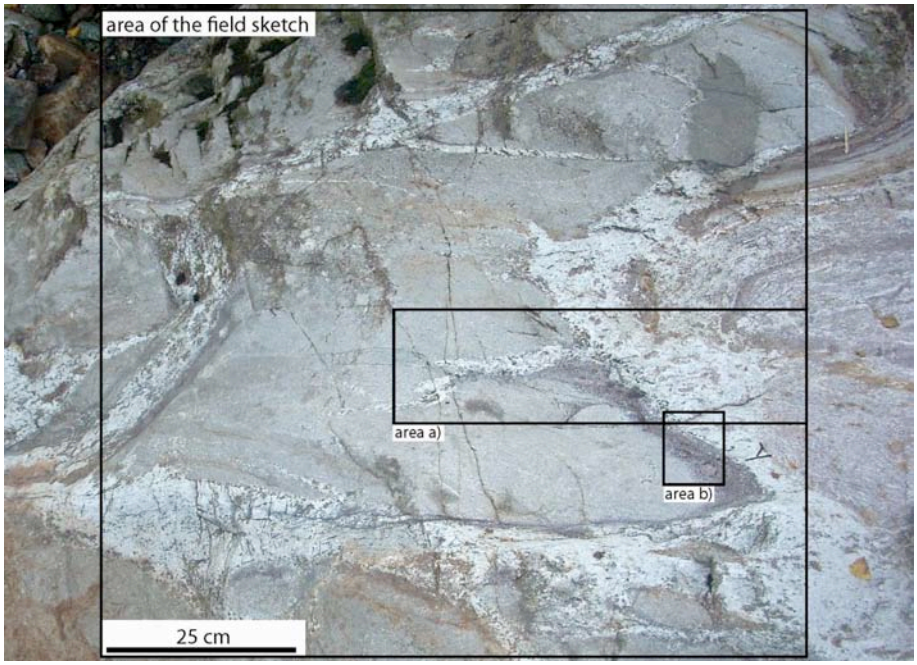

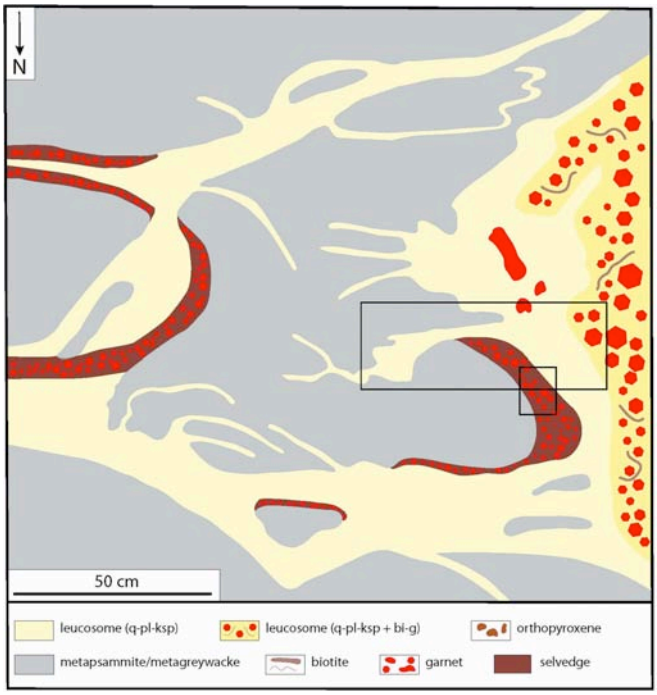

Figure 4.2.21. Field photograph and sketch (8) illustrating a diatexitic metapelites with schollen of metapsammite/metagreywackes. The *in situ* leucosomes of the metapsammites/metagreywackes consists of plagioclase, quartz and K-feldspar and are best observed in the middle of the sketch. Towards the right hand side they cross over into a pool of melt that is bounded between the metapsammite/metagreywacke and the metapelite. On the right hand side garnet is enriched within the leucosomes. Melanocratic selvedges (brown) several cm wide may occur between the metapsammite/metagreywacke and leucosome, consisting of biotite, sillimanite and garnet. At the right side of the sketch a large proportion of leucosome is present and contains abundant garnet and minor biotite and sillimanite (not illustrated).

Next page:

Figure 4.2.22. Field photograph and sketch (8a) illustrating a detailed view of a part of sketch (8), marked as area a) in the appropriate picture (Fig. 4.2.21). It shows the relationships between different leucosomes. On the left side the leucosomes are *in situ* to in-source segregated from the metapsammite/metagreywacke. Evidence for this is the presence of substantial amounts of small orthopyroxene grains that are absent from the metapelite. Further to the right side this leucosome migrates out of its layer and merges into larger leucosome. The larger leucosome, illustrated with light yellow in this sketch, contains orthopyroxene on the left side and becomes more garnet rich to

the right side. It seems to be a mixture of two different leucosomes, one segregated from the metapsammite/metagreywacke and the other one segregated from the metapelite. Further to the right, the leucosome contains abundant garnet and minor biotite. A melanosome that still contains minor leucosomes is visible in the upper right part of the sketch and is rich in biotite, sillimanite and garnet. Another important part of this sample are the selvedges around the leucosomes (dark brown). They are of limited extent around the *in situ* leucosomes of the metapsammite/metagreywacke and become much expanded between the in-source leucosome (middle part) and the metapsammite/metagreywacke scholle. The selvedges consist of mostly biotite with garnet porphyroblasts and minor felsic minerals. The biotite is aligned parallel to the leucosome and is also concentrated in some areas (light brown inside the dark brown).

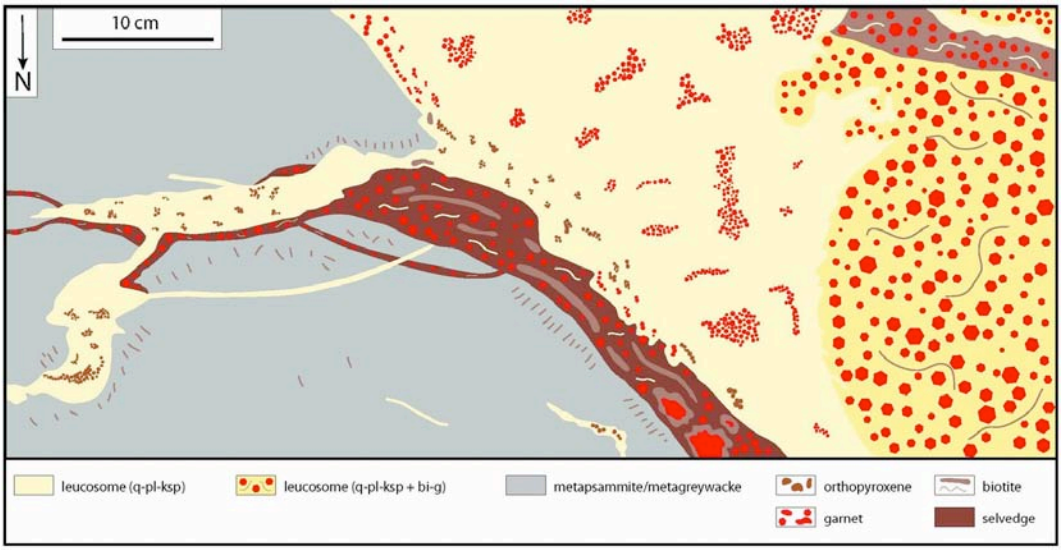

Figure 4.2.23. Field photograph and sketch (8b) illustrating a detailed view to a part of sketch 8, marked as area b) in the appropriate picture (Fig. 4.2.21). It shows a biotite-rich selvedge that contains large garnet porphyroblasts, which are surrounded by a rim of biotite that replaces the garnet. Also visible are some small garnets that are located in the leucosome and into the selvedge.

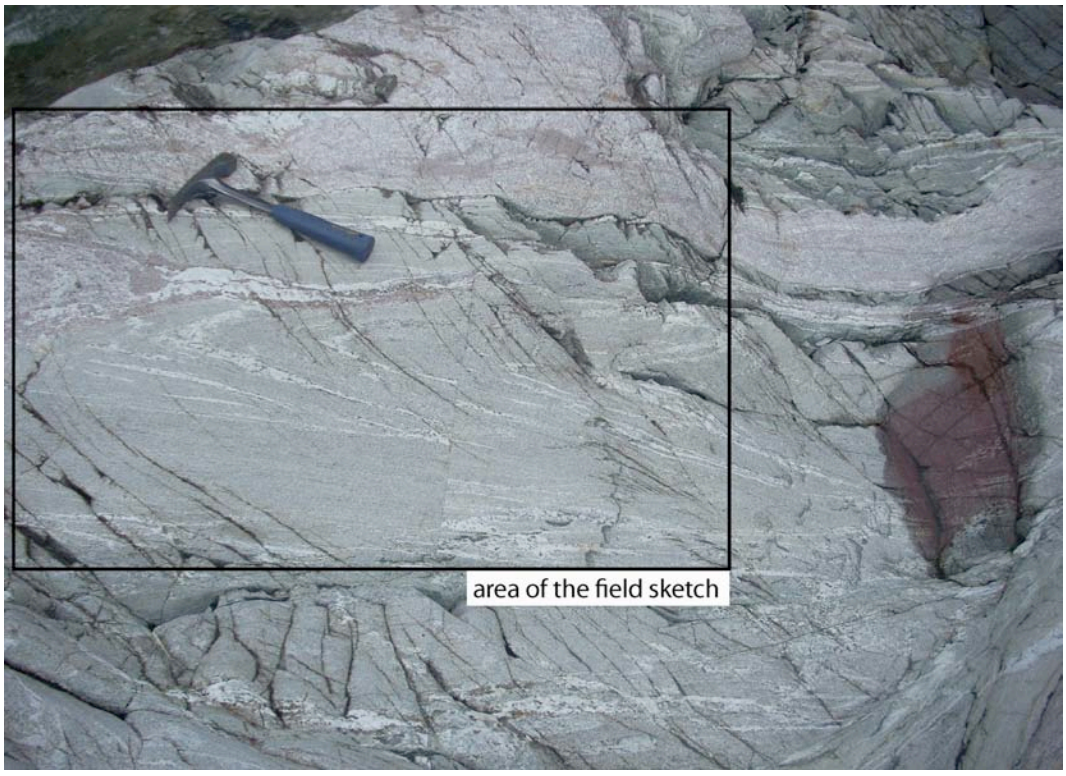

Figure 4.2.24 (also next page). Field photograph and sketch (9) illustrating a diatexitic metapelite with schollen of metapsammite/metagreywacke, which are affected by a small shear zone in the lower part. The metapsammites/metagreywackes show more evidence for partial melting. They contain abundant *in situ* leucosomes (plagioclase, quartz, K-feldspar), which may merge with larger in-source leucosomes. These leucosomes contain abundant orthopyroxene. In the lower part of the

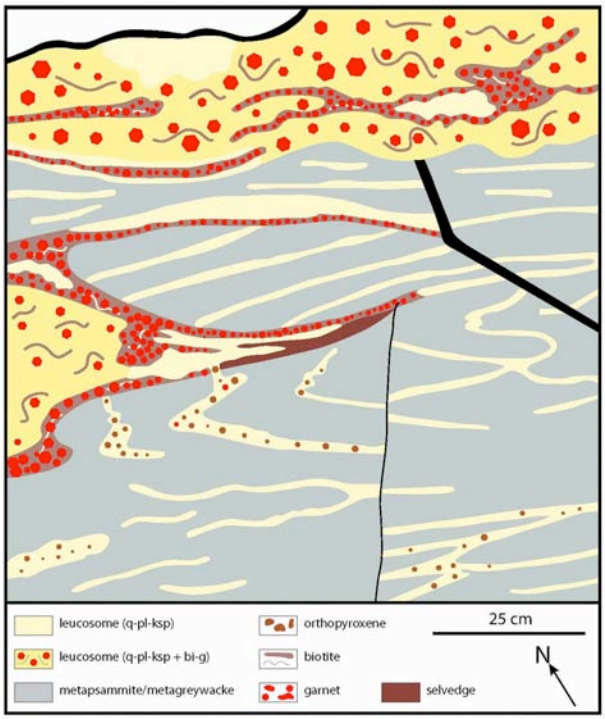

sketch a narrow shear zone crosses the leucosomes. The metapelite contains the same structures as described in former sketches. The light yellow parts are in-source leucosomes, while the yellow parts illustrated garnet- and biotite-rich leucosomes. A small selvedge is observable between an in-source leucosome and the metapsammite/metagreywacke in the middle of the sketch. Around the leucosomes small rims of selvedge occur, consisting of garnet, biotite and sillimanite. They contain rarely felsic minerals. *Scale on the photo*: the hammer is 28 cm long.

In thin sections, garnet is very common in the metapelites. It consists of larger elongated grains (2–4 mm) with a poikiloblastic texture (Fig. 4.2.25 a and c). Inclusions in the garnet are mostly quartz, biotite and rutile. In addition, more rounded grains are also present in the metapelites (Fig. 4.2.25 b). Abundant prismatic sillimanite and minor biotite occur interstitial to the garnet grains. K-feldspar and plagioclase have an average grain size of approximate 3 mm in the leucosomes. Some sericitization is visible at the rims of some plagioclase grains, while K-feldspar may exhibit a myrmekitic texture. Retrograde muscovite cross-cuts the fabric defined by biotite and is not intergrown with sillimanite. Muscovite most commonly occurs next to K-feldspar or partially replaces it. In the metapsammites/metagreywackes subhedral garnet commonly has a smaller grain size of approximately 0.25 mm, but larger grains of 0.5–1 mm are also present (Fig. 4.2.25 d and e). Orthopyroxene is a common mineral in the metapsammites/metagreywackes (Fig. 4.2.25 c and d). The grain size varies between 0.25–0.75 mm and the orthopyroxene shows a mostly anhedral but in places subhedral, grain shape. In the leucosomes larger orthopyroxene grains are present that have a grain size of 1–2 mm. Additionally, biotite and plagioclase are common minerals in these rocks (Fig. 4.2.25 d).

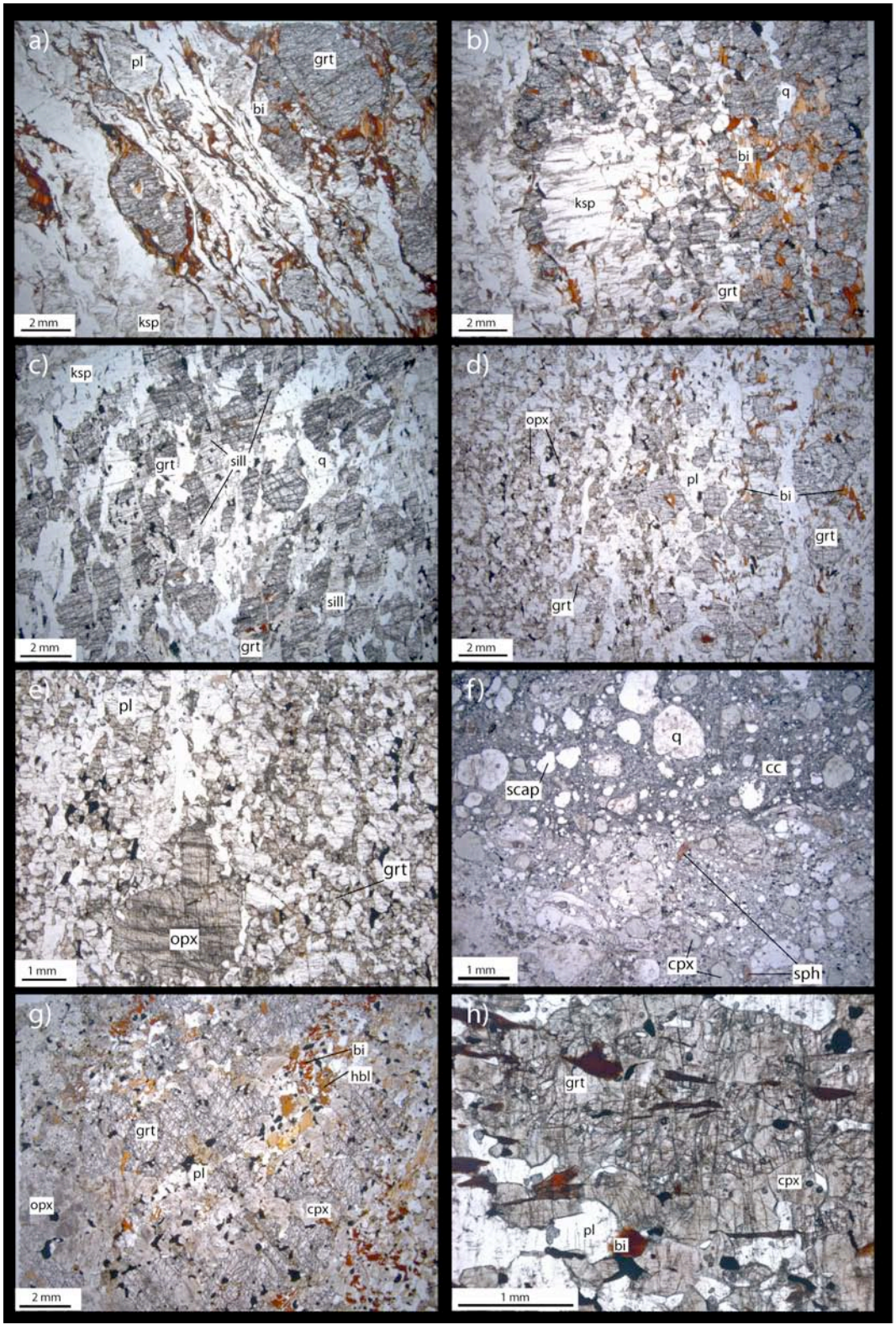

Figure 4.2.25. Photomicrographs illustrating the textures of the rocks in zone 4 between Forno and Piana di Forno: **a)** This sample (IZ 156, located 1 km west of Forno) contains garnet, plagioclase, biotite, quartz, K-feldspar and prismatic sillimanite. In this rock a proto-mylonitic texture is present (in the middle) but also the development of a leucosome (on the left side). In contrast to this, the right side is rich in biotite and garnet. **b)** Another sample of a metapelite (IZ 158) from the same locality as a). Garnet and biotit are enriched on the right side, while the felsic minerals are concentrated mostly on the left side. This sample contains leucosome (left hand side) and residuum

(right hand side). **c)** This sample (IZ 136) is located approximately 1.2 km west of Forno. It contains mostly garnet and sillimanite, additionally quartz and K-feldspar. Biotite is only present as inclusions in garnet. Garnet is in places elongated. The rock has a granoblastic texture with mostly melanocratic minerals. **d)** Illustrated in this picture is a sample (IZ 120) of a metapsammite/metagreywacke from approximate 1 km west of Forno. It is fine grained but has an equigranular texture and contains the mineral assemblage g-opx-pl with minor biotite and quartz. **e)** Orthopyroxene porphyroblast in a metapsammite/metagreywacke (IZ 120). This sample is equigranular and also contains garnet, plagioclase and finer-grained orthopyroxene. **f)** Collected from a river section 1 km west of Forno this sample (IZ 157) shows an ultramylonitic calcsilicate. It comprises porphyroblasts of clinopyroxene, sphene, scapolite and quartz. The dark and light grey matrix is build up by different amounts of calcite. **g)** An example of a metabasite (IZ 138) located 2 km west of Forno. It contains garnet, brown hornblende, plagioclase, orthopyroxene, clinopyroxene and minor biotite. This sample seems to be layered, one layer with biotite, hornblende and plagioclase and another layer with garnet and pyroxenes. **h)** This sample shows a more residual composition of a metabasite (IZ 077), located 1.5 km west of Forno. It consists of mostly garnet and clinopyroxene with minor plagioclase and biotite. Biotite is only present between clinopyroxene and plagioclase grains. The sample has a granoblastic texture.

4.2.5 Zone 5 – Piana di Forno through Campello Monti to the Insubric Line

Zone 5 ranges from the biotite-out isograd at Piana di Forno to the Insubric Line, which is located approximately 500 m west of Campello Monti (Fig. 4.2.26). Beyond the Insubric Line greenschist facies rocks of the Sesia-Lanzo Zone occur (Fig, 4.2.27 f). The Insubric Line consists of a 1 km wide fault zone of extensive faulting and mylonitisation.

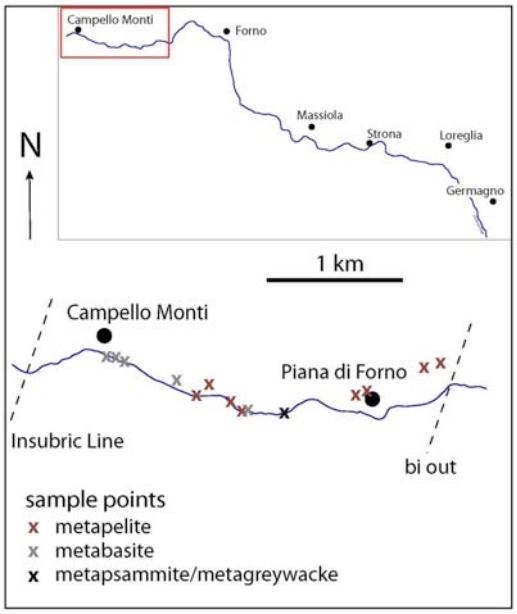

Figure 4.2.26. Overview of zone 5 in Val Strona di Omegna, including sample locations.

The metapelites in zone 5 consist largely of assemblages containing sillimanite, garnet, plagioclase, quartz and K-feldspar. The quartzofeldspatic minerals are concentrated in leucosomes, whereas sillimanite and garnet are concentrated in the melanosome. Rutile and ilmenite are the dominant accessory minerals. The metapelites are predominantly diatexites (Fig. 4.2.27 a and b), with abundant schollen of metapsammite/ metagreywacke and, less commonly,

metabasite. Metatexitic metapelites with a high proportion of leucosome (commonly greater than 15 %; Fig. 4.2.28) also occur in this zone. One metapsammite/metagreywacke sample was found 1 km west of Piana di Forno, containing garnet, plagioclase and orthopyroxene. It contains abundant small leucosomes that contain larger orthopyroxene grains.

The metabasites contain brown hornblende, plagioclase, clinopyroxene and in most samples, orthopyroxene, garnet and minor biotite. The garnet is variable in grain size. 1 km east of Campello Monti at Pian Pennino garnet forms large porphyroblasts (up to 5 cm in diameter) as well as smaller grains within particular layers (less than 0.5 cm) (Fig. 4.2.27 c). This is similar to the garnet in metabasites in a river section around Campello Monti where they also forms porphyroblasts and additionally occur as smaller grains in particular layers of the rock (Fig. 4.2.27 d). Additionally, areas of metabasite without garnet porphyroblasts occur around Campello Monti (Fig. 4.2.27 e).

In thin section two different types of quartz are present. One has a coarse grain size of 2 mm and exists only in the leucosomes (Fig. 4.2.29 b). The second type is very fine grained (0.05–0.1 mm), recrystallised and occurs between garnet and K-feldspar in the melanosomes (Fig. 4.2.29 d). Abundant graphic intergrowth of feldspar and quartz can be observed (Fig. 4.2.29 b). Sillimanite and garnet form elongated grains (Fig. 4.2.29 c) while the latter contains inclusions of biotite, rutile and minor quartz. Additionally, retrograde muscovite can be observed with a similar grain size and orientation as in zone 4.

Figure 4.2.27. Field photographs illustrating the rocks of zone 5 between Piana di Forno and Campello Monti/Insubric Line: **a)** Schollen of metapsammite/metagreywacke and metabasite in a diatexitic metapelite. **b)** Diatexitic metapelite with abundant leucosomes. **c)** Metabasite next to Pian Pennino, 1 km east of Campello Monti. This rock contains abundant garnet in the compositional layering as well as bigger porphyroblasts of garnet (the hammer head is 17 cm long). **d)** Garnet porphyroblasts in a layered metabasite near Campello Monti. The garnet is also exposed in the layering (the hammer head is 17 cm long). **e)** Layered metabasite without garnet porphyroblasts. The garnet only occurs as small grains in the different layers. This outcrop is a few metres away from d). **f)** Greenschist facies rocks north from the Insubric Line.

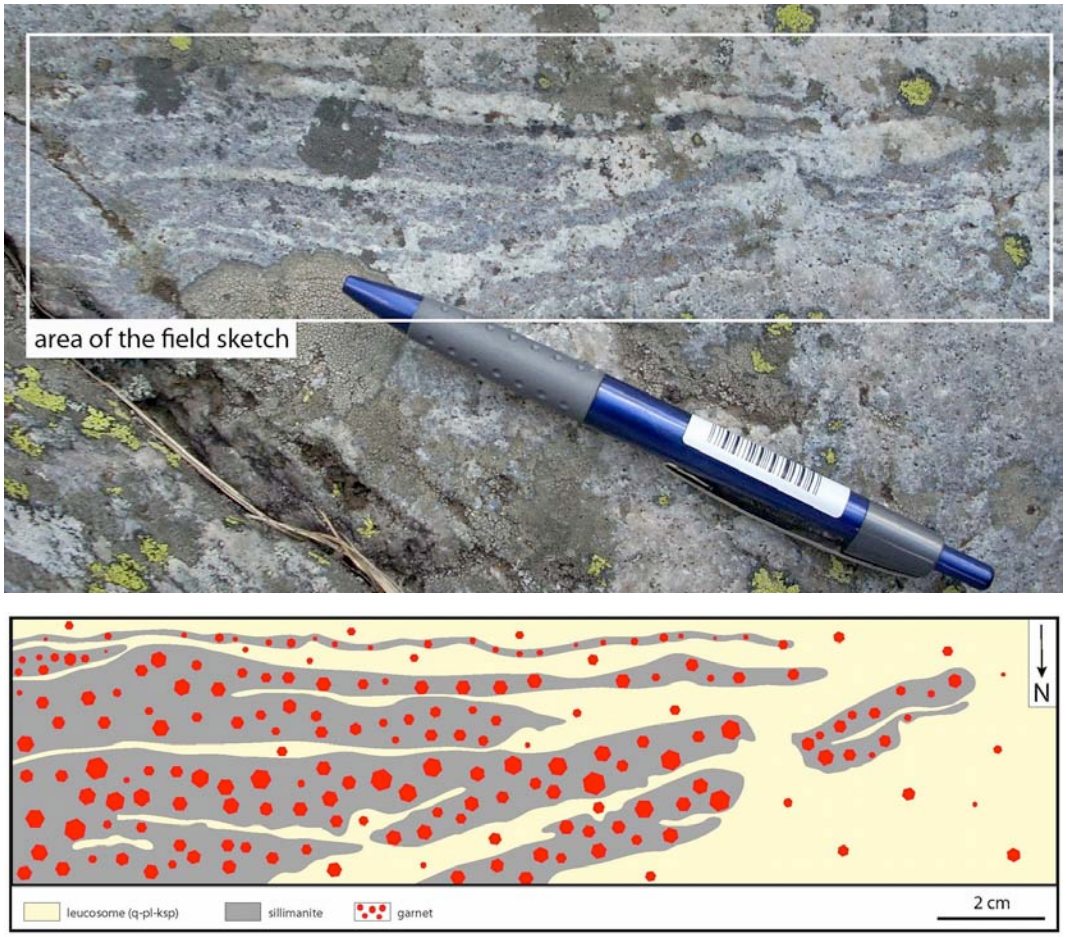

Figure 4.2.28. Field photograph and sketch (10) illustrating a diatexitic metapelite in the high-grade part of granulite facies, located between Piana di Forno and Campello Monti in a river section, approximately 1 km west of Piana di Forno. The diatexitic metapelite consists predominantly of quartz rich leucosome with additionally plagioclase and K-feldspar. This leucosome contains less garnet. The melanosome contains abundant garnet and sillimanite. *Scale on the photo*: the pen is 15 cm long.

Next page:

Figure 4.2.29. Photomicrographs illustrating the textures of the rocks in zone 5 between Piana di Forno and the Insubric Line: **a)** This sample (IV 006) is located approximate 400 m east of Piana di Forno. It consists of garnet, sillimanite with minor K-feldspar (right side) and quartz (left side). Sillimanite occurs between elongated garnet grains. Biotite is only visible as inclusions in the poikiloblastic garnet (upper left part). **b)** A more felsic part of sample IZ 050 located near Piana di Forno dominated by K-feldspar (upper left), plagioclase and quartz. The bigger grain in the middle (right side from the marked plagioclase) shows a mesoperthitic texture. **c)** In contrast to b) this picture of sample IZ 004 located 1 km west of Piana di Forno shows a more melanocratic part of a metapelite. In the middle, elongated garnets and sillimanite prism are present, together with minor biotite and plagioclase on the right hand side. **d)** Same sample as c) under crossed polars (IZ 004). **e)** Garnet, quartz and feldspar from sample IZ 102 (located approximate 500 m east of Campello Monti). The quartz is strongly recrystallised into fine-grained aggregate. In the lower left part larger deformed quartz grains are present. **f)** A pyroxenite (IZ 047) from 500 m east of Campello Monti. It consists of clinopyroxene and brown hornblende and minor ilmenite. **g)** Metabasite (IZ 100) from 100 m south of Campello Monti. It contains granoblastic garnet, clinopyroxene, orthopyroxene, plagioclase and some oxide minerals. **h)** Another section of sample IZ 100. The clinopyroxene grain

in the middle is partly replaced by brown hornblende and minor biotite that is present within the hornblende. Additionally the garnet in the lower part is partially replaced by hornblende.

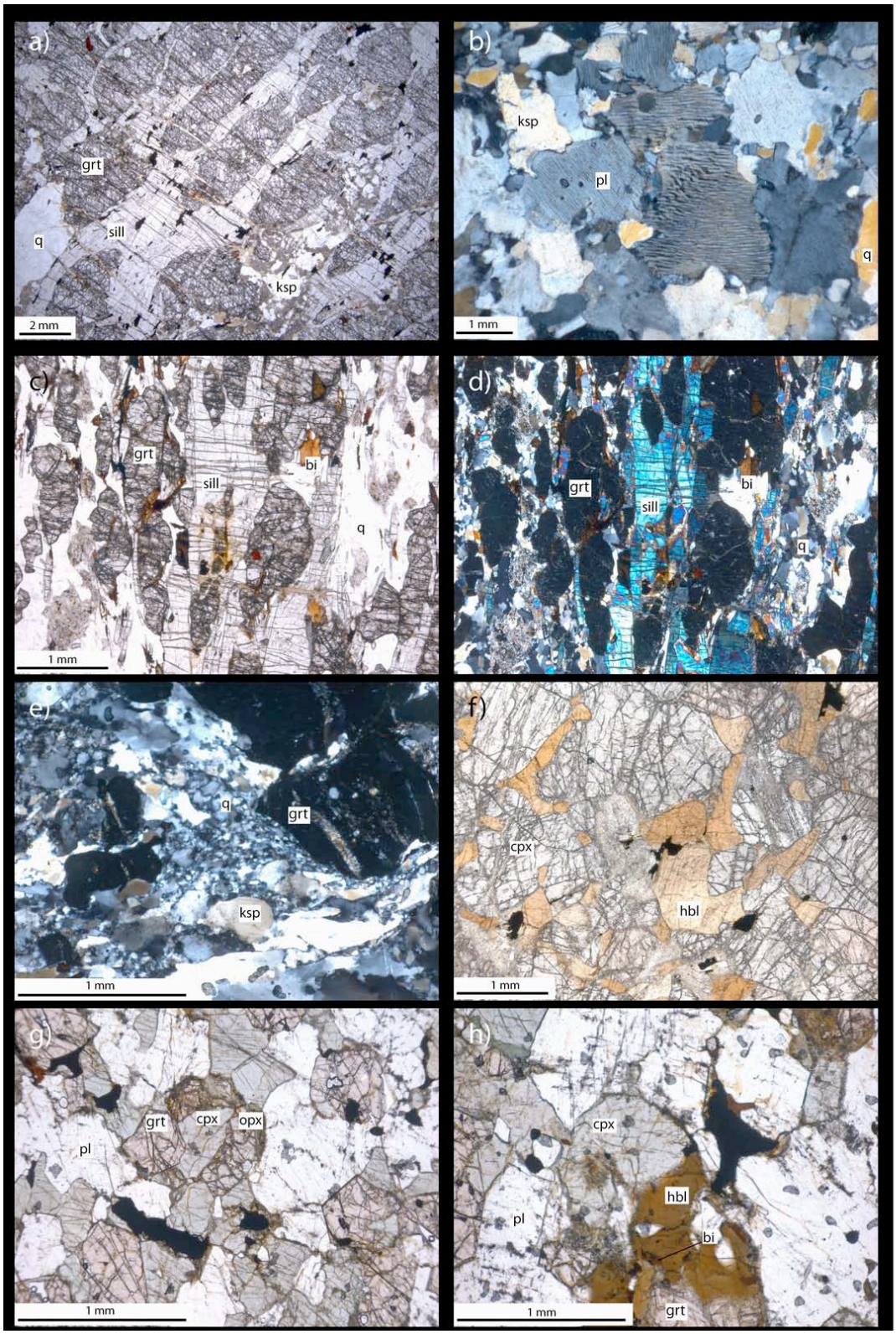

4.3 Val Sesia

Val Sesia represents a section through the Kinzigite Formation and the Mafic Complex (Fig. 4.3.1), although the rocks are very poorly exposed. It is a wide and flat valley with many small lateral valleys. The hillsides around are steeper to the east than to the west, and range up to 1200 m above sea level. Because of the width of the valley, the Sesia river and the vegetation, the rocks of the Kinzigite Formation crop out only sparsely. The dominantly north-south orientation of the river valley is also problematic for establishing mineral isograds, which also trend broadly north-south. According to the geological map of Quick *et al.* (2003), within the Kinzigite Formation only amphibolite facies rocks occur.

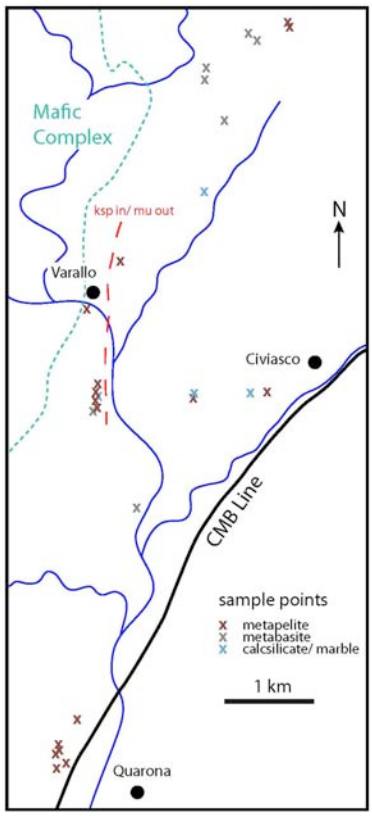

Figure 4.3.1. Overview for Val Sesia, including sample locations and the extrapolated mineral isograd mu-out/ksp-in. The border with the Mafic Complex is defined according to Quick *et. al* (2003).

The metapelites in Val Sesia vary in their mineral assemblage. Around Civiasco they consist of biotite, muscovite, fibrolitic sillimanite, plagioclase and quartz. One sample also contains garnet. The rocks are foliated and exhibit a schistosity (Fig. 4.3.2 a and b). In the neighbouring valley to the northwest the metapelites are also mica-schists with biotite, plagioclase, sillimanite and garnet, some with muscovite and some with K-feldspar. To the south of Varallo and west of Quarona (Fig. 4.3.1) the rocks consist of biotite, garnet, plagioclase, fibrolitic sillimanite, quartz and minor cordierite. One sample contains additionally K-feldspar, while others contain muscovite. Near to Varallo in a river section, the metapelites are strongly folded metatexites (Fig. 4.3.2 d). These rocks consist of garnet, biotite, plagioclase, K-feldspar, fibrolitic to prismatic sillimanite and minor cordierite, but no muscovite occurs. The muscovite-out/K-feldspar-in isograd can therefore be assumed to lie east of Varallo (Fig. 4.3.1).

Metabasites are less abundant in Val Sesia compared with Val Strona di Omegna. To the north of Varallo, they comprise green hornblende and plagioclase. In one sample biotite, clinopyroxene and garnet are also present. The rocks are compositionally layered (defined by variations in the proportions of hornblende and plagioclase) and show no evidence for partial melting. South of Varallo, metabasites are also compositionally layered and contain green and brown hornblende, plagioclase, clinopyroxene, biotite, orthopyroxene and garnet, also without evidence for partial melting. Based on the presence of both ortho- and clinopyroxene, these rocks record granulite facies conditions. Next to Civiasco and north of Varallo calcsilicates with clinopyroxene and plagioclase are exposed (Fig. 4.3.2 c).

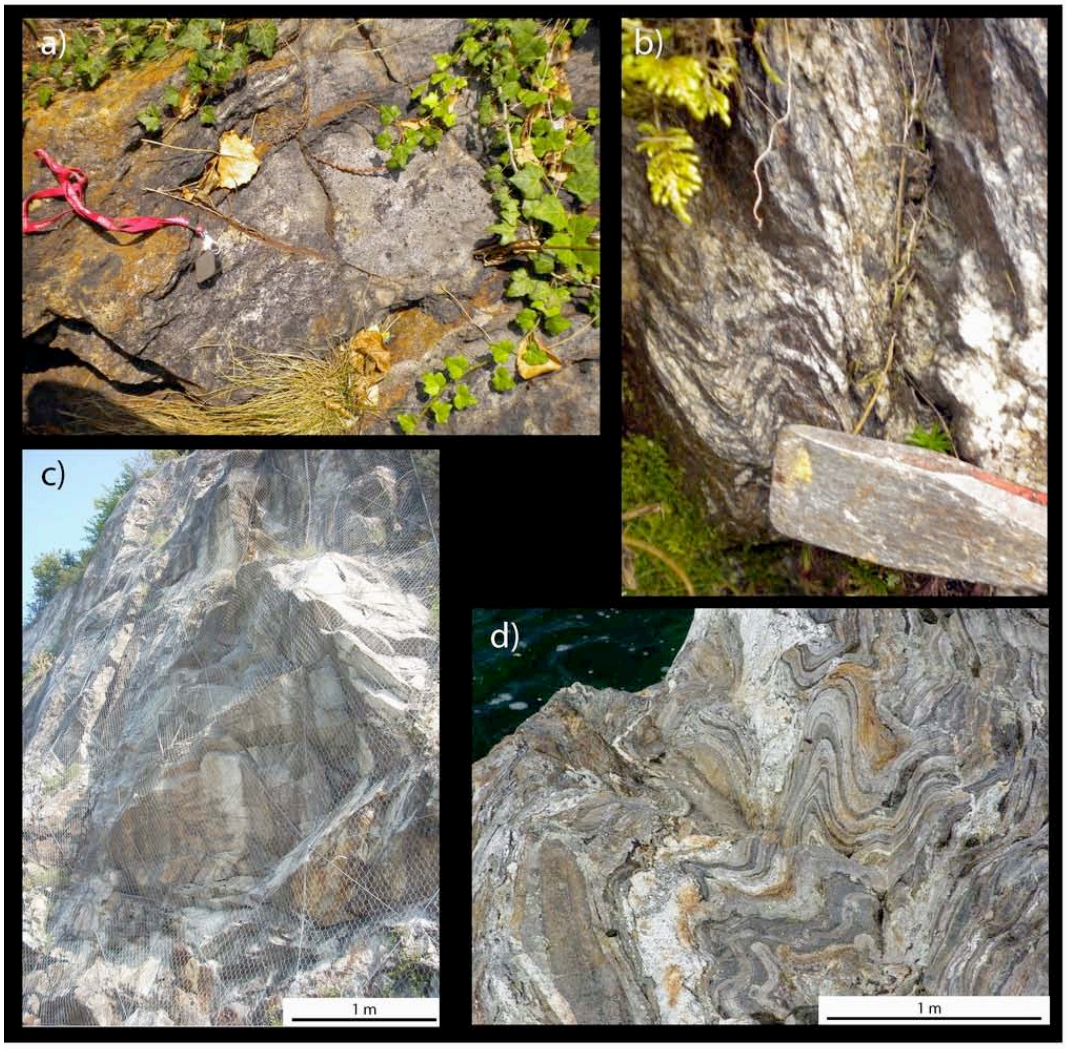

Figure 4.3.2. Field photographs illustrating the rocks in Val Sesia: **a)** Cursory weathered mica-schist near Civiasco. **b)** Folded mica-schist (the chisel is 4 cm wide). **c)** Street outcrop of calcsilicates between Civiasco and Varallo **d)** Metatexitic and folded metapelites in a river section next to Varallo.

In thin section, quartz is the most common mineral in the metapelites. The grains are mostly anhedral and sub-rounded with an average grain size of 1–2 mm. Plagioclase is also common and commonly shows multiple twinning. The grains are subhedral to anhedral and rarely euhedral with a variable grain size of 0.2 to 2 mm. In some samples sericitization occurs at the rims of the plagioclase grains. K-feldspar is very rare and only present in samples around Varallo, where it occurs as anhedral grains that are commonly sericitized. In the highest grade sample (IZ 201) K-feldspar exhibits a myrmekitic texture and also minor intergrowth between K-feldspar and quartz (granophyre) are present. Garnet in the lower grade part of Val Sesia has an average grain size of 0.5–1 mm. It is commonly poikiloblastic with inclusions of quartz, biotite and oxide minerals and in places elongated (Fig. 4.3.3 a and b). Towards the border of the Mafic Complex garnet occurs as smaller rounded grains (average size 0.25–0.5 mm) and has very few inclusions (Fig. 4.3.3 c and e). Biotite is also a common mineral in the metapelites and is in places overgrown by sillimanite (Fig. 4.3.3 e). In addition, intergrowths of biotite and sillimanite are common (Fig. 4.3.3 a and b). Some samples contain retrograde muscovite, which cross cuts the foliation defined by biotite and sillimanite. Muscovite is commonly in contact with K-feldspar. Cordierite is present in sample IV 026 and IZ 201 next to the border of the Mafic Complex and in sample IV 034 next to the granites of the Strona-Ceneri Zone. The grain size of cordierite varies between 0.25–1 mm with grains typically anhedral. In places the grains are more rounded. Cordierite appears in general adjacent to sillimanite, biotite and K-feldspar.

Next page:

Figure 4.3.3. Photomicrographs illustrating the textures of the rocks in Val Sesia: **a)** This picture from sample IV 028 shows a typical biotite rich mica-schist in Val Sesia. The biotite and sillimanite anastomoses the larger garnet grains. In the upper left a mat of fibrolitic sillimanite is observable. **b)** Illustrated here (IV 028) is a kink fault in a band of biotite and sillimanite between garnet and plagioclase. The garnet is minor elongated and contains inclusions of biotite. **c)** Rounded garnet grains of sample IZ 201 located next to Varallo. The garnets generally lack inclusions. This sample also contains K-feldspar, quartz and biotite. **d)** Another picture from sample IZ 201 illustrating deformed biotite-sillimanite intergrowth. These intergrowths enclose a deformed quartz grain (middle) and garnet grains. The garnet in this part of the rock contains rare inclusions of quartz. **e)** A former biotite fish from sample IZ 201 that is now almost completely pseudomorphed by fibrolitic sillimanite. A small cordierite grain is also visible here. **f)** This picture shows an example of a metabasite in Val Sesia (IV 030) located 1 km south of Varallo. It contains green hornblende, plagioclase, garnet and minor biotite. The garnets have a skeletal shape and contain inclusions of quartz and oxides. **g)** Compositional layering of a metabasite on a microscopic scale from sample

IZ 171. On the left side green hornblende, clinopyroxene and minor plagioclase are dominant. To the middle this changes to minor green hornblende, clinopyroxene, plagioclase and biotite. On the right side garnet is the dominant mineral, together with plagioclase and biotite. The garnet is skeletal and has inclusions of oxides**. h)** This picture shows a typical marble in Val Sesia located approximately 1 km southeast of Varallo (IZ 175).

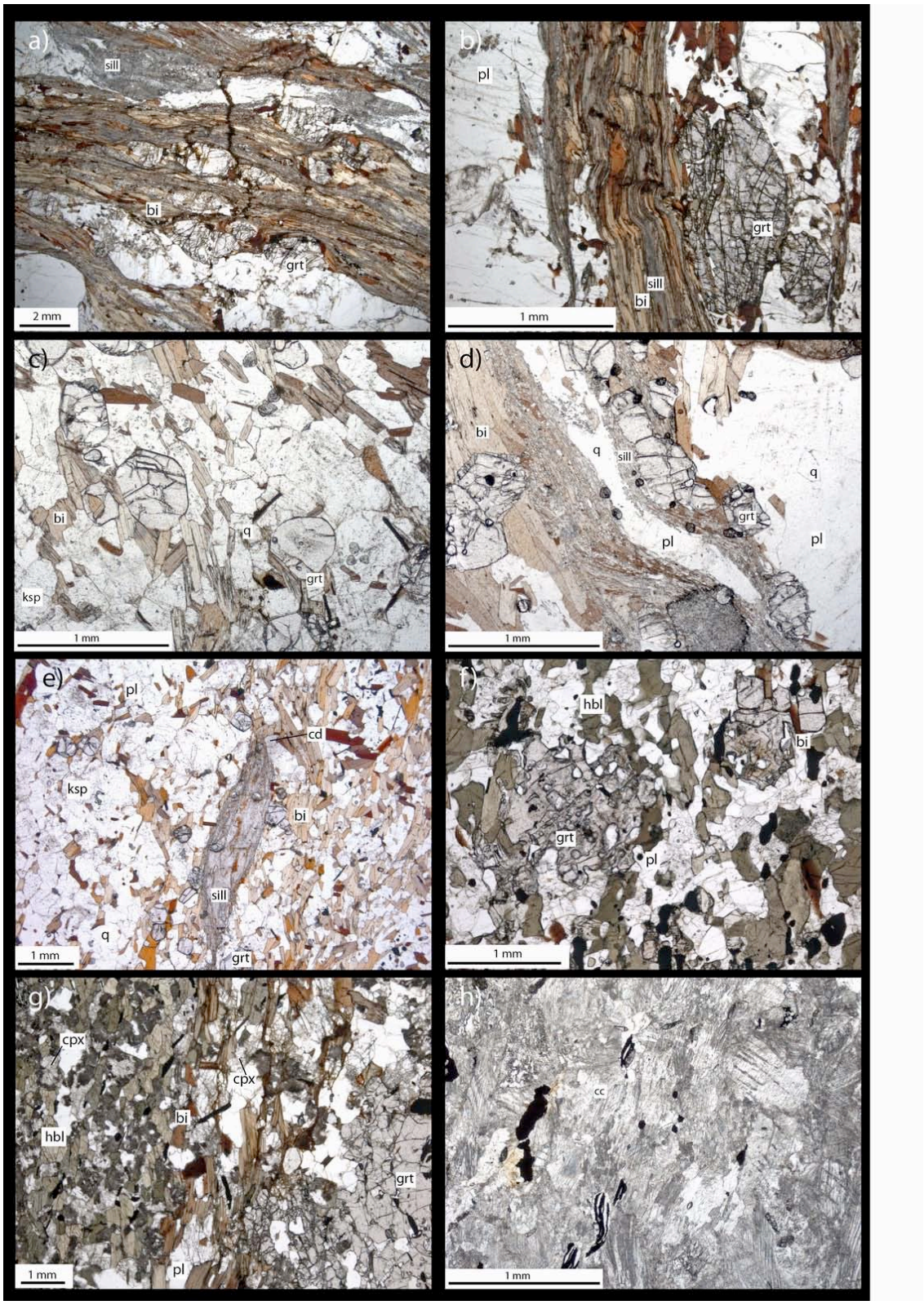

4.4 Val Strona di Postua

Val Strona di Postua is an approximately 10 km long section through the southern part of the Ivrea Zone and traverses the rocks of the Kinzigite Formation and the Mafic Complex. It is a flat-floored valley with steep hillsides and ranges from Crevacuore at 377 m above sea level to the spring of the Strona di Postua river in the mountains at around 1400 m above sea level. The section through the Kinzigite Formation is nearly perpendicular to the strike direction of the rocks. In the southern part of Val Strona di Postua no useful outcrops were found, and studied outcrops starts at Roncole village and extend to the north/northwest to the border with the Mafic Complex (Fig. 4.4.1), a distance of around 2–3 km. According to Quick *et al.* (2003), the exposed rocks are all amphibolite facies rocks. No mineral isograds were identified and the rocks are described from southeast to northwest.

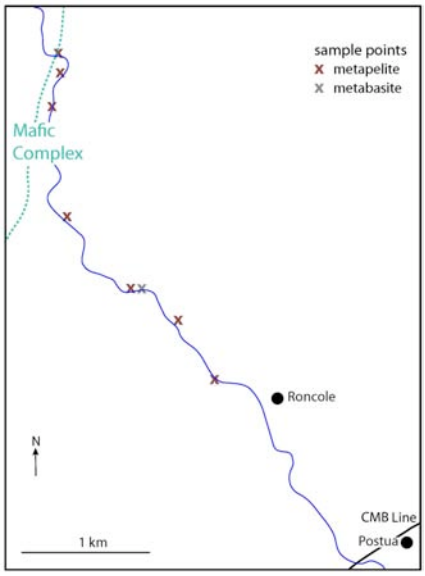

Figure 4.4.1. Overview for Val Strona di Postua, including sample locations. The boundary to the Mafic Complex is defined according to Quick *et. al.* (2003).

Approximately 300 m northwest of Roncole, schistose metapelites contain garnet, biotite, plagioclase, sillimanite, quartz, cordierite and spinel. Further to the northwest thin layers of metabasite and meta-semipelite are intercalated with the metapelites. Around 1 km northwest of Roncole the metapelites contain garnet, biotite, plagioclase, fibrolitic sillimanite, quartz, cordierite, K-feldspar and rutile. One exposed metabasite 1 km northwest of Roncole is fine grained and contains green hornblende and plagioclase in varying proportions defining a compositional layering. There is no evidence for partial melting. Further to north, the rocks have a gneissose structure and have a variable composition. All contain garnet, biotite, plagioclase, cordierite and quartz, but vary in their proportions of K-feldspar and fibrolitic to prismatic sillimanite. The metapelites contain abundant quartz veins (Fig. 4.4.2 a), similar to the rocks of zone 2 in Val Strona di Omegna (Strona to

Massiola). Further to northwest rare metabasites crop out and exhibit a metatexitic to diatexitic structure. At the point where a walking track crosses the river, next to the border with the Mafic Complex, the rocks show evidence for partial melting. The metapelites have a diatexitic structure and contain schollen of metabasite and/or metapsammite/metagreywacke (Fig. 4.4.2 b and c). The metabasites also have a diatexitic structure. Rocks of the Mafic Complex are not exposed, although according to the map of Quick *et al.* (2003) leucotonalites and granodiorites of the Mafic Complex should crop out here.

Figure 4.4.2. Field photographs illustrating the rocks in Val Strona di Postua, north of Roncole: **a)** Biotite-schist with abundant quartz veins 1.5 km of northwest of Roncole. **b)** Schollen of metabasites in a leucosome rich partial melted metapelite. The metabasites also contain small leucosomes. **c)** A metapsammite/metagreywacke scholle (green grey) with a selvedge of biotite (brownish) in a partial melted metapelite. The metapelite contains abundant garnet and many leucosomes of different sizes whereby the rock show a diatexitic structure (the part of the shoe is 18 cm long). **d)** In this picture another metatexitic to diatexitic metapelite is visible. The leucosomes contain garnet and biotite, while the dark parts between them consist only of biotite. On the left side schollen of metapsammite/metagreywacke with a small selvedge of biotite are present (the visible part of the shoe is 12 cm long).

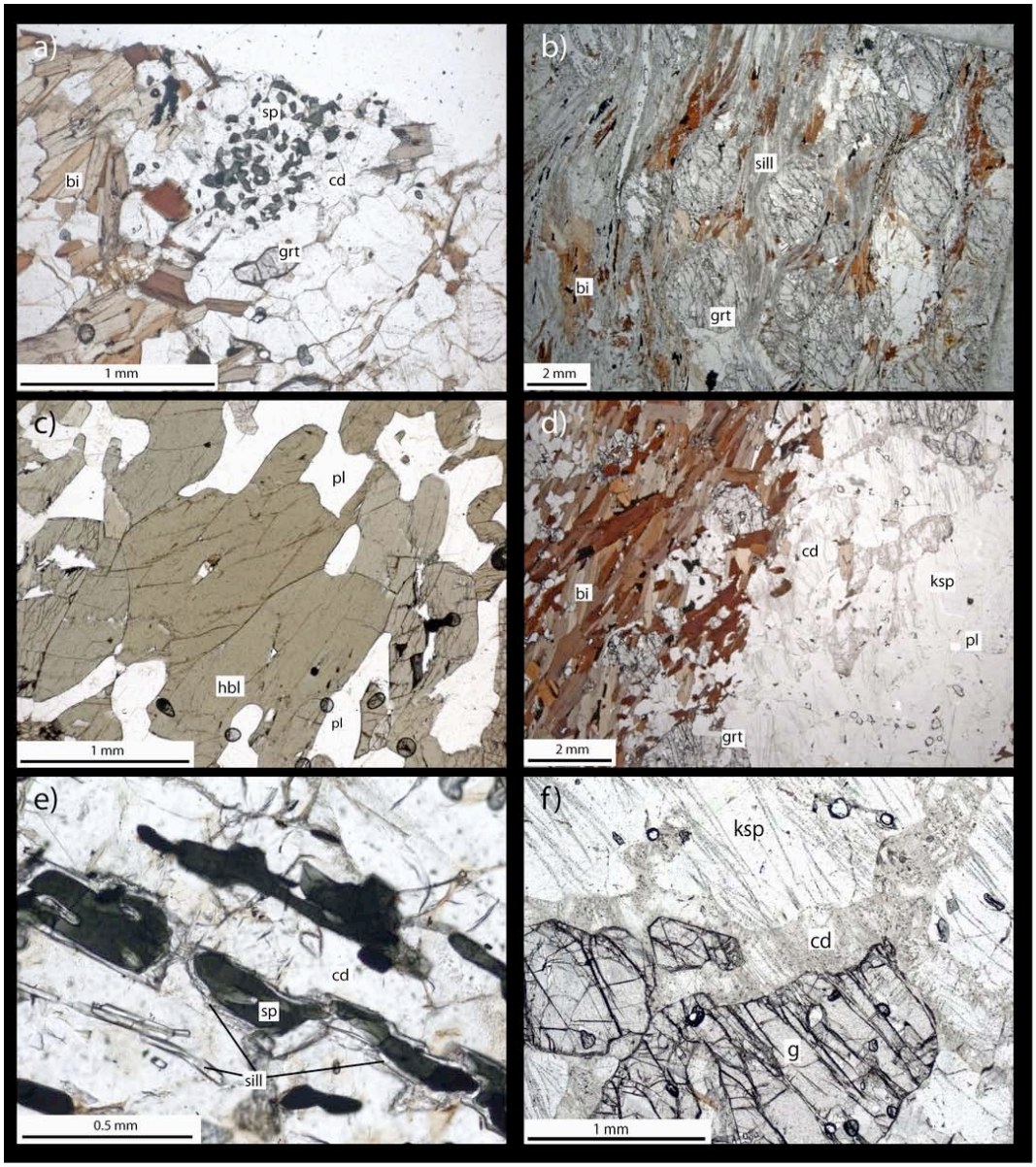

Figure 4.4.3. Photomicrographs illustrating the textures of the rocks in Val Strona di Postua: **a)** A section from sample IZ 132 approximately 250 m west of Roncole. It contains garnet, biotite, plagioclase, quartz and fibrolitic sillimanite. Also observable are small grains of hercynitic spinel within cordierite grains. **b)** This sample (IZ 133) is located around 500 to 750 m northwest of Roncole and contains garnet, biotite, fibrolitic sillimanite, plagioclase and quartz. Sillimanite overgrowths and replaces the biotite and also enclosed larger garnet grains. **c)** Typical appearance of a metabasite in the lower part of this valley (IZ 134). It comprises mostly green hornblende and plagioclase. **d)** This picture shows a cordierite-bearing metapelite (IZ 165). On the left side it is dominated by biotite, garnet and minor sillimanite, while to the right side cordierite, K-feldspar and plagioclase are observable. Cordierite is always in contact with garnet and/or K-feldspar. **e)** A more detailed look to spinel grains in sample IZ 132. Spinel is within cordierite grains, while sillimanite forms a corona around spinel. **f)** Illustrated in this picture of sample IZ 165 are garnet grains that are surrounded by cordierite and K-feldspar. On the left hand side cordierite also occurs between two K-feldspar grains. The garnet contains inclusion of quartz and minor oxides.

In the thin sections of metapelite, quartz is one of the most common minerals with anhedral grains of an average size of 0.5–2 mm. Plagioclase is also common, forming mostly subhedral to anhedral and rarely euhedral grains with a variable grain size of 0.2 to 2 mm. Anhedral K-feldspar is present in two samples and is very commonly sericitized. It is mostly present adjacent to cordierite in the samples. The felsic minerals exhibit myrmekitic textures and intergrowths of feldspar and quartz are abundant. Garnet in Val Strona di Postua has an average grain size around 2–4 mm. In the lower grade samples the grains are slightly elongated and poikiloblastic with minor inclusions of quartz. Towards the boundary of the Mafic Complex garnet becomes more skeletal and contains abundant inclusions of quartz, biotite and oxide minerals. Biotite is very common and commonly intergrown with fibrolitic sillimanite. Cordierite is also common in the rocks of Val Strona di Postua. It is anhedral with an average grain size of 2–3 mm and mostly concentrated around garnet and K-feldspar grains. Cordierite is pinitized in the highest grade rock. Spinel is present in two samples. It has a dark green colour characteristic for hercynitic spinel, and occurs as small rounded anhedral grains (< 0.05 mm). Spinel only occurs within cordierite grains and has in places a corona of sillimanite (Fig. 4.4.3 a and e), suggesting this mineral is not necessarily in equilibrium with the other matrix minerals, especially quartz.

Chapter 5
Whole rock and mineral geochemistry

5.1 Introduction

In this Chapter the results of whole rock and mineral element analysis are presented. For Val Strona di Omegna and Val Strona di Postua the data are ordered from low-grade to high-grade conditions, while in Val Sesia the data are ordered up river from Quarona through Civiasco to Varallo (Chapter 5.2). Harker diagrams are presented only for samples from Val Strona di Omegna. For the mineral geochemistry (Chapter 5.3) the results from all three valleys are presented together. Detailed data including values for whole rock analyses and mean values for single mineral (with standard division) are given in Appendix A and B.

5.2 Whole rock analyses

5.2.1 Val Strona di Omegna

For whole rock analyses of major elements, 33 representative samples of metapelites and 3 samples of metapsammite/metagreywacke were chosen. These are organised from low-grade to high-grade conditions appropriate to their location in the valley in Table 5.2.1 (Appendix A). In this study, 13 samples from the amphibolite facies (zone 1 and 2), 13 samples from the transition zone (zone 3) and 7 samples from the granulite facies (zone 4 and 5) are presented. One sample of the metapsammites/metagreywackes is located in the amphibolite

facies north of Germagno, while both others samples are from the granulite facies, located to the southwest of Forno and east of Piana di Forno.

		q	ksp	pl	g	sill	bi	mu	ru	cd	opx
IZ 008	amphibolite facies	x	(x)	x		x	x	x			
IZ 009		x	(x)	x		x	x	x		x	
IZ 010		x		x		x	x	x			
IZ 011		x		x		x	x	x	x		
IZ 015		x		x			x	x	x		
IZ 017		x		x		x	x	x	x	x	
IZ 018		x	x	x		x	x	x			
IZ 013		x		x		x	x	x		x	
IZ 019		x		x			x	x			
IV 059		x	x	x		x	x	x			
IZ 061		x		x		x	x	x			
IV 019		x	x	x			x	x			
IZ 029		x	x	x		x	x	x			
IZ 028	transition zone	x	x	x	x	x	x				
IV 058		x		x	x	x	x	x			
IZ 033		x	x	x	x	x					
IV 020		x	x	x	x	x	x				
IZ 030		x		x	x	x	x				
IZ 036		x	x	x	x	x	x				
IZ 112		x	x	x	x	x	x				
IV 054		x	x	x	x	x	x				
IV 052		x	x	x	x	x	x				
IZ 066		x	x	x	x	x	x		x		
IV 048		x	x	x	x	x	x				
IV 049		x	x	x	x	x	x				
IZ 146		x		x	x		x				
IZ 156	granulite facies	x	x	x	x		x				
IV 044		x	x	x	x			x			
IZ 072		x	x		x	x	x				
IZ 005		x	x	x	x	x	x		x		
IZ 070		x	x		x	x	x	x	x		
IZ 049		x	x	x	x	x			x		
IZ 102		x	x	x	x				x		
IZ 140		x		x	x		x				
IZ 120		x		x	x		x				x
IZ 129		x		x	x		x				x

Table 5.2.1. Major mineral assemblages in samples from Val Strona di Omegna sorted from low-grade (top) to high-grade conditions (bottom). The top 33 samples show the assemblages typical of the metapelites. The last three samples are from metapsammites/metagreywackes (IZ 140: amphibolite facies, IZ 120 and IZ 129: granulite facies).

In general, metapelites throughout the valley show a more or less continuous trend in TiO_2, FeO, P_2O_5 and LOI from low-grade to high-grade conditions (Fig. 5.2.1, 5.2.3). The values for TiO_2 and FeO slightly increase, while the values for P_2O_5 and LOI slightly decrease. For some elements (e.g. SiO_2, TiO_2 and FeO) the highest/lowest values are present in more than one zone, which results from the

strong variation in the composition of the samples, and will be described in the following.

Most of the amphibolite facies samples do not show any clear continuous trend in major element oxides other than MnO (Fig. 5.2.2). MnO values decrease from sample IZ 008–IZ 017 and increase from sample IZ 017–IV 059. Sample IZ 017 has the lowest MnO content in the valley. Another trend can be observed in the increasing LOI contents from samples IZ 061–IV 058 across the muscovite-out isograd. For all other major elements, the values are highly variable. The highest values for SiO_2, MgO, Na_2O, K_2O, P_2O_5 and LOI as well as the lowest values for Al_2O_3, FeO, MnO, MgO, CaO and Na_2O are present in diverse samples in the amphibolite facies.

In the transition zone, a trend in the concentration of CaO, Na_2O, K_2O and P_2O_5 can be observed (Fig. 5.2.2, 5.2.3). The values for K_2O and P_2O_5 decrease upgrade, while the values for CaO and Na_2O increase upgrade. Further, a trend with increasing (IZ 029–IV 020) and decreasing (IV 020–IV 049) values for MnO is evident, with sample IZ 066 containing higher values and the highest MnO content in sample IV 020. The highest values for TiO_2, Al_2O_3, FeO, MnO and LOI as well as the lowest values for SiO_2, TiO_2, P_2O_5 and LOI are present in samples from the transition zone.

In the granulite facies, no clear trend for any major element can be observed. Samples from this facies contain the highest values for TiO_2, FeO, MnO and CaO and the lowest values for TiO_2, Al_2O_3, CaO, K_2O and P_2O_5 and LOI in the valley.

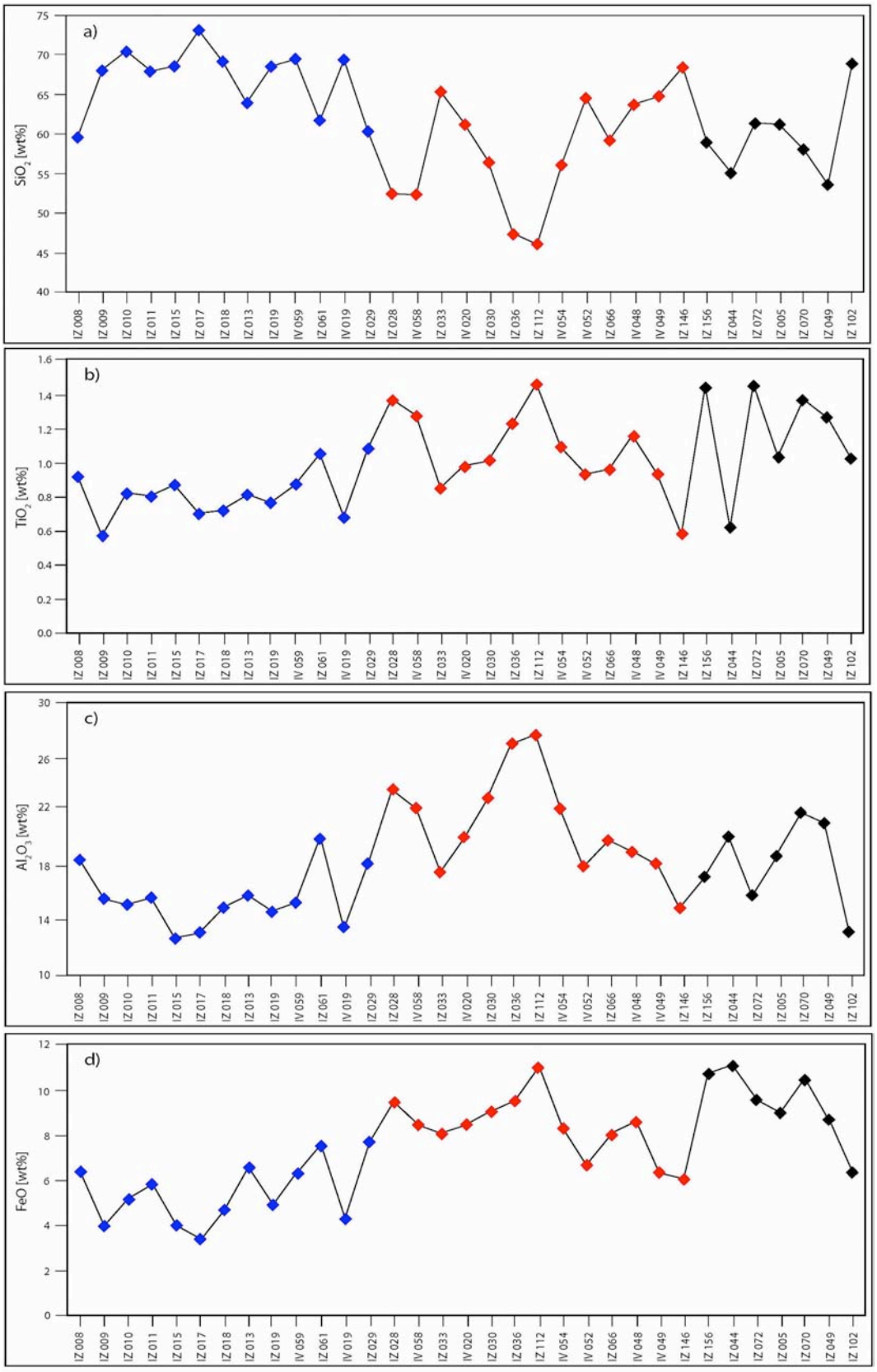

Figure 5.2.1. Bulk rock concentrations of SiO_2 (a), TiO_2 (b), Al_2O_3 (c) and FeO (d) ordered from low-grade (left) to high-grade (right) conditions. Blue, red and black samples are from the amphibolite facies, the transition zone and the granulite facies respectively, identical with Tab. 5.2.1.

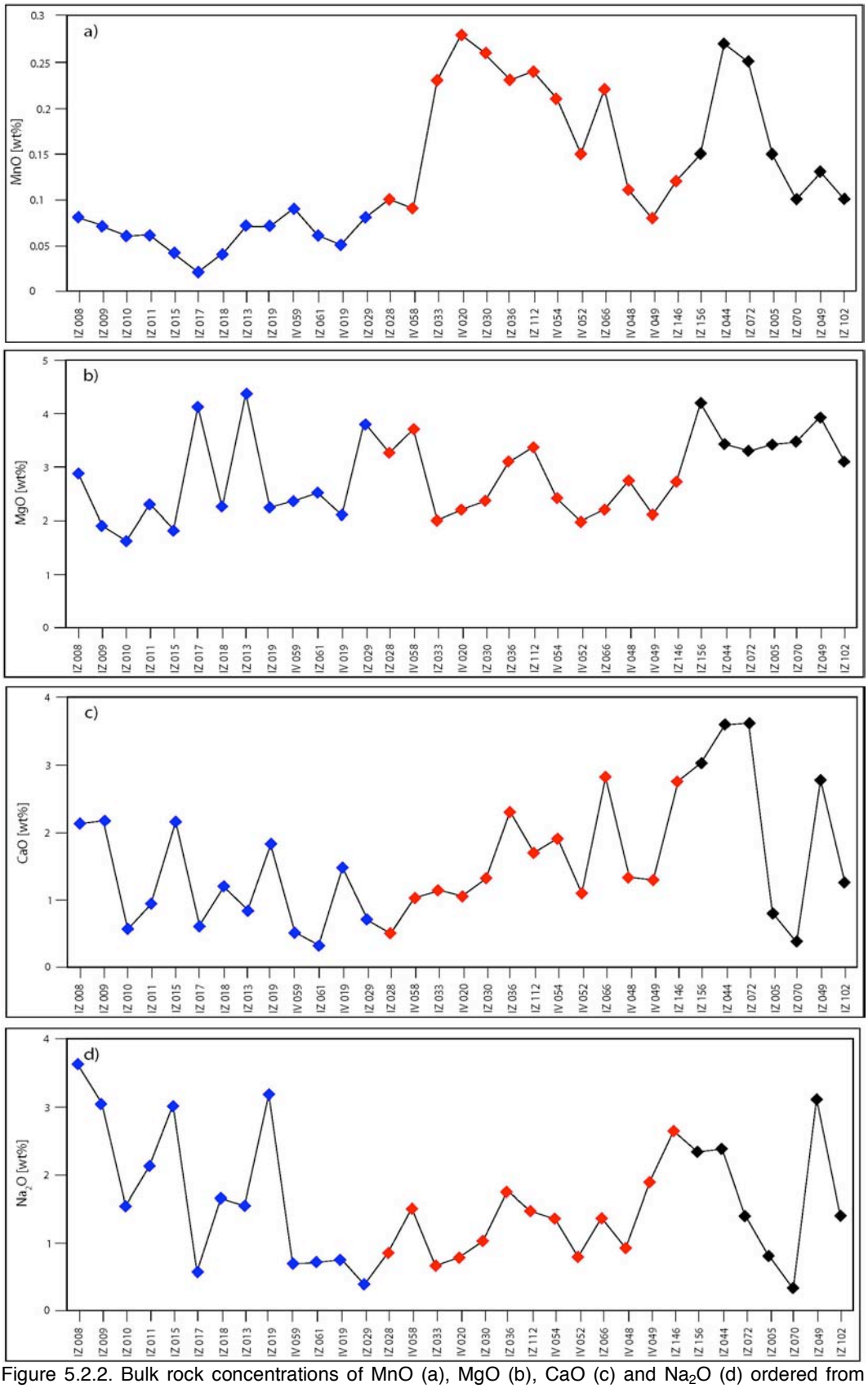

Figure 5.2.2. Bulk rock concentrations of MnO (a), MgO (b), CaO (c) and Na_2O (d) ordered from low-grade (left) to high-grade (right) conditions. Blue, red and black samples are from the amphibolite facies, the transition zone and the granulite facies respectively, identical with Tab. 5.2.1.

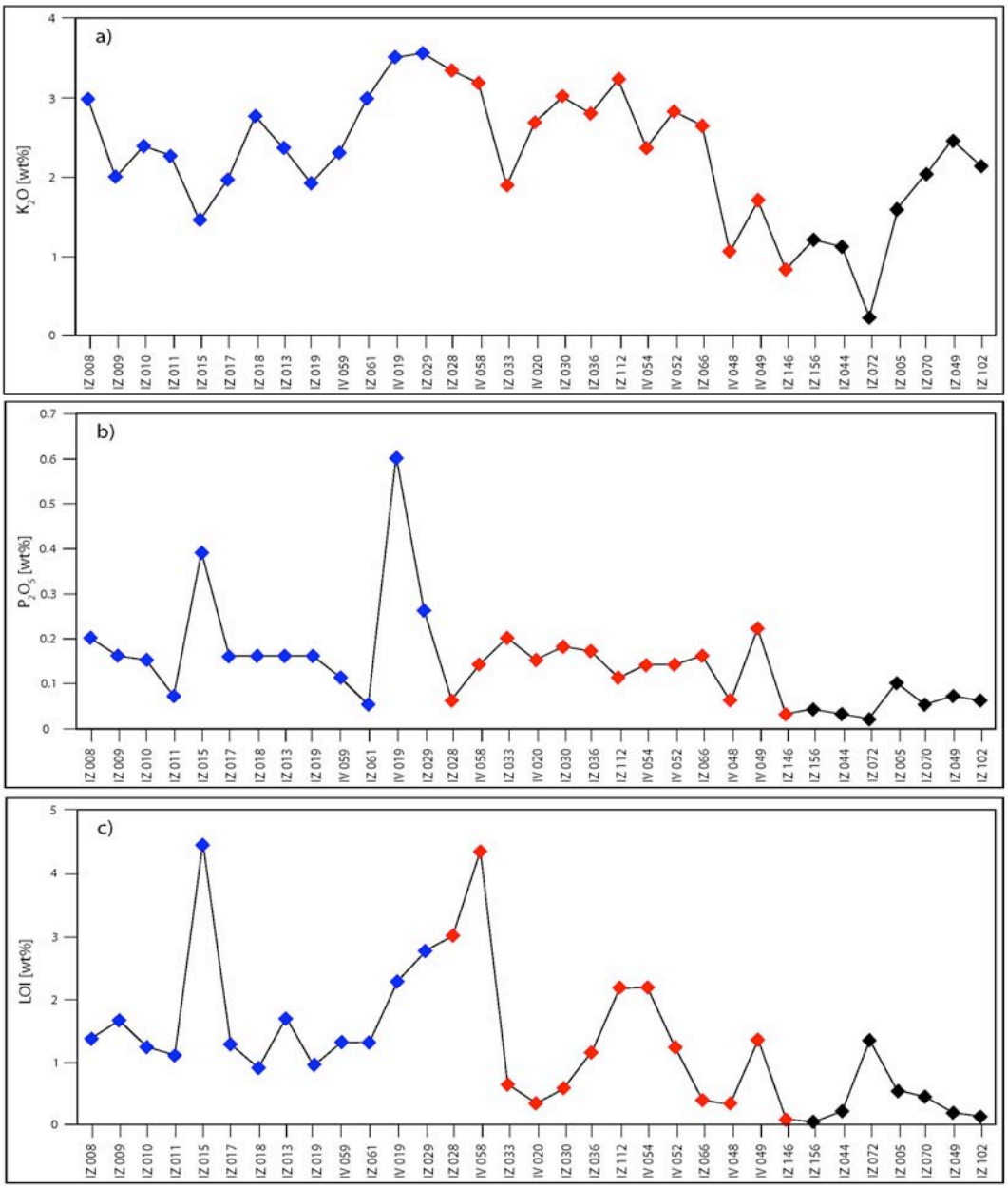

Figure 5.2.3. Bulk rock values for K_2O (a), P_2O_5 (b) and LOI (c) sorted from low-grade (left) to high-grade (right) conditions. Blue, red and black samples are from the amphibolite facies, the transition zone and the granulite facies respectively, identical with Tab. 5.2.1.

In Fig. 5.2.4 the amount of $Na_2O + K_2O$ is compared with the amount of $Fe_2O_3 + MgO + TiO_2$ (here, Fe_2O_3 is the amount of total Fe measured by XRF, Appendix A). In general the amphibolite facies samples are richer in $Na_2O + K_2O$ than the granulite facies samples, which contain more $Fe_2O_3 + MgO + TiO_2$. The granulite facies samples with lower $Fe_2O_3 + MgO + TiO_2$ contains more leucosome than melanosome in the field. One of the amphibolite facies samples (IZ 013) with a higher amount of $Fe_2O_3 + MgO + TiO_2$ contains cordierite. Another sample (IZ

008) is very rich in $Na_2O + K_2O$ that can be explained by the high amount of muscovite and also K-feldspar in the appropriate sample. Samples from the transition zone range in their $Na_2O + K_2O$ and $Fe_2O_3 + MgO + TiO_2$ contents between those of the amphibolite and those of the granulite facies samples, while samples from the granulite facies show a higher amount of $Fe_2O_3 + MgO + TiO_2$ with lower values for $Na_2O + K_2O$. These observations are consistent with the granulite facies samples having lost some melt. Figure 5.2.5 supports this suggestion by showing more silica-rich samples in the amphibolite facies and more $Fe_2O_3 + MgO$-rich samples in the granulite facies that are poorer in SiO_2. Four samples (IZ 008, IZ 013, IZ 061 and IZ 029) from the amphibolite facies are different and plot between amphibolite and granulite facies samples. These samples contain cordierite or a large amount of biotite. Further evidence that samples in the granulite facies lost melt is shown in Fig 5.2.6. Amphibolite facies samples in general are richer in both $Na_2O + K_2O$ and SiO_2 but poorer in Al_2O_3 than samples from the granulite facies (Fig. 5.2.7). For one of the granulite facies samples (IZ 102), all values are similar to values of the amphibolite facies samples. This suggests that the amphibolite facies samples can be considered as appropriate protoliths for the granulite facies migmatites.

In an isocon diagram (following Grant, 1986; Grant, 2005) the average concentration of major elements in the amphibolite facies is compared with the average concentration of major elements in the granulite facies (Fig. 5.2.8). Assuming TiO_2 is an immobile phase the slope of the isocon yields a change in the mass of the oxides, due to some open-system process such as the lost of melt in the granulite facies. The diagram suggests a stronger depletion of SiO_2 and K_2O and a weaker depletion of Al_2O_3 outside their uncertainty bars in granulite facies samples in comparison to amphibolite facies samples. All other elements may reflect a loss or gain in mass but within the error of constant mass. The slope of the isocon suggests that the granulite facies samples lost an amount of around 40% mass/melt, which is consistent to the depletion of the oxides mentioned above.

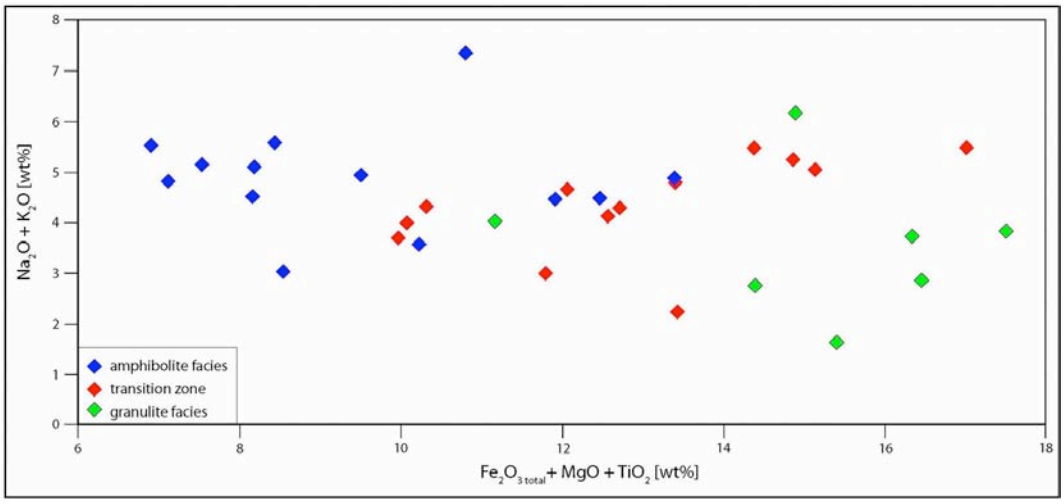

Figure 5.2.4. Diagram for the amount of $Na_2O + K_2O$ against $Fe_2O_{3\ total} + MgO + TiO_2$ in metapelites from Val Strona di Omegna. $Fe_2O_{3\ total}$ is the amount of all Fe measured from XRF ($FeO + Fe_2O_3$).

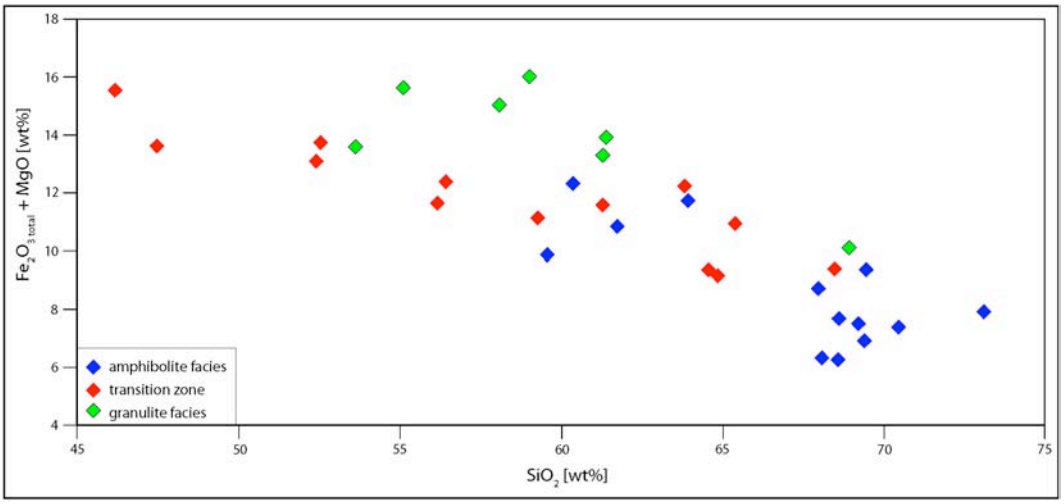

Figure 5.2.5. Diagram for the amount of SiO_2 against $Fe_2O_{3\ total} + MgO$ in metapelites from Val Strona di Omegna. $Fe_2O_{3\ total}$ is the amount of all Fe measured from XRF ($FeO + Fe_2O_3$).

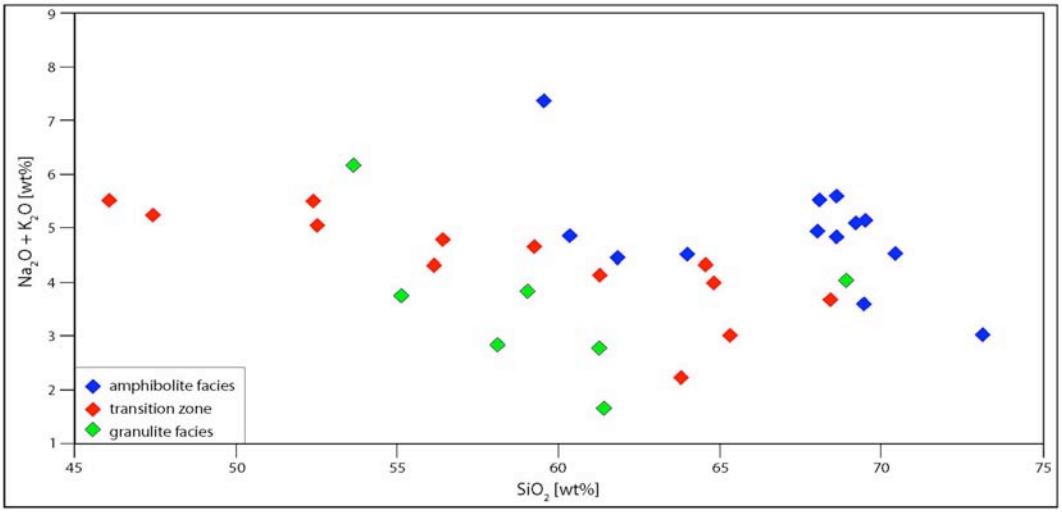

Figure 5.2.6. Diagram for the amount of SiO_2 against $Na_2O + K_2O$ in metapelites from Val Strona di Omegna.

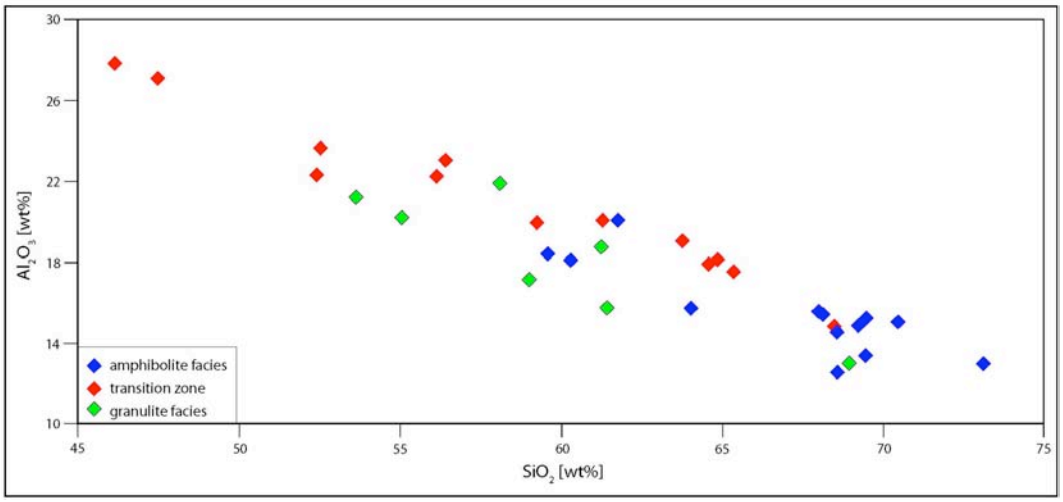

Figure 5.2.7. Diagram for the amount of SiO_2 against Al_2O_3 in metapelites from Val Strona di Omegna.

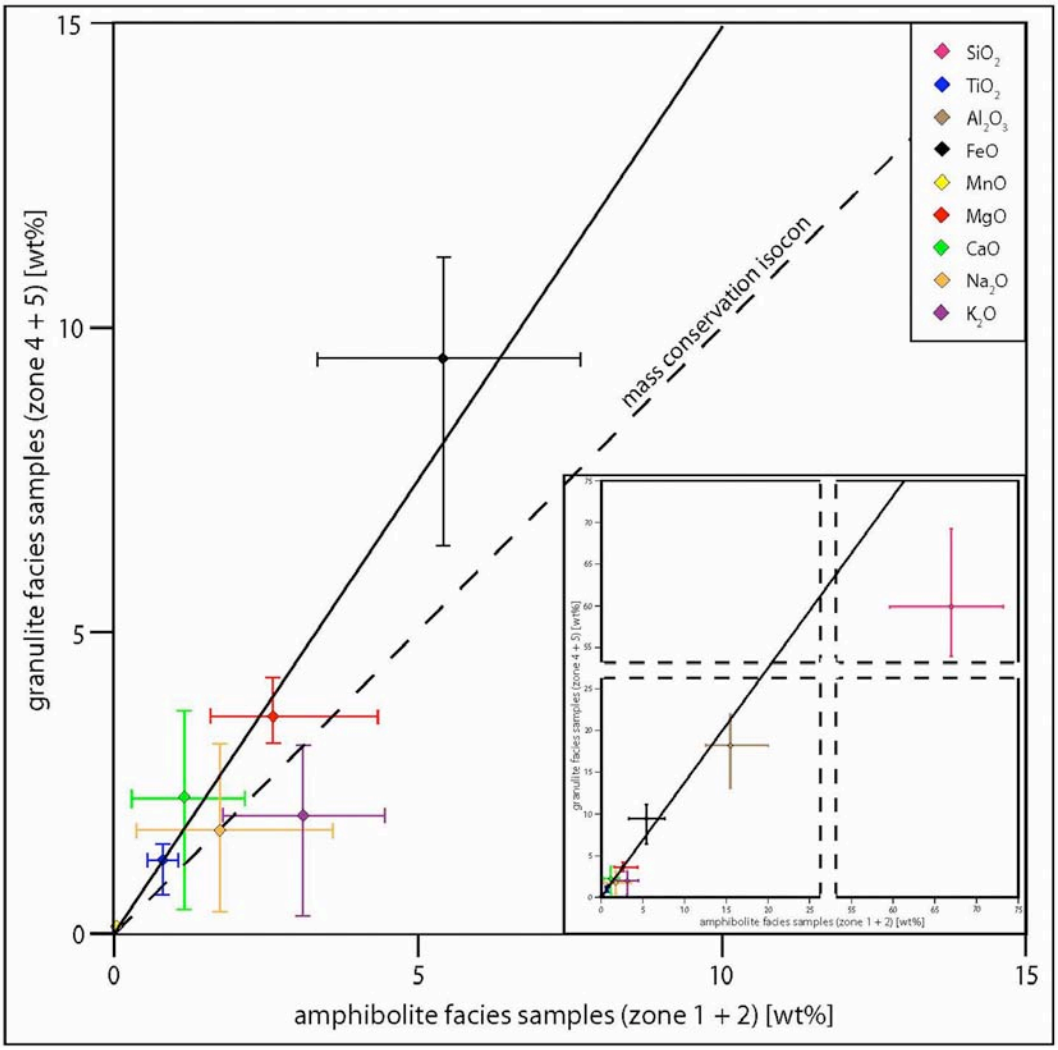

Figure 5.2.8. Isocon diagram (according to Grant, 1986) for the average element concentrations in amphibolite facies metapelites compared with the average element concentrations in granulite

metapelites, both with maximum and minimum range. The isocon is defined by the immobile phase TiO_2 and is straight through the origin. The uncertainty bars for each element show the maximum range of values for samples from amphibolite facies and granulite facies.

Based on the limited numbers of samples of metapsammite/metagreywacke, no general trend from low-grade to high-grade conditions can be discerned (Fig. 5.2.9).

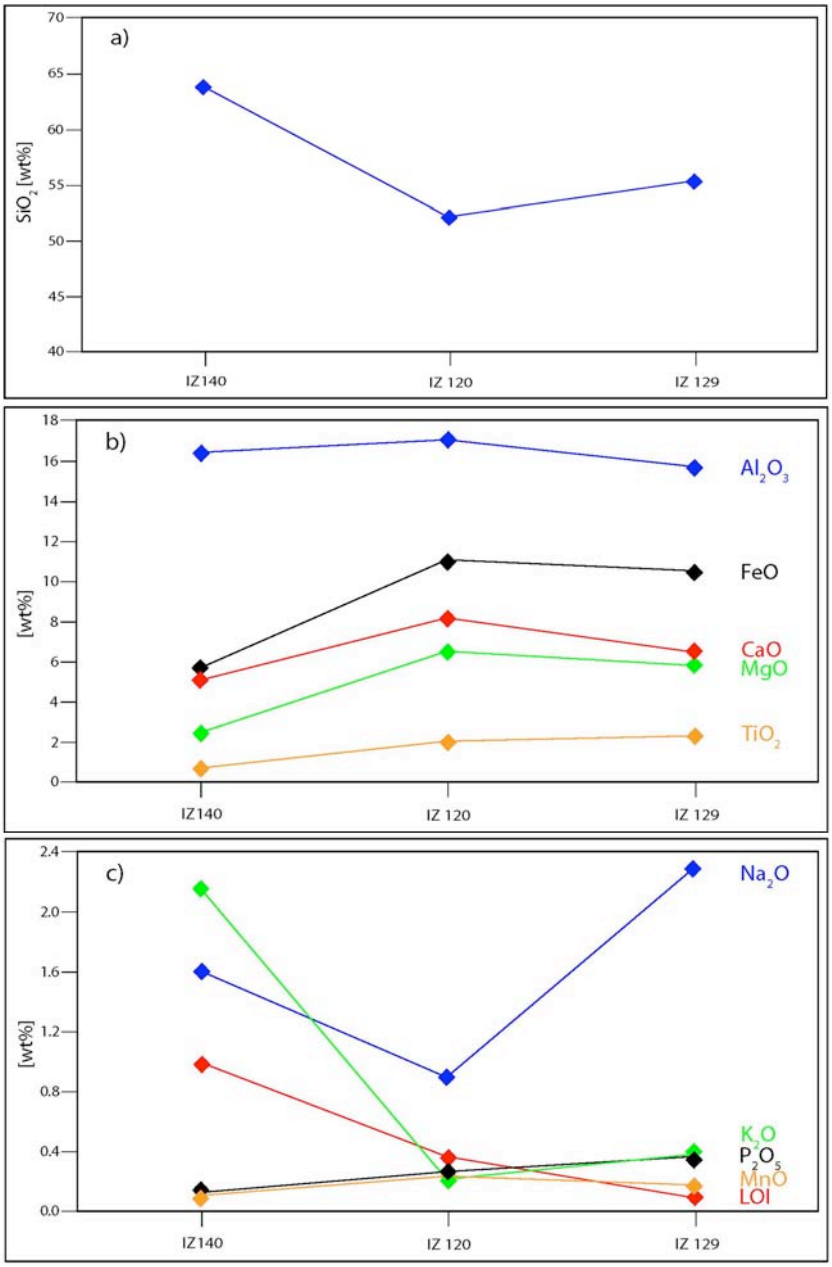

Figure 5.2.9. Bulk rock concentrations of SiO_2 (a), Al_2O_3, FeO, CaO, MgO and TiO_2 (b) and Na_2O, K_2O, P_2O_5, MnO and LOI (c) in metapsammite/metagreywacke samples from low-grade to high-grade conditions in Val Strona di Omegna.

5.2.2 Val Sesia

For Val Sesia, whole rock analyses of 6 metapelite samples are presented. Due to the broadly north-south orientation of both the valley and the mineral isograds, it is not possible to clearly order all the samples into increasing metamorphic grade. Instead, they are sorted based on their distance from the CMB Line (IV 034) towards the Mafic Complex (IZ 210), which is assumed to be broadly from low-grade to high-grade conditions (Tab. 5.2.2).

	q	ksp	pl	g	sill	bi	mu	ru	cd
IV 034	x		x	x	x	x			x
IZ 114	x		x	x	x	x	x		
IZ 168	x		x	x	x	x	x		
IZ 169	x		x		x	x	x		
IV 026	x	x	x	x	x	x	x		x
IZ 201	x	x	x	x	x	x			x

Table 5.2.2. Major minerals in metapelite samples from Val Sesia. The samples are sorted from their distance from the CMB Line towards the Mafic Complex.

In general, no continuous trend from near Quarona (near CMB Line) to Varallo (Mafic Complex) can be observed (Fig. 5.2.10). From samples IZ 114 to IZ 169 the values for SiO_2 and Al_2O_3 increase, while they decrease from samples IZ 169 to IZ 201. A decrease in FeO can also be observed from samples IZ 169–IZ 201. An increase in CaO and Na_2O is present from IZ 168–IZ 201. Further, for samples IV 034 to IZ 168 and from IZ 169 to IZ 201, the values for TiO_2 increase. The values for LOI decrease from IZ 114 to IV 026. A sharp increase in values for CaO and P_2O_5 can be observed for samples IV 026 to IZ 201. Sample IV 034 contains the highest values for SiO_2 and Na_2O and the lowest value for TiO_2. By contrast, the lowest value for SiO_2 is present in sample IZ 114, which also contains the highest values for Al_2O_3, FeO, K_2O and LOI. For MnO and K_2O, the highest values occur in sample IZ 186, which additionally contains the lowest values for CaO and P_2O_5. Sample IZ 169 has the lowest values of Al_2O_3, FeO, MnO, Na_2O and K_2O, while the lowest value for LOI is present in sample IV 026. In addition, the highest values for TiO_2, CaO and P_2O_5 are present in sample IZ 201.

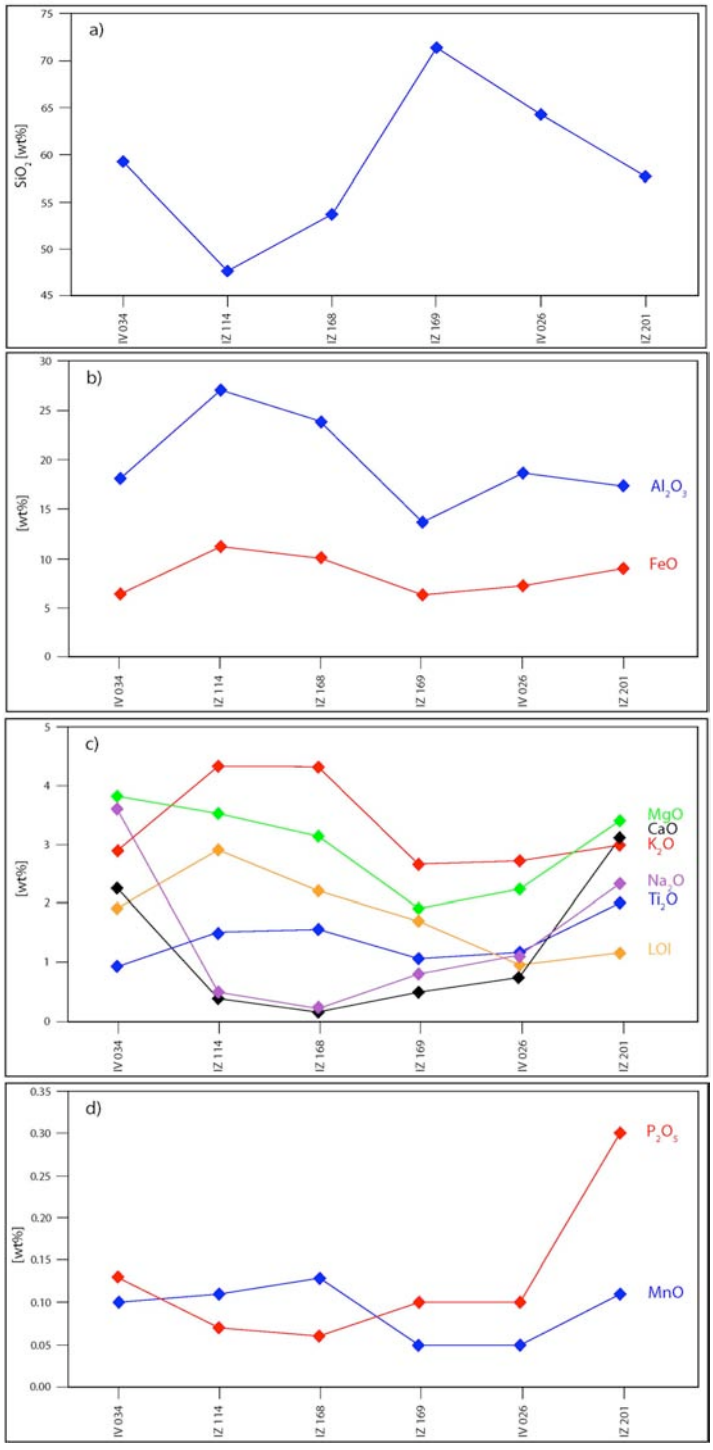

Figure 5.2.10. Bulk rock concentrations of SiO_2 (a), Al_2O_3 and FeO (b), MgO, CaO, K_2O, Na_2O, TiO_2 and LOI (c) and P_2O_5 and MnO (d) sorted from down river (Quarona) to up river (Varallo) in Val Sesia.

5.2.3 Val Strona di Postua

In Val Strona di Postua 5 samples of metapelite were analysed (Tab. 5.2.3) with results sorted from low-grade to high-grade conditions.

	q	ksp	pl	g	sill	bi	mu	ru	cd	sp
IZ 132	x		x	x	x	x			x	x
IZ 133	x		x	x	x	x			x	x
IZ 135	x		x	x	x	x		x	x	
IZ 165	x	x	x	x	x	x		x	x	
IZ 163	x	x	x	x					x	

Table 5.2.3. Major minerals in metapelite samples from Val Strona di Postua. The samples are sorted from low-grade to high-grade conditions.

The values from metapelites in Val Strona di Postua show no clear or continuous trend from low-grade to high-grade conditions (Fig. 5.2.11). For Al_2O_3 and LOI the values decrease from IZ 133 to IZ 163, while for these samples the values of CaO and Na_2O increase. Sample IZ 132 contains the overall lowest value for K_2O. In contrast, the highest value for K_2O, together with highest values for Al_2O_3, FeO, MnO, MgO and LOI are present in sample IZ 133. This sample also has the lowest values of SiO_2, TiO_2, CaO and Na_2O. In sample IZ 165 the highest values for TiO_2 and P_2O_5 occur. The highest values for SiO_2, CaO and Na_2O are present in the highest grade sample IZ 163, which also has the lowest values for Al_2O_3, FeO, MnO, MgO, P_2O_5 and LOI.

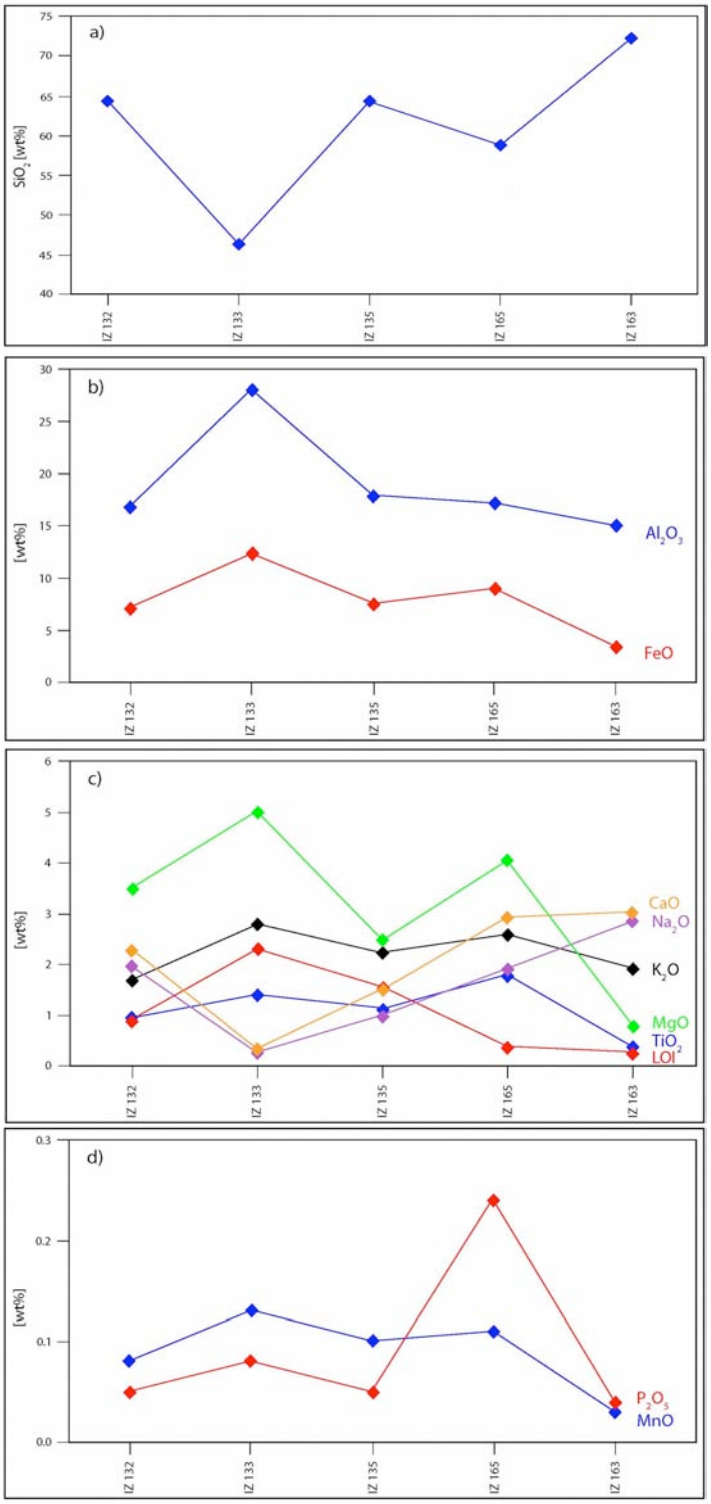

Figure 5.2.11. Bulk rock concentrations of SiO_2 (a), Al_2O_3 and FeO (b), MgO, CaO, K_2O, Na_2O, TiO_2 and LOI (c) and P_2O_5 and MnO (d) sorted from low-grade to high-grade conditions in Val Strona di Postua.

5.3 Mineral chemistry

In the following section the chemical analyses of major minerals in thin sections from metapelites from Val Strona di Omegna, Val Sesia and Val Strona di Postua as well as from metapsammites/metagreywackes from Val Strona di Omegna are described.

The ternary diagrams presented for garnet, K-feldspar and plagioclase are based on analyses of single minerals in the appropriate sample. The ranges of the proportion of end-members (e.g. X_{alm}, X_{py}, X_{grs} etc.) in metapelites are given in Tab. 5.3.1–5.1.4 for Val Strona di Omegna, Tab. 5.3.5 for Val Sesia, Tab. 5.3.6 for Val Strona di Postua and in Tab. 5.3.7 for metapsammites/metagreywackes from Val Strona di Omegna. The diagrams showing the variation of mineral major element compositions from low-grade to high-grade conditions in each valley are based on mean values with their maximum and minimum variance of the appropriate mineral in the samples. The mean values are given in Appendix B along with their standard division and the number of analyses per sample.

	sample	IZ 008	IZ 009	IZ 079	IZ 010	IZ 011	IZ 015	IZ 016
mineral								
garnet	X_{alm}			0.65–0.77				
	X_{py}			0.04–0.15				
	X_{grs}			0.06–0.32				
	X_{spess}			0.02–0.14				
plag	X_{ab}	0.74–0.76	0.66–0.72	0.71–0.77	0.85–0.88	0.79–0.85	0.73–0.7	0.49–0.58
	X_{an}	0.20–0.25	0.27–0.33	0.23–0.28	0.11–0.15	0.15–0.21	0.23–0.26	0.42–0.51
	X_{or}	0.01	0.01	0–0.01	0–0.01	0–0.01	0.01	0.01
ksp	X_{ab}	0.13–0.15						0.28
	X_{an}	0						0.09
	X_{or}	0.84–0.87						0.63
biotite	X_{Fe}	0.5–0.52	0.46–0.55	0.43–0.51	0.61–0.63	0.54–0.59	0.35–0.4	0.52–0.54
	Ti	0.15–0.17	0.09–0.2	0.11–0.15	0.17–0.2	0.12–0.18	0.12–0.15	0.17–0.18
	Al	1.71–1.78	1.72–1.82	1.65–1.73	1.71–1.82	1.71–1.8	1.65–1.74	1.71–1.72

Table 5.3.1. Proportions of end-members for garnet, plagioclase, K-feldspar and biotite in amphibolite facies metapelites from Val Strona di Omegna (sorted from low-grade (left) to high-grade (right). Ti and Al are given in atoms per formula unit (a.p.f.u.) based on 11 oxygens.

	sample	IZ 017	IZ 018	IZ 013	IZ 059	IZ 002	IV 019	IZ 029
mineral								
garnet	X_{alm}							
	X_{py}							
	X_{grs}							
	X_{spess}							
plag	X_{ab}	0.61–0.71	0.7–0.75	0.8–0.82	0.73–0.75	0.77–0.83		0.62
	X_{an}	0.29–0.38	0.24–0.29	0.18–0.19	0.24–0.25	0.16–0.22		0.37
	X_{or}	0–0.01	0.01–0.02	0–0.01	0.01–0.02	0.01–0.02		0.01
ksp	X_{ab}		0.13–0.14		0.03–0.09		0.07–0.11	0.05–0.14
	X_{an}		0		0		0	0
	X_{or}		0.86–0.87		0.91–0.96		0.89–0.93	0.86–0.95
biotite	X_{Fe}	0.3–0.33	0.47–0.51	0.43–0.46	0.6	0.6–0.64	0.5–0.51	0.46–0.51
	Ti	0.11–0.14	0.15–0.16	0.07–0.14	0.11–0.16	0.16–0.22	0.16–0.19	0.12–0.17
	Al	1.69–1.73	1.75–1.81	1.71–1.82	1.72–1.85	1.76–1.81	1.7–1.73	1.71–1.81

Table 5.3.2. Proportions of end-members for garnet, plagioclase, K-feldspar and biotite in amphibolite facies metapelites from Val Strona di Omegna (sorted from low-grade (left) to high-grade (right)). Ti and Al are given in atoms per formula unit (a.p.f.u.) based on 11 oxygens.

	sample	IV 058	IZ 034	IV 020	IV 054	IV 052	IZ 066	IZ 085
mineral								
garnet	X_{alm}	0.65–0.66	0.77–0.79	0.73–0.76	0.72–0.75	0.70–0.73	0.66–0.69	0.57–061
	X_{py}	0.14–0.15	0.16–0.19	0.15–0.18	0.16–0.19	0.19–0.21	0.22–0.26	0.32–0.36
	X_{grs}	0.16–0.2	0.02–0.03	0.04–0.05	0.05–0.06	0.05–0.06	0.05	0.04–0.05
	X_{spess}	0.03–0.07	0.01–0.02	0.04–0.05	0.03–0.04	0.03	0.02–0.03	0.02–0.03
plag	X_{ab}	0.70–0.74	0.74–0.78	0.62	0.53–0.58	0-53–0.58	0.46–0.51	0.55–0.58
	X_{an}	0.25–0.29	0.21–0.25	0.36–0.3	0.41–0.46	0.42–0.46	0.48–0.53	0.41–0.44
	X_{or}	0.01	0.01	0.01–0.02	0.01	0.01	0–0.01	0.01
ksp	X_{ab}		0.09–0.28	0.09–0.23		0.1–0.13	0.11	0.06–0.14
	X_{an}		0	0		0	0	0–0.01
	X_{or}		0.71–0.91	0.77–0.91		0.87–0.89	0.88	0.85–0.94
biotite	X_{Fe}	0.47–0.51	0.52–0.54	0.51–0.55	0.44–0.53	0.47–0.53	0.42–0.44	0.32–0.33
	Ti	0.15–0.18	0.21–0.26	0.21–0.26	0.24–0.32	0.24–0.3	0.25–0.32	0.25–0.33
	Al	1.74–1.88	1.63–1.69	1.59–1.67	1.53–1.66	1.52–1.58	1.47–1.52	1.4–1.41

Table 5.3.3. Proportions of end-members for garnet, plagioclase, K-feldspar and biotite in transition zone metapelites from Val Strona di Omegna (sorted from low-grade (left) to high-grade (right)). Ti and Al are given in atoms per formula unit (a.p.f.u.) based on 11 oxygens.

	sample	IZ 156	IV 044	IZ 005	IZ 070	IZ 004	IZ 048	IZ 102
mineral								
garnet	X_{alm}	0.57–0.67	0.58–0.61	0.56–0.59	0.63–0.64	0.61–0.62	0.56–0.58	0.48–0.49
	X_{py}	0.26–0.35	0.33–0.36	0.36–0.39	0.33–0.35	0.34–0.36	0.38–0.39	0.45–0.47
	X_{grs}	0.04–0.08	0.04–0.06	0.04	0.02	0.03	0.04	0.04–0.05
	X_{spess}	0.01	0.01–0.02	0.01	0–0.01	0–0.01	0.01	0.01
plag	X_{ab}	0.64–0.68	0.58–0.62	0.62			0.69–0.74	0.7–0.72
	X_{an}	0.3–0.35	0.37–0.41	0.37			0-25–0.3	0.28–0.3
	X_{or}	0–0.05	0.01–0.02	0.01			0–0.02	0.01
ksp	X_{ab}		0.09–0.13	0.09–0.13	0.06–0.12		0.08–0.19	0.14
	X_{an}		0.01	0.01	0		0–0.02	0
	X_{or}		0.86–0.91	0.85–0.9	0.88–0.94		0.8–0.91	0.86
biotite	X_{Fe}	0.34–0.4		0.21	0.24			
	Ti	0.27–0.38		0.3	0.31			
	Al	1.34–1.55		1.28	1.27			

Table 5.3.4. Proportions of end-members for garnet, plagioclase, K-feldspar and biotite in granulite facies metapelites from Val Strona di Omegna (sorted from low-grade (left) to high-grade (right)). Ti and Al are given in atoms per formula unit (a.p.f.u.) based on 11 oxygens.

	sample	IV 034	IZ 114	IZ 168	IV 026	IZ 201
mineral						
garnet	X_{alm}	0.68–0.69		0.72–0.74	0.77–0.81	0.72–0.76
	X_{py}	0.18–0.19		0.09–011	0.13–0.18	0.16–0.19
	X_{grs}	0.03		0.02	0.03	0.04–0.05
	X_{spess}	0.1		0.14–0.16	0.02–0.03	0.04
plag	X_{ab}	0.74–0.75	0.75	0.84	0.71–0.72	0.54–0.68
	X_{an}	0.24–0.26	0.22	0.15	0.26–0.28	0.31–0.45
	X_{or}	0–0.01	0.02	0.01	0.01	0.01–0.02
ksp	X_{ab}				0.08–0.1	
	X_{an}				0	
	X_{or}				0.9–0.92	
biotite	X_{Fe}	0.42–0.46	0.56–0.62	0.6–0.61	0.55–0.6	0.47–0.51
	Ti	0.13–0.18	0.11–0.19	0.19–0.21	0.16–0.27	0.22–0.26
	Al	1.34–1.44	1.37–1.54	1.35–1.43	1.27–1.38	1.22–1.33

Table 5.3.5. Proportions of end-members for garnet, plagioclase, K-feldspar and biotite in metapelites from Val Sesia (sorted from down river to up river). Ti and Al are given in atoms per formula unit (a.p.f.u.) based on 11 oxygens.

	sample	IZ 132	IZ 165	IZ 163
mineral				
garnet	X_{alm}	0.69–0.71	0.66–0.69	0.64–0.67
	X_{py}	0.24–0.26	0.26–0.28	0.29–0.31
	X_{grs}	0.03	0.03–0.04	0.03
	X_{spess}	0.02	0.01–0.02	0.01
plag	X_{ab}	0-61–0.65	0.57–0.61	0.6–0.63
	X_{an}	0.34–0.37	0.37–0.4	0.35–0.38
	X_{or}	0.01–0.02	0.01–0.02	0.01–0.02
ksp	X_{ab}		0.08–0.1	0.07–0.12
	X_{an}		0	0–.0.2
	X_{or}		0.90–0.92	0.86–0.92
biotite	X_{Fe}	0.39–0.46	0.33–0.38	0.29
	Ti	0.16–0.31	0.23–0.29	0.22
	Al	1.2–1.33	1.14–1.19	1.16

Table 5.3.6. Proportions of end-members for garnet, plagioclase, K-feldspar and biotite metapelites from Val Strona di Postua (sorted from low-grade to high-grade). Ti and Al are given in atoms per formula unit (a.p.f.u.) based on 11 oxygens.

	sample	IZ 120	IZ 129	IZ 129
mineral				
garnet	X_{alm}	0.52–0.55	0.55–0.57	
	X_{py}	0.32–0.37	0.31–0.34	
	X_{grs}	0.09–0.1	0.08–0.12	
	X_{spess}	0.02–0.03	0.02	
plag	X_{ab}	0.31–0.47	0.14–0.27	0.43–0.5
	X_{an}	0.53–0.69	0.73–0.86	0.48–0.55
	X_{or}	0–0.03	0–0.01	0.01–0.02
opx	X_{Fe}	0.33–0.43	0.37–0.4	
	X_{Ca}	0–0.01	0.01	
	X	0.06–0.12	0.07–0.09	
biotite	Al (oct.)	0.3–0.33	0.32–0.34	
	Ti	0.35–0.38	0.37–0.39	
	Al_{tot}	1.01–1.05	0.98–1	

Table 5.3.7. Proportions of end-members for garnet, plagioclase, orthopyroxene and biotite in granulite facies metapsammites /metagreywackes from Val Strona di Omegna (sorted from low-grade to high-grade). Al (oct. = octahedral), Ti and Al_{tot} (total) are given in atoms per unit (a.p.f.u.) based on 11 oxygens.

5.3.1 Garnet

In general no garnet in the metapelites and metapsammites/metagreywackes from the three valleys shows any significant major element zoning. As shown in Fig. 5.3.4, garnet in the metapelite samples from Val Strona di Omegna is almandine-rich in the amphibolite facies and becomes more pyrope-rich through the transition zone towards the granulite facies. In comparison, amphibolite facies samples from Val Sesia are similar in X_{alm} and X_{py} values to those in Val Strona di Omegna. Garnet in Val Strona di Postua samples is more pyrope-rich, consistent with granulite facies samples from Val Strona di Omegna. Garnet in granulite facies metapsammite/metagreywacke samples shows similar X_{alm} and X_{py} ratios to the metapelites under these conditions. The proportion of spessartine (X_{spess}) is generally low in both metapelites and metapsammites/metagreywackes.

sample	IZ 079	IV 020	IZ 005	IV 034	IZ 201	IZ 132	IZ 163	IZ 120	IZ 129
SiO_2	37.66	38.12	38.95	38.64	37.78	38.23	38.01	39.06	38.89
TiO_2	0.03	0.00	0.00	0.00	0.00	0.05	0.03	0.00	0.14
Al_2O_3	21.25	21.87	22.13	21.57	21.41	21.59	21.86	22.04	21.78
FeO	32.89	33.99	27.97	31.62	33.93	32.29	30.55	25.21	26.83
MnO	4.28	1.94	0.51	4.57	1.68	0.83	0.31	0.95	0.81
MgO	3.21	4.37	9.85	4.60	4.87	6.58	7.88	9.65	8.97
CaO	1.92	1.41	1.38	1.11	1.34	1.27	1.16	3.45	2.84
Na_2O	0.00	0.00	0.02	0.01	0.09	0.01	0.05	0.03	0.02
K_2O	0.01	0.01	0.00	0.00	0.03	0.03	0.00	0.02	0.02
Cr_2O_3	0.00	0.06	0.06	0.04	0.06	0.07	0.08	0.06	0.01
Total	101.24	101.77	100.87	102.16	101.19	100.95	99.92	100.47	100.32
Si	2.995	2.988	2.975	3.014	2.981	2.985	2.969	2.982	2.990
Al^{tet}	0.005	0.012	0.025	0.000	0.019	0.015	0.031	0.018	0.010
Al^{oct}	1.986	2.009	1.968	1.983	1.972	1.972	1.981	1.966	1.964
Ti	0.001	0.000	0.000	0.000	0.000	0.003	0.001	0.000	0.008
Fe	2.187	2.228	1.787	2.063	2.239	2.108	1.995	1.610	1.725
Mn	0.288	0.129	0.033	0.302	0.112	0.055	0.021	0.062	0.052
Mg	0.381	0.511	1.122	0.535	0.573	0.766	0.918	1.098	1.028
Ca	0.164	0.118	0.113	0.093	0.113	0.106	0.097	0.282	0.234
Na	0.000	0.000	0.002	0.002	0.014	0.002	0.007	0.004	0.004
K	0.001	0.001	0.000	0.000	0.003	0.003	0.000	0.002	0.002
Cr	0.000	0.004	0.003	0.002	0.004	0.004	0.005	0.004	0.001
X_{Fe}	0.85	0.81	0.61	0.79	0.8	0.73	0.68	0.59	0.63

Table 5.3.8. Selected representative values for garnet in metapelites in the amphibolite facies (IZ 079), the transition zone (IV 020) and the granulite facies (IZ 005) from Val Strona di Omegna, for garnet from Val Sesia (IV 034, IZ 201), for garnet from Val Strona di Postua (IZ 132, IZ 163) and for garnet in metapsammites/metagreywackes from Val Strona di Omegna (IZ 120, IZ 129). Cations are calculated for 12 oxygens.

In Val Strona di Omegna the values for X_{alm} decreases from low-grade (0.77–0.65) to high-grade (0.49–0.48) conditions, while X_{py} increases (0.04–0.15 to 0.45–0.47). A decrease in X_{Fe} = Fe/(Fe + Mg) from 0.88 (± 0.06/0.07) in the lowest grade sample to 0.51 (± 0.01) in the highest grade sample (Fig. 5.3.1) is also present. The highest value for X_{alm} is present in sample IZ 034 in the transition zone, while the lowest value is present in sample IZ 102 from the granulite facies. For X_{py} the lowest value is present in the lowest grade sample (IZ 079). Values for X_{grs} range from 0.06–0.32 in the amphibolite facies to 0.04–0.05 in the granulite facies with little systematic variation. The values for X_{spess} vary from 0.02–0.14 to 0–0.01 through the valley. The composition of garnet changes from approximately $Alm_{70}Py_{10}Grs_{15}Spess_5$ in the amphibolite facies to approximately $Alm_{47}Py_{47}Grs_3Spess_1$ in the granulite facies. The values for Mn (atoms per formula unit = a.p.f.u.) slightly decreases from low-grade (0.144 + 0.28/- 0.08) to high-grade (0.026 ± 0.07) conditions, except from IV 058 and IZ 034.

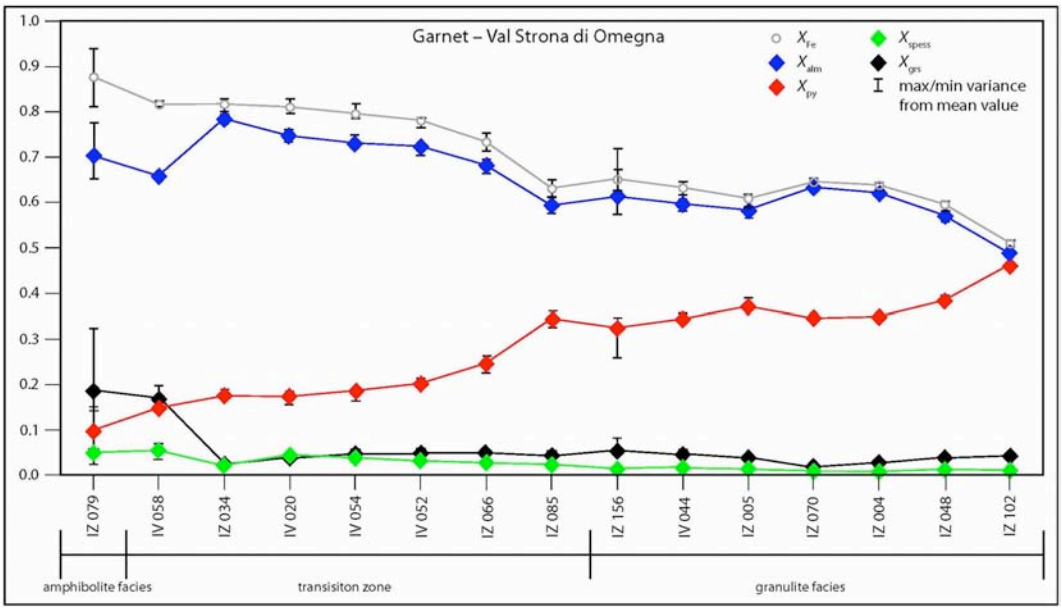

Figure 5.3.1. Trend and variation for X_{alm}, X_{py}, X_{grs}, X_{spess} and X_{Fe} in garnet from Val Strona di Omegna sorted from low-grade to high-grade conditions.

In comparison to the metapelites, garnet in the two metapsammite/metagreywacke samples from Val Strona di Omegna is richer in Ca and Mg but lower in Fe (atoms per formula unit) with X_{Fe} = 0.59–0.64, while the other elements have similar contents to garnets in the metapelites. The composition is around $Alm_{53}Py_{33}Grs_{9}Spess_{2}$.

Garnet in Val Sesia shows no significant continuous major element trend in the samples from down river near Quarona to up river near Varallo (Fig. 5.3.2). The composition of garnet here is similar to that in samples from the amphibolite facies and the transition zone from Val Strona di Omegna (Fig. 5.3.1). Sample IZ 168 is rich in Mn, while sample IV 026 shows the highest Fe contents in Val Sesia. The composition of the garnet is highly variable, with $Alm_{65-79}Py_{10-19}Grs_{2-4}Spess_{2-15}$ along the valley. No consistent trend in X_{Fe} (0.79–0.84) is observable. Sample IZ 168 has the highest X_{spess} values (0.14–0.16).

In general, there is no obvious variation in the major element concentrations from low-grade to high-grade from the very limited number of samples investigated from Val Strona di Postua (Fig. 5.3.3), but X_{alm} slightly decreases, while X_{py} increases along this valley. In addition the values for X_{Fe} decrease from 0.74 to 0.68. The composition of garnet is $Alm_{66-70}Py_{25-30}Grs_{3-4}Spess_{1-2}$.

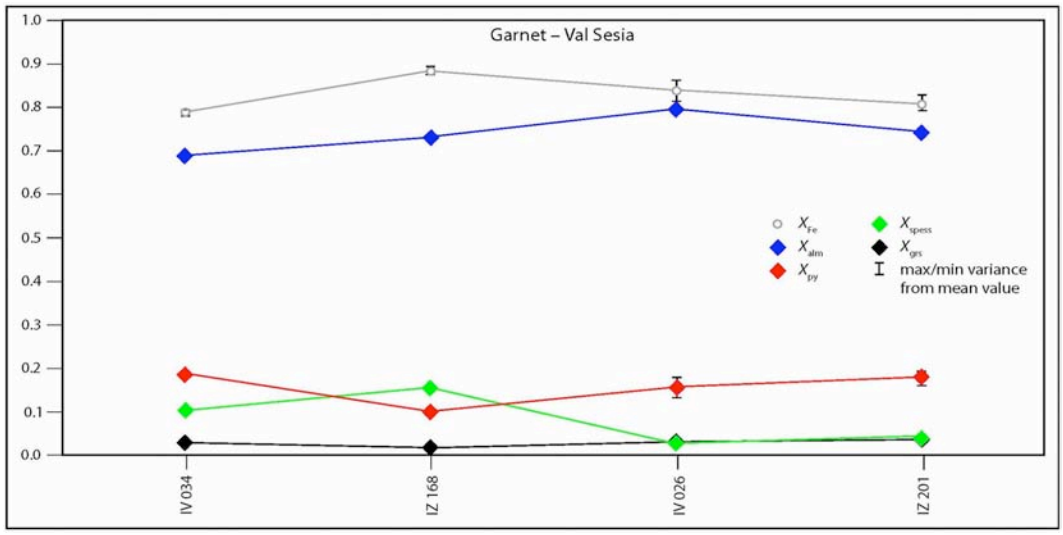

Figure 5.3.2. Trend and variation for X_{alm}, X_{py}, X_{grs}, X_{spess} and X_{Fe} in garnet from Val Sesia sorted from low-grade to high-grade conditions.

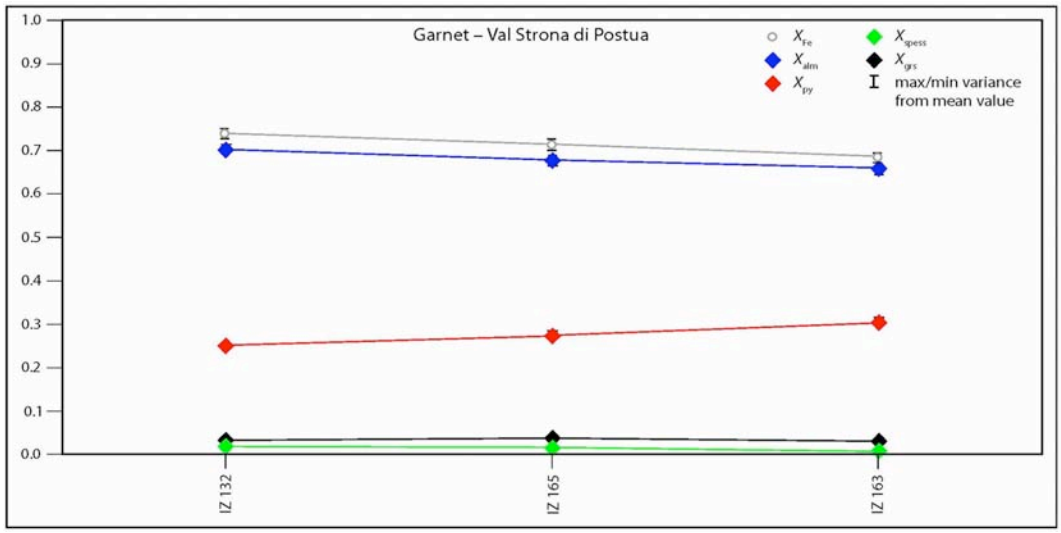

Figure 5.3.3. Variation for X_{alm}, X_{py}, X_{grs}, X_{spess} and X_{Fe} in garnet from Val Strona di Postua.

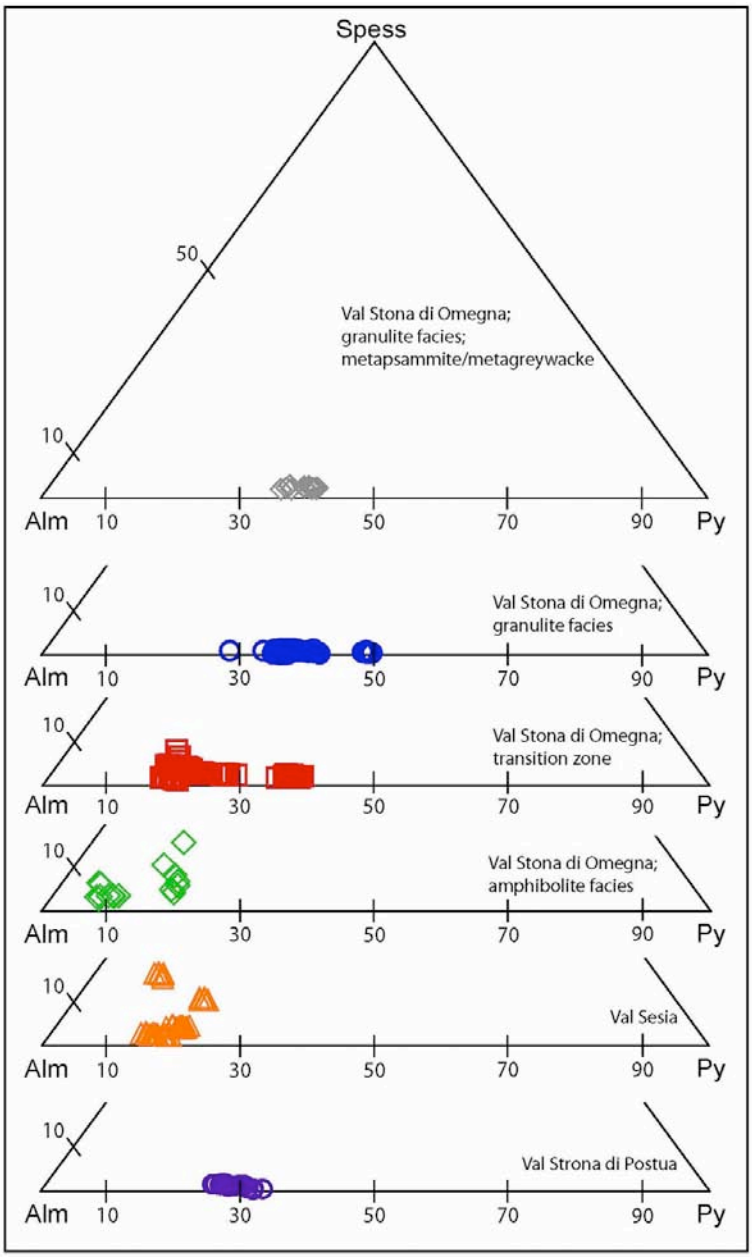

Figure 5.3.4. Ternary diagrams showing the variation of X_{alm}, X_{py} and X_{spess} in garnet from metapelites from Val Strona di Postua, Val Sesia and Val Strona di Omegna (divided into the facies). In addition the variation in garnet from metapsammite/metagreywacke samples in Val Strona di Omegna is illustrated.

5.3.2 Orthopyroxene, Cordierite & Spinel

The composition of orthopyroxene in two samples of metapsammite/metagreywacke from Val Strona di Omegna shows X_{Fe} values varying from 0.33–0.43 with X_{Ca} 0–0.01. The calculated amount of octahedral Al

(a.p.f.u. based on 6 oxygens) is 0.06–0.12. Orthopyroxene was analysed in two samples and hence no trend or variations through the valley can be inferred.

The composition of the rare cordierite grains in amphibolite facies from Val Strona di Omegna samples shows an X_{Fe} value of 0.19–0.37 but without any systematic trend. Cordierite is strongly pinitised in the samples from Val Sesia. This is visible in the chemistry based on the content of K_2O, which is too high for cordierite, best observed in sample IV 034 (Appendix B). In other samples no analyses of this mineral could be undertaken due to the degree of pinitisation. The composition of cordierite in sample IV 034 gives X_{Fe} values of 0.29–0.38. In Val Strona di Postua cordierite has almost the same composition in every sample. In sample IZ 163 this mineral is strongly pinitised. This mineral shows no obvious trend in the major elements and has an $X_{Fe} = 0.24–0.39$.

Spinel was analysed in only one sample from Val Strona di Postua, although it is present in other samples, but mostly too small for measurement. Spinel is Fe rich with $X_{Fe} = 0.76$

	Orthopyroxene		Cordierite						Spinel
sample	**IZ 120**	**IZ 129**	**IZ 009**	**IZ 017**	**IZ 013**	**IV 034**	**IZ 132**	**IZ 163**	**IZ 132**
SiO_2	51.18	51.56	47.87	48.88	48.43	42.51	48.13	41.27	0.03
TiO_2	0.07	0.06	0.00	0.05	0.01	0.00	0.00	0.03	0.00
Al_2O_3	2.30	1.68	32.73	33.43	33.20	28.78	32.14	30.28	58.48
FeO	24.45	24.76	8.04	4.56	6.83	5.69	6.39	7.51	31.74
MnO	0.44	0.36	0.59	0.11	0.38	0.10	0.09	0.00	0.10
MgO	21.00	20.30	7.64	10.45	9.10	7.57	9.57	6.69	5.35
CaO	0.22	0.49	0.05	0.01	0.02	0.04	0.01	0.53	0.03
Na_2O	0.03	0.00	0.51	0.36	0.30	0.14	0.09	0.06	0.12
K_2O	0.02	0.00	0.01	0.00	0.02	9.41	0.01	1.17	0.00
Cr_2O_3	0.03	0.12	0.03	0.00	0.00	0.02	0.00	0.04	0.23
Total	99.72	99.33	97.46	97.85	98.30	94.25	96.42	87.57	96.07
Si	1.932	1.957	4.987	4.977	4.967	4.836	5.012	4.831	0.001
Al^{tet}	0.068	0.043							
Al^{oct}	0.034	0.032	4.018	4.012	4.013	3.859	3.944	4.177	1.991
Ti	0.002	0.002	0.000	0.004	0.001	0.000	0.000	0.002	0.000
Fe	0.772	0.786	0.700	0.388	0.586	0.541	0.556	0.735	0.767
Mn	0.014	0.012	0.052	0.009	0.033	0.010	0.007	0.000	0.002
Mg	1.182	1.148	1.187	1.586	1.391	1.284	1.486	1.167	0.230
Ca	0.009	0.020	0.005	0.002	0.002	0.005	0.001	0.066	0.001
Na	0.002	0.000	0.103	0.070	0.059	0.030	0.017	0.014	0.006
K	0.001	0.000	0.002	0.000	0.003	1.366	0.002	0.175	0.000
Cr	0.001	0.003	0.002	0.000	0.000	0.001	0.000	0.004	0.005
X_{Fe}	0.39	0.40	0.36	0.20	0.29	0.29	0.27	0.39	0.77
X_{Mg}	0.60	0.59	0.61	0.80	0.69	0.70	0.72	0.61	0.23
X_{Ca}	0.00	0.01	–	–	–	–	–	–	–

Table 5.3.9. Selected representative values for orthopyroxene in granulite facies metapsammite/metagreywacke samples from Val Strona di Omegna (IZ 120, IZ 129), for cordierite in amphibolite facies metapelites samples from Val Strona di Omegna (IZ 009, IZ 017, IZ 013), Val Sesia (IV 034) and Val Strona di Postua (IZ 132, IZ 163) and for spinel in metapelites samples from Val Strona di Postua (IZ 132). Cations are calculated for 6 oxygens (orthopyroxene), for 18 oxygens cordierite) and for 4 oxygens (spinel).

5.3.3 Biotite

In Val Strona di Omegna the biotite has an X_{Fe} = 0.32–0.63, but towards the biotite-out isograd it becomes richer in Mg (X_{Fe} = 0.21–0.37). In general there is no continuous trend in X_{Fe} in the amphibolite facies, while the composition of biotite decreases in X_{Fe} through the transition zone and in the granulite facies (Fig. 5.3.5). From the beginning of the transition zone to the high-grade parts of the granulite facies an increase in Ti (0.16 ± 0.01 to 0.31 (atoms per formula unit)) and a decrease in Al (total) is recorded (1.75 ± 0.03 to 1.27 (atoms per formula unit)).

sample	IZ 009	IV 020	IZ 005	IV 034	IZ 201	IZ 132	IZ 163	IZ 120	IZ 129
SiO_2	35.56	35.70	37.85	36.19	35.74	35.81	35.82	37.09	36.46
TiO_2	1.62	4.54	5.41	2.35	4.68	4.13	3.94	6.74	6.43
Al_2O_3	20.52	17.91	14.95	19.53	17.77	17.47	16.26	14.27	13.68
FeO	17.19	19.43	8.55	15.88	18.10	15.63	11.35	12.56	12.50
MnO	0.39	0.03	0.038	0.15	0.01	0.03	0.00	0.05	0.01
MgO	10.60	9.33	17.9	11.81	9.88	11.79	15.76	14.53	14.37
CaO	0.00	0.00	0.02	0.00	0.00	0.00	0.00	0.00	0.05
Na_2O	0.17	0.08	0.17	0.41	0.10	0.12	0.14	0.09	0.13
K_2O	9.04	8.81	9.89	8.81	9.85	9.32	9.37	9.38	8.93
Cr_2O_3	0.02	0.09	0.207	0.04	0.04	0.16	0.07	0.13	0.16
Total	95.11	95.92	94.99	95.17	96.17	94.47	92.71	94.83	92.73
Si	2.674	2.692	2.760	2.699	2.688	2.705	2.708	2.757	2.771
Al^{tet}	0.326	0.308	0.240	0.301	0.312	0.295	0.292	0.243	0.229
Al^{oct}	1.492	1.284	1.044	1.415	1.264	1.260	1.157	1.008	0.996
Ti	0.092	0.257	0.297	0.132	0.265	0.235	0.224	0.377	0.368
Fe	1.081	1.225	0.521	0.990	1.138	0.987	0.718	0.781	0.794
Mn	0.025	0.002	0.002	0.009	0.001	0.002	0.000	0.003	0.001
Mg	1.188	1.049	1.946	1.313	1.108	1.328	1.776	1.610	1.628
Ca	0.000	0.000	0.002	0.000	0.000	0.000	0.000	0.000	0.004
Na	0.025	0.011	0.024	0.060	0.014	0.018	0.021	0.012	0.019
K	0.867	0.847	0.920	0.838	0.945	0.898	0.904	0.889	0.866
Cr	0.001	0.005	0.012	0.002	0.002	0.009	0.004	0.007	0.010
X_{Fe}	0.47	0.54	0.21	0.43	0.51	0.43	0.29	0.33	0.33

Table 5.3.10. Selected representative values for biotite in metapelites in the amphibolite facies (IZ 009), the transition zone (IV 020) and the granulite facies (IZ 005) from Val Strona di Omegna; for biotite from Val Sesia (IV 034, IZ 201); for biotite from Val Strona di Postua (IZ 132, IZ 163) and for biotite in metapsammites/metagreywackes from Val Strona di Omegna (IZ 120, IZ 129). Cations are calculated for 11 oxygens.

Biotite in the metapsammite/metagreywacke samples has similar values to biotite in the metapelites, with X_{Fe} varying from 0.33–0.43. Biotite has slightly higher values of Ti (0.35–0.39 (atoms per formula unit)) and slightly lower values of Al (0.98–1.05 (atoms per formula unit)) than that in the metapelites.

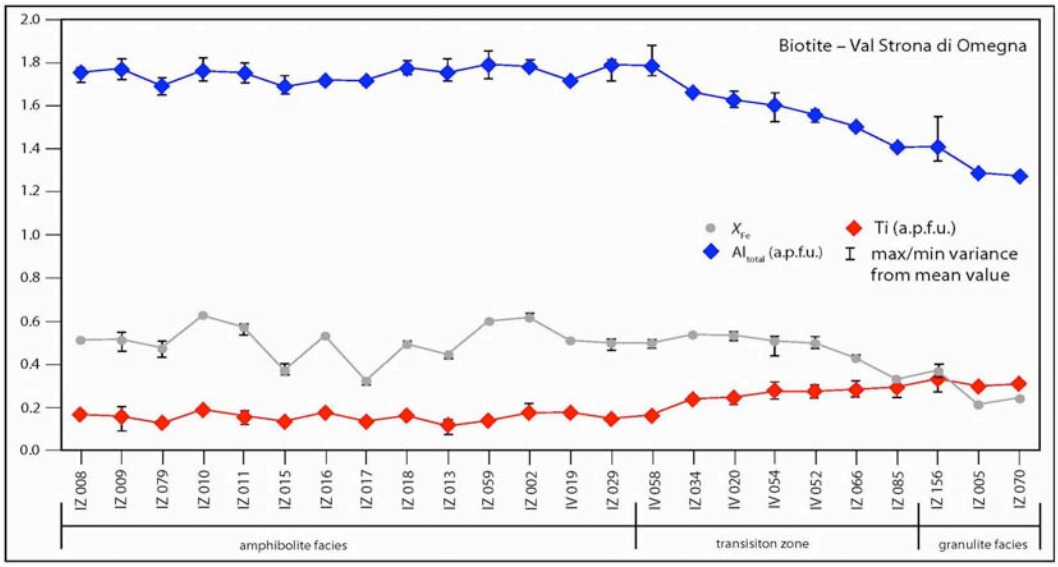

Figure 5.3.5. Trend and variation for X_{Fe}, Ti (a.p.f.u.) and Al (total, a.p.f.u.) in biotite from Val Strona di Omegna.

Biotite compositions in Val Sesia show some variations in the major elements from down river to up river (Fig. 5.3.6). Ti (atoms per formula unit) increases from sample IV 034 (0.13–0.18) to IZ 201 (0.22–0.26). With the increase of Ti the Al (total) content of the biotite slightly decreases (1.64–1.44 to 1.22–1.33). Fe and Mg show an opposite trend from down river to up river. With increasing Fe the Mg content decreases and vice versa. Also the values for X_{Fe} slightly decreases from sample IZ 114 (0.56–0.62) to IZ 201 (0.47–0.51), while X_{Fe} in sample IV 034 (0.46–0.42) is the lowest value in this valley (0.44).

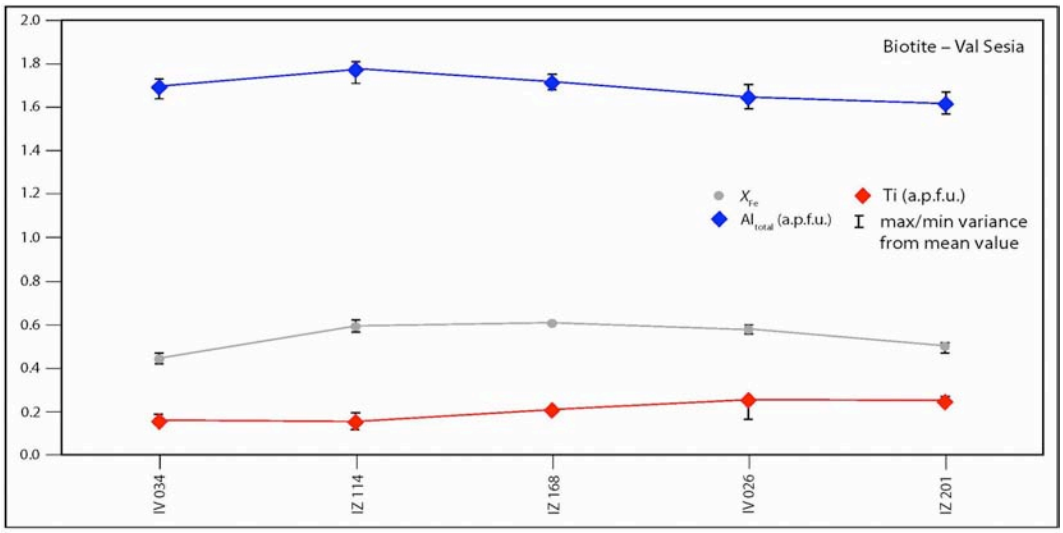

Figure 5.3.6. Trend and variation for X_{Fe}, Ti (a.p.f.u) and Al (total, a.p.f.u.) in biotite from Val Sesia.

Investigation of the biotite compositions in Val Strona di Postua samples show, similar to Val Strona di Omegna and Val Sesia, a decrease in X_{Fe} from 0.46–0.39 in sample IZ 132 to X_{Fe} = 0.22 in sample IZ 163. All other elements show no clear or continuous trend in this valley.

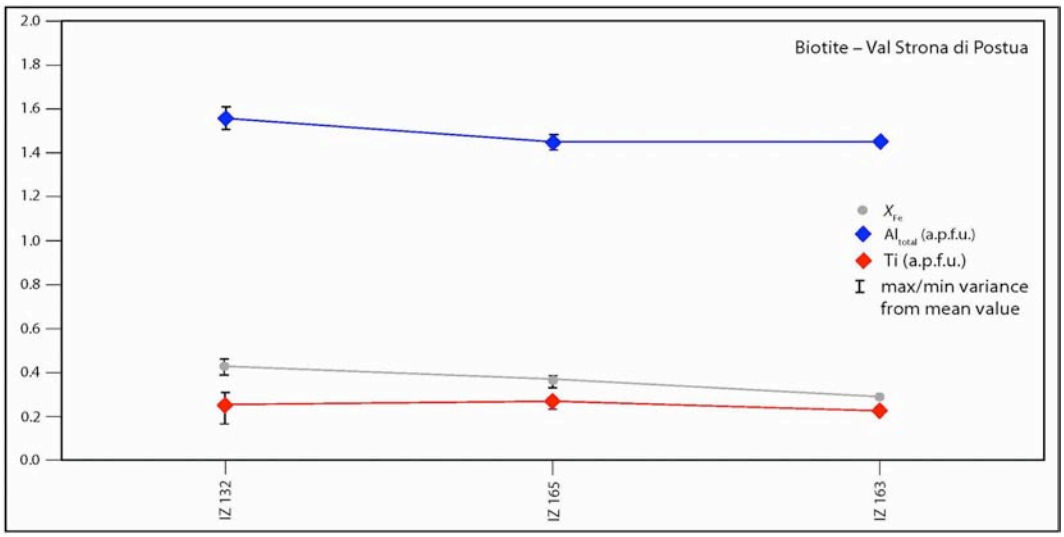

Figure 5.3.7. Variation for X_{Fe}, Ti (a.p.f.u.) and Al (total, a.p.f.u.) in biotite from Val Strona di Postua.

5.3.4 Muscovite

Muscovite occurs in metapelite samples from Val Strona di Omegna and Val Sesia but is absent from samples from Val Strona di Postua. Neither in Val Strona di Omegna nor Val Sesia does muscovite show any systematic variation in major element chemistry. In Val Strona di Omegna samples in the transition zone (IV 058) and the granulite facies (IV 044 and IZ 070) contain muscovite as a retrograde mineral with X_{Na} = Na/(Na + K) = 0.02–0.06. This overlaps with, but is typically lower, than that in amphibolite facies samples (X_{Na} = 0.06–0.21). In the granulite facies retrograde muscovite is poorer in Ti and Al but richer in Si, Fe and Mg in comparison to muscovite from the amphibolite facies rocks. In Val Sesia the composition of the muscovite shows a slight decrease in Na (X_{Na} =Na/(Na + K) = 0.11–0.05) going up river but in general no systematic trend in the major elements can be observed. Sample IV 026 contains muscovite as a retrograde mineral with a higher SiO_2 content in comparison to prograde/peak muscovite, similar to granulite facies samples from Val Strona di Omegna.

sample	IZ 010	IV 058	IZ 070	IZ 114	IZ 168	IV 026
SiO_2	45.16	45.89	48.50	45.32	45.03	47.21
TiO_2	0.85	0.13	0.11	0.25	1.01	0.10
Al_2O_3	36.08	35.56	30.17	35.64	34.74	35.02
FeO	0.90	1.07	1.83	1.08	1.16	1.22
MnO	0.01	0.01	0.00	0.04	0.00	0.04
MgO	0.44	0.78	1.87	0.47	0.50	0.52
CaO	0.03	0.01	0.12	0.00	0.00	0.00
Na_2O	0.60	0.40	0.17	0.83	0.67	0.32
K_2O	10.63	10.13	10.28	9.74	9.88	9.62
Cr_2O_3	0.01	0.03	0.02	0.05	0.13	0.01
Total	94.71	94.00	93.07	93.41	93.11	94.07
Si	3.025	3.082	3.299	3.064	3.061	3.152
Al^{tet}	1.975	1.918	1.701	1.936	1.939	1.848
Al^{oct}	1.874	1.896	1.718	1.903	1.845	1.907
Ti	0.043	0.007	0.006	0.013	0.051	0.005
Fe	0.050	0.060	0.104	0.061	0.066	0.068
Mn	0.001	0.000	0.000	0.002	0.000	0.002
Mg	0.044	0.078	0.190	0.047	0.050	0.052
Ca	0.002	0.001	0.009	0.000	0.000	0.000
Na	0.078	0.052	0.022	0.108	0.088	0.042
K	0.908	0.868	0.892	0.840	0.857	0.819
Cr	0.001	0.001	0.001	0.002	0.007	0.001
X_{Fe}	0.53	0.43	0.35	0.55	0.57	0.56
X_{Na}	0.08	0.06	0.02	0.11	0.09	0.05

Table 5.3.11. Selected representative values for muscovite in metapelites in the amphibolite facies (IZ 010), the transition zone (IV 058) and the granulite facies (IZ 070) from Val Strona di Omegna and for muscovite from Val Sesia (IZ 114, IZ 168, IV 026). Cations are calculated for 22 oxygens.

5.3.5 K-feldspar

For K-feldspar in metapelites from Val Strona di Omegna no continuous composition trend exists (Fig. 5.3.8). In general the mineral shows X_{or} varying from 0.71–0.94 with X_{ab} = 0.03–0.28. Especially at the beginning of the transition zone K-feldspar has lower X_{or} and higher X_{ab} values than in other parts of the valley. In addition, K-feldspar in samples IZ 034 and IV 020 shows a wide range for X_{or} and X_{ab}. K-feldspar is always a partly sericitised in the samples.

Analyses of K-feldspar in Val Sesia could be undertaken in only one sample (IV 026) because in other samples K-feldspar is too sericitised for analysis (Fig. 5.3.9). In sample IV 026 K-feldspar is similar to those from Val Strona di Omegna (X_{Or} = 0.9–0.92, X_{Ab} = 0.08–0.1).

From Val Strona di Postua samples values for K-feldspar with X_{Or} = 0.86–0.92 and X_{Ab} = 0.07–0.12 were measured in two samples (Fig. 5.3.9).

sample	IZ 016	IV 020	IZ 005	IV 026	IZ 165	IZ 163
SiO_2	64.38	64.56	63.90	64.30	63.16	63.41
TiO_2	0.05	0.04	0.10	0.00	0.00	0.04
Al_2O_3	20.08	18.81	18.57	18.83	18.31	17.92
FeO	0.03	0.00	0.04	0.04	0.06	0.02
MnO	0.00	0.01	0.05	0.01	0.00	0.02
MgO	0.01	0.00	0.00	0.00	0.01	0.01
CaO	1.70	0.08	0.09	0.04	0.05	0.05
Na_2O	3.05	2.08	1.32	0.90	0.97	1.24
K_2O	10.45	12.77	14.74	15.07	14.66	14.26
Cr_2O_3	0.05	0.05	0.13	0.05	0.07	0.02
Total	99.80	98.40	98.94	99.25	97.30	96.99
Si	2.928	2.990	2.976	2.982	2.987	3.002
Ti	0.002	0.001	0.004	0.000	0.000	0.001
Al	1.076	1.027	1.019	1.029	1.020	1.000
Fe	0.001	0.000	0.002	0.002	0.002	0.001
Mn	0.000	0.000	0.002	0.000	0.000	0.001
Mg	0.001	0.000	0.000	0.000	0.001	0.001
Ca	0.083	0.004	0.005	0.002	0.003	0.003
Na	0.269	0.187	0.119	0.081	0.089	0.114
K	0.606	0.754	0.876	0.891	0.884	0.861
Cr	0.002	0.002	0.005	0.002	0.003	0.001
X_{Av}	0.28	0.20	0.12	0.08	0.09	0.12
X_{An}	0.09	0.00	0.00	0.00	0.00	0.00
X_{Or}	0.63	0.80	0.88	0.91	0.91	0.88

Table 5.3.12. Selected representative values for K-feldspar in metapelites in the amphibolite facies (IZ 016), the transition zone (IV 020) and the granulite facies (IZ 005) from Val Strona di Omegna; for K-feldspar from Val Sesia (IV 026) and for K-feldspar from Val Strona di Postua (IZ 165, IZ 163). Cations are calculated for 8 oxygens.

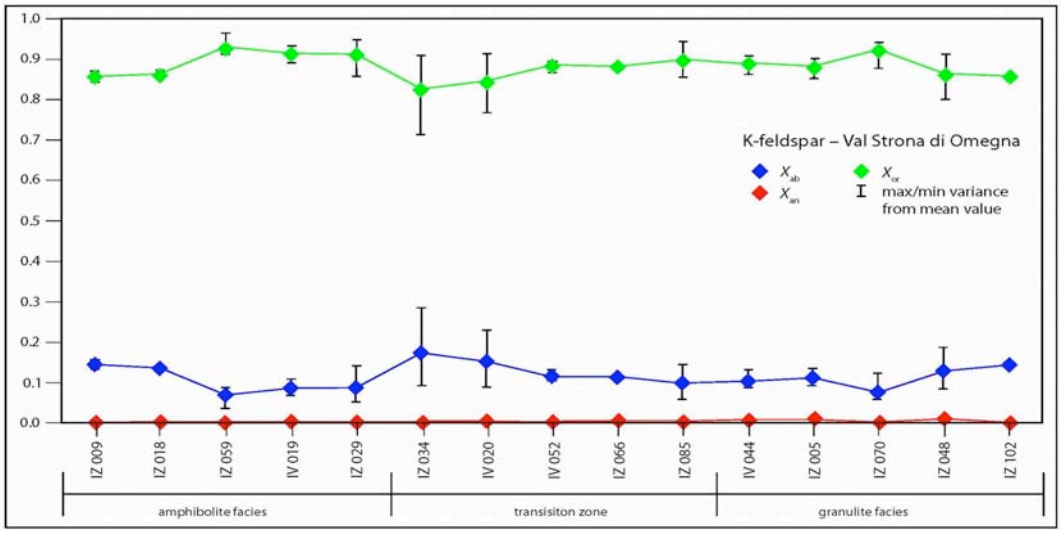

Figure 5.3.8. Trend and variation for X_{ab}, X_{an} and X_{or} in K-feldspar from Val Strona di Omegna.

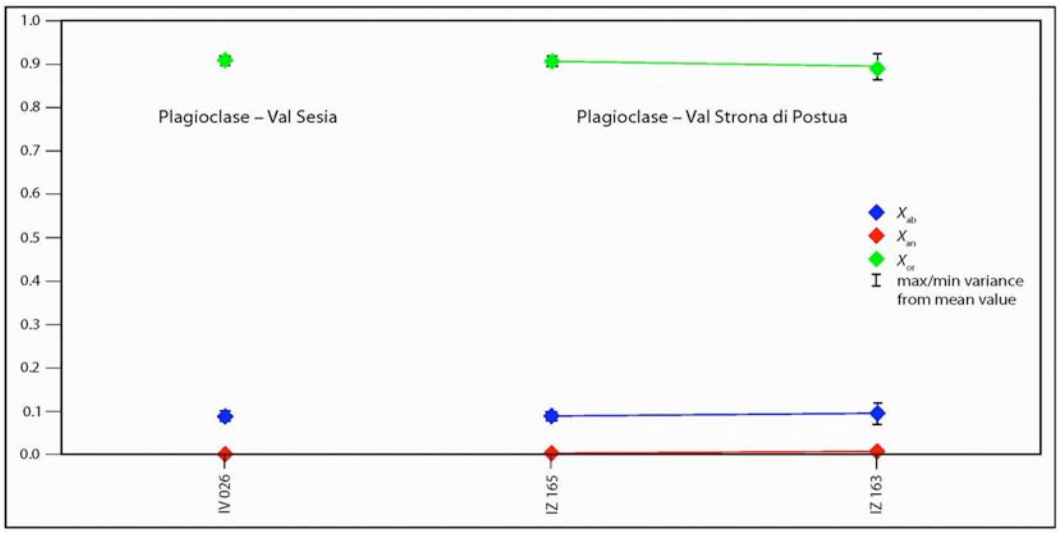

Figure 5.3.9. Values for X_{ab}, X_{an} and X_{or} in K-feldspar from Val Sesia (left) and Val Strona di Postua (right).

As shown in Fig. 5.3.10 the composition of K-feldspar is similar in all of the three valleys, all with high X_{or} contents. In samples from the transition zone and the granulite facies in Val Strona di Omegna K-feldspar has a wide range in X_{or} and X_{ab} contents.

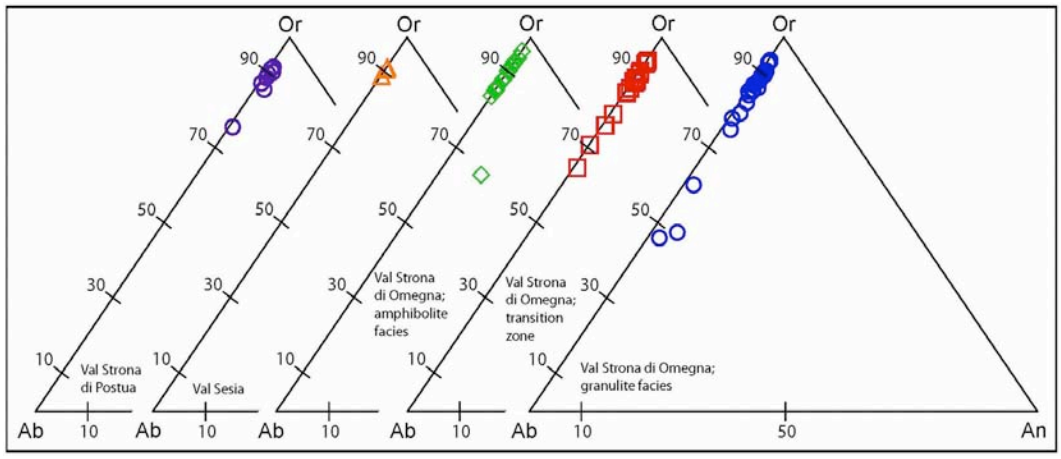

Figure 5.3.10. Ternary diagrams showing the variation of X_{ab}, X_{an} and X_{or} in K-feldspar from metapelites from Val Strona di Postua, Val Sesia and Val Strona di Omegna (divided into the facies).

5.3.6 Plagioclase

In general no continuous trend in plagioclase compositions occurs in any of the three valleys. As shown in Fig. 5.3.12, plagioclase compositions range widely in amphibolite facies samples from Val Strona di Omegna but are more clustered in the transition zone and the granulite facies. Analyses of plagioclase in Val Strona di Postua are similar to granulite facies samples in Val Strona di Omegna. In Val Sesia analyses of plagioclase can be divided into two groups of which one is richer in X_{ab} and the other is richer in X_{an}. The latter are from plagioclase in sample IZ 201 located next to the Mafic Complex. Plagioclase in metapsammite/metagreywacke samples from Val Strona di Omegna shows a wide range in values varying from $X_{ab} < 50$ to $X_{ab} > 80$.

According to Schmid & Wood (1976), a trend in chemistry of plagioclase in metapelites from Val Strona di Omegna is recognizable through the valley, with plagioclase becoming more Ca-rich from low-grade to high-grade conditions. This variation is not obvious from the data from this study, and higher grade samples do not tend to be more anorthite-rich (Fig. 5.3.11). The albite contents of this mineral vary between X_{ab} = 0.46–0.88 throughout the valley. Plagioclase in amphibolite facies samples is Na-rich with X_{ab} = 0.49–0.88 (oligoclase to andesine), in the transition zone the composition varies from oligoclase to labradorite (X_{ab} = 0.46–0.78) and under granulite facies conditions andesine and oligoclase are present (X_{ab} = 0.62–0.74). In every facies the plagioclase contains X_{or} = 0–0.02 with a maximum of X_{or} = 0.05 at the beginning of the granulite facies.

In the metapsammites/metagreywackes plagioclase is more anorthite rich than in the metapelites. In sample IZ 120 X_{Ab} varies between 0.31 and 0.47 with X_{Or} = 0–0.03. The other sample, IZ 129 has two types of plagioclase, one with X_{Ab} = 0.14–0.27 (oligoclase) and X_{Or} = 0–0.01 and a second variant with X_{Ab} = 0.43–0.5 (andesine) and X_{Or} = 0.01–0.02. These two types of plagioclase could be explained as the albite component of the plagioclase fractionates into

the melt during partial melting and the remaining plagioclase becomes more anorthite rich (Bowen, 1913; Sawyer, 2008).

ample	IZ 010	IV 020	IV 044	IV 034	IZ 201	IZ 132	IZ 163	IZ 120	IZ 129
SiO_2	65.32	58.06	58.27	61.96	56.60	58.07	58.00	50.49	48.67
TiO_2	0.00	0.00	0.00	0.00	0.00	0.00	0.00	0.05	0.00
Al_2O_3	21.45	25.92	26.24	23.86	26.81	25.48	25.13	30.28	31.45
FeO	0.01	0.04	0.05	0.03	0.00	0.00	0.03	0.03	0.02
MnO	0.03	0.00	0.01	0.04	0.01	0.02	0.02	0.00	0.00
MgO	0.00	0.00	0.00	0.00	0.00	0.00	0.01	0.01	0.00
CaO	2.39	7.37	8.19	5.22	9.06	7.64	7.62	14.05	15.36
Na_2O	10.39	7.04	6.96	8.58	6.55	7.04	6.99	3.52	2.80
K_2O	0.17	0.31	0.18	0.16	0.16	0.33	0.25	0.07	0.11
Cr_2O_3	0.05	0.04	0.01	0.00	0.04	0.00	0.01	0.03	0.03
Total	99.80	98.78	99.91	99.85	99.24	98.59	98.06	98.54	98.44
Si	2.881	2.625	2.610	2.751	2.561	2.633	2.642	2.332	2.261
Ti	0.000	0.000	0.000	0.000	0.000	0.000	0.000	0.002	0.000
Al	1.115	1.381	1.385	1.249	1.430	1.362	1.349	1.649	1.722
Fe	0.000	0.002	0.002	0.001	0.000	0.000	0.001	0.001	0.001
Mn	0.001	0.000	0.000	0.002	0.000	0.001	0.001	0.000	0.000
Mg	0.000	0.000	0.000	0.000	0.000	0.000	0.001	0.001	0.000
Ca	0.113	0.357	0.393	0.248	0.439	0.371	0.372	0.695	0.764
Na	0.888	0.617	0.604	0.739	0.575	0.619	0.617	0.315	0.252
K	0.009	0.018	0.010	0.009	0.009	0.019	0.015	0.004	0.006
Cr	0.002	0.002	0.000	0.000	0.002	0.000	0.000	0.001	0.001
X_{Av}	0.88	0.62	0.60	0.74	0.56	0.61	0.61	0.31	0.25
X_{An}	0.11	0.36	0.39	0.25	0.43	0.37	0.37	0.69	0.75
X_{Or}	0.01	0.02	0.01	0.01	0.01	0.02	0.01	0.00	0.01

Table 5.3.13. Selected representative values for plagioclase in metapelites in the amphibolite facies (IZ 010), the transition zone (IV 020) and the granulite facies (IV 044) from Val Strona di Omegna; for plagioclase from Val Sesia (IV 034, IZ 201); for plagioclase from Val Strona di Postua (IZ 132, IZ 163) and for plagioclase in metapsammites/metagreywackes from Val Strona di Omegna (IZ 120, IZ 129). Cations are calculated for 8 oxygens.

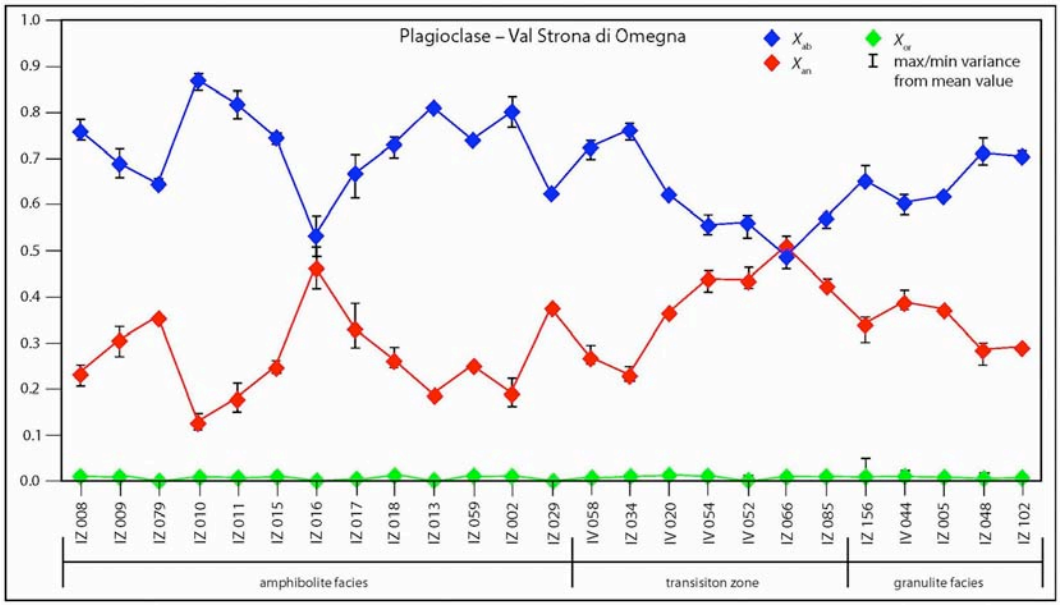

Figure 5.3.11. Trend and variation for X_{ab}, X_{an} and X_{or} in plagioclase from Val Strona di Omegna.

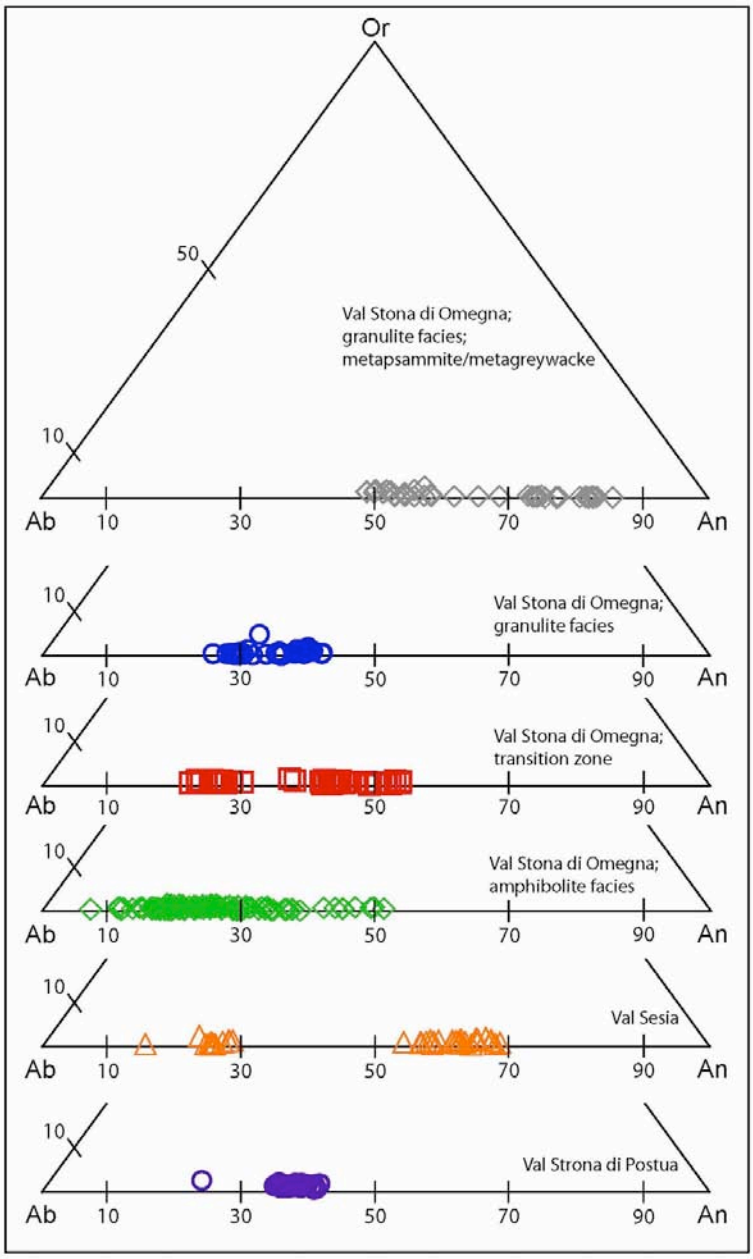

Figure 5.3.12. Ternary diagrams showing the variation of X_{ab}, X_{an} and X_{or} in plagioclase from metapelites from Val Strona di Postua, Val Sesia and Val Strona di Omegna (divided into the facies). In addition the variation in plagioclase from metapsammite/metagreywacke samples in Val Strona di Omegna is illustrated.

Plagioclase in metapelite samples from Val Sesia has X_{ab} = 0.54–0.84 (andesine to oligoclase) and X_{or} = 0.01–0.02. The proportion of X_{an} shows a decrease for the lowest grade samples (IV 034–IZ 168) and an increase (sample IZ 168–IZ 201) towards the border with the Mafic Complex, which is vice versa for X_{ab} in these samples (Fig. 5.3.13). The composition of plagioclase in metapelites from Val Strona di Postua shows neither an increase nor a decrease in any major

element (Fig. 5.3.14). The plagioclase is andesine with X_{Ab} = 0.57–0.65 and X_{Or} = 0.01–0.02.

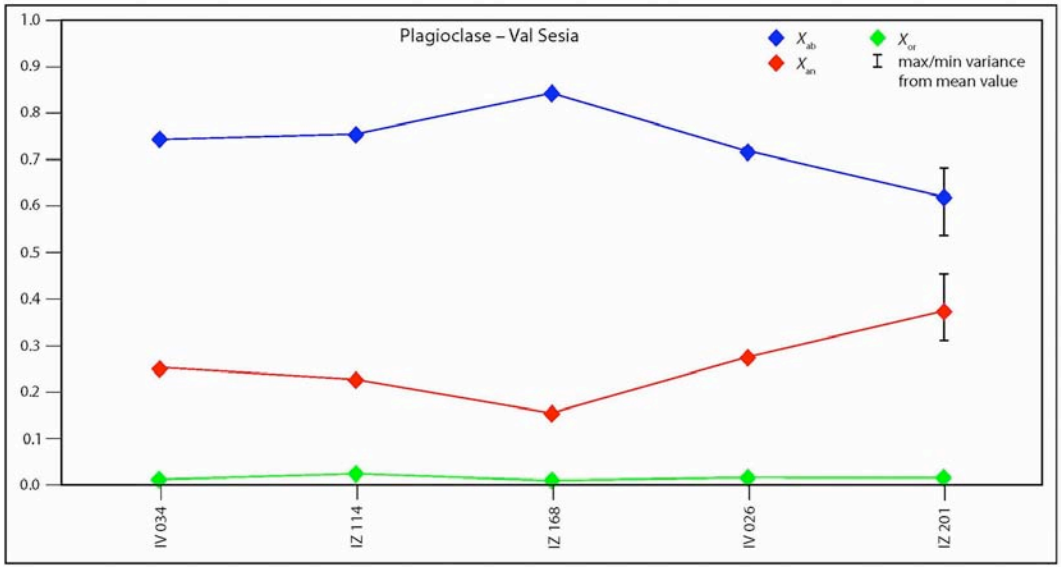

Figure 5.3.13. Trend and variation for X_{ab}, X_{an} and X_{or} in plagioclase from Val Sesia.

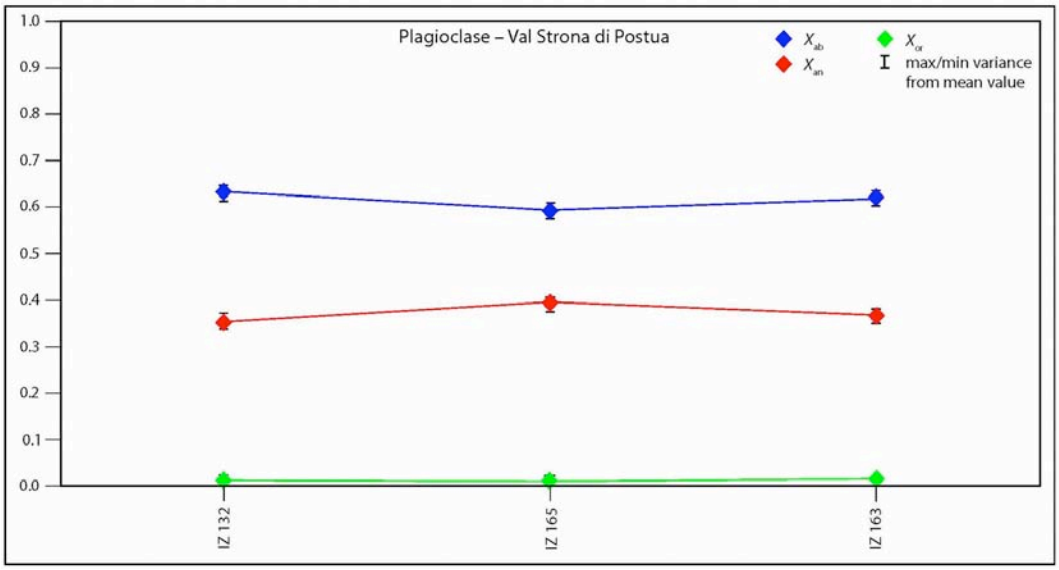

Figure 5.3.14. Variation for X_{ab}, X_{an} and X_{or} in plagioclase from Val Strona di Postua.

5.4 Summary

In summary, whole rock and mineral chemistry of major elements are consistent with the field and thin section observations reflecting that granulite facies

samples are partially molten and lost varying amounts of melt. As a consequence, the granulite facies samples are depleted in elements (SiO_2, Al_2O_3, Na_2O and K_2O) that are preferably mobile and enriched in the melt phase. In places this melt crystallised as leucosomes that are rich in quartz and feldspars. Consistent to this the granulite facies samples are enriched in immobile phases such as TiO_2 and FeO. The mineral chemistry shows only a trend for garnet and biotite in Val Strona di Omegna with a decrease in X_{Fe}.

Chapter 6
Calculated phase equilibria constraints on the metamorphic *P–T* conditions

6.1 Introduction

In this chapter the calculated *P–T* pseudosections will be described. In each *P–T* pseudosection the red highlighted field shows the inferred preserved metamorphic assemblage for the appropriate sample. These assemblages are not necessarily peak metamorphic assemblages, because some of the minerals investigated in thin sections could be metastable or formed on the retrograde path. The bulk rock H_2O contents during cooling exert a strong influence on the preserved assemblages and degree of retrogression of the appropriate samples (e.g. White & Powell, 2002). In the *P–T* pseudosections the blue dashed lines display contours for the modal abundance of melt/*liquid*, while the black dotted line shows the position of the solidus.

6.2 Conditions for the calculated *P–T* pseudosections

Pseudosections were calculated in the NCKFMASHTO (Na_2O–CaO–K_2O–FeO–MgO–SiO_2–H_2O–TiO_2–O) system using THERMOCALC 3.30i and 3.33i (Powell & Holland, 1988) and the internally consistent dataset of Holland & Powell (1998, ds55, updated 22 November 2003). The *a–x* models used are: garnet, biotite and melt (White *et al.*, 2007), K-feldspar and plagioclase (Holland & Powell, 2003), cordierite (Holland & Powell, 1998), orthopyroxene, spinel and magnetite (White

et al., 2002), ilmenite and hematite (White *et al.*, 2000) and muscovite and paragonite (Coggon & Holland, 2002). Manganese was not considered for the reasons given in White *et al.* (2007). The following mineral abbreviations are used in the *P–T* pseudosections: g – garnet; opx – orthopyroxene; di – diopside (clinopyroxene); cd – cordierite; sp – spinel; hb – hornblende; ged – gedrite; bi – biotite; mu – muscovite; pa – paragonite; sill – sillimanite; ky – kyanite; ksp – K-feldspar; pl – plagioclase; ilm – ilmenite; mt – magnetite; ru – rutile; q – quartz; liq – silicate melt*/liquid*; H_2O – fluid phase. The pseudosections use bulk rock compositions based on major element XRF analyses (Appendix A). The values for the bulk rock H_2O contents were estimated from the measured 'loss on ignition' (LOI), which decrease with increasing grade of metamorphism. These H_2O values based on LOI represent maximum values given that LOI typically involves other volatile species. Furthermore, any hydrous retrogression due to fluid influx subsequent to high-grade metamorphism will result in the LOI values being an overestimate of peak H_2O content for a given sample. Three samples modelled (IV 058, IZ 114 and IZ 168) had unusually high LOI values, resulting in wide fields of coexisting H_2O and melt, and the H_2O contents were subsequently reduced such that only a small proportion (< 1%) of fluid co-exists with melt at the solidus. The *P–T* pseudosections for these three samples calculated using the measured LOI contents (IV 058, IZ 114 and IZ 168) are given in Appendix C. For Fe_2O_3, a fixed content of 0.1 mol% was assumed, consistent with the results of Fe^{3+} titration on a limited number of samples, which were mostly around 0.1 mol%.

To further constrain the *P–T* estimates most of the pseudosections were contoured for the modal abundances of minerals, mostly garnet and biotite, additionally sillimanite, muscovite and cordierite. These calculated modes were compared with estimated of modal proportions of minerals in thin section.

6.3 Val Strona di Omegna

P–T pseudosections were calculated for six samples of metapelite and three samples of metapsammite/metagreywacke from Val Strona di Omegna (Fig. 6.3.1) The *P–T* pseudosections for the metapelites are shown in Figs. 6.3.2–6.3.7 and described from low-grade to high-grade conditions. Two samples from each of the amphibolite facies (zone 1, 2), the transition zone (zone 3) and the granulite facies (zone 4, 5) were modelled. The *P–T* pseudosections for the metapsammites/metagreywackes samples are shown in Figs. 6.3.8–6.3.10. One sample contains an amphibolite facies assemblage (zone 1), whereas both other samples are from the granulite facies (zone 4) and these are also described from low-grade to high-grade. The bulk rock compositions (mol%) used for each pseudosection are listed in Tab. 6.3.1, while the *P–T* estimates for the inferred peak metamorphic assemblage fields are summarised in Tab. 6.3.2. To further constrain the *P–T* estimates of the assemblages fields contours for the modal abundance of major minerals were calculated and are summarised in Fig. 6.3.11 (upper part). In addition, the results of *P–T* estimates for metapsammites/metagreywackes are summarised in Fig. 6.3.11 (lower part).

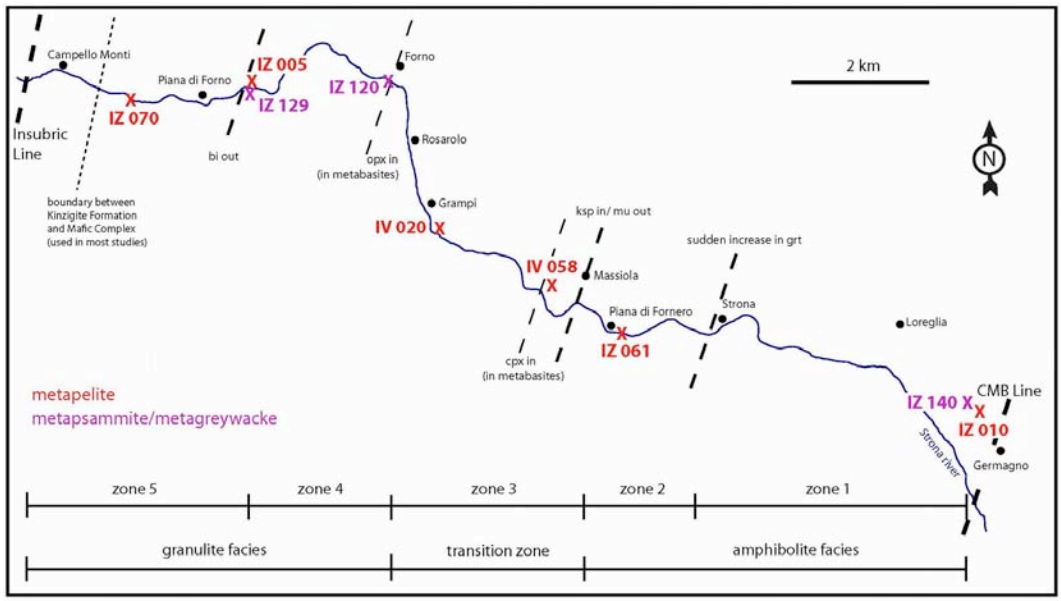

Figure 6.3.1. Schematic map of Val Strona di Omegna with locations of the samples that were used for calculation of *P–T* pseudosections.

	H_2O	SiO_2	Al_2O_3	CaO	MgO	FeO	K_2O	Na_2O	TiO_2	O
IZ 010	4.34	74.46	9.40	0.38	2.54	4.55	2.01	1.57	0.65	0.1
IZ 061	4.72	67.00	12.80	0.30	4.04	6.83	2.60	0.75	0.86	0.1
IV 058	6.13*	58.52	14.67	0.99	6.14	7.91	2.83	1.63	1.08	0.1
IV 020	1.26	68.71	13.27	1.02	3.64	7.93	2.40	0.85	0.82	0.1
IZ 005	1.97	67.90	12.22	0.75	5.62	8.32	1.39	0.87	0.86	0.1
IZ 070	1.65	64.72	14.37	0.36	5.73	9.75	1.81	0.36	1.15	0.1
IZ 140	3.52	68.05	10.30	5.55	3.83	5.02	1.47	1.65	0.51	0.1
IZ 120	1.28	55.84	10.79	8.98	10.39	9.93	0.14	0.93	1.62	0.1
IZ 129	0.32	59.60	9.94	6.87	9.25	9.45	0.26	2.38	1.83	0.1

Table 6.3.1. Bulk rock compositions (mol%) of six metapelite and three metapsammite/metagreywacke samples used for the calculation of *P–T* pseudosections from Val Strona di Omegna. The bulk rock compositions are normalised to 100%. The H_2O value for IV 058 (*) was analysed with 14.57 mol%, which is unrealistically high for peak conditions and a value of 1 mol% fluid phase was assumed for the calculation of the pseudosection above the solidus. "O" is used for the amount of Fe_2O_3.

Metapelites

The lowest grade sample of metapelite, IZ 010 (Fig. 6.3.2), is located north of Germagno (Fig. 6.3.1) and contains the assemblage sill-bi-mu-pl-q-ilm ± H_2O/*liq*. The contours for the modal abundance of *liquid* (blue dashed lines) shows that a sample with the measured bulk rock composition and assemblage can contain a maximum of 3 to 4 % melt, an amount which is unlikely to be observable as leucosomes in the field. It is not clear if sample IZ 010 contained a small amount of melt, H_2O or both, so three assemblage fields for this sample are highlighted. The pseudosection shows that this sample could produce 30 to 40 % melt under higher grade conditions with temperatures above 850 °C. The *P–T* estimates for the three assemblage fields of this sample define a range of < 640 °C to 730 °C and < 3.4 to 8.4 kbar (Tab. 6.3.2) with the solidus located at around 650 °C. With the calculation of contours for the modal abundances of minerals (Fig. 6.3.11) a similar *P–T* range (< 640–710 °C and < 3.4–7.9 kbar) is defined (Tab. 6.3.2). The contouring was undertaken for the abundance of muscovite and sillimanite in the sample (investigated in thin sections), which is less than 9 % and less than 6 % respectively.

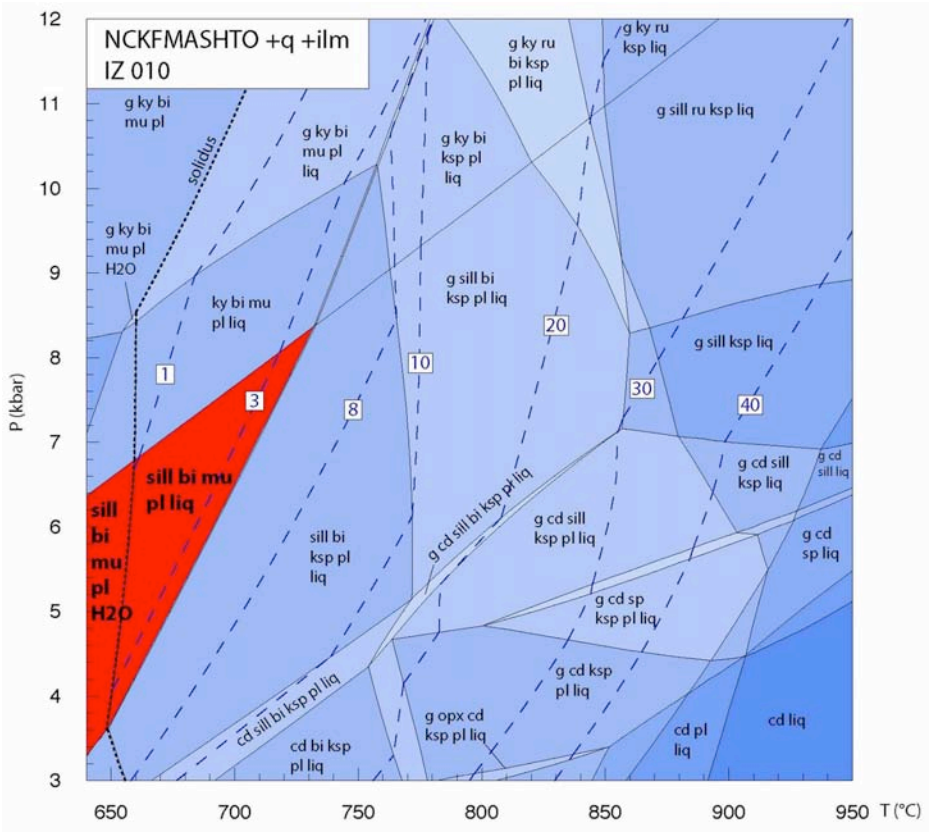

Figure 6.3.2. *P–T* pseudosection for sample IZ 010.

In sample IZ 061 (Fig. 6.3.3), located next to Piana di Fornero (Fig. 6.3.1), K-feldspar occurs as an additional phase within the otherwise identical assemblage to that in sample IZ 010 (sill-bi-mu-ksp-pl-q-ilm-*liq*). The stability of this assemblage is confined to a very narrow field. Based on the small amount of K-feldspar in the sample, it is possible, or likely, that the peak temperature was at slightly higher *T* than this field and muscovite either persisted metastably or formed on the retrograde path. Consequently, a larger possible assemblage field that extends to higher T is highlighted. The field is bordered by the amount of melt (< 5 %) in this sample because field observations show no evidence for partial melting for this sample. The amount of melt that can result from this sample under higher grade conditions (T > 850 °C) is similar to those of sample IZ 010 with approximately 30 to 40 % melt. The *P–T* estimates of the assemblage field give temperatures of 650–780 °C and pressures of 3.5–9.1 kbar, similar to the *P–T* estimates from sample IZ 010 (Tab. 6.3.2). The solidus occurs at around

650 °C at pressure of around 3.5 kbar and moves to higher temperatures with increasing pressure.

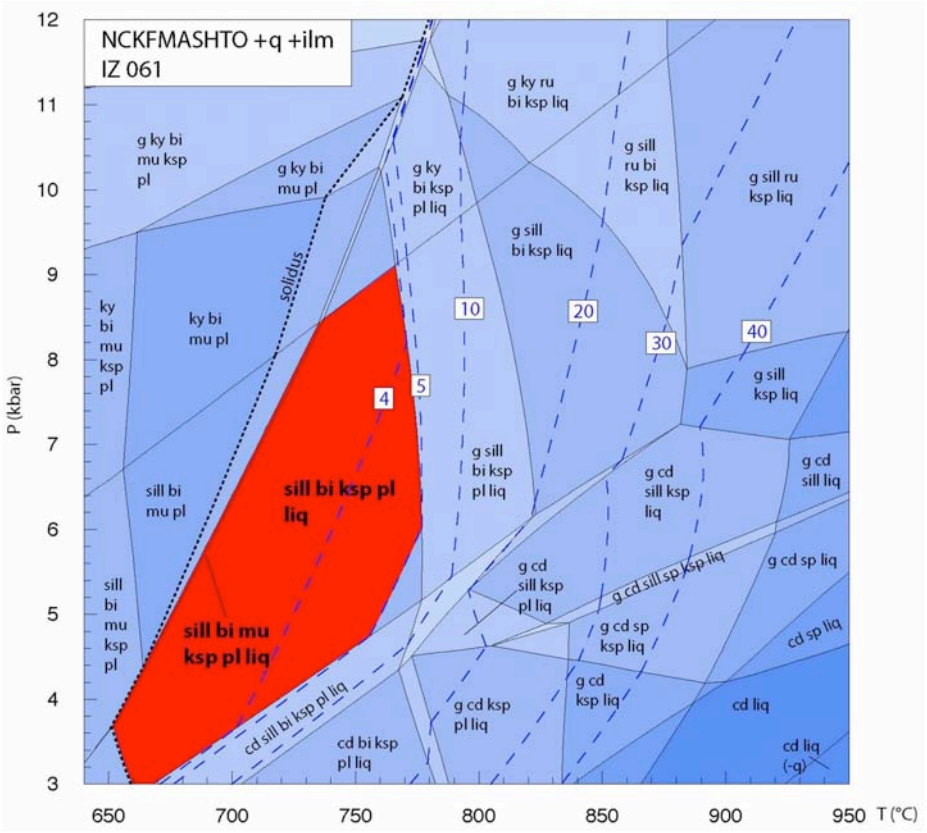

Figure 6.3.3. *P–T* pseudosection for sample IZ 061.

Sample IV 058 (Fig. 6.3.4) is the first sample within the transition zone, located west of Massiola (Fig. 6.3.1), and preserves the assemblage g-sill-bi-pl-q-ilm-*liq*. This sample does not contain K-feldspar, which should be present in the transition zone based on the position of the muscovite-out/K-feldspar-in isograd. Further, an unrealistically high LOI content resulted from the measurements. Consequently, the *P–T* pseudosection from sample IV 058 was calculated with an amount of around 1 mol% fluid phase above the solidus (Chapter 6.2). The assemblage field is consistent with temperatures of 730–800 °C and pressure of 5.7–9.6 kbar and with the production of around 5–10 % *liquid*. With contours for the modal abundance of minerals (Fig. 6.3.11) it is possible to further constrain the temperature estimates to 750–800 °C at similar pressures (Tab. 6.3.2). The

constraints using contours for sample IV 058 were made with the amount of garnet (< 5 %) biotite (35–40 %) present in the sample.

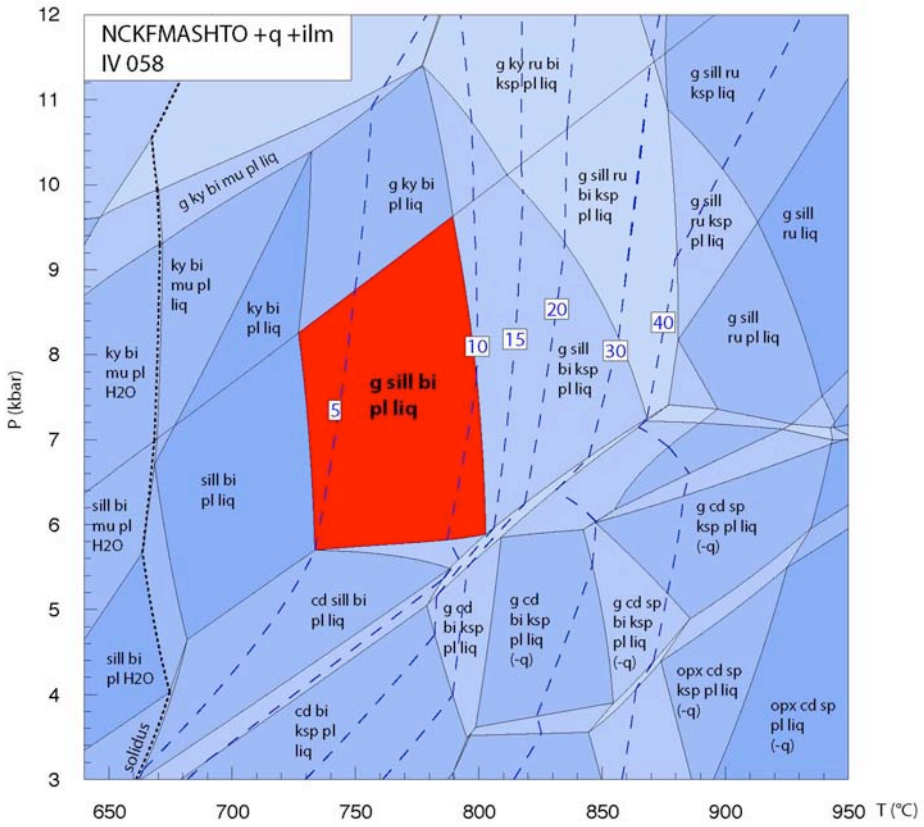

Figure 6.3.4. *P–T* pseudosection for sample IV 058.

The next sample, IV 020, was collected from south of Grampi (Fig. 6.3.1) and has the typical mineral assemblage of the transition zone with g-sill-bi-ksp-pl-q-ilm-*liq* (Fig. 6.3.5). With this present assemblage the sample contains a maximum of 5 % *liquid* but it would produce up to 10 % melt under temperature conditions higher than 850 °C. The *P–T* estimates for this sample are 810–850 °C and 6–10 kbar. The mineral mode contours constrain the temperature conditions to a minimum temperature of 815 °C at 6–10 kbar (Tab. 6.3.2), as this sample contains more than 10 % biotite (Fig. 6.3.11). The solidus occurs at around 810 °C but at higher temperatures of 850 °C at pressures lower than 5 kbar.

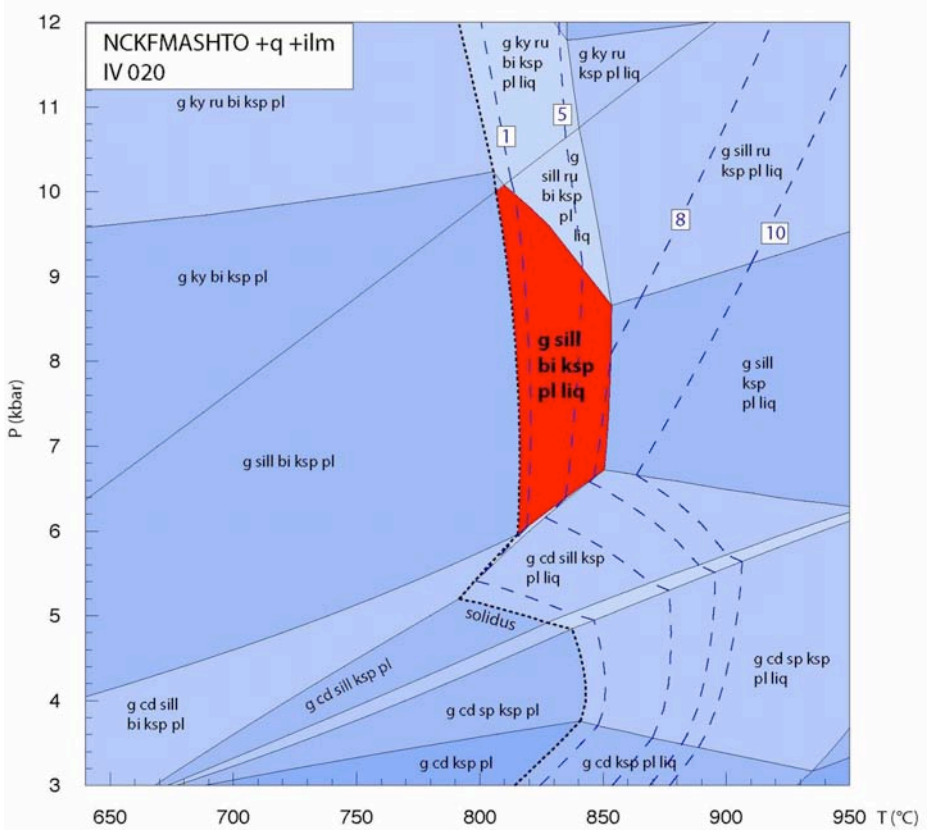

Figure 6.3.5. *P–T* pseudosection for sample IV 020.

The first calculated sample from the granulite facies, IZ 005 (Fig. 6.3.6), was collected from east of Piana di Forno (Fig. 6.3.1). Sample IZ 005 contains the assemblage g-sill-ru-bi-ksp-pl-q-ilm-*liq* with an amount of melt estimated at 1–10 %. The *P–T* estimates suggest temperatures between 820 and 870 °C with corresponding pressures of 7.3 to 11.2 kbar. Similar to the previous sample the solidus occurs at around 800 °C. The result of constraining the *P–T* conditions using contours for the modal abundance of minerals gives pressures that are almost the same (7.6 to 11.2 kbar) but temperatures are constrained to approximately 860 °C (Fig. 6.3.11; Tab. 6.3.2) based on the presence of more than 30 % garnet and more than 1–5 % biotite within the sample.

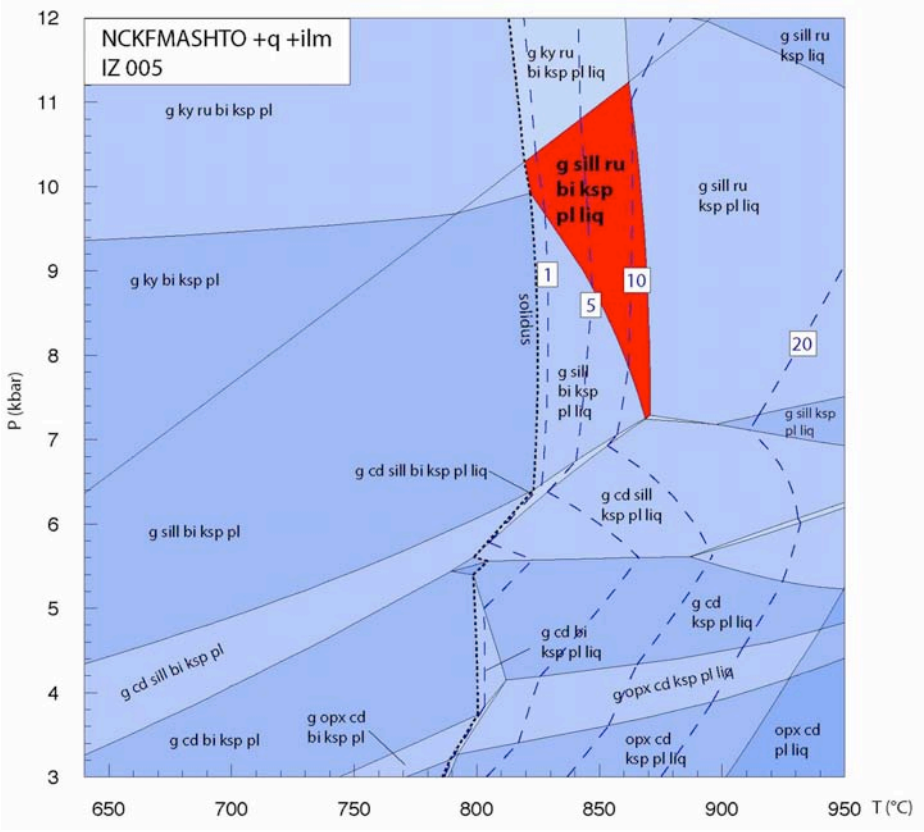

Figure 6.3.6. *P–T* pseudosection for sample IZ 005.

Sample IZ 070 (Fig. 6.3.7) is the highest grade metapelites modelled and was collected west of Piana di Forno (Fig. 6.3.1). The inferred peak mineral assemblage is similar to IZ 005 but without biotite or plagioclase. *P–T* estimates are 870 to > 950 °C and 7.2 to > 12 kbar. The amount of melt predicted at these conditions is 8–20 %. The solidus occurs, as typical for the high-grade samples, at around 800 °C. With the calculation of contours for the modal abundance of minerals (Fig. 6.3.11) the pressure estimates can further be constrained from 9.5 to > 12 kbar at similar temperatures (Tab. 6.3.2). The restricted *P* range was based on the large amount of garnet, which is more than 35 % in this sample.

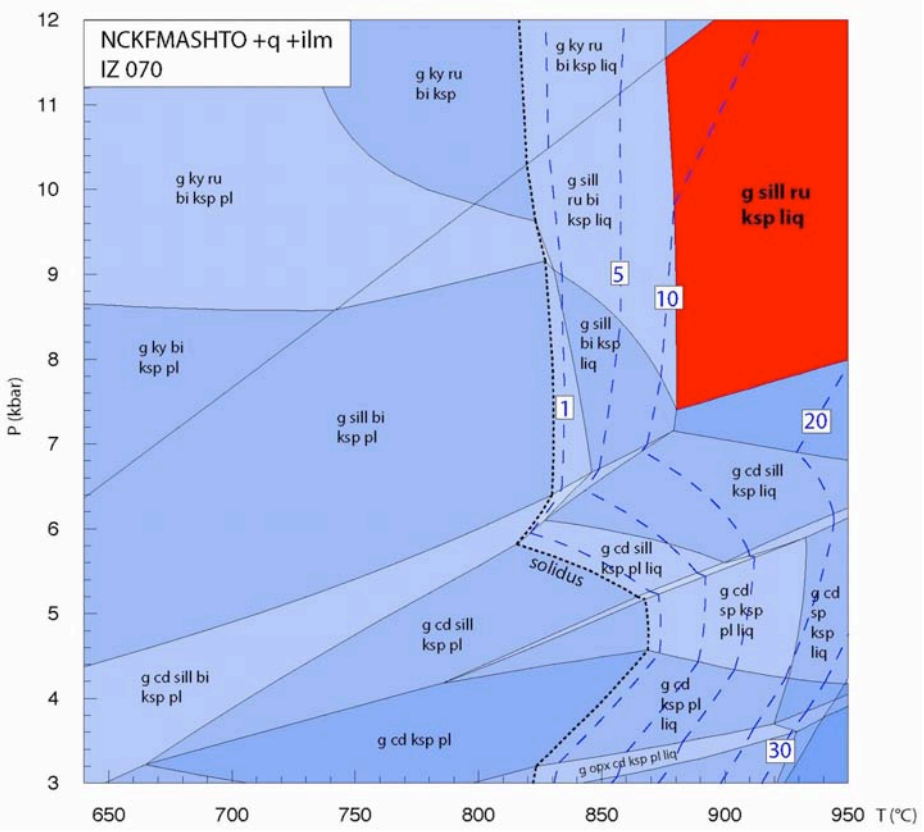

Figure 6.3.7. *P–T* pseudosection for sample IZ 070.

Metapsammites/Metagreywackes

Sample IZ 140 (Fig 6.3.8) is located north of Germagno (Fig. 6.3.1) and is the lowest grade sample of metapsammite/metagreywacke. It contains the assemblage g-bi-pl-q-ilm-*liq* ± H_2O. Although the field observations show no evidence for partial melting, the production of a small amount (less than 5%) melt cannot be precluded. This sample contains neither sillimanite nor cordierite and the only assemblage fields consistent with this contain a small amount of melt. *P–T* estimates are 720–785 °C and 5.8–10.4 kbar (Tab. 6.3.2). A rock with this composition can produce up to 20 % melt at higher grade conditions at $T > 850$ °C. The wet solidus is present at around 750 °C, which is 100 °C higher than the wet solidus in the metapelites from nearby locations (IZ 010).

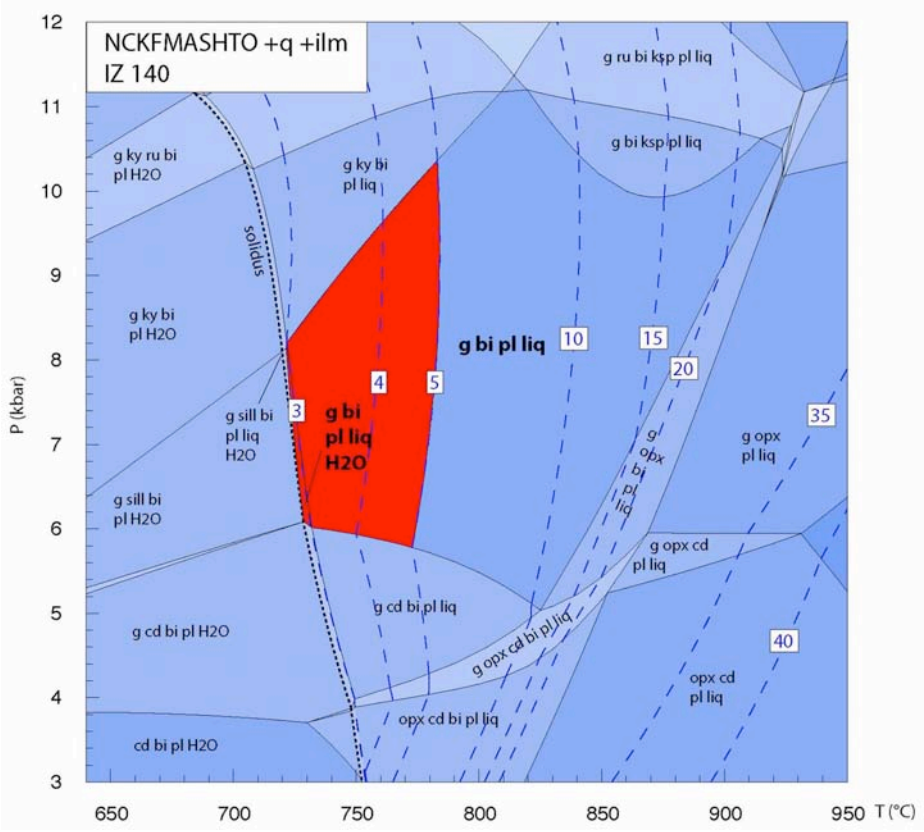

Figure 6.3.8. *P–T* pseudosection for sample IZ 140.

The second sample of the metapsammites/metagreywackes, IZ 120 (Fig 6.3.9), was collected from near Forno at the boundary between the transition zone and the granulite facies (Fig. 6.3.1). Sample IZ 120 contains the assemblage g-opx-bi-pl-q-ilm-*liq* and field observations show evidence for a small amount of partial melting. The small field defined by this assemblage yield *P–T* estimates of 790–830 °C and 7.9–8.5 kbar (Tab. 6.3.2). At the inferred *P–T* conditions the sample should contain 1–5 % *liquid* and could produce only 5–7 % melt at higher grade conditions ($T > 850$ °C). The appearance of small leucosomes in the field is consistent with these predicted melt contents. The solidus is present at around 800 °C at the inferred peak pressures.

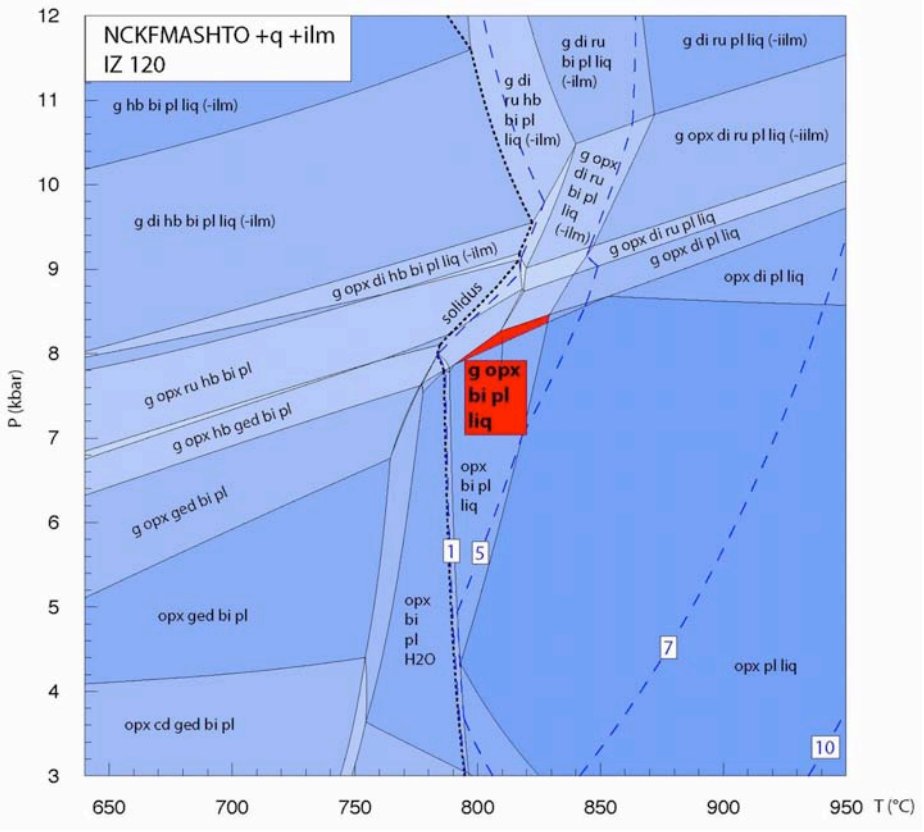

Figure 6.3.9. *P–T* pseudosection for sample IZ 120.

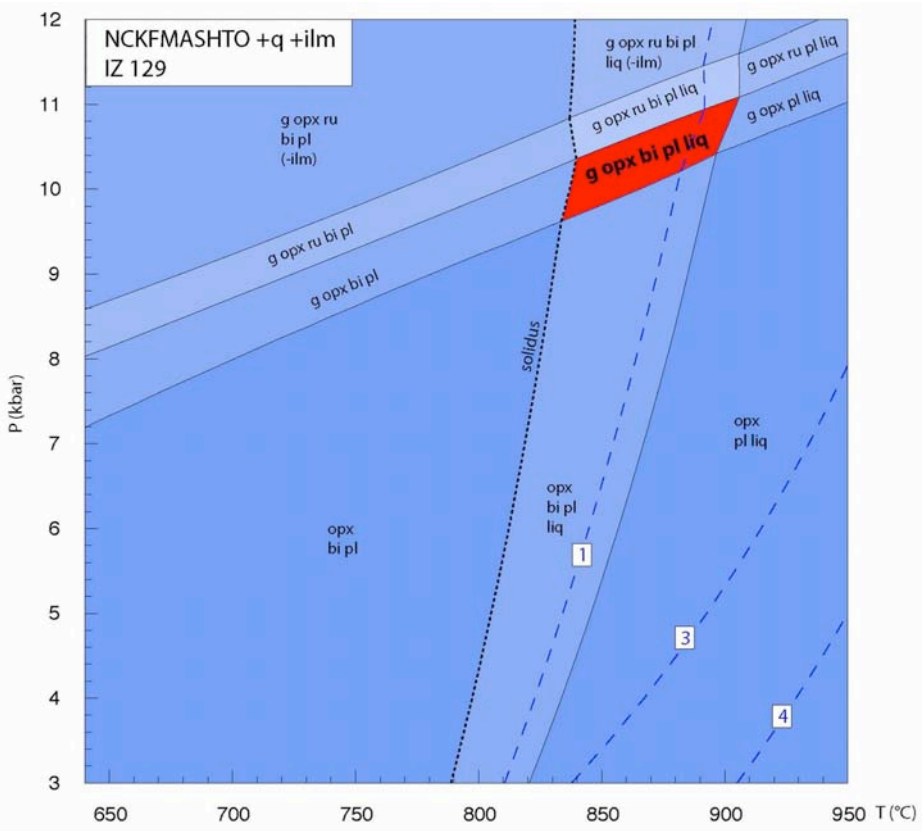

Figure 6.3.10. *P–T* pseudosection for sample IZ 129.

The highest grade metapsammite/metagreywacke sample, IZ 129 (Fig 6.3.10), was collected from near Piana di Forno, close to the biotite-out isograd (Fig. 6.3.1) and contains the assemblage g-opx-bi-pl-q-ilm-*liq*. *P–T* estimates are constrained to 830 to 910 °C and 9.6 to 11.1 kbar (Tab. 6.3.2). According to the model calculations, this sample should contain around 1 % *liquid*, but field observations suggest a higher degree of partial melting which may reflect melt loss subsequent to the crystallisation of some of the melt. The solidus is present at around 800 °C, similar to the solidus of all the metapelites in the granulite facies.

Summary

The inferred *P–T* assemblage fields appropriate to peak conditions in each of the metapelites suggest a continuous increase in both pressure and temperature occurs throughout the valley from low-grade (southeast) to high-grade (northwest) (Fig. 6.3.11 upper part; Table 6.3.2). The upper pressure limit for all the samples is the sillimanite/kyanite boundary, because sillimanite is the only stable Al_2SiO_5-polymorph in the rocks. The metamorphic field gradient in the metapelites is constrained to extend from amphibolite facies conditions of around 3.5–7.9 kbar and 650–710 °C (IZ 010), through 750–815 °C and 5.7–10 kbar in the transition zone (IV 058 and IV 020) and to granulite facies conditions at more than 870 °C and more than 9.5 kbar (IZ 070). All *P–T* pseudosections are contoured for the modal abundance of melt/*liquid* as well as for solid minerals such as garnet and biotite to narrow the *P–T* constraints. For the metapsammites/metagreywackes an increase in both pressure and temperature also occurs throughout the valley from low-grade to high-grade conditions (Fig. 6.3.11 lower part; Tab. 6.3.2), similar to the trend of the metapelites. The *P–T* estimates extends from around 725 °C and 6 kbar in the amphibolite facies (IZ 140) to 830–910 °C and 9.6–11 kbar in the granulite facies (IZ 120 and IZ 129).

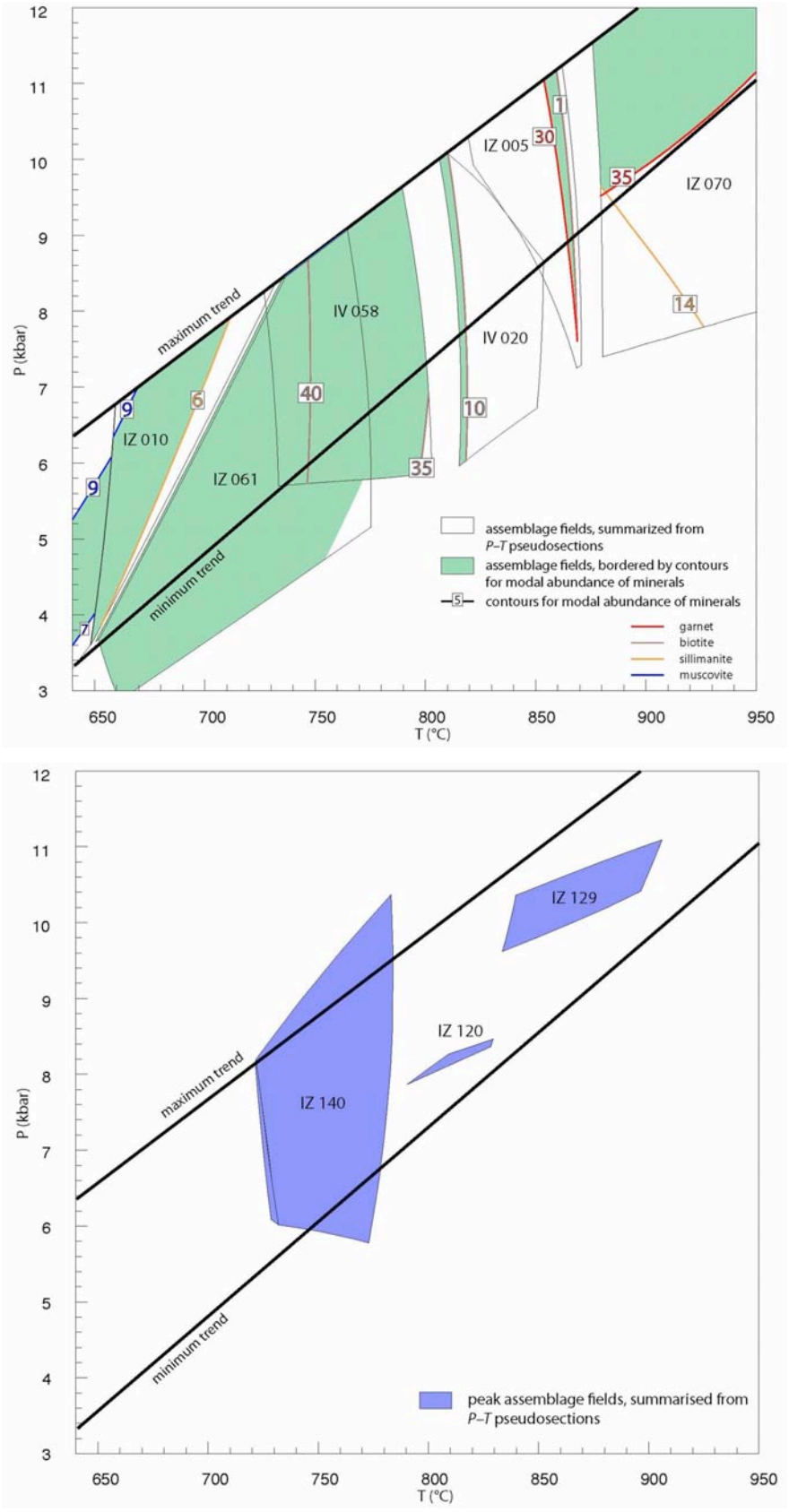

Figure 6.3.11. Summarised *P–T* conditions from the pseudosections for Val Strona di Omegna. The upper diagram shows the inferred peak assemblage fields for the metapelites, in the lower diagram the inferred peak assemblage fields for the metapsammites/metagreywackes are illustrated. In the

upper diagram the grey borders mark the peak assemblage fields from Figs. 6.3.2–6.3.7, while the green fields illustrate the *P–T* conditions constrained using contours of modal abundance of minerals (garnet, biotite, sillimanite, muscovite). The lower diagram shows the assemblage fields from Figs 6.3.8–6.3.10 but without contouring. The bold black lines in both pseudosections border the minimum and maximum trend for pressures and temperatures in this valley.

	***P–T* estimates without contouring**		***P–T* estimates with contouring**	
sample	**T (°C)**	**P (kbar)**	**T (°C)**	**P (kbar)**
IZ 010	< 640 – 730	< 3.5 – 8.4	< 640 – 710	< 3.5 – 7.9
IZ 061	650 – 780	3 – 9.1		
IV 058	730 – 800	5.7 – 9.6	750 – 800	5.7 – 9.6
IV 020	810 – 850	6 – 10	~ 815	6 – 10
IZ 005	820 – 870	7.3 – 11.2	~ 860	7.6 – 11.2
IZ 070	> 870	> 7.2	> 870	> 9.5
IZ 140	720 – 785	5.8 – 10.4		
IZ 120	790 – 830	7.9 – 8.5		
IZ 129	830 – 910	9.6 – 11.1		

Table 6.3.2. Summarised results of *P–T* estimates for Val Strona di Omegna samples. The P–T estimated are given for assemblage fields without (left) and with (right) contours for the modal abundance of minerals.

6.4 Val Sesia

Figure 6.4.1 shows the locations of the five samples in Val Sesia for which *P–T* pseudosections were calculated. Figures 6.4.2–6.4.6 show the pseudosections ordered from south/southeast to north/northwest, which correspond to low-grade to high-grade conditions.

	H_2O	SiO_2	Al_2O_3	CaO	MgO	FeO	K_2O	Na_2O	TiO_2	O
IV 034	6.65	61.94	11.12	2.34	5.95	5.60	1.92	3.65	0.73	0.1
IZ 114	6.74*	53.51	17.92	0.35	5.90	10.55	3.10	0.54	1.29	0.1
IZ 168	6.61*	58.91	15.43	0.09	5.13	9.20	3.01	0.23	1.29	0.1
IV 026	3.44	69.63	11.90	0.72	3.63	6.55	1.87	1.19	0.97	0.1
IZ 201	4.15	62.12	10.93	3.11	5.42	8.09	2.04	2.43	1.61	0.1

Table 6.4.1. Bulk rock compositions (mol%) of five metapelite samples used for the calculated *P–T* pseudosections from Val Sesia. The bulk rock compositions are normalised to 100%. The H_2O values for IZ 114 and IZ 168 (*) were analysed with 10.21 mol% and 7.9 mol% respectively, which is unrealistic and a value with 1 mol% fluid phase was assumed for the calculation of the pseudosection above the solidus. "O" is used for the amount of Fe_2O_3.

All the samples collected were considered to be amphibolite facies by Quick *et al.*, 2003, with sample IV 026 and IZ 201 from the transition zone based on field observations and thin sections. In Tab. 6.4.1 the bulk rock compositions (mol%) used for each sample modelled are listed, while in Tab. 6.4.2 the *P–T* estimates for the peak assemblage fields are summarised. To further constrain the *P–T* estimates, contours for the modal abundance of major minerals were calculated and the results are summarised in Fig. 6.4.7.

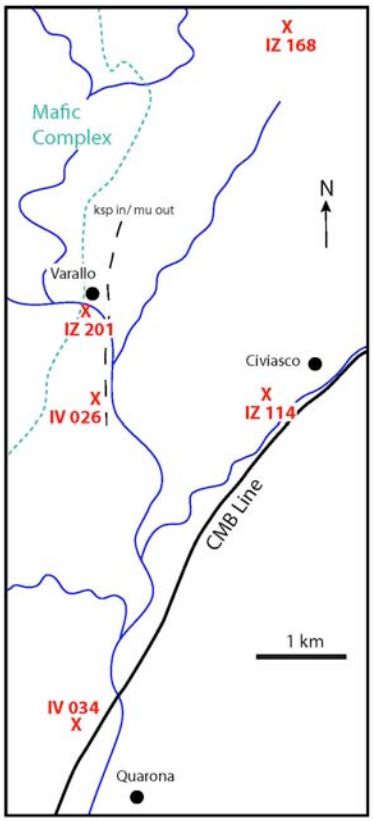

Figure 6.4.1. Schematic map of Val Sesia with locations of the samples that were used for calculation of *P–T* pseudosections.

Sample IV 034 was located northwest of Quarona, next to the CMB Line (Fig. 6.4.1) and contains the mineral assemblage g-cd-sill-bi-pl-q-ilm-*liq* ± H_2O. Based on whether the assemblage equilibrated with H_2O or not, two assemblage fields are highlighted (Fig. 6.4.2). Under the *P–T* conditions defined by these fields this sample could have up to 30% melt depending on temperature conditions. The *P–T* estimates for the two fields are 680 to 860° C and 5.9 to 7.5 kbar. To further constrain these *P–T* conditions contours for the modal abundance of minerals were calculated (Fig. 6.4.7). For the observed abundances of approximately 5 % garnet and 25 % biotite, temperatures of 735 to 770 °C with corresponding pressures of 6.5 to 6.8 kbar result. Under these conditions the amount of *liquid* is 10 to 15 % consistent with the appearance of abundant leucosomes in the field.

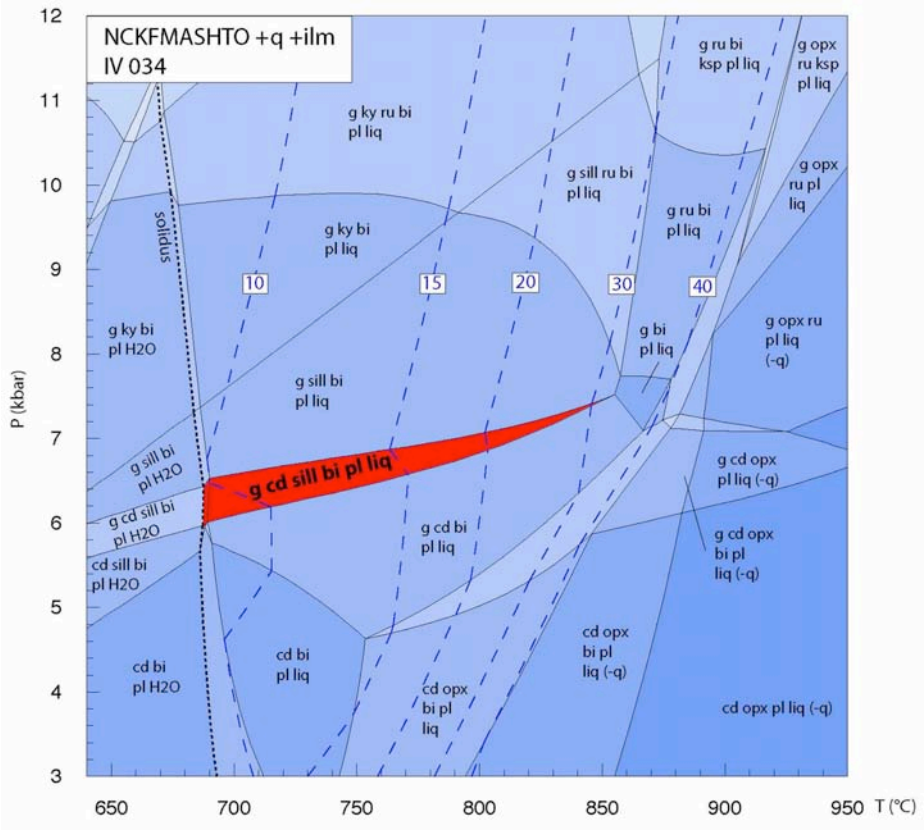

Figure 6.4.2. *P–T* pseudosection for sample IV 034.

The next sample IZ 114 is located southwest of Civiasco (Fig. 6.4.1) and is also near the CMB Line, at a similar distance as sample IV 034. Sample IZ 114 contains the assemblage g-sill-bi-pl-q-ilm. Three assemblage fields are highlighted because it is not clear, based on field relations, whether this rock contained H_2O, *liquid* or both (Fig. 6.4.3). Similar to sample IV 058 in Val Strona di Omegna, sample IZ 114 has an unusually high H_2O content based on LOI, which is inconsistent with the proportion of hydrous minerals present. The composition was adjusted for H_2O such that the model composition was just saturated in H_2O at the solidus with an amount of 1 mol% fluid phase. Pressure and temperature estimates of < 4.7 to 9.2 kbar and < 640 to 780 °C result. The highlighted assemblage fields contain 0 to 10 % *liquid* (Fig. 6.4.3). Contouring for the modal amount of minerals better constrains the *P–T* estimates to 670–720 °C and 5.2–7.8 kbar (Fig. 6.4.7). This gives less than 5 % *liquid* for the present assemblage. The *P–T* conditions using contouring for minerals was based on the assemblage having more than 50 % biotite and less than 2 % garnet. An

additional problem is that this sample contains a small amount of muscovite. Muscovite is not stable in the pseudosection together with the other investigated minerals and it is possible that muscovite formed during the retrograde history.

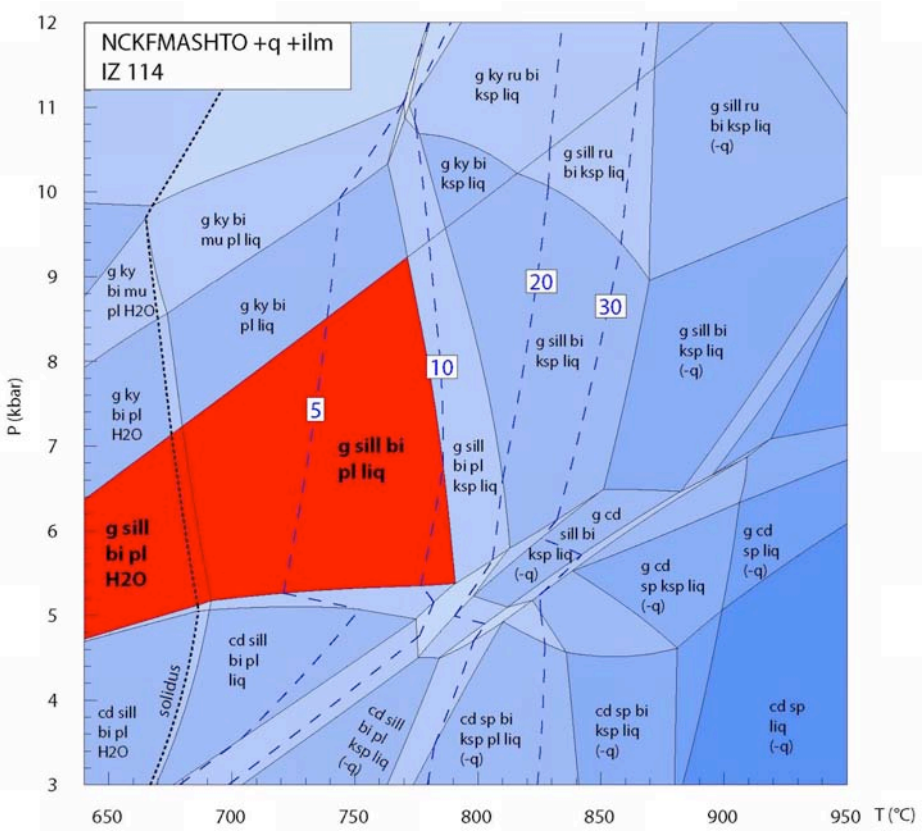

Figure 6.4.3. *P–T* pseudosection for sample IZ 114.

Sample IZ 168 was collected from a small valley perpendicular to the main Sesia valley around 3 km north of Civiasco (Fig. 6.4.1). The assemblage is similar to those of both previous samples (g-sill-bi-pl-q-ilm-*liq*). This sample also yield an unrealistically high H_2O content (7.9 mol%), so it was recalculated from the solidus up to higher pressure and temperatures with an amount of 1 mol% H_2O at the solidus similar to IZ 114. Based on the resulting narrow field, temperatures of 760 to 785 °C and pressures of 5.3 to 9.2 kbar results. This assemblage contains around 7–10 % *liquid*. Under higher grade conditions 30 % *liquid* or higher could result (Fig. 6.4.4). Similar to the amphibolite facies metapelites of Val Strona di Omegna, the solidus occurs at around 650 °C. As with sample IZ 114 muscovite is present in small amounts, but no assemblage field containing the observed

assemblage additionally with muscovite is present. Muscovite likely either persisted metastably or formed on the retrograde path.

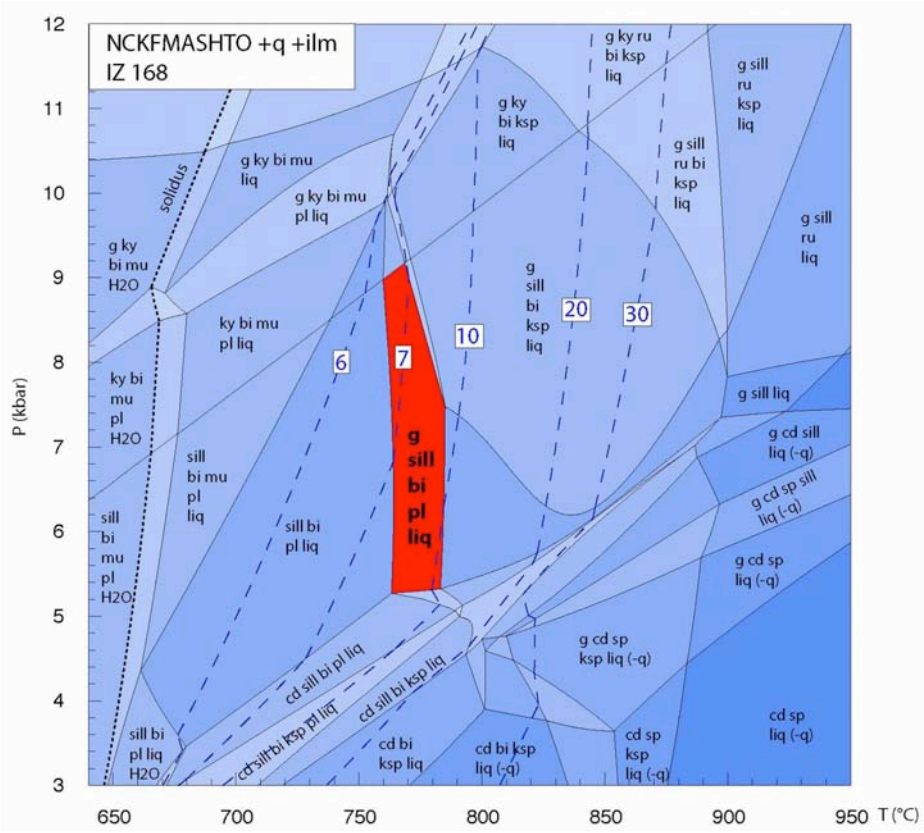

Figure 6.4.4. *P–T* pseudosection for sample IZ 168.

The fourth sample IV 026 was collected south of Varallo (Fig. 6.4.1). The assemblage differs from those of the three previous samples by containing both cordierite and K-feldspar additionally to g-sill-bi-pl-q-ilm-*liq*. Two peak assemblage fields are highlighted because it is not clear if biotite is part of the assemblage or resulted from growth on the retrograde path. Inferred temperatures are 760–940 °C but pressures are lower than in the other three samples (4.9–7.1 kbar). The mineral assemblage contains 5 to 30 % *liquid* depending on the position in the assemblage field. By contouring the modal abundance of garnet and biotite these *P–T* conditions can be narrowed to 770–890 °C and 4.7–6 kbar (Fig. 6.4.5). This is based on the sample containing 5–10 % garnet and 0–15 % biotite, based on the assumption that some of the biotite is retrograde. The large amount of leucosome present in the field is consistent

with 10–20 % melt or more being present. The solidus occurs at around 680 °C but shifts to higher *T* (> 700 °C) at pressures lower than 5 kbar.

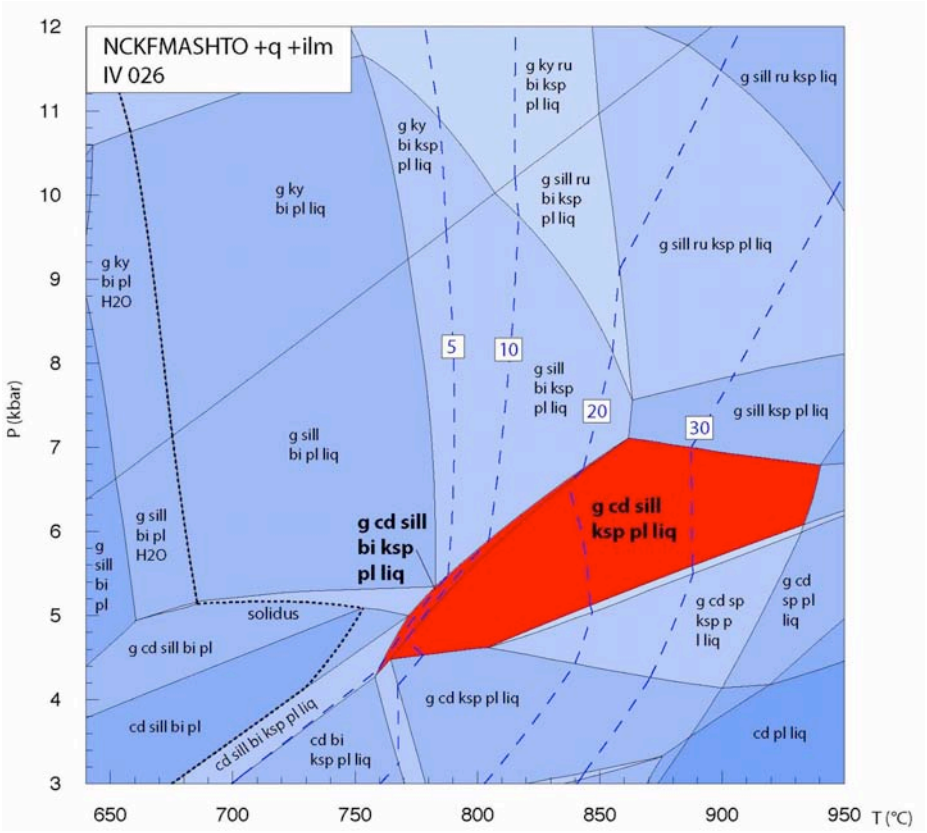

Figure 6.4.5. *P–T* pseudosection for sample IV 026.

The highest grade sample in Val Sesia, IZ 201 is located next to Varallo at the border with the Mafic Complex (Fig. 6.4.1). The inferred mineral assemblage (g-cd-sill-bi-ksp-pl-q-ilm-*liq*) as well as the pressure and temperature estimates are similar to sample IV 026. Two assemblage fields are highlighted because it is not clear whether one of the minerals (sillimanite) is retrograde. Peak temperatures of between 820 and 860 °C and pressures between 4.7 and 6.7 kbar are inferred (Fig. 6.4.6). The amount of *liquid* is between 10 to 20 %, consistent with the appearance of metatexitic structure and presence of leucosomes in the field. The solidus occurs at ~ 700 °C and at slightly higher temperatures at pressures lower than 5 kbar. This is similar to pseudosections of granulite facies samples from Val Strona di Omegna.

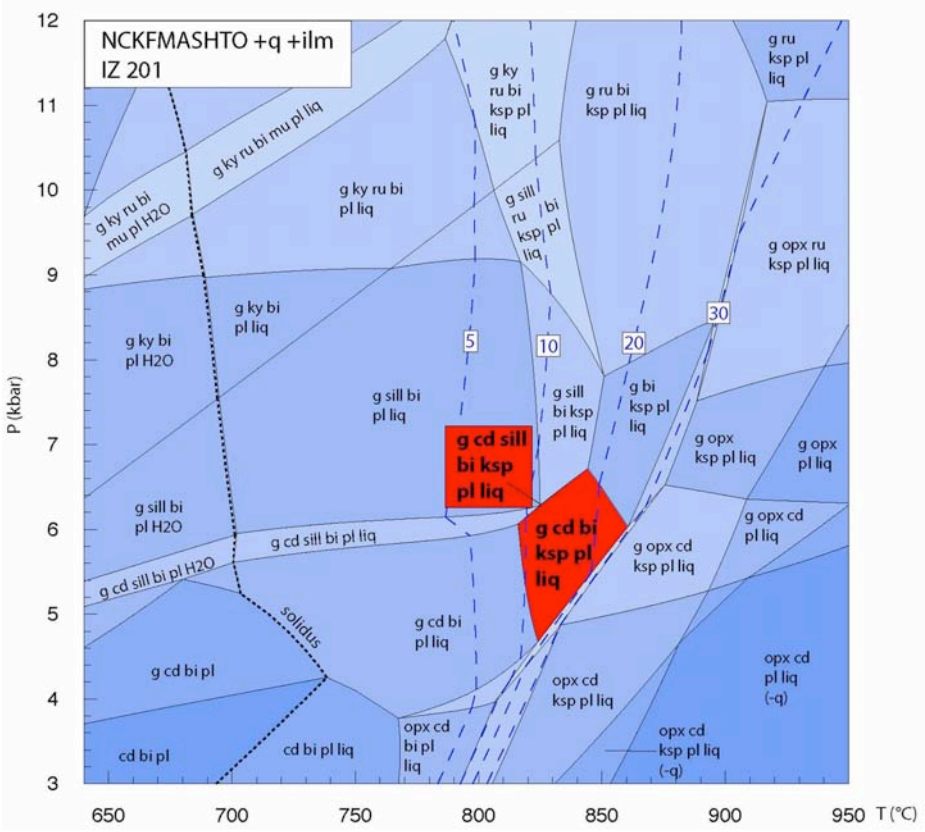

Figure 6.4.6. *P–T* pseudosection for sample IZ 201.

Summary

In summarising the inferred metamorphic peak assemblage fields on a single diagram (Fig. 6.4.7), no continuous trend is visible. The metamorphic field gradient is less well constrained and does not extend to the high pressures and temperatures recorded in Val Strona di Omegna. However, based on the pressure and temperature estimates, the samples can be divided into two groups. The three samples distant from Varallo (IV 034, IZ 114, IZ 168) have *P–T* values of 5 to 9 kbar and 670 to 780 °C. The other two samples (IV 026, IZ 201) define lower pressures of 4.5 to 6 kbar and higher temperatures of 800–850 °C (IV 026 and IZ 201).

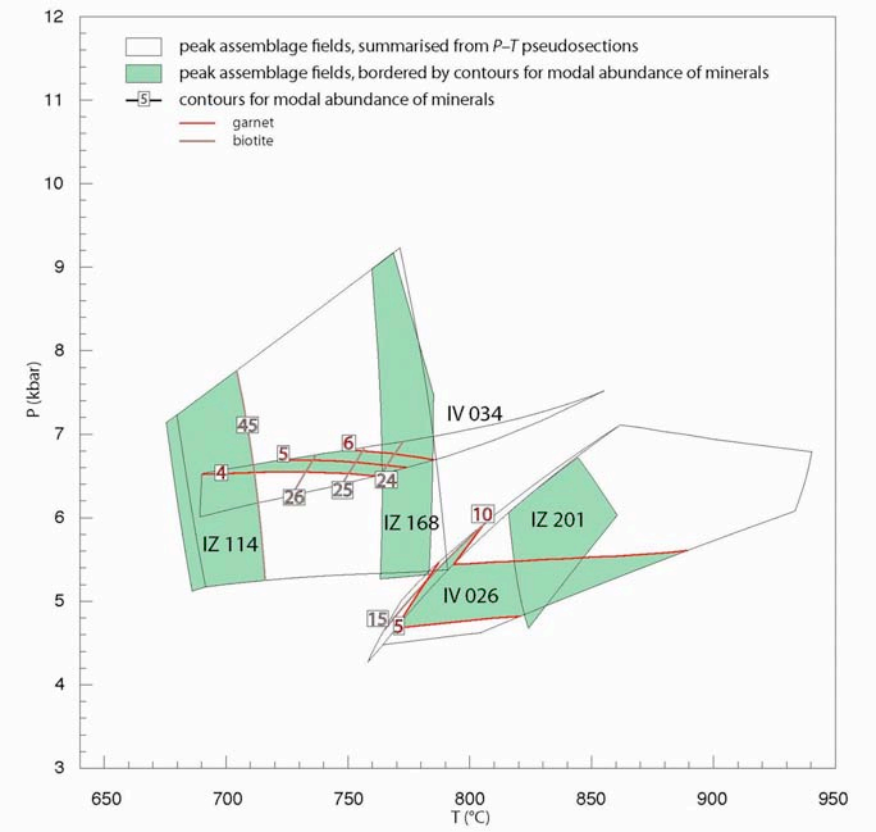

Figure 6.4.7. Summary *P–T* conditions from the pseudosections for Val Sesia. The grey borders mark the assemblage fields from Fig. 6.4.2–6.4.6, while the green fields illustrate the *P–T* conditions constrained using contours of modal abundance of minerals (garnet, biotite).

	***P–T* estimates without contouring**		***P–T* estimates with contouring**	
sample	**T (°C)**	**P (kbar)**	**T (°C)**	**P (kbar)**
IV 034	680 – 860	5.9 – 7.5	735 – 770	6.5 – 6.8
IZ 114	< 640 – 780	< 4.7 – 9.2	670 – 720	5.2 – 7.8
IV 168	760 – 785	5.3 – 9.2		
IV 026	760 – 940	4.9 – 7.1	770 – 890	4.7 – 6
IZ 201	820 – 860	4.7 – 6.7		

Table 6.4.2. Summarized results of *P–T* estimates for Val Sesia samples. The P–T estimated are given for assemblage fields without (left) and with (right) contours for the modal abundance of minerals.

6.5 Val Strona di Postua

Figure 6.5.1 illustrates the locations in Val Strona di Postua of the three samples for which *P–T* pseudosections were calculated, while Figs. 6.5.2–6.5.4 shows the pseudosections sorted from lower grade to higher grade conditions. All the samples are part of the amphibolite facies zone of Quick *et al.*, 2003, although field observations and thin section investigations suggest granulite facies conditions for the high-grade samples in this valley. In Tab. 6.5.1 the bulk rock compositions (mol%) used for each calculated sample are listed, while in Tab. 6.5.2 the *P–T* estimates for the peak assemblage fields are summarised. To further constrain the *P–T* estimates contours for the modal abundance of major minerals were calculated (Fig. 6.5.5).

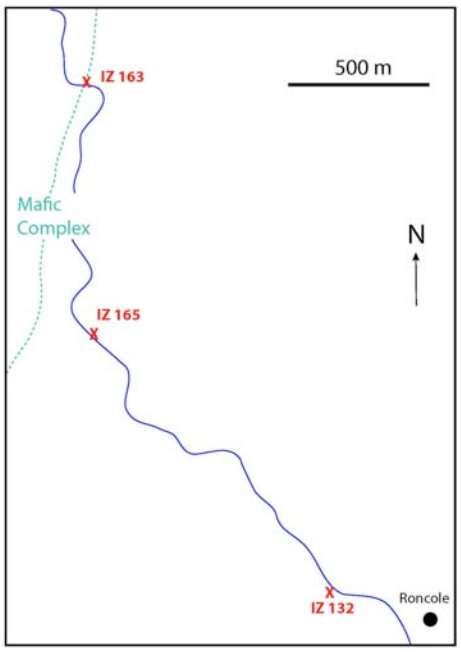

Figure 6.5.1. Schematic map of Val Strona di Postua with locations of the samples that were used for calculation of *P–T* pseudosections.

	H_2O	SiO_2	Al_2O_3	CaO	MgO	FeO	K_2O	Na_2O	TiO_2	O
IZ 132	3.16	68.17	10.43	2.51	5.50	6.27	1.13	1.99	0.74	0.1
IZ 165	1.34	64.45	11.03	3.05	6.59	8.16	1.80	2.02	1.47	0.1
IZ 163	0.92	77.41	9.42	3.41	1.25	2.96	1.30	2.94	0.29	0.1

Table 6.5.1. Bulk rock compositions (mol%) of five metapelite samples used for the calculated *P–T* pseudosections from Val Strona di Postua. The bulk rock compositions are normalised to 100%. "O" is used for the amount of Fe_2O_3.

The lowest grade sample of this valley, IZ 132 is located near the village Roncole (Fig. 6.5.1). It contains the inferred peak mineral assemblage g-cd-sill-pl-q-ilm-*liq* as field relations show small leucosomes. The amount of *liquid* in this assemblage field ranges from 1 to 20 % (Fig. 6.5.2). The *P–T* estimates are 700–

870 °C and 6–7.4 kbar. The contours of modal abundance of minerals constrain the *P–T* conditions to 700–780 °C and 6–7.3 kbar (Fig. 6.5.5), based on between 5 to 10 % cordierite, 10 to 15 % garnet and more than 15 % biotite within the sample. Based on this the amount of *liquid* is between 1 and 5 %, consistent with field observations. The solidus is present at around 700 °C.

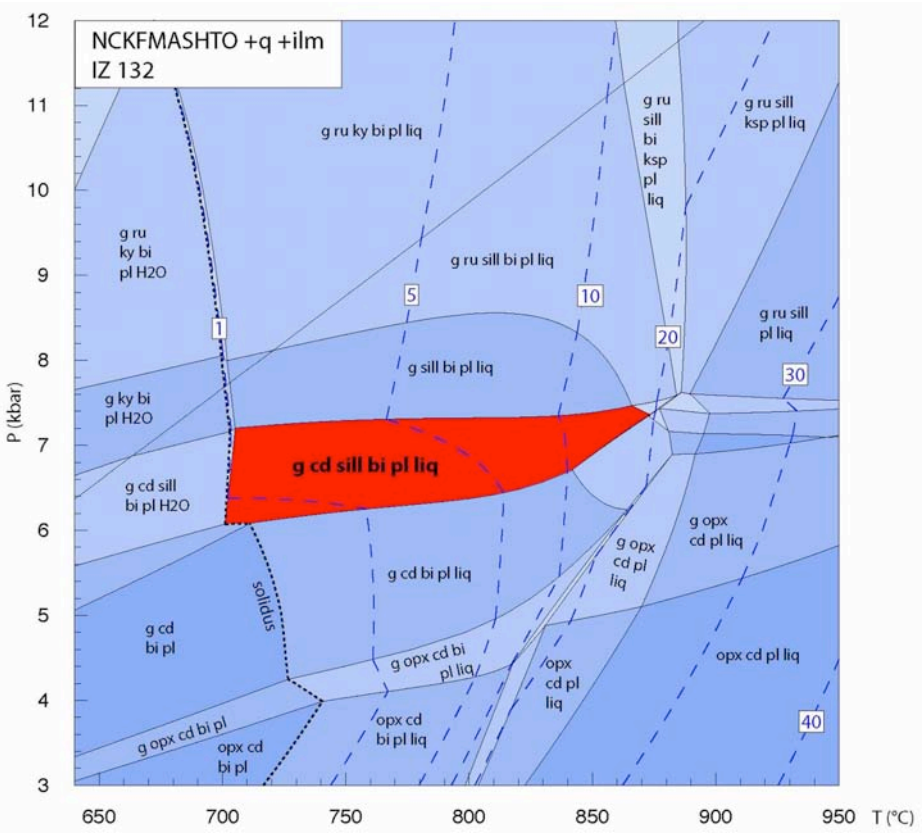

Figure 6.5.2. *P–T* pseudosections for sample IZ 132.

Sample IZ 165 was collected from approximately 500 m northwest of Roncole (Fig. 6.5.1), and contains the assemblage g-cd-sill-ru-bi-ksp-pl-q-ilm-*liq*, but it is more likely that one of these minerals (e.g. sillimanite) is not part of the peak metamorphic assemblage. Consequently two assemblage fields are highlighted. Temperatures are 870–890 °C with pressure of 6.8–7.2 kbar (Fig. 6.5.3). These fields contain an amount of 1 to 5 % melt, while this rock can produce between 10 to 20 % *liquid* at higher grade conditions (T > 850°). In comparison to the previous sample the position of the solidus shifts up temperature to around 800 °C.

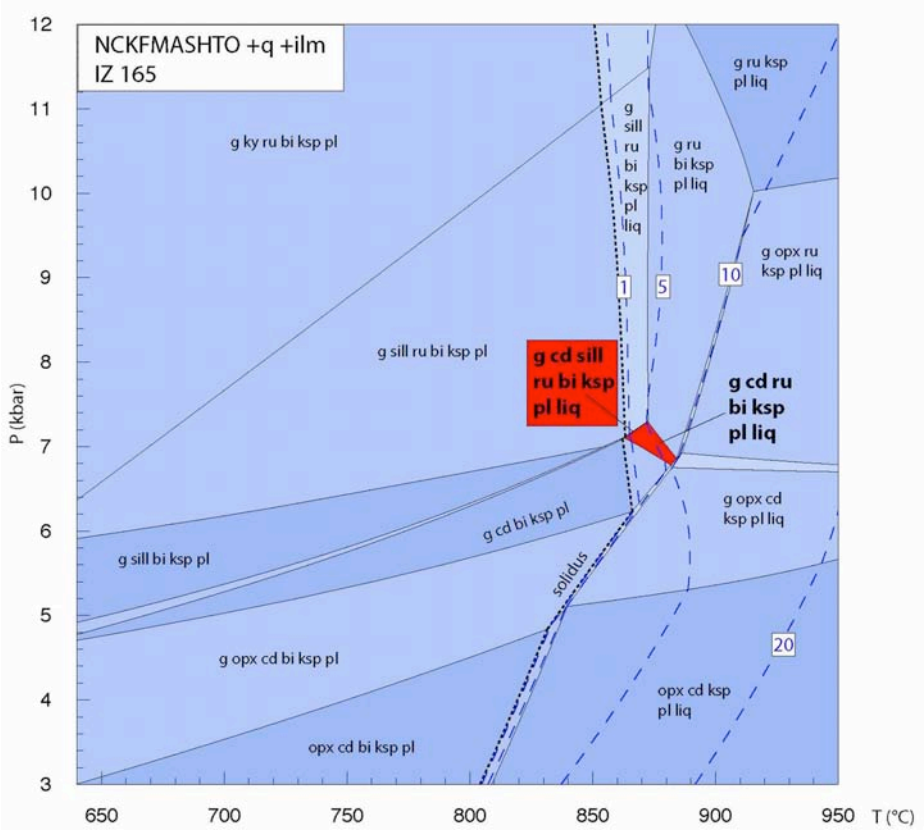

Figure 6.5.3. *P–T* pseudosections for sample IZ 165.

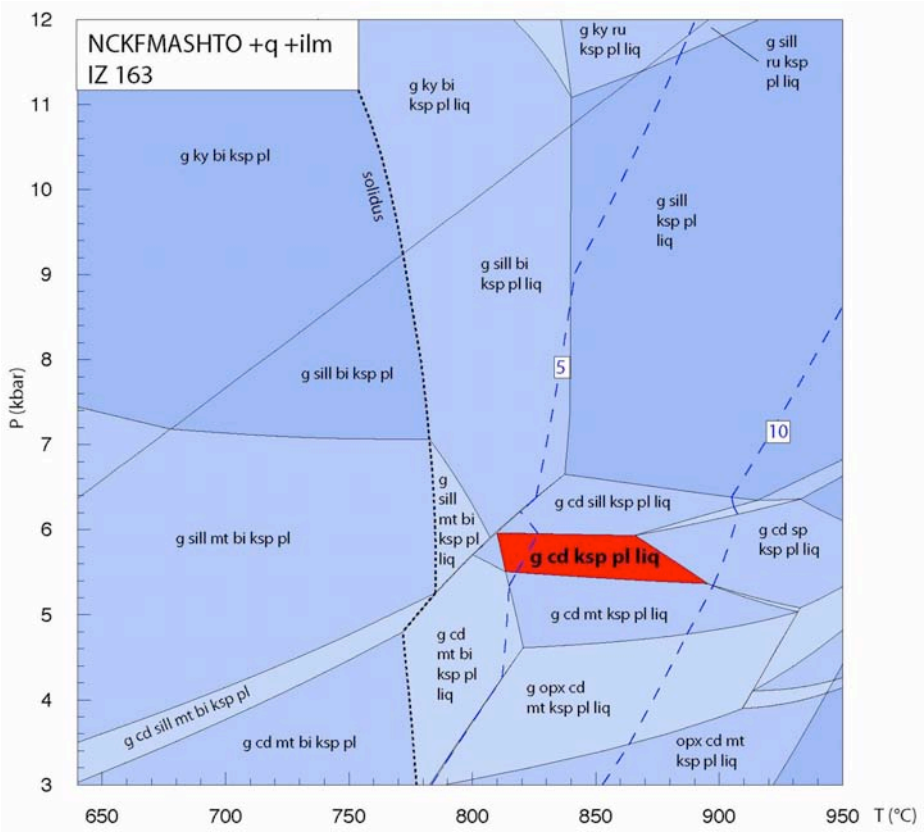

Figure 6.5.4. *P–T* pseudosections for sample IZ 163.

The highest grade sample IZ 163 is located next to the border with the Mafic Complex (Fig. 6.5.1), and contains the mineral assemblage g-cd-ksp-pl-q-ilm-*liq*. This assemblage occurs at lower pressures than that inferred for the other two samples. As illustrated with the blue dashed line this sample would contain 5 to 10 % *liquid* in this field. *P–T* estimates are 810 to 900 °C and 5.3 to 6 kbar (Fig. 6.5.4). The solidus occurs at around 780 °C.

Summary

The calculated *P–T* pseudosections illustrate no systematic trend for the metamorphic field gradient but a significant jump in temperature and a slightly decrease in pressure over a very short distance of 2–3 km through this valley.

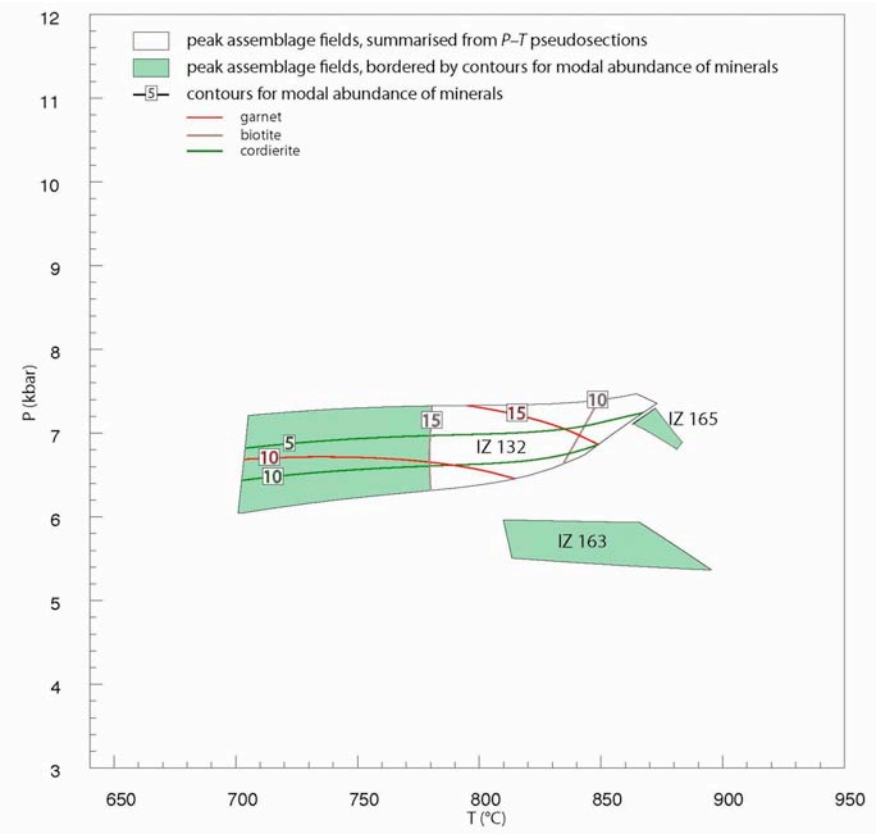

Figure 6.5.5. Summarised *P–T* pseudosections of Val Strona di Postua. The white borders mark the assemblage fields from Fig. 6.5.2–6.5.4, while the green fields illustrate the assemblage fields bordered with contours of modal abundance of minerals (garnet, biotite, and cordierite).

Next to the contact to the Mafic Complex temperatures are around 100 °C higher and/or pressures are around 1–2 kbar lower (IZ 163 and IZ 165) than in the

lowest grade sample (IZ 132). The temperatures range from 700 to 900 °C with corresponding pressures of 5.3–7.5 kbar (Fig. 6.5.5).

	***P–T* estimates without contouring**		***P–T* estimates with contouring**	
sample	**T (°C)**	**P (kbar)**	**T (°C)**	**P (kbar)**
IZ 132	700 – 870	6 – 7.4	700 – 780	6 – 7.3
IZ 165	870 – 890	6.8 – 7.2		
IZ 163	810 – 900	5.3 – 6		

Table 6.5.2. Summarised results of *P–T* estimates for Val Strona di Postua samples. The P–T estimated are given for assemblage fields without (left) and with (right) contours for the modal abundance of minerals.

Chapter 7
Discussion

7.1 Introduction

In this Chapter the results of field investigations, petrography geochemical analysis and mineral equilibria modelling are presented, interpreted and discussed in context to previous work and the main question asked in the introduction. In the following sub-chapters the field relations of the various rock types, metapelites, metapsammites/metagreywackes and metabasites (Chapters 7.2, 7.3, 7.5) as well as the evidence for partial melting and melt loss (Chapters 7.6, 7.7) in Val Strona di Omegna are discussed and compared with those in Val Sesia and Val Strona di Postua. Further, the ranges of *P–T* conditions, which are recorded within the metamorphic field gradient in Val Strona die Omegna, Val Sesia and Val Strona di Postua are discussed in Chapter 7.4. Some local characteristics in the field observations are discussed in Chapter 7.8. Another main aspect in the discussion is the relationship between the Mafic Complex and the granulite facies metamorphism in Val Strona di Omegna and whether the Mafic Complex is the source of heat for the high-grade metamorphism in the Ivrea Zone.

7.2 Field evidence for regional and contact metamorphism

In Val Strona di Omegna the metapelites of the Kinzigite Formation evolve from amphibolite facies schistose metapelites into metatexitic metapelites in the transition zone and to commonly diatexitic structures in the granulite facies. The

results of mapping, petrography and phase equilibria modelling are consistent with this change reflecting a continuous or near continuous progression in metamorphic grade. This is in contrast to Schmid & Wood (1976), who reported that it is questioned, whether the rocks present in Val Strona di Omegna represent a continuous metamorphic sequence. The development of the migmatitic structures is in contrast to the investigations of Zingg (1978), who argued that there is no clear evidence for partial melting and melt migration in the metapelites in Val Strona di Omegna and that only rocks in contact with the Mafic Complex are partially melted across the entire Ivrea Zone. The field observations, together with petrography and calculated *P–T* conditions (Chapter 7.4) lack any evidence for more than one metamorphic event in Val Strona di Omegna. Based on the calculated *P–T* estimates that increase continuously from low-grade to high-grade conditions, this metamorphic event can be interpreted as regional metamorphism. In contrast to several previous studies (Chapter 2) neither structures nor do mineral assemblages (e.g. the absence of cordierite in high-grade metapelites, Chapter 7.3) show any evidence for typical contact metamorphism, which would be expected if the Mafic Complex caused the metamorphism in Val Strona di Omegna. In Val Strona di Omegna, the high-grade rocks lack any clear evidence for a metamorphic overprint caused by the intrusion of the Mafic Complex. However, the extent, if any, of the Mafic Complex in this valley is unclear. Although mafic rocks do occur in the valley, they occur mostly as narrow (10's–100's of metres thick) units intercalated with the metasediments and contain assemblages consistent with the *P–T* conditions of the surrounding metasediments (Chapter 7.4). In the amphibolite facies the metabasites are amphibolites and in the granulite facies they contain orthopyroxene and a higher proportion of *in-situ* leucosome as evidence for partial melting. These observations are consistent with most, if not all, of the mafic rocks in this valley having a shared metamorphic history with the host metasediments (i.e. having undergone a series of prograde dehydration and partial melting reactions (Kunz, 2011)). The absence of a discrete contact metamorphic effect in Val Strona di Omegna likely reflects an absence or paucity of Mafic Complex intrusions here. Alternatively, if the rocks were metamorphosed, and as a consequence dehydrated, to temperatures in excess of 900 °C prior to the intrusion of Mafic Complex rocks, then a noticeable contact

effect would likely be highly restricted, as only the area immediately adjacent the intrusion is likely to exceed the temperatures associated with the regional metamorphism.

The map of Quick *et al.* (2003) illustrates only amphibolite facies rocks in the Kinzigite Formation in Val Sesia and in Val Strona di Postua and defines granulite facies rocks by the absence of a schistosity, a high abundance of garnet and a lower abundance of biotite. Further the rocks at the contact to the Mafic Complex exhibit a diatexitic structure, while schistose metapelites are present only at a distance of 2 km or more away from the contact with the Complex. It can be argued that diatexitic metapelites with their mineral assemblage of a high abundance of garnet and a lower abundance or absence of biotite are related to granulite facies conditions. The absence of a continuous metamorphic sequence as it is present in Val Strona di Omegna, can be explained with a second metamorphic event, likely a contact metamorphic overprint of earlier regional metamorphic mineral assemblages resulting from the intrusion of the Mafic Complex into the rocks of the Kinzigite Formation. Further evidence for this interpretation will be given in Chapter 7.3 and 7.4 with the presence of cordierite ± spinel as a typical contact metamorphic assemblage (e.g. corona structures of cordierite around garnet porphyroblasts) and with pressure and temperature estimates, which are different from the continuous metamorphic sequence in Val Strona di Omegna.

In Val Sesia the metapelites in contact with the Mafic Complex exhibit a metatexitic structure, which can be interpreted as an evidence from transition zone to granulite facies conditions, which is in contrast to the map of Quick *et al.* (2003). Further arguments for this interpretation are the presence of K-feldspar together with the absence of muscovite as a peak metamorphic mineral (i.e. mu-out/ksp-in isograd). In addition, assemblages containing orthopyroxene, brown hornblende, plagioclase, quartz and garnet in the metabasites next to the contact with the Mafic Complex in Val Sesia also suggest granulite facies conditions. This is in contrast to metabasites in Val Strona di Omegna from similar locality (north of Massiola, Fig. 7.4.1), which preserve upper amphibolite facies mineral assemblages (green hornblende-plagioclase-clinopyroxene ± garnet). It can be

argued that rocks in Val Sesia, similar to rocks in Val Strona di Postua, underwent a second metamorphic event that can be interpreted as a contact metamorphic overprint as a result from the intrusion of the Mafic Complex. Further, metapelite samples next to the CMB Line in Val Sesia, which should be schists of the amphibolite facies based on their relative location compared to samples from Val Strona di Omegna, have a metatexitic structure. It is possible that the onset of this fault zone and maybe also the intrusion of the Permian granites caused overprinting of mineral assemblages and structures. These assumptions are supported by the presence of cordierite in samples next to the Mafic Complex and other intrusions (Chapter 7.3) as well as the pressure and temperature estimates (Chapter 7.4).

Altogether, field observations in Val Strona di Omegna, Val Sesia and Val Strona di Postua lead to the assumptions that a regional metamorphic event took place in all the three valleys but in Val Sesia and Val Strona di Postua this first event was followed by a contact metamorphic overprint caused from the intrusion of the Mafic Complex. Further evidence for these interpretations are given in the following Chapters.

7.3 Minerals as indicators for a contact metamorphic overprint

Cordierite was observed in the metapelites in each valley but is only present in samples adjacent to intrusions. Cordierite is very rare in Val Strona di Omegna but more common in Val Sesia and Val Strona di Postua. In Val Strona di Omegna cordierite-bearing samples are located directly in contact to pegmatitic and granitic veins that were mapped as intrusions of unknown age (Bertolani, 1968). It is not clear if and how these dykes relate to the intrusion of the Permian granites in the Serie dei Laghi (e.g. Hunziker & Zing, 1980; Peressini *et al.,* 2007; Schaltegger & Brack, 2007), but the field observations suggest that the granites are younger than the inferred peak metamorphism of the amphibolite facies and granulite facies rocks of the Kinzigite Formation. For the age of peak

metamorphism, various authors (e.g. Köppel, 1974; Henk *et al.*, 1997; Demarchi *et al.*, 1998) reported ages between 250 and 290 Ma, while Peressini *et al.* (2007) suggested ages of around 310 Ma for the high-grade metamorphism in the Kinzigite Formation and ages of around 288 Ma for the formation of the upper Mafic Complex. This leads to the interpretation that cordierite in the metapelites in Val Strona di Omegna is not part of the peak metamorphic assemblage, resulting neither from regional metamorphism nor from retrograde reactions, but developed by a contact overprint caused by the granitic intrusions. In contrast to the studies of Reinsch (1969) and Zingg (1978), cordierite was not found in general in amphibolite facies and transition zone samples (Germagno to Forno) in Val Strona di Omegna and particularly not in the high-grade metapelites west of Forno and around Campello Monti, where the Mafic Complex is inferred to crop out according to some studies (e.g. Zingg, 1978; Zingg, 1983; Sills, 1984).

Metapelites in Val Sesia and Val Strona di Postua contain cordierite. In addition, samples in Val Strona di Postua contain variable amounts of spinel (IZ 132) and rutile (IZ 165) together with prismatic sillimanite and cordierite-bearing coronas around garnet, while biotite is absent from the highest grade sample (IZ 163). The growth of cordierite could be attributed to contact metamorphism related to the intrusion of the Mafic Complex that locally overprinted the pre-existing upper amphibolite facies and/or granulite facies regionally metamorphosed rocks. This interpretation was also suggested by Barboza & Bergantz (2000). The presence of cordierite together with spinel ± prismatic sillimanite is consistent with the assumed granulite facies conditions in Val Sesia and Val Strona di Postua (Chapter 7.2). This is consistent with the interpretation that the overprinting contact metamorphic effect was at high *T* but lower *P* than the earlier regional metamorphic event that is recorded in Val Strona di Omegna (Chapter 7.4). These interpretations are consistent with published ages of 285–295 Ma (Peressini *et al.,* 2007) for the intrusion of the upper Mafic Complex, which are around 20 Ma younger than ages for the high-grade metamorphism in the Kinzigite Formation.

Rocks adjacent to the Mafic Complex in Val Sesia and Val Strona di Postua were partially melted, whereas rocks that are 2–3 km away from the Complex are still

largely schistose and lack leucosomes, but retain a subsolidus contact metamorphic overprint. The small amount of hercynitic spinel in Val Strona di Postua samples is similarly consistent with lower pressures and suggests the replacement of garnet-biotite-sillimanite by cordierite and spinel with or without melt present (White *et al.,* 2001).

7.4 Pressure and temperature estimates

In general, phase equilibria modelling of the samples from Val Strona di Omegna and Val Sesia shows an increase in both pressure and temperature from lower grade (close to the CMB Line) to higher grade conditions (towards the Insubric Line), while in Val Strona di Postua no distinct trend is obvious.

The regional metamorphic field gradient in Val Strona di Omegna is constrained to extend from 3.5–6.5 kbar at < 650–730 °C under amphibolite facies conditions to > 12 kbar and > 950 °C under granulite facies conditions. The sample set defines a continuous increase in pressure and temperature without any major discontinuities in Val Strona di Omegna, though this does not preclude the presence of smaller scale fault structures with movements smaller than can be resolved using the calculated pseudosections. This trend is consistent with a section through the mid to lower crust (e.g. Taylor & McLennan, 1985; Rudnick and Gao, 2003) with pressures evolving from 3 to > 12 kbar and a metamorphic field gradient involving 20–25 °C/km along the valley. The modelled peak pressures and temperatures for the highest grade rocks presented here are higher than those suggested in most earlier studies (e.g. Schmid & Wood, 1976; Hunziker & Zingg, 1980; Henk *et al.*, 1997). The modelled peak temperatures here are around 100 °C higher for the granulite facies rocks (850 °C to > 950 °C) than those of Henk *et al.* (1997), based on Fe–Mg exchange thermometry (e.g. garnet-biotite, garnet-orthopyroxene thermometer), suggesting significant retrograde resetting of mineral compositions (e.g. Pattinson *et al.*, 2003). The model calculations are based on whole rock chemistry and are independent of mineral compositions, meaning that retrograde cation exchange have no

influence on the results of the calculations. The model constraints on peak temperatures of the granulite facies metamorphism are broadly consistent with those of Luvizotto & Zack (2009), based on Zr-in-rutile thermometry (850–930 °C).

In Val Strona di Omegna the metamorphic conditions calculated for metapsammite/metagreywacke samples established a similar trend to the metapelites with a continuous increase in pressure and temperature. These rocks have not been investigated in detail in previous studies. The metamorphic field gradient for the metapsammites/metagreywackes is constrained to extend from a minimum of 6 kbar at 725 °C to a maximum of 11.1 kbar at 910 °C under granulite facies conditions. A metamorphic field gradient, similar to those from Val Strona di Omegna, of around 20 °C/km for these rocks can be inferred. However, the metapsammites/metagreywackes are less abundant in Val Strona di Omegna and were only investigated over a shorter lateral distance than the metapelites so the results from these rocks are less well constrained.

In Val Sesia the less well-constrained metamorphic field gradient changes from regional metamorphic in amphibolite facies rocks to contact metamorphic assemblages in samples close to the Mafic Complex. Pressure and temperature estimates of the lowest grade samples are similar to amphibolite facies assemblages in Val Strona di Omegna (Fig. 7.4.1). Samples next to the Mafic Complex in Val Sesia suggest temperatures of more than 800 °C (granulite facies conditions) at pressures of around 6 kbar, which is inconsistent with similar samples from Val Strona di Omegna (750 to 800 °C and 6 to 9 kbar). The *P–T* estimates of Val Strona di Postua are similar to those of Val Sesia with temperatures of 800 to 900 °C at pressures of around 6 kbar. Based on the pressure and temperature differences between high-grade rocks in Val Strona di Omegna and those in the high-grade rocks in Val Sesia and Val Strona di Postua it is likely that the intrusion of the Mafic Complex occurred subsequent to some decompression in the rocks from Val Sesia and Val Strona di Postua. The amount of decompression is poorly constrained in Val Sesia, but is likely to be around 1–2 kbar in Val Strona di Postua. This interpretation was also suggested by Barboza & Bergantz (2000), who argued that the lower pressures of 5–8 kbar

at 800 to 900 °C recorded close to the Mafic Complex were consistent with some decompression from regional metamorphic peak conditions prior to the intrusion of the Mafic Complex.

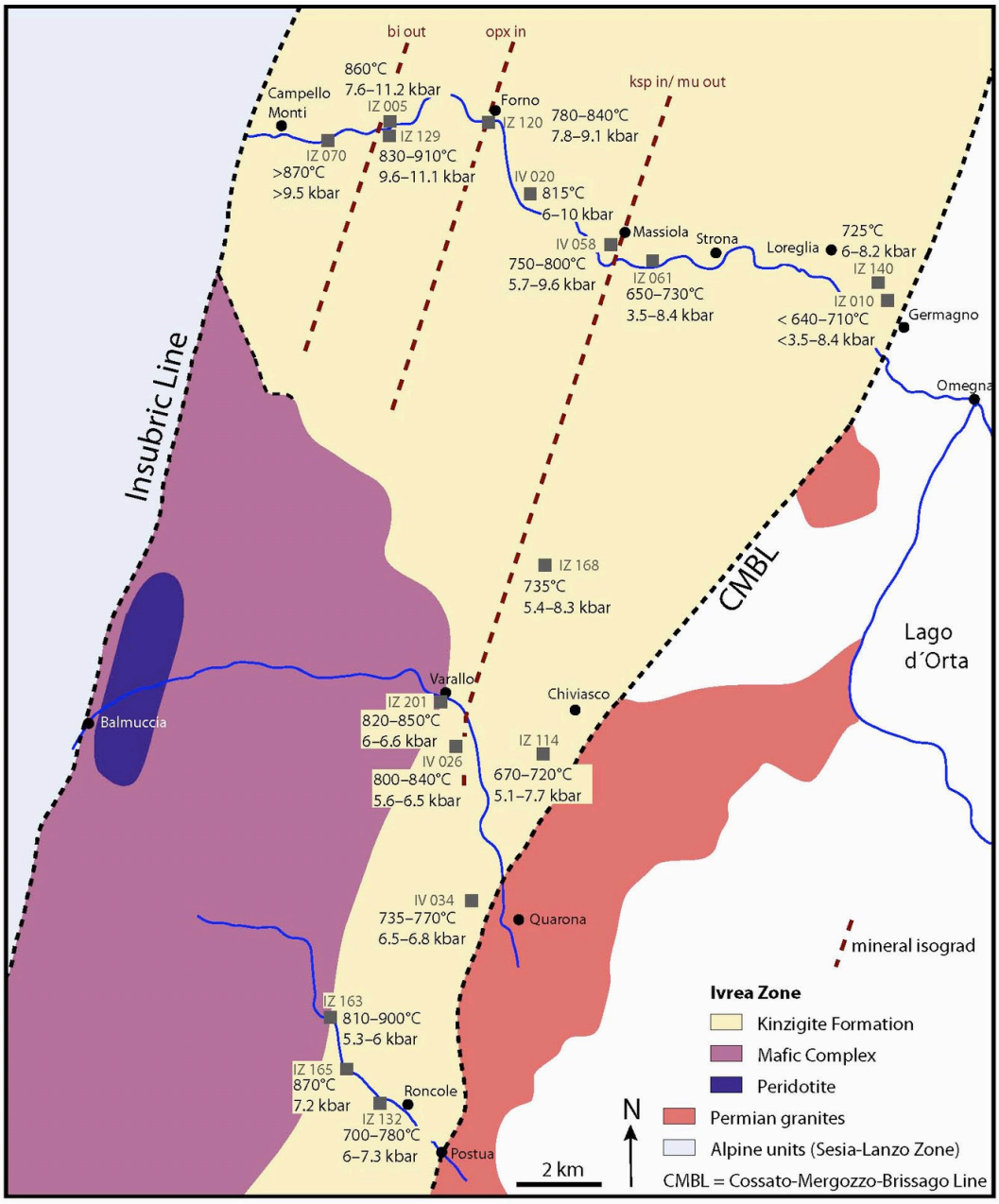

Figure 7.4.1. New schematic geological map of Val Strona di Omegna, Val Sesia and Val Strona di Postua including calculated *P–T* estimates. In comparison to most previous maps no Mafic Complex is illustrated in Val Strona di Omegna. The exact position of the border between Mafic Complex and Kinzigite Formation is unknown and illustrated here with dashed lines, according to several previous studies (e.g. Rutter *et al.*, 1993; Sinigoi *et al.*, 1994; Quick *et al.*, 2003; Peressini *et al.*, 2007). The higher grade extrapolated mineral isograds are cut by the Mafic Complex in the south, while the low-grade isograd also can be found in Val Sesia.

Based on the field observations and the distribution of cordierite in Val Sesia and Val Strona di Postua samples, a contact aureole of 2–3 km around the Mafic Complex is suggested. If the Mafic Complex also intruded in Val Strona di Omegna, a similar aureole should be observed (i.e. approximately between Piana di Forno to the Insubric Line north of Campello Monti), but no evidence for this could be found.

The results of the quantitative phase equilibria modelling presented here place much more robust constraints on the *P–T* conditions of metamorphism and the preserved metamorphic field gradient. The combined results suggest a clockwise *P–T* path with 1) increasing pressure and temperature and 2) decompression at still high temperatures or with an increase in temperature. Based on the present discussion, the data add to the burgeoning metamorphic and geochronological evidence (e.g. Barboza *et al.*, 1999; Barboza & Bergantz, 2000; Peressini *et al.*, 2007) that the metamorphic field gradient preserved in the Ivrea Zone is a regional metamorphic feature and that this metamorphism was unrelated to the intrusion of the Mafic Complex.

7.5 Mineral isograds

In Val Strona di Omegna several regional metamorphic mineral isograds can be defined but only the muscovite-out/K-feldspar-in isograd occurs in Val Sesia, while no isograd was identified in Val Strona di Postua. The extrapolated high-grade isograds in Val Strona di Omegna (orthopyroxene-in and biotite-out) are cut by the Mafic Complex to the south of Val Strona di Omegna (Fig. 5.2.1). If the Mafic Complex caused the high-grade regional metamorphism in the Ivrea Zone, these isograds should be present in every valley at more or less the same distance from the Mafic Complex. Based on this, it is unlikely that 1) the intrusion of the Mafic Complex caused the granulite facies metamorphism and the development of mineral isograds in the regional metamorphic area of Val Strona di Omegna and 2) the Mafic Complex is present in Val Strona di Omegna. A biotite-out/cordierite-in isograd suggested by Schmid (1968) and later by Zingg

(1980) in Val Sesia could not established in this work, because samples next to the CMB Line contain both cordierite and biotite.

7.6 Migmatites and melt generations

In the Ivrea Zone several variations of migmatites occur. North of Forno in Val Strona di Omegna two apparent generations of leucosomes occur. The first leucosome consists of mostly quartz and minor feldspars, while the second leucosome is rich in garnet and varies in the amount of biotite. It is also likely that the quartz-rich leucosomes represents quartz- and feldspar-rich veins that are not directly related to partial melting of the metapelites (Chapter 7.8.1) and so there is only one generation of leucosome. The garnet- and biotite-rich leucosome, which is present in almost every diatexite, may reflect limited segregation of melt and residuum or selective entrainment of garnet. It could also reflect different episodes of melt segregation, based on the varying amount of garnet and biotite in the leucosomes. This type of leucosome could also result from melt infiltration into the neosome so that there is now a mixture of former neosome and crystallised foreign melt. The quartz-rich leucosome without garnet can be interpreted as in-source leucosome, resulting from melt migration. Around Pian Pennino and further to the north most of the leucosome does not contain any garnet and biotite or only small amounts of garnet. Here, the segregation of the diatexite into melt and residue is better developed than in the lower grade part of the valley. Furthermore, in-source leucosomes are more abundant in this area.

According to Sawyer (2008), different generations of leucosome coexisting as anatectic melt along the prograde *P–T* path could reflect different melting reactions (Chapter 7.7). These various melting reactions could be defined by 1) H_2O-present melting, 2) muscovite-dehydration melting and 3) biotite-dehydration melting. It is likely that the structures and leucosomes in the migmatites from Val Strona di Omegna resulted from these melting reactions (Fig. 7.7.1). Alternatively, different generations of leucosomes may simply record different episodes of melt segregation from the solid fraction (Sawyer, 2008).

In Val Sesia next to the contact with the Mafic Complex the metapelites occur as metatexites, while in Val Strona di Postua they occur as diatexites. These rocks may have formed as a consequence of the intrusion of the Mafic Complex. The diatexites in Val Strona di Postua contains garnet-rich leucosomes similar to those from Val Strona di Omegna north of Forno, but purely quartzofeldspathic leucosomes are rare.

7.7 Partial melting, melt loss and maximum melt (*P–T* pseudosections)

As mentioned before (Chapter 7.2) rocks in the Ivrea Zone, especially in Val Strona di Omegna partially melted under high-grade conditions. Based on the continuous change in structures, mineral assemblages and pressure and temperature estimates that show a regional metamorphic trend, it might be suggested that schists similar to those in the lower grade part of Val Strona di Omegna were protoliths for the metatexitic and diatexitic metapelites. The *P–T* pseudosection of the lowest grade sample IZ 010 (Fig. 6.3.2) illustrates that a rock with such a composition can produce around 30–40 % melt under high-grade conditions. This amount is consistent with the results from the geochemical analyses and the isocon diagram (Chapter 5.2). In comparison, the lowest grade samples in Val Sesia (IZ 114; Fig. 6.3.3) and Val Strona di Postua (IZ 132; Fig. 6.4.2) can produce an amount of 40–45 % melt and 20–25 % melt respectively, under the same pressure and temperature conditions. Further, the three melt/mineral mode–temperature plots (Fig. 7.7.1–7.7.3) show the degree of partial melting resulting from different partial melting reactions. In Val Strona di Omegna the majority of the melt proportions resulted from the breakdown of muscovite and biotite reflected in the sharp increases from 3 to 7 % melt and from 8 to 11 % melt, respectively (Fig. 7.7.1). With the decrease of biotite the proportions of garnet increases, until biotite is exhausted. In the lowest grade sample IZ 114 from Val Sesia changes in the rate of melt proportion as a function of temperature seem to be accompanied by the disappearance of first H_2O and later plagioclase and quartz (Fig. 7.7.2). The amount of melt sharply increases

from 0–3 % (H_2O-out), 8–15 % (plagioclase-out) and 30–34 % (quartz-out). This is incorrect as the increase of melt is caused by the breakdown and decrease of biotite (e.g. 41–30 % at 780–800 °C) and the accompanying increase of garnet (e.g. 5–13 % at 780–800 °C). The diagram for Val Strona di Postua shows a more monotonous rate of melt production and the breakdown of biotite together with an increase in the proportion of garnet caused an increase in the amount of melt (Fig. 7.7.3).

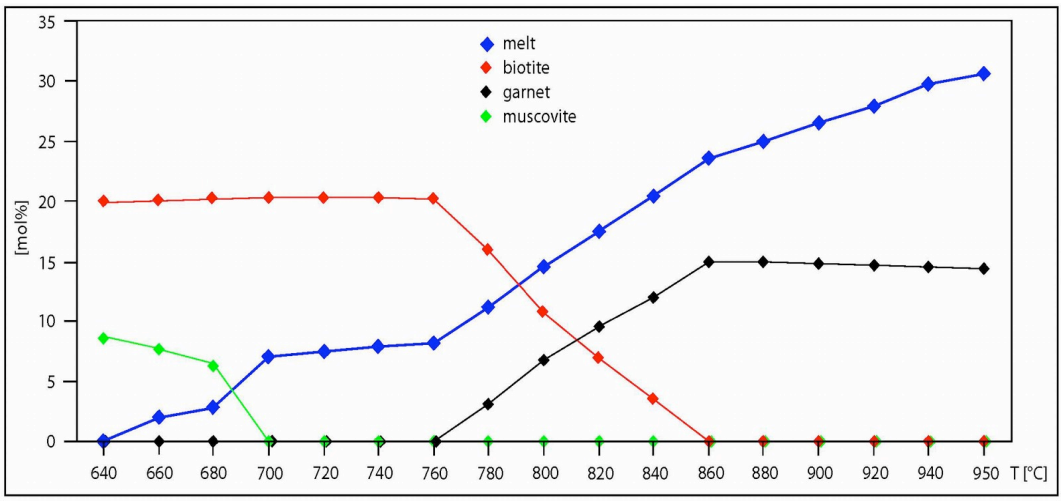

Figure 7.7.1. Profile through the lowest grade *P–T* pseudosection IZ 010 in Val Strona di Omegna illustrating the increase of melt and garnet and the decrease of muscovite and biotite with increasing temperature. The diagram only shows the increasing temperatures but also pressures increases from 5 kbar at 640 °C to 11.9 kbar at 950 °C. The used temperature/pressure pairs are: 640 °C/5 kbar; 660 °C/5.5 kbar; 680 °C/5.9 kbar; 700 °C/6.3 kbar; 720 °C/6.8 kbar; 740 °C/7.2 kbar; 760 °C/7.7 kbar; 780 °C/8.1 kbar; 800 °C/8.5 kbar; 820 °C/9 kbar; 840 °C/9.4 kbar; 860 °C/9.9 kbar; 880 °C/10.3 kbar; 900 °C/10.7 kbar; 920 °C/11.2 kbar; 940 °C/11.6 kbar and 950 °C/11.9 kbar.

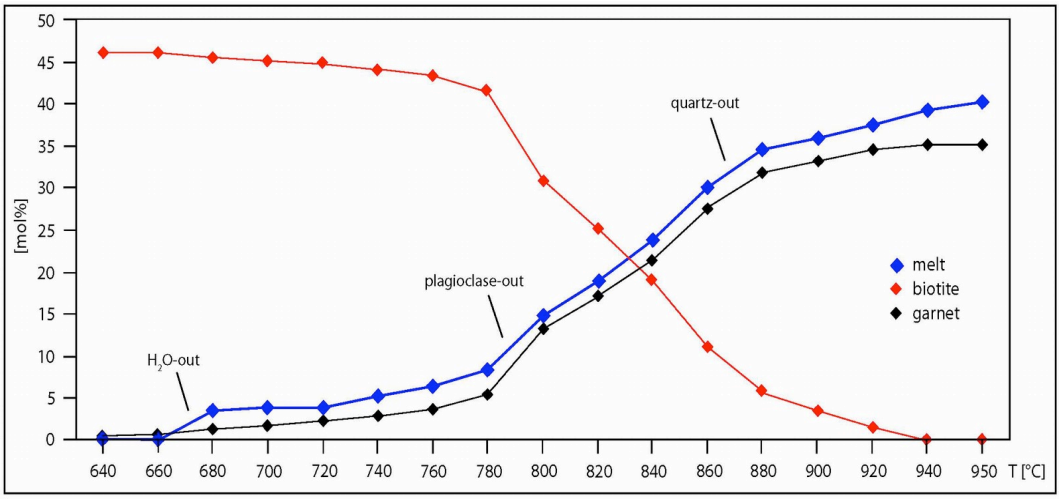

Figure 7.7.2. Profile through the inferred lowest grade *P–T* pseudosection IZ 114 in Val Sesia illustrating the increase of melt and garnet and the decrease of biotite with increasing temperature. The diagram only shows the increasing temperatures but also pressures increases from 5 kbar at

640 °C to 11.9 kbar at 950 °C. The temperature/pressure pairs used are the same as in the diagram for Val Strona di Omegna (Fig. 7.7.1).

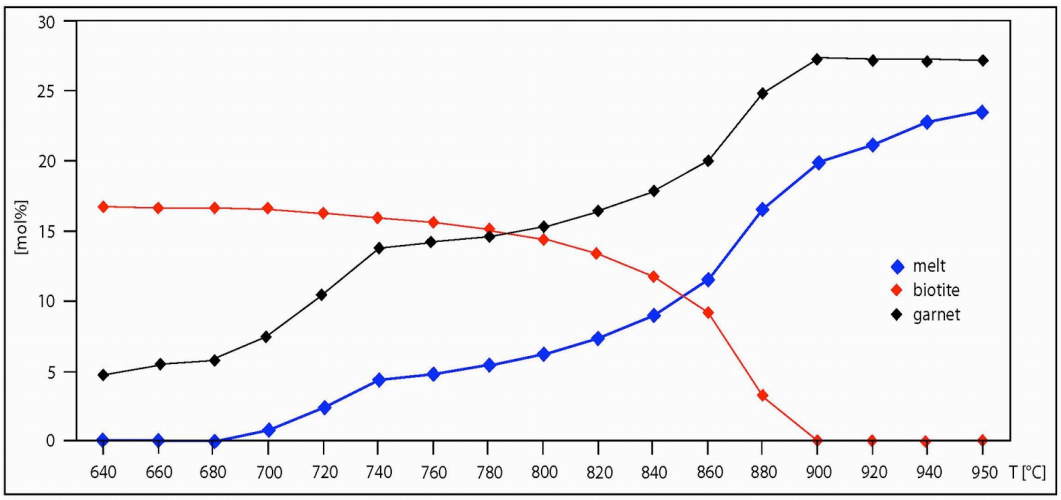

Figure 7.7.3. Profile through the lowest grade *P–T* pseudosection IZ 132 in Val Strona di Postua illustrating the increase of melt and garnet and the decrease of biotite with increasing temperature. The diagram only shows the increasing temperatures but also pressures increases from 5 kbar at 640 °C to 11.9 kbar at 950 °C. The temperature/pressure pairs used are the same as in the diagram for Val Strona di Omegna (Fig. 7.7.1).

In the high-grade samples from Val Strona di Omegna IV 020 (transition zone), IZ 005 and IZ 070 (granulite facies) the solidus is shifted to higher temperatures in comparison to the low-grade samples and no wet solidus is present. The elevated solidus for the high-grade samples is consistent with them having lost a substantial proportion of their melt prior to cooling (e.g. White & Powell, 2002). An example of the shift of the solidus from low-grade to high-grade compositions is given in Fig. 7.7.4. As presented in the results (Chapter 6.2), sample IV 020 is able to produce 5% or maximum 10 % melt with the measured composition. In contrast, the lowest grade sample IZ 010 used here as an approximate protolith is able to produce around 10–20 % melt at estimated *P–T* similar to the present assemblage field of IV 020. Therefore, it can be assumed that sample IV 020 lost approximately 5–10 % melt of a predicted 20 % melt produced at metamorphic peak. Similarly, sample IZ 005 is still able to produce 10 % melt with the measured composition. In comparison, the low-grade sample IZ 010 can produce 20–30 % melt at *P–T* conditions similar to those of IZ 005, which is shown in Fig. 7.7.4, where sample IZ 010 (x=0) contains 30 % melt at 860 °C that decreases towards the composition of IZ 005 (x=1) to around 10 % melt at the same temperature, where the peak metamorphic assemblage of IZ 005 can be inferred.

Sample IZ 005 must have lost 10–20 % melt. Identical, the highest grade sample IZ 070 lost 20–30 % melt. This is similar to suggestions of Schnetger (1994), who reported a possible melt loss of 20–40 % for granulite facies rocks. The loss of melt can be also inferred in the high-grade samples in Val Strona di Postua, where the solidus is also shifted to higher temperatures and no wet solidus occurs. According to this, samples IZ 165 and IZ 163 must have lost around 15% melt based on the predicted melt production of the low-grade sample IZ 132, which can be assumed as a approximate protolith. This melt loss is consistent with sample IZ 005 in Val Strona di Omegna.

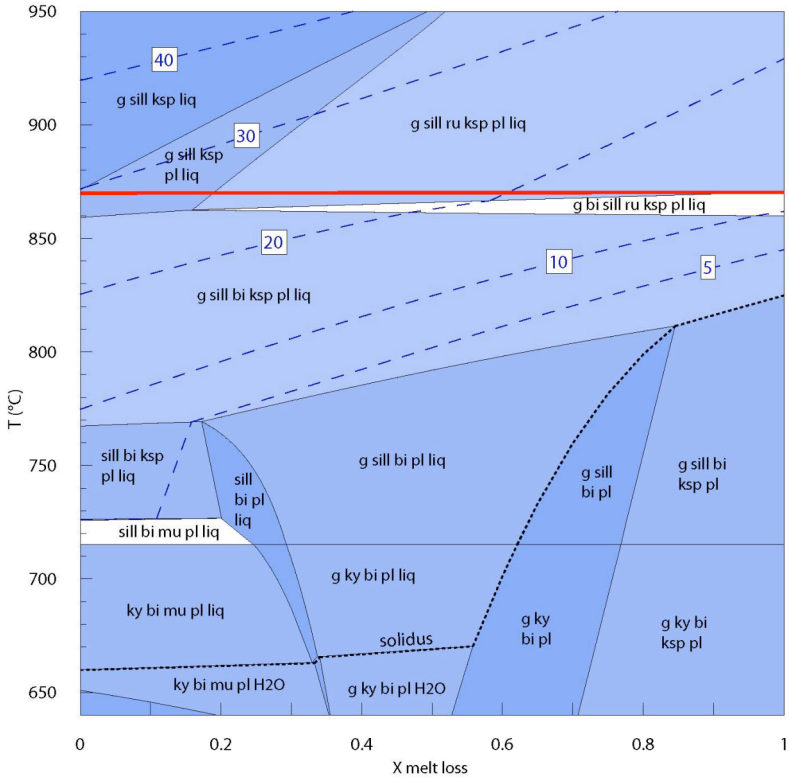

Figure 7.7.4. Calculated T–$x_{\text{melt loss}}$ pseudosection (fixed P = 6 kbar) showing the shifting of the solidus from 660 °C at x = 0 to higher temperatures of 820 °C at x = 1 (black dotted line) and also the removal of melt at around 870 °C from 30 % at x = 0 to 10% at x = 1 (along the red line). The bulk rock compositions are from IZ 010 at x = 0 and IZ 005 at x =1. With the blue dashed lines the amount of *liquid* is illustrated. The white fields marked roughly the fields with the peak assemblage of sample IZ 010 (left) and IZ 005 (right).

The high-grade samples (IV 026 and IZ 201) in Val Sesia differ from these observations and in comparison to high-grade pseudosections from Val Strona di Omegna the solidus does not shift to higher temperatures (800–850 °C) and is still present at around 650 °C as a water saturated solidus, which suggest that

these samples did not lose melt or were hydrated later. In contrast to this, the field observation and the comparison with the low-grade sample IZ 114, which is used as an approximate protolith for high-grade Val Sesia samples, suggest that the high-grade samples lost around 10–15 % melt and 10–20 % melt, respectively.

7.8 Local characteristics in field observations and *P–T* pseudosections

7.8.1 Leucocratic veins instead of partial melting

In Val Strona di Omegna (around Piana di Fornero) and Val Strona di Postua areas with an unusual high amount of quartz dominated leucocratic veins (quartz-plagioclase-K-feldspar) are located in the upper part of the amphibolite facies, close to the muscovite-out/K-feldspar-in isograd (e.g. Chapter 4, Fig. 4.2.7c, 4.2.8). The rocks around these veins are schistose and contain biotite-sillimanite-quartz-plagioclase ± muscovite. Given the very high quartz contents of these veins, it is unlikely that the leucocratic veins resulted from partial melting of the schists and no evidence for this could be established, which imply that these rocks are not migmatites using the definition from Sawyer (2008). It is more likely that the leucocratic veins represent H_2O-rich fluids derived from the schists. Evidence for this interpretation is the coarser grain size of the leucocratic veins. In addition, most of the leucocratic veins are folded or boudinaged, which seems to be the result of deformation during or after their migration and crystallisation. This interpretation is consistent with an interpretation of Bea & Montero (1999), who suggested locally abundant quartz-rich veins resulted from hydrothermal mobilisation instead of partial melting. Sawyer (2008) illustrated in fig. G17 and G18 the typical occurrence of the rocks with the extensive amount of leucocratic veins in Val Strona di Omegna. The current interpretation in this study is consistent with the interpretation of Sawyer (2008), that no evidence for a genetic link between leucocratic and melanocratic parts could established for these rocks. The samples in these areas together with samples from a small area in Val

Sesia (all in the strike direction of the Ivrea Zone and more or less around the muscovite-out/K-feldspar-in isograd) contain an unusual high LOI content that will be discussed below (Chapter 7.8.3).

7.8.2 Depletion of felsic minerals

In addition to the areas rich in leucocratic veins, an area of rocks with a more residual composition occurs between Rosarolo and Forno in Val Strona di Omegna. Here, metatexitic metapelites occur together with boudinaged and partially melted metabasites. The bulk rock chemistry suggests that the metapelites are H_2O-depleted (very low LOI content) in comparison to samples north of Forno and south of Rosarolo and that the mineral assemblages (dominated by garnet-sillimanite-biotite) are residual. The depletion of the felsic minerals is not related to the development of numerous shear zones with various displacements (e.g. Fig. 4.2.13), mylonites and pseudotachylites, which seems to be a later tectonic event of likely alpine age. Siegesmund *et al*. (2008) define this whole area as the Rosarolo shear zone. Further, this area is also consistent with the transition zone between Kinzigite Zone and Stronalite Zone defined by Bea & Montero (1999), based on the modal values biotite and garnet (Chapter 2.3). In contrast to this, the present study defines the transition zone between amphibolite and granulite facies rocks based on the mineral isograds.

7.8.3 High LOI content and its effect to the *P–T* pseudosections

As mentioned previously, in each of the three valleys an area with unusual high bulk rock LOI contents occur. Samples from this area were using these high LOI values for the calculation of the *P–T* pseudosections in Val Strona di Omegna (IV 058) and Val Sesia (IZ 114 and IZ 168) resulted in pseudosections with an usually wide field of coexisting melt and H_2O (Appendix C). Recalculations of the *P–T* pseudosections (Fig. 6.3.4, 6.4.3 and 6.4.4) using lower values show that

the LOI content has an influence to the position of the inferred peak assemblage fields and to the amount of melt. For sample IV 058 and IZ 114 the recalculated pseudosections are much more consistent with the field observations and the inferred amount of melt. It can be assumed that H_2O contents were lower than the measured LOI during the development of the peak metamorphic assemblage, while the higher H_2O contents measured resulted from fluids that migrated into the rocks during cooling or from the migration and crystallisation of the leucocratic veins. For sample IZ 168 (Val Sesia) it is not clear whether the *P–T* pseudosection with the high LOI content is more realistic than the recalculated pseudosection. Both are consistent with the field and thin section observations with respect to the preserved assemblage and amount of melt in the inferred peak assemblage field. The lower temperatures (and also pressures) resulting from the calculations on this sample are more consistent with those of sample IZ 061 in Val Strona di Omegna at similar position near the muscovite-out/K-feldspar-in isograd. Further explanation for this high LOI content could be the presence of retrograde muscovite and the high proportions of quartz veins, which are not part of the peak metamorphic assemblages.

Chapter 8
Conclusions and future research

8.1 Introduction

In the following Chapter the conclusions of this study are presented together with an outline to possible future research in the Ivrea Zone.

8.2 Conclusions

The present study arrives at the conclusion that some important and for long-held views on the history and the development of the metamorphic rocks in the Ivrea Zone need rethinking. It is unlikely that the Mafic Complex was the source of heat for the widespread metamorphism in the Ivrea Zone and no evidence for this assumption could be established in this study. The results of the phase equilibria modelling are consistent with the findings of Barboza *et al.* (1999) and Barboza & Bergantz (2000) in that a) the contact metamorphic effects of the Mafic Complex are spatially-limited to a few kilometres extent, and: b) that the contact metamorphic rocks preserve evidence for lower pressures than the earlier regional metamorphic conditions, consistent with some decompression between the regional metamorphic peak and the intrusion of the Mafic Complex. Altogether, the field gradient in the investigated part of the Ivrea Zone defines a deep crustal section with rocks that experienced a clockwise *P*–*T* path with 1) increasing pressure and temperature largely through the sillimanite zone and 2) decompression at still high temperatures, accompanied by the intrusion of the Mafic Complex. The Mafic Complex likely crystallised under granulite facies conditions similar to the granulites facies metapelites in Val Strona di Omegna at the same crustal level. This is in agreement with the interpretation of Rivalenti *et*

al. (1984) and Sinigoi *et al.* (1994). Furthermore, this study finds no evidence for the presence of the Mafic Complex in Val Strona di Omegna; the Mafic Complex only exists in Val Sesia and Val Strona di Postua, which is the southern part of the Ivrea Zone. These conclusions are based on the development of the continuous transition from schists through metatexites to diatexites in Val Strona di Omegna without any evidence for contact effects present in Val Sesia and Val Strona di Postua. Also the map of Quick *et al.* (2003) is incorrect, because the study presented here points out that not only amphibolite facies rocks but also granulite facies rocks occur in Val Sesia and Val Strona di Postua near the contact with the Mafic Complex in an aureole of around 2–3 km. Based on the results of this study, with the exception of Peressini *et al.* (2007), the age determinations from other studies are likely to be cooling ages. The conclusions are supported by a study on the detailed field and petrological investigations on the metabasites that are interlayered with the metapelites and the calculations of their pressure and temperature estimates (Kunz, 2011). This study describes a similar metamorphic field gradient for Val Strona di Omegna, based on metabasites as it is presented here and also show that the mafic rock present all underwent prograde metamorphism from hydrated protoliths.

8.3 Suggestions for future research

Several important aspects that are not included in this work require further study to enable a more complete understanding of the evolution of the Ivrea Zone. First, it would be useful to investigate if there is a clear contact effect from the intrusion of the Permian granites of the Strona-Ceneri Zone to the rocks of the Kinzigite Formation. Such a contact effect has been observed next to granitic dykes (unknown age) in the lower grade rocks of Kinzigite Formation but for clear evidence of this too few samples were investigated in this study. The phase equilibrium modelling should also be extended to include the northern part of the Ivrea Zone to get a more complete picture of the metamorphic pattern and how the northern part relates to the present results. Lastly, it would be important to revisit the age determinations in the whole of Val Strona di Omegna, for

metapelites as well as for metabasites, under the consideration of the peak metamorphic pressures and temperatures detailed here.

Bibliography

Abart, R., Schmud, R. & Harlov, D., 2001. Metasomatic coronas around hornblendite xenoliths in granulite facies marble, Ivrea Zone, N Italy: constraints on component mobility. *Contributions to Mineralogy and Petrology*, **141,** 473–493.

Ahrendt, H., Hoefs, J., Strackenbrock, I. & Weber, K., 1989. A geothermal gradient of the lower crustal section of the Ivrea-Zone during Hercynian time deduced from carbon isotopes. In: Consiglio Nazionale della Ricerca, eds., *Varallo Conference on the Lower Continental Crust, Varallo Italy, Special Publications Consiglio Nazionale delle Ricerche, Varallo*, **27,** 17.

Barboza, S.A. & Bergantz, G.W., 2000. Metamorphism and Anatexis in the Mafic Complex Contact Aureole, Ivrea Zone, Northern Italy. *Journal of Petrology*, **41,** 1307–1327.

Barboza, S.A., Bergantz, G.W. & Brown, M., 1999. Regional granulite facies metamorphism in the Ivrea Zone: Is the Mafic Complex the smoking gun or red herring?. *Geology*, **27,** 447–450.

Barrow, G., 1893. On an intrusion of muscovite-biotite gneiss in the south-eastern highland of Scotland, and its accompanying metamorphism. *Quarterly Journal of the Geological Society*, **49,** 330–358.

Bea, F. & Montero, P., 1999. Behaviour of accessory phases and redistribution of Zr, REE, Y, Th and U during metamorphism and partial melting of metapelites in the lower crust: An example from the Kinzigite Formation of Ivrea-Verbano, NW Italy. *Geochemica et Cosmochimica Acta*, **63,** 1133–1153.

Berman, R.G., 1991. Thermobarometry using multiequilibrium calculations: a new technique with petrologic applications. *Canadian Mineralogist*, **29,** 833–885.

Bertolani, M., 1968. La petrografia della Valle Strona (Alpi Occidentali Italiane). *Schweizer Mineralogische und Petrographische Mitteilungen*, **48,** 695–732.

Binns, R.A., 1964. Zones of progressive regional metamorphism in the Willyama Complex, Broken Hill district, New South Wales. *Australian Journal of Earth Science*, **11,** 283–330.

Boriani, A. & Villa, I.M., 1997. Geochronology of regional metamorphism in the Ivrea-Verbano Zone and Serie die Laghi, Italian Alps. *Schweizer Mineralogische und Petrographische Mitteilungen,* **77,** 381–401.

Boriani, A. & Giobbi, E., 2004. Does the basement of western southern Alps display a tilted section through the continental crust? A review and discussion. *Periodico di Mineralogia*, **73,** 5–22.

Boriani, A., Bigioggero, B. & Origoni Giobbi, E., 1977. Metamorphism, tectonic evolution, and tentative stratigraphy of the `Serie die Laghi´–geological map of the Verbania area (northern Italy). *Memorie degli Instituti di Geologia e Mineralogia dell´Universita di Padova*, **32,** 1–25.

Boriani, A., Burlini, L., Caironi, V., Giobbi Origoni, E., Sassi, A. & Sesana, E., 1988. Geological and petrological studies on the Hercynian plutonism of Serie die Laghi–Geologial map of its occurrence between Valsesia and Lago Maggiore (N-Italy). *Rendiconti della Società Italiana di Mineralogia e Petrologia*, **43,** 367–384.

Bowen, N.L., 1913. The melting phenomena of the plagioclase feldspars. *American Journal of Science*, **185,** 557–559.

Brodie, K.H. & Rutter, E.H., 1987. Deep crustal extensional faulting in the Ivrea Zone of Northern Italy. *Tectonophysics*, **140,** 193–212.

Brodie, K.H., Rex, D. & Rutter, E.H., 1989. On the age of deep crustal faulting in the Ivrea Zone, northern Italy. *Geological Society, London, Special Publications*, **45,** 203–210.

Bürgi, A. & Klötzli, U., 1990. New data on the Evolutionary History of the Ivrea Zone (Northern Italy). *Bulletin of the Suiss Association of Petroleum Geologists and Engineers*, **56,** 49–70.

Carmichael, D.M., 1970. Intersecting isograds in the Whetstone Lake area, Ontario. *Journal of Petrology,* **11,** 147–217.

Coggon, R. & Holland, T.J.B., 2002. Mixing properties of phengitic micas and revised garnet-phengite themobarometers. *Journal of Metamorphic Geology,* **20,** 683–969.

Demarchi, G., Quick, J.E., Sinigoi, S. & Mayer, A., 1998. Pressure Gradient and Original Orientation of a Lower-Crustal Intrusion in the Ivrea-Verbano Zone, Northern Italy. *Journal of Geology*, **106,** 609–622.

Ellis, D.H. & Green, E.H., 1979. An experimental study of the effect of Ca upon garnet-clinopyroxene Fe-Mg exchange equilibria. *Contributions to Mineralogy and Petrology*, **71,** 13–22.

Franz, L. & Harlov, D., 1998. High-Grade K-feldspar Veining in Granulites from the Ivrea-Verbano Zone, Northern Italy: Fluid Flow in the Lower Crust and Implications for Granulite Facies Genesis. *Journal of Geology*, **106,** 455–472.

Fuhrman, M.L. & Lindsley, D.H., 1988. Ternary feldspar modelling and thermometry. *American Mineralogist*, **73,** 201–215.

Gansser, A., 1968. The Insubric Line, a Major Geotectonic Problem. *Schweizer Mineralogische und Petrographische Mitteilungen,* **48,** 123–143.

Garuti, G., Bea, F., Zaccarini, F. & Montero, P., 2001. Age, geochemistry and petrogenesis of the ultramafic pipes in the Ivrea Zone, NW Italy. *Journal of Petrology*, **42,** 433–457.

Gebauer, D., 1993. The pre-alpine evolution of the continental crust of the central alps–an overview. In: von Raumer J.F., Neubauer, F., eds., Pre-Mesozoic geology in the alps. Springer, Berlin Heidelberg New York, 93–117.

Graham, C.M. & Powell, R., 1986. A garnet-hornblende geothermometer: Calibration, testing, and application to the Pelona schists, southern California. *Journal of Metamorphic Geology*, **2,** 13–31.

Grant, J.A., 1986. The isocon diagram – a simple solution to Gresens´equation from Metasomatic alteration. *Economic Geology*, **81,** 1976–1982.

Grant, J.A., 2005. Isocon analysis: A brief review of the method and applications. *Physics and Chemistry on the Earth*, **30,** 997–1004.

Handy, M. R. & Zingg, A., 1991. The tectonic and rheological evolution of an attenuated cross section of the continental crust: Ivrea crustal section, southern Alps, northwestern Italy and southern Switzerland. *Geological Societey of American Bulletin*, **103,** 236–253.

Harlov. D. & Förster, H.J., 2002. High-Grade Fluid Metasomatism on both a Local and Regional Scale: the Seward Peninsula, Alaska and the Val Strona di Omegna, Ivrea-Verbano Zone, Northern Italy. Part II: Phosphate Mineral Chemistry. *Journal of Petrology*, **43,** 801–824.

Harlov, D. & Wirth, R., 2000. K-feldspar-quartz and K-feldspar-plagioclase phase boundary interactions in garnet-orthopyroxene gneiss´s from the Val Strona di Omegna, Ivrea-Verbano Zone, northern Italy. *Contributions to Mineralogy and Petrology*, **140,** 148–162.

Henk, A., Franz, L., Teufel, S. & Oncken, O., 1997. Magmatic Underplating, Extension and Crustal Reequilibration: Insights from a Cross-Section through the Ivrea Zone and Strona-Ceneri Zone, Northern Italy. *Journal of Geology*, **105,** 367–377.

Hodges, K.V. & Fountain, D.M., 1984. Pogallo Line, South Alps, northern Italy: An intermediate crystal level, low-angle normal fault?. *Geological Society of America*, **12,** 151–155.

Hoisch, T.D., 1990. Empirical calibration of six geobarometers for the mineral paragenesis quartz+muscovite+biotite+plagioclase+garnet. *Contributions to Mineralogy and Petrology*, **104,** 225–234.

Holland, T.J.B & Powell, R., 1985. An internally consistent thermodynamic dataset with uncertainties and correlations: 2. Data and results. *Journal of Metamorphic Geology*, **3,** 343–370.

Holland, T.J.B. & Powell, R., 1990. An enlarged and updated internally consistent thermodynamic dataset with uncertainties and correlations: the system K_2O–Na_2O–CaO–MgO–MnO–FeO–Fe_2O_3–Al_2O_3–TiO_2–SiO_2–C–H_2–O_2. *Journal of Metamorphic Geology*, **8,** 89–124.

Holland, T.J.B. & Powell, R., 1996a. Thermodynamics of order-disorder in minerals: 1. Symmetric formalism applied to minerals of fixed composition. *American Mineralogist*, **81,** 1413–1424.

Holland, T.J.B. & Powell, R., 1996b. Thermodynamics of order-disorder in minerals: 2. Symmetric formalism applied to solid solutions. *American Mineralogist*, **81,** 1425–1437.

Holland, T.J.B. & Powell, R., 1998. An internally consistent thermodynamic data set for the phases of petrological interest. *Journal of Metamorphic Geology*, **16,** 309–343.

Holland, T.J.B. & Powell, R., 2001. Calculation of Phase Relations Involving Haplogranitic Melts Using an Internally Consistent Thermodynamic Dataset. *Journal of Metamorphic Geology*, **42,** 673–683.

Holland, T.J.B. & Powell, R., 2003. Activity-composition relations for phases in petrological calculations: an asymmetric multicomponent formulation. *Contributions to Mineralogy and Petrology*, **145,** 492–501.

Holland, T.J.B. & Powell, R., 2006. Mineral activity-composition relations and petrological calculations involving cation equipartition in multisite minerals: a logical inconsistency. *Journal of Metamorphic Geology*, **24,** 851–861.

Hunziker, J.C., 1974. Rb-Sr and K-Ar age determination and the Alpine tectonic history of the Western Alps. *Memorie degli Instituti di Geologia e Mineralogia dell´Universita di Padova*, **31,** 1–154.

Hunziker, J.C. & Zingg, A., 1980. Lower Paleozoic Amphibolite to Granulite Facies Metamorphism in the Ivrea Zone (Southern Alps, Northern Italy). *Schweizer Mineralogische und Petrographische Mitteilungen,* **60,** 181–213.

Köppel, V., 1974. Isotopic U-Pb ages of Monazites and Zircons from the Crust-Mantle Transition and Adjacent Units of the Ivrea and Ceneri Zones (Southern Alps, Italy): *Contributions to Mineralogy and Petrology*, **43,** 55–70.

Kohn, M. & Spear, F.S., 1990. Two new geobaromaters for garnet amphibolites, with applications to south-east Vermont. *American Mineralogist*, **75,** 89–96.

Koziol, A.M. & Newton, R.C., 1988. Redetermination of the anorthite breakdown reaction and improvement of the plagioclase-garnet-Al_2SiO_5-quartz geobarometer. *American Mineralogist*, **73,** 216–223.

Kunz, B.E., 2011. Mid-crustal metamorphic field gradient in Val Strona di Omegna, Ivrea Zone, Italy: constraints from metabasic rocks. Diploma thesis, Johannes Gutenberg-Universität Mainz, 142p.

Lal, R.K., 1993. Internally consistent recalibrations of mineral equilibria for geothermobarometry involving garnet-orthopyroxene-plagioclase-quartz assemblages and their application to the south Indian granulites. *Journal of Metamorphic Geology*, **11,** 855–866.

Lu, M., Hofman, A.W., Mazzucchelli, M., Rivalenti, G., 1997. The mafic–ultramafic complex near Finero (Ivrea-Verbano Zone), II Geochronology and isotope geochemistry. *Chemical Geology*, **140,** 223–235.

Luvizotto, G.L. & Zack, T., 2009. Nb and Zr behavior in rutile during high-grade metamorphism and retrogression: An example from the Ivrea-Verbano Zone. *Chemical Geology*, **261,** 303–317.

Maher, E.M., Baker, J.M., Powell, R., Holland, T.J.B. & Howell, N., 1997. The effect of Mn on mineral stability in metapelites. *Journal of Metamorphic Geology*, **15,** 223–238.

Massonne, H.-J., 1990. High-pressure, low-temperature metamorphism of pelitic and other protoliths based on experiments in the system K_2O–MgO–Al_2O_3–SiO_2–H_2O. Habilitation thesis, Ruhr Universität, Bochum, Germany, 172p.

McDowell, F.W. & Schmid, R., 1968. Potassium-Argon Ages from the Valle d´Ossola Section of the Ivrea-Verbano Zone (Northern Italy). *Schweizer Mineralogische und Petrographische Mitteilungen,* **48,** 205–210.

Mehnert, K.R., 1975. The Ivrea Zone - A model for the deep crust. *Neues Jahrbuch für Mineralogie, Abhandlungen*, **125,** 156–199.

Newton, R.C. & Perkins, D. (III.), 1982. Thermodynamic calibrations of geobarometers based on the assemblages garnet-plagioclase-orthopyroxene (clinopyroxene)-quartz. *American Mineralogist*, **67,** 203–222.

Pattinson, D.R.M., Chacko, T., Farquhar, J., McFarlane, C.R.M., 2003. Temperatures of Granulite-facies Metamorphism: Constraints from Experimental Phase Equilibria and Thermobarometry Corrected for Retrograde Exchange. *Journal of Petrology*, **44,** 867–900.

Peressini, G., Quick, J.E., Sinigoi, S., Hofmann, A.W. & Fanning, M., 2007. Duration of a Large Mafic Intrusion and Heat Transfer in the Lower Crust: a SHRIMP U-Pb Zircon Study in the Ivrea–Verbano Zone (Western Alps, Italy). *Journal of Petrology*, **48,** 1185–1218.

Pin, C., 1986. Datation U-Pb sur zircons a 285 Ma du complexe gabbro-dioritique du Val Sesia–Val Mastallone etage tardi-hercynien du métamorphisme granulitique de la zone Ivrea-Verbano (Italie). *Comptes Rendus de l´Académie des Sciences, Paris*, **303,** 827–830.

Pin, C. & Sills, J.D., 1986. Petrogenesis of layered gabbros and ultramafic rocks from Val Sesia, the Ivrea Zone, NW Italy: trace elements and isotop geochemistry. *Geological Society, London, Special Publications*, **24,** 231–249.

Powell, R., 1987. Darken's quadratic formalism and the thermodynamic of minerals. *American Mineralogist*, **72,** 1–11.

Powell, R. & Holland, T.J.B., 1985. An internally consistent thermodynamic dataset with uncertainties and correlations: 1. Methods and a worked example. *Journal of Metamorphic Geology*, **3,** 327–342.

Powell, R. & Holland, T.J B., 1988. An internally consistent thermodynamic dataset with uncertainties and correlations: 3. Applications to geobarometry, worked examples and a computer program. *Journal of Metamorphic Geology*, **6,** 173–204.

Powell, R., Holland, T.J.B. & Worley, B., 1998. Calculating phase diagrams involving solid solutions via non-linear equations, with examples using THERMOCALC. *Journal of Metamorphic Geology*, **16,** 577–588.

Powell, R. & Holland, T.J.B., 1993. On the formulation of simple mixing models for complex phases. *American Mineralogist*, **78,** 1174–1180.

Quick, J.E., Sinigoi, S. Mayer, A., 1994. Emplacement dynamics of a large mafic intrusion in the lower crust of the Ivrea-Verbano Zone, northwest Italy. *Journal of Geophysical Research*, **99,** 559–573.

Quick, J.E., Sinigoi, S. Mayer, A., 1995. Emplacement of mantle peridotite in the lower continental crust, Ivrea-Verbano Zone, northern Italy. *Geology*, **23,** 739–742

Quick, J.E., Sinigoi, S., Snoke, A.W., Kalakay, T.J., Mayer, A. & Peressini, G., 2003. Geologic map of the southern Ivrea-Verbano Zone, Northwestern Italy: *U.S. Geological Survey*, Geologic Investigations Series Map I-2776, scale 1:25,000, 22p.

Quick, J.E., Sinigoi, S., Peressini, G. Demarchi, G., Wooden, J.L. & Sbisà, A., 2009. Magmatic plumbing of a large Permian caldera exposed to a depth of 25 km. *Geology*, **37,** 603–606.

Reinsch, D., 1969. Zur Petrographie des Valle Strona (Ivrea-Zone). *Neues Jahrbuch für Mineralogie, Abhandlungen, Monatsheft*, 885–869.

Rivalenti, G., Garuti, G. & Rossi, A., 1975. The origin of the Ivrea–Verbano basic formation (western Italian Alps). Whole rock geochemistry. *Bollettino della Società Geologica Italiana*, **94,** 1149–1186.

Rivalenti, G., Garuti, G., Rossi, A. ,Siena, F. & Sinigoi, S., 1981. Existence of different peridotite types and of a layered igneous complex in the Ivrea Zone of the Western Alps. *Journal of Petrology*, **22,** 127–153.

Rivalenti, G., Rossi, A. ,Siena, F. & Sinigoi, S., 1984. The Layered Series of the Ivrea-Verbano Igneous Complex, Western Alps, Italy. *Tschermaks Mineralogische und Petrogrographische Mitteilungen*, **33,** 77–99.

Rudnick, R.L. & Gao, S., 2003. Composition of the Continental Crust, In: Holland, H.D. & Turekian, K.K., eds., Treatise on Geochemistry: Pergamin, Oxford, **2,** 1–64.

Rutter, E.H., Brodie, K.H. & Evans, P., 1993. Structural geometry, lower crustal magmatic underplating and lithospheric stretching in the Ivrea-Verbano Zone, northern Italy. *Journal of Structural Geology*, **15,** 647–662.

Rutter, E.H. & Brodie, K.H., 1996. A summary of the Geology of the Ivrea-Verbano Zone, to accompany the Valle d´Ossola and Val Sesia Field excursion, 5 and 6 September 1996, 16p.

Rutter, E., Brodie, K., James, T. & Burlini, L., 2007. Large-scale folding in the upper part of the Ivrea-Verbano zone, NW Italy. *Journal of Structural Geology*, **29,** 1–17.

Sawyer, E.W., 2008. Atlas of Migmatites. *The Canadian Mineralogist, Special Publication 9*. NRC Research Press, Ottawa, Ontario, Canada, 371p.

Schaltegger, U. & Brack, P., 2007. Crustal-scale magmatic systems during intercontinental strike-slip tectonics: U, Pb and Hf isotopic constraints from Permian magmatic rocks of the Southern Alps. *International Journal of Earth Science*, **96,** 1131–1151.

Schmid, R., 1967. Zur Petrographie und Struktur der Zone Ivrea-Verbano zwischen Valle d´Ossola und Val Grande (Prov. Novara Italien). *Schweizer Mineralogische und Petrographische Mitteilungen,* **47,** 935–1117.

Schmid, R., 1968. Schwierigkeiten der Nomenklatur und Klassifikation massiger Katametamorphite, erläutert am Beispiel der Zone Ivrea-Verbano (Norditalien). *Schweizer Mineralogische und Petrographische Mitteilungen*, **48,** 81–90.

Schmid, R. & Wood, B.J., 1976. Phase Relationships in Granulitic Metapelites from the Ivrea-Verbano Zone (Northern Italy). *Contributions to Mineralogy and Petrology,* **54,** 255–279.

Schmid, S.M., Zingg, A. & Handy, M., 1987. The kinematics of movements along the Insubric Line and the emplacement of the Ivrea Zone. *Tectonophysics*, **135,** 47–66.

Schmid, S.M., 1993. Ivrea Zone and Adjacent Southern Alpine Basement, In: v. Raumer, J.F. and Neubauer, F., eds., Pre-Mesozoic Geology in the Alps: Berlin Heidelberg Springer-Verlag, 567–583.

Schnetger, B., 1988. Geochemische Untersuchungen an den Kinzigiten und Stronaliten der Ivrea-Zone, Norditalien. Dissertation, Georg-August-Universität, Göttingen, 118p.

Schnetger, B., 1994. Partial melting during evolution of the amphibolite- to granulite-facies gneisses of the Ivrea Zone. *Chemical Geology*, **113,** 71–101.

Siegesmund, S., Layer, P., Dunkl, I., Vollbrecht, A. Steenken, A., Wemmer, K. & Ahrendt, H., 2008. Exhumation and deformation history of the lower crustal section of the Valstrona di Omegna in the Ivrea Zone, southern Alps. *Geological Society, London, Special Publications*, **298,** 45–68.

Sills, J.D., 1984. Granulite facies metamorphism in the Ivrea Zone, NW Italy. *Schweizer Mineralogische und Petrographische Mitteilungen*, **64,** 69–91.

Sills, J.D. & Tarney, J., 1984. Petrogenesis and tectonic significance of amphibolites interlayerd with metasedimentary gneisses in the Ivrea Zone, Southern Alps, northwest Italy. *Tectonophysics,* **107,** 187–208.

Sinigoi, S., Quick, J.E., Clemens-Knott, D., Mayer, A., Demarchi, G., Mazzucchelli, M., Negrini, L. and Rivalenti, G., 1994. Chemical evolution of the large mafic intrusion in the lower crust, Ivrea-Verbano Zone, northern Italy. *Journal of Geophysical Research*, **99,** 575–590.

Sinigoi, S., Quick, J.E., Demarchi, G. & Klötzli, U., 2011. The role of crustal fertility in the generation of large silicic magmatic systems triggered by intrusion of mantel magma in the deep crust. *Contributions to Mineralogy and Petrology*,**162,** 691–707.

Snoke, A.W., Kalakay, T.J., Quick, J.E., Sinigoi, S., 1999. Development of a deep-crustal shear zone in response to syntectonic intrusion of mafic magma into the lower crust, Ivrea–Verbano zone, Italy. *Earth and Planetary Science Letters*, **166,** 31–45.

Spear, F.S., Kohn, M.J., Cheney, J.T. & Florence, F., 2002. Metamorphic, thermal, and tectonic evolution of central New England. *Journal of Petrology*, **43,** 2097–2120.

Taylor, S.R. & McLennan, S.M., 1985. The Continental crust: Its Composition and Evolution. Blackwell, Oxford.

Teufel, S. & Schärer, U., 1989. Unravelling the age of high-grade metamorphism of the Ivrea Zone: a monazite single-grain and small fraction study. Terra Abstract, **1,** 350.

Vavra, G. & Schaltegger, U., 1999. Post-granulite facies monazite growth and rejuvenation during Permian to Lower Jurassic thermal and fluid events in the Ivrea Zone (Southern Alps). *Contributions to Mineralogy and Petrology*, **122,** 337–358.

Vavra, G., Schmid, R. & Gebauer, D., 1999. Internal morphology, habit and U-Th-Pb microanalysis of amphibolite-to-granulite facies zircons: geochronology of the Ivrea Zone (Southern Alps). *Contributions to Mineralogy and Petrology,* **98,** 257–276.

Voshage, H., Hunziker, J.C., Hofmann, A.W. & Zingg, A., 1987. A Nd and Sr isotopic study of the Ivrea Zone, Southern Alps, N-Italy. *Contributions to Mineralogy and Petrology*, **97,** 31–42.

Voshage, H., Hofmann, A.W., Mazzucchelli, M., Rivalenti, G., Sinigoi, S., Raczek, I. & Demarchi, G., 1990. Isotopic evidence from the Ivrea Zone for a hybrid lower crust formed by magmatic underplating. *Nature*, **347,** 731–736.

White, R.W. & Powell, R., 2002. Melt loss and the preservation of granulite facies mineral assemblages. *Journal of Metamorphic Geology*, **20,** 621–632.

White, R.W., Powell ,R. & Holland, T.J.B. & Worley, B.A., 2000. The effect of TiO_2 and Fe_2O_3 on metapelitic assemblages at greenschist and amphibolite facies conditions: mineral equilibria calculations in the system K_2O–FeO–MgO–Al_2O_3–SiO_2–H_2O–TiO_2–Fe_2O_3. *Journal of Metamorphic Geology*, **18,** 497–511.

White, R.W., Powell, R. & Holland, T.J.B., 2001. Calculation of partial melting equilibria in the system Na_2O–CaO–K_2O–FeO–MgO–Al_2O_3–SiO_2–H_2O (NCKFMASH). *Journal of Metamorphic Geology*, **19,** 139–153.

White, R.W., Powell, R. & Clarke, G.L., 2002. The interpretation of reaction textures in Fe-rich metapelitic granulites from the Musgrave Block, central Australia: constraints from mineral equilibria calculations in the system K_2O–FeO–MgO–Al_2O_3–SiO_2–H_2O–TiO_2–Fe_2O_3. *Journal of Metamorphic Geology*, **20,** 41–55.

White, R.W., Powell, R. & Clarke, G.L., 2003. Prograde metamorphic assemblage evolution during partial melting of metasedimentary rocks at low pressures: migmatites from Mt Stafford, Central Australia. *Journal of Petrology*, **44,** 1– 4.

White, R.W., Powell, R. & Holland, T.J.B., 2007. Progress relating to calculation of partial melting equilibria for metapelites. *Journal of Metamorphic Geology*, **25,** 522–527.

Williams, M.L. & Grambling, J.A., 1990. Manganese, ferric iron, and the equilibrium between garnet and biotite. *American Mineralogist*, **75,** 886–908.

Zhu, C. & Sverjensky, D.A., 1992. F–Cl–OH partitioning between biotite and apatite. *Geochemica et Cosmochimica Acta*, **56,** 3435–3467.

Zingg, A., 1978. Regionale Metamorphose in der Ivrea Zone (Nord-Italien). Dissertation, Eidgenoessische Technische Hochschule, Zürich, 230p.

Zingg, A., 1980. Regional Metamorphism in the Ivrea Zone (Southern Alps, N-Italy): Field and microscopic Investigations. *Schweizerische Mineralogische und Petrographische Mitteilungen,* **60,** 153–173.

Zingg, A., 1983. The Ivrea and Strona-Ceneri Zones (Southern Alps, Ticino and N-Italy) - A Review. *Schweizer Mineralogische und Petrographische Mitteilungen,* **63,** 361–392.

Appendix A

XRF analyses

- Val Strona di Omegna, metapelites
- Val Strona di Omegna, metaspammites/metagreywackes
- Val Sesia, metapelites
- Val Strona di Postua, metapelites

Val Strona di Omegna (metapelite, amphibolite facies)

Sample	IZ 008	IZ 009	IZ 010	IZ 011	IZ 015	IZ 017	IZ 018	IZ 013	IZ 019	IV 059	IZ 061	IV 019	IZ 029
SiO_2	59.58	68.10	70.46	67.99	68.58	73.15	69.22	64.01	68.60	69.48	61.76	69.46	60.33
TiO_2	0.92	0.57	0.82	0.80	0.87	0.70	0.72	0.81	0.76	0.87	1.05	0.68	1.08
Al_2O_3	18.41	15.48	15.09	15.61	12.60	13.01	14.89	15.76	14.58	15.24	20.03	13.40	18.13
FeO	6.33	4.00	5.16	5.76	3.99	3.37	4.69	6.58	4.90	6.31	7.52	4.29	7.68
MnO	0.08	0.07	0.06	0.06	0.04	0.02	0.04	0.07	0.07	0.09	0.06	0.05	0.08
MgO	2.86	1.89	1.61	2.29	1.82	4.11	2.25	4.35	2.23	2.35	2.50	2.09	3.79
CaO	2.12	2.16	0.54	0.92	2.15	0.60	1.18	0.83	1.82	0.50	0.31	1.46	0.69
Na_2O	3.61	3.05	1.54	2.12	3.01	0.57	1.65	1.54	3.18	0.69	0.71	0.75	0.39
K_2O	3.73	2.48	2.98	2.81	1.81	2.45	3.46	2.95	2.39	2.88	3.74	4.39	4.46
P_2O_5	0.20	0.16	0.15	0.07	0.39	0.16	0.16	0.16	0.16	0.11	0.05	0.60	0.26
SO_3	0.86	0.23	0.01	0.02	0.65	0.01	0.11	0.37	0.11	0.03	0.04	0.12	0.40
Cr_2O_3	0.01	0.01	0.01	0.01	0.01	0.01	0.01	0.01	0.01	0.01	0.01	0.01	0.02
NiO	0.00	0.00	0.00	0.00	0.01	0.00	0.00	0.01	0.00	0.00	0.01	0.00	0.01
Sum	**100.80**	**100.28**	**100.25**	**100.21**	**100.82**	**99.81**	**99.81**	**99.88**	**100.30**	**100.58**	**99.95**	**100.06**	**100.92**
LOI	1.38	1.65	1.24	1.10	4.45	1.28	0.91	1.70	0.95	1.31	1.32	2.27	2.76
$Fe_2O_3(t)$	7.03	4.44	5.73	6.40	4.43	3.74	5.21	7.31	5.44	7.01	8.36	4.77	8.53

Val Strona di Omegna (metapelite, transition zone)

Sample	IZ 028	IV 058	IZ 033	IV 020	IZ 030	IZ 036	IZ 112	IV 054	IV 052	IZ 066	IV 048	IV 049	IZ 146
SiO_2	52.51	52.40	65.36	61.28	56.42	47.47	46.12	56.17	64.57	59.27	63.80	64.82	68.49
TiO_2	1.37	1.28	0.85	0.98	1.01	1.23	1.46	1.09	0.93	0.96	1.15	0.93	0.58
Al_2O_3	23.63	22.28	17.52	20.08	23.03	27.09	27.74	22.22	17.95	19.87	18.98	18.12	14.83
FeO	9.47	8.47	8.06	8.46	9.03	9.52	10.99	8.32	6.67	8.01	8.59	6.34	6.02
MnO	0.10	0.09	0.23	0.28	0.26	0.23	0.24	0.21	0.15	0.22	0.11	0.08	0.12
MgO	3.25	3.69	1.99	2.18	2.35	3.07	3.35	2.39	1.97	2.20	2.73	2.10	2.71
CaO	0.48	1.01	1.12	1.04	1.30	2.29	1.68	1.90	1.08	2.81	1.32	1.28	2.74
Na_2O	0.85	1.50	0.66	0.78	1.02	1.74	1.46	1.35	0.79	1.36	0.92	1.88	2.65
K_2O	4.19	3.98	2.35	3.36	3.76	3.50	4.03	2.96	3.53	3.30	1.31	2.12	1.03
P_2O_5	0.06	0.14	0.20	0.15	0.18	0.17	0.11	0.14	0.14	0.16	0.06	0.22	0.03
SO_3	0.01	0.02	0.07	0.06	0.05	0.00	0.03	0.02	0.02	0.12	0.13	0.01	0.11
Cr_2O_3	0.02	0.02	0.02	0.02	0.02	0.03	0.03	0.02	0.02	0.02	0.02	0.01	0.01
NiO	0.01	0.01	0.01	0.01	0.01	0.01	0.01	0.01	0.01	0.01	0.01	0.00	0.00
Sum	**99.99**	**100.18**	**99.97**	**99.96**	**100.03**	**98.56**	**100.64**	**99.90**	**99.80**	**99.58**	**100.42**	**99.96**	**100.08**
LOI	2.99	4.35	0.64	0.34	0.58	1.16	2.17	2.18	1.23	0.39	0.34	1.35	0.09
$Fe_2O_3(t)$	10.52	9.41	8.96	9.40	10.04	10.58	12.21	9.24	7.41	8.90	9.54	7.04	6.69

Val Strona di Omegna (metapelite, granulite facies)

Sample	IZ 156	IV 044	IZ 072	IZ 005	IZ 070	IZ 049	IZ 102
SiO_2	59.03	55.10	61.41	61.28	58.12	53.65	68.95
TiO_2	1.44	0.62	1.45	1.03	1.37	1.27	1.03
Al_2O_3	17.14	20.12	15.76	18.71	21.89	21.14	13.07
FeO	10.71	11.08	9.60	8.97	10.47	8.73	6.34
MnO	0.15	0.27	0.25	0.15	0.10	0.13	0.10
MgO	4.17	3.41	3.29	3.40	3.45	3.92	3.10
CaO	3.02	3.59	3.62	0.78	0.36	2.77	1.24
Na_2O	2.33	2.37	1.39	0.81	0.33	3.10	1.39
K_2O	1.51	1.39	0.27	1.98	2.54	3.07	2.66
P_2O_5	0.04	0.03	0.02	0.10	0.05	0.07	0.06
SO_3	0.09	0.02	0.15	0.04	0.03	0.93	0.04
Cr_2O_3	0.02	0.02	0.02	0.03	0.02	0.02	0.01
NiO	0.01	0.00	0.01	0.01	0.01	0.01	0.01
Sum	**100.90**	**99.46**	**99.65**	**98.82**	**100.36**	**99.98**	**98.84**
LOI	0.05	0.21	1.35	0.54	0.45	0.19	0.14
$Fe_2O_3(t)$	11.90	12.31	10.67	9.97	11.64	9.70	7.04

Val Strona di Omegna (metapsammite/metagreywacke, amphibolite (IZ 140) and granulite facies (IZ 120, IZ 129))

Sample	IZ 140	IZ 120	IZ 129
SiO_2	63.78	52.07	55.27
TiO_2	0.64	1.99	2.25
Al_2O_3	16.37	16.99	15.65
FeO	5.63	11.02	10.47
MnO	0.10	0.23	0.17
MgO	2.41	6.46	5.75
CaO	5.02	8.11	6.42
Na_2O	1.60	0.89	2.28
K_2O	2.15	0.21	0.38
P_2O_5	0.12	0.26	0.36
SO_3	0.01	0.01	0.09
Cr_2O_3	0.01	0.03	0.03
NiO	0.00	0.01	0.01
Sum	**99.48**	**99.87**	**100.38**
LOI	0.99	0.36	0.09
$Fe_2O_3(t)$	6.26	12.25	11.64

Val Sesia (metapelite)

Sample	IV 034	IZ 114	IZ 168	IZ 169	IV 026	IZ 201
SiO_2	59.16	47.60	53.64	71.28	64.18	57.61
TiO_2	0.93	1.52	1.56	1.06	1.18	2.00
Al_2O_3	18.03	27.06	23.84	13.62	18.62	17.27
FeO	6.40	11.22	10.02	6.29	7.23	9.02
MnO	0.10	0.11	0.13	0.05	0.05	0.11
MgO	3.81	3.52	3.13	1.91	2.24	3.39
CaO	2.26	0.38	0.16	0.50	0.75	3.10
Na_2O	3.59	0.49	0.22	0.81	1.13	2.33
K_2O	2.88	4.32	4.30	2.66	2.71	2.98
P_2O_5	0.13	0.07	0.06	0.10	0.10	0.30
SO_3	0.56	0.73	0.06	0.01	0.04	0.58
Cr_2O_3	0.02	0.02	0.02	0.01	0.01	0.01
NiO	0.01	0.01	0.01	0.00	0.01	0.01
Sum	**99.79**	**99.95**	**99.36**	**100.00**	**99.20**	**99.86**
LOI	1.92	2.90	2.21	1.69	0.96	1.16
$Fe_2O_3(t)$	7.11	12.47	11.14	6.99	8.03	10.02

Val Strona di Postua (metapelite)

Sample	IZ 132	IZ 133	IZ 135	IZ 165	IZ 163
SiO_2	64.42	46.28	64.39	58.79	72.15
TiO_2	0.93	1.39	1.10	1.78	0.36
Al_2O_3	16.72	27.95	17.79	17.06	14.90
FeO	7.08	12.23	7.46	8.90	3.30
MnO	0.08	0.13	0.10	0.11	0.03
MgO	3.49	5.00	2.46	4.03	0.78
CaO	2.28	0.32	1.50	2.91	3.02
Na_2O	1.94	0.25	0.98	1.90	2.83
K_2O	1.67	2.78	2.22	2.57	1.90
P_2O_5	0.05	0.08	0.05	0.24	0.04
SO_3	0.45	0.18	0.02	0.29	0.00
Cr_2O_3	0.01	0.02	0.01	0.02	0.00
NiO	0.01	0.01	0.01	0.01	0.00
Sum	**100.03**	**98.91**	**99.64**	**98.98**	**99.58**
LOI	0.90	2.29	1.55	0.37	0.26
$Fe_2O_3(t)$	7.87	13.59	8.29	9.89	3.67

Appendix B

EMP analyses

- Garnet
- Orthopyroxene
- Cordierite
- Spinel
- Biotite
- Muscovite
- K-feldspar
- Plagioclase

Garnet Val Strona di Omegna, metapelite

(number of cations based on 12 O atoms)

Sample	IZ 079		IV 058		IZ 034		IV 020		IV 054		IV 052		IZ 066		IZ 085		IZ 156	
	n=16	sd	n=4	sd	n=15	sd	n=12	sd	n=10	sd	n=13	sd	n=14	sd	n=20	sd	n=11	sd
SiO_2	37.60	0.29	37.73	0.26	37.97	0.17	38.11	0.20	37.52	0.25	38.41	0.45	38.53	0.24	39.14	0.13	38.97	0.19
TiO_2	0.04	0.04	0.01	0.01	0.02	0.03	0.01	0.01	0.01	0.01	0.02	0.02	0.00	0.01	0.02	0.02	0.03	0.03
Al_2O_3	21.29	0.18	21.67	0.23	21.92	0.13	21.83	0.10	21.64	0.10	21.92	0.17	22.10	0.13	22.37	0.15	21.96	0.21
FeO	31.59	1.79	31.34	0.28	35.63	0.29	33.90	0.38	33.01	0.37	33.17	0.47	31.57	0.23	28.10	0.40	28.70	0.94
MnO	2.14	1.41	5.53	0.16	0.83	0.07	1.94	0.07	1.63	0.07	1.33	0.07	1.16	0.05	1.01	0.09	0.57	0.06
MgO	2.46	1.06	3.87	0.25	4.42	0.25	4.38	0.23	4.68	0.21	5.15	0.15	6.37	0.25	9.13	0.27	8.52	0.70
CaO	5.45	1.73	1.08	0.04	0.95	0.06	1.45	0.08	1.78	0.11	1.78	0.11	1.84	0.07	1.67	0.10	2.00	0.36
Na_2O	0.02	0.03	0.02	0.02	0.02	0.02	0.02	0.01	0.04	0.05	0.01	0.02	0.02	0.03	0.02	0.02	0.01	0.01
K_2O	0.00	0.01	0.00	0.01	0.01	0.01	0.01	0.01	0.01	0.01	0.04	0.11	0.01	0.01	0.01	0.01	0.01	0.01
Cr_2O_3	0.05	0.03	0.06	0.05	0.03	0.03	0.03	0.03	0.04	0.02	0.04	0.03	0.05	0.03	0.06	0.04	0.07	0.04
Total	100.63	0.45	101.30	0.66	101.80	0.34	101.68	0.26	100.36	0.33	101.87	0.33	101.63	0.46	101.53	0.34	100.85	0.35
Si	2.994		2.985		2.980		2.990		2.976		2.990		2.982		2.979		2.993	
Al^{tet}	0.006		0.015		0.020		0.010		0.024		0.010		0.018		0.021		0.007	
Al^{oct}	1.992		2.005		2.008		2.008		1.999		2.001		1.998		1.984		1.981	
Ti	0.002		0.000		0.001		0.001		0.001		0.001		0.000		0.001		0.002	
Fe	2.104		2.073		2.339		2.224		2.190		2.160		2.043		1.788		1.844	
Mn	0.144		0.370		0.055		0.129		0.109		0.088		0.076		0.065		0.037	
Mg	0.291		0.456		0.517		0.512		0.554		0.598		0.735		1.035		0.975	
Ca	0.465		0.091		0.080		0.122		0.151		0.149		0.152		0.136		0.165	
Na	0.003		0.004		0.003		0.002		0.006		0.002		0.003		0.003		0.002	
K	0.000		0.000		0.001		0.001		0.001		0.004		0.001		0.001		0.001	
Cr	0.003		0.004		0.002		0.002		0.003		0.002		0.003		0.004		0.004	
X_{Fe}	0.88		0.82		0.82		0.81		0.80		0.78		0.74		0.63		0.65	
Almandine	69.90		69.24		78.12		74.46		72.63		72.11		67.71		58.48		60.68	
Pyrope	9.74		15.29		17.34		17.14		18.61		19.99		24.63		34.76		32.57	
Spessartine	4.82		12.41		1.86		4.31		3.67		2.93		2.55		2.18		1.24	
Grossular	15.26		2.86		2.59		3.99		4.96		4.85		4.95		3.89		4.69	
Andradite	0.11		0.00		0.00		0.00		0.00		0.00		0.00		0.51		0.62	
Uvarovite	0.16		0.20		0.10		0.10		0.13		0.12		0.15		0.18		0.20	

Garnet

Val Strona di Omegna, metapelite

metapsammite/metagreywacke

(number of cations based on 12 O atoms)

Sample	IV 044		IZ 005		IZ 070		IZ 004		IZ 048		IZ 102		IZ 120		IZ 129	
	n=21	sd	n=19	sd	n=20	sd	n=19	sd	n=17	sd	n=14	sd	n=13	sd	n=3	sd
SiO_2	39.54	0.16	39.09	0.18	38.70	0.17	39.12	0.10	39.41	0.13	39.20	0.16	39.17	0.16	38.87	0.16
TiO_2	0.02	0.02	0.02	0.02	0.02	0.02	0.03	0.03	0.02	0.02	0.02	0.03	0.02	0.03	0.07	0.06
Al_2O_3	22.22	0.16	22.23	0.15	22.02	0.11	22.38	0.11	22.48	0.14	22.35	0.09	22.02	0.11	21.82	0.10
FeO	28.27	0.35	27.90	0.40	30.09	0.20	29.32	0.16	27.10	0.30	23.32	0.20	25.30	0.35	26.22	0.54
MnO	0.71	0.04	0.52	0.04	0.32	0.04	0.28	0.03	0.49	0.04	0.40	0.02	1.00	0.09	0.84	0.05
MgO	9.12	0.25	9.95	0.27	9.17	0.10	9.22	0.11	10.21	0.18	12.41	0.11	9.49	0.35	8.47	0.44
CaO	1.79	0.11	1.46	0.04	0.72	0.03	1.05	0.04	1.46	0.04	1.68	0.08	3.56	0.13	3.82	0.85
Na_2O	0.02	0.02	0.02	0.02	0.02	0.02	0.02	0.02	0.03	0.03	0.02	0.02	0.01	0.02	0.03	0.01
K_2O	0.01	0.01	0.01	0.01	0.01	0.01	0.00	0.01	0.01	0.01	0.01	0.01	0.01	0.01	0.02	0.01
Cr_2O_3	0.08	0.03	0.04	0.03	0.06	0.04	0.04	0.02	0.07	0.03	0.08	0.03	0.09	0.05	0.06	0.08
Total	101.79	0.44	101.25	0.39	101.14	0.27	101.45	0.24	101.29	0.29	99.49	0.28	100.67	0.30	100.22	0.13
Si	2.998		2.973		2.970		2.980		2.982		2.973		2.987		2.992	
Al^{tet}	0.002		0.027		0.030		0.020		0.018		0.027		0.013		0.080	
Al^{oct}	1.702		1.966		1.963		1.989		1.987		1.972		1.966		1.971	
Ti	0.001		0.001		0.001		0.001		0.001		0.001		0.001		0.004	
Fe	1.793		1.775		1.932		1.867		1.715		1.479		1.613		1.688	
Mn	0.046		0.033		0.021		0.018		0.032		0.026		0.064		0.055	
Mg	1.031		1.128		1.050		1.048		1.152		1.403		1.078		0.972	
Ca	0.146		0.119		0.059		0.085		0.118		0.136		0.291		0.315	
Na	0.003		0.003		0.002		0.003		0.005		0.003		0.002		0.004	
K	0.001		0.001		0.001		0.000		0.001		0.001		0.001		0.002	
Cr	0.005		0.003		0.004		0.002		0.004		0.005		0.005		0.004	
X_{Fe}	0.63		0.61		0.65		0.64		0.60		0.51		0.60		0.63	
Almandine	59.22		56.93		61.97		61.38		56.35		47.36		52.01		55.16	
Pyrope	34.40		37.93		35.34		35.15		38.63		47.19		36.10		32.48	
Spessartine	1.53		1.12		0.70		0.61		1.06		0.87		2.16		1.84	
Grossular	4.11		2.43		0.20		2.42		3.42		3.25		8.10		9.37	
Andradite	0.50		1.46		1.61		0.32		0.32		1.09		1.37		0.96	
Uvarovite	0.24s		0.13		0.18		0.12		0.22		0.25		0.27		0.18	

Garnet

Val Sesia, metapelite

Val Strona di Postua, metapelite

(number of cations based on 12 O atoms)

Sample	IV 034		IZ 168		IV 026		IZ 201		IZ 132		IZ 165		IZ 163	
	n=5	sd	n=8	sd	n=20	sd	n=15	sd	n=13	sd	n=9	sd	n=6	sd
SiO_2	38.37	0.17	37.33	0.15	38.28	0.18	37.84	0.16	38.25	0.11	38.34	0.18	38.05	0.30
TiO_2	0.01	0.01	0.01	0.01	0.01	0.01	0.00	0.01	0.02	0.02	0.02	0.02	0.02	0.02
Al_2O_3	21.76	0.16	21.08	0.15	21.57	0.13	21.43	0.11	21.64	0.08	21.66	0.11	21.83	0.12
FeO	31.55	0.12	32.55	0.21	36.25	0.36	34.08	0.30	32.40	0.36	31.36	0.41	30.60	0.32
MnO	4.49	0.08	6.73	0.17	1.08	0.08	1.77	0.11	0.80	0.04	0.67	0.04	0.32	0.04
MgO	4.78	0.16	2.45	0.16	3.95	0.37	4.61	0.26	6.47	0.20	7.08	0.27	7.91	0.18
CaO	1.05	0.06	0.71	0.03	1.04	0.06	1.49	0.11	1.16	0.07	1.34	0.08	1.16	0.04
Na_2O	0.02	0.00	0.03	0.02	0.04	0.02	0.04	0.03	0.02	0.02	0.01	0.01	0.03	0.03
K_2O	0.00	0.00	0.01	0.01	0.01	0.01	0.01	0.01	0.01	0.01	0.01	0.01	0.02	0.04
Cr_2O_3	0.03	0.03	0.02	0.02	0.03	0.03	0.04	0.03	0.04	0.02	0.04	0.02	0.06	0.03
Total	102.06	0.20	100.91	0.39	102.25	0.34	101.34	0.28	100.82	0.33	100.52	0.25	99.99	0.15
Si	2.996		3.000		3.002		2.985		2.990		2.990		2.971	
Al^{tet}	0.004		0.000		0.000		0.015		0.010		0.010		0.029	
Al^{oct}	1.998		1.997		1.994		1.977		1.983		1.981		1.979	
Ti	0.000		0.001		0.001		0.000		0.001		0.001		0.001	
Fe	2.059		2.187		2.377		2.248		2.118		2.046		1.997	
Mn	0.297		0.458		0.072		0.118		0.053		0.044		0.021	
Mg	0.557		0.294		0.462		0.542		0.754		0.823		0.920	
Ca	0.088		0.061		0.087		0.126		0.097		0.112		0.097	
Na	0.003		0.004		0.006		0.007		0.004		0.002		0.004	
K	0.000		0.001		0.001		0.001		0.001		0.001		0.002	
Cr	0.002		0.001		0.002		0.003		0.003		0.002		0.004	
X_{Fe}	0.79		0.88		0.84		0.81		0.74		0.71		0.68	
Almandine	68.58		72.90		79.27		73.64		69.76		67.26		65.05	
Pyrope	18.58		9.80		15.42		18.16		25.20		27.53		30.97	
Spessartine	9.91		15.28		2.40		3.97		1.78		1.47		0.71	
Grossular	2.83		1.93		2.79		3.14		2.51		2.92		2.33	
Andradite	0.00		0.02		0.02		0.95		0.61		0.70		0.76	
Uvarovite	0.09		0.07		0.10		0.14		0.14		0.12		0.18	

Orthopyroxene

Val Strona di Omegna, metapsammite/metagreywacke

(number of cations based on 6 O atoms)

Sample	IZ 120		IZ 129	
	n=20	sd	n=13	sd
SiO_2	51.25	0.29	51.62	0.29
TiO_2	0.08	0.04	0.09	0.04
Al_2O_3	1.93	0.42	1.81	0.14
FeO	25.09	1.15	24.18	0.65
MnO	0.51	0.09	0.31	0.06
MgO	20.23	0.83	20.99	0.49
CaO	0.34	0.08	0.46	0.04
Na_2O	0.02	0.02	0.02	0.01
K_2O	0.01	0.01	0.00	0.01
Cr_2O_3	0.08	0.04	0.09	0.04
Total	99.55	0.25	99.56	0.30
Si	1.945		1.948	
Al^{tet}	0.055		0.052	
Al^{oct}	0.031		0.028	
Ti	0.002		0.002	
Fe	0.796		0.763	
Mn	0.017		0.010	
Mg	1.144		1.181	
Ca	0.014		0.019	
Na	0.001		0.002	
K	0.001		0.000	
Cr	0.002		0.003	
Enst	41		39	
Ferro	59		60	
Wolla	1		1	

Cordierite

Val Strona di Omegna | Val Sesia | Val Strona di Postua

(number of cations based on 18 O atoms)

Sample	IZ 009		IZ 017		IZ 013		IZ 034		IZ 132		IZ 165		IZ 163	
	n=5	sd	n=2	sd	n=2	sd	n=3	sd	n=15	sd	n=10	sd	n=3	sd
SiO_2	47.66	0.28	49.14	0.37	48.56	0.18	42.25	0.47	48.40	0.20	48.37	0.19	41.98	1.77
TiO_2	0.00	0.00	0.03	0.04	0.01	0.01	0.01	0.01	0.01	0.02	0.02	0.03	0.02	0.01
Al_2O_3	32.67	0.16	33.47	0.06	33.23	0.04	28.68	0.22	32.29	0.20	32.46	0.16	30.24	0.35
FeO	8.14	0.14	4.46	0.15	6.93	0.14	6.98	1.15	6.15	0.29	6.19	0.25	6.86	0.92
MnO	0.63	0.03	0.11	0.01	0.35	0.04	0.08	0.02	0.05	0.03	0.04	0.03	0.01	0.01
MgO	7.64	0.11	10.45	0.01	9.07	0.05	7.35	0.60	9.80	0.18	9.63	0.17	6.23	0.92
CaO	0.03	0.02	0.02	0.01	0.02	0.00	0.02	0.01	0.02	0.02	0.01	0.01	0.54	0.05
sNa_2O	0.56	0.03	0.35	0.01	0.28	0.02	0.10	0.04	0.07	0.02	0.05	0.02	0.06	0.02
K_2O	0.02	0.01	0.01	0.01	0.01	0.02	8.99	0.61	0.01	0.01	0.00	0.01	1.64	0.93
Cr_2O_3	0.03	0.03	0.03	0.04	0.00	0.00	0.02	0.02	0.02	0.02	0.03	0.03	0.04	0.00
Total	97.39	0.29	98.06	0.29	98.45	0.21	94.48	0.38	96.82	0.32	96.79	0.44	87.62	1.38
Si	4.975		4.989		4.973		4.815		5.012		5.010		4.899	
Al	0.000		0.002		0.000		0.001		0.001		0.001		0.002	
Ti	4.019		4.005		4.010		3.851		3.941		3.961		4.160	
Fe	0.710		0.378		0.593		0.665		0.533		0.536		0.671	
Mn	0.055		0.010		0.031		0.008		0.004		0.004		0.001	
Mg	1.189		1.581		1.384		1.249		1.514		1.487		1.086	
Ca	0.004		0.002		0.002		0.003		0.003		0.001		0.068	
Na	0.114		0.069		0.056		0.021		0.014		0.009		0.014	
K	0.003		0.001		0.002		1.307		0.001		0.001		0.243	
Cr	0.003		0.002		0.000		0.002		0.001		0.002		0.003	
X_{Mg}	0.61		0.80		0.69		0.65		0.74		0.73		0.62	

Spinel

Val Strona d. Postua

(number of cations based on 4 O atoms)

Sample	IZ 132	
	n=7	sd
SiO_2	0.41	0.65
TiO_2	0.03	0.03
Al_2O_3	57.94	0.66
FeO	30.93	1.27
MnO	0.09	0.03
MgO	5.48	0.31
CaO	0.02	0.01
Na_2O	0.12	0.03
K_2O	0.01	0.01
Cr_2O_3	0.34	0.21
Total	95.37	0.62
Si	0.012	
Al	0.001	
Ti	1.980	
Fe	0.750	
Mn	0.002	
Mg	0.237	
Ca	0.000	
Na	0.007	
K	0.000	
Cr	0.008	
X_{Mg}	0.24	

Biotite Val Strona di Omegna, metapelite

(number of cations based on 11 O atoms)

Sample	IZ 008		IZ 009		IZ 079		IZ 010		IZ 011		IZ 015		IZ 016		IZ 017		IZ 018	
	n=15	sd	n=10	sd	n=5	sd	n=11	sd	n=16	sd	n=12	sd	n=4	sd	n=17	sd	n=9	sd
SiO_2	35.56	0.17	35.52	0.16	35.25	0.63	34.80	0.12	35.29	0.19	36.13	0.51	35.52	0.18	37.09	0.17	34.18	0.27
TiO_2	2.88	0.11	2.75	0.72	2.22	0.35	3.26	0.19	2.79	0.37	2.37	0.16	3.06	0.07	2.43	0.14	2.67	0.06
Al_2O_3	19.74	0.24	19.93	0.40	18.85	0.34	19.62	0.30	19.64	0.30	19.15	0.28	19.19	0.07	19.93	0.16	19.17	0.21
FeO	18.19	0.25	18.24	0.77	18.01	1.29	21.66	0.30	20.45	0.53	13.96	0.72	18.80	0.15	12.16	0.22	16.32	0.58
MnO	0.26	0.03	0.36	0.07	0.11	0.02	0.22	0.03	0.21	0.03	0.29	0.03	0.42	0.03	0.06	0.03	0.15	0.04
MgO	9.61	0.12	9.51	0.73	11.13	0.77	7.18	0.21	8.52	0.34	13.19	0.45	9.11	0.13	14.34	0.18	9.38	0.19
CaO	0.00	0.01	0.00	0.01	0.03	0.02	0.01	0.02	0.01	0.01	0.02	0.03	0.02	0.02	0.00	0.00	0.00	0.00
Na_2O	0.12	0.03	0.14	0.04	0.29	0.05	0.18	0.04	0.27	0.06	0.14	0.05	0.11	0.03	0.28	0.04	0.11	0.02
K_2O	9.06	0.09	8.99	0.08	8.36	0.47	9.41	0.12	8.93	0.12	9.04	0.52	8.78	0.15	9.03	0.11	8.99	0.13
Cr_2O_3	0.07	0.02	0.05	0.04	0.07	0.04	0.06	0.02	0.06	0.02	0.10	0.05	0.08	0.02	0.07	0.02	0.07	0.03
Total	95.51	0.22	95.51	0.26	94.33	0.64	96.41	0.30	96.17	0.37	94.40	0.76	95.09	0.17	95.38	0.25	91.06	0.55
Si	2.677		2.675		2.681		2.650		2.667		2.698		2.694		2.706		2.686	
Al^{tet}	1.323		1.325		1.319		1.350		1.333		1.302		1.306		1.294		1.314	
Al^{oct}	0.429		0.443		0.371		0.411		0.417		0.383		0.409		0.419		0.462	
Ti	0.163		0.156		0.127		0.187		0.159		0.133		0.175		0.133		0.158	
Fe	1.145		1.149		1.146		1.379		1.292		0.872		1.192		0.742		1.073	
Mn	0.017		0.023		0.007		0.014		0.014		0.018		0.027		0.004		0.010	
Mg	1.079		1.068		1.262		0.816		0.960		1.468		1.030		1.560		1.099	
Ca	0.000		0.000		0.002		0.001		0.000		0.001		0.002		0.000		0.000	
Na	0.017		0.021		0.042		0.026		0.040		0.021		0.016		0.039		0.017	
K	0.870		0.864		0.811		0.914		0.861		0.861		0.849		0.841		0.901	
Cr	0.004		0.003		0.004		0.003		0.004		0.006		0.005		0.004		0.004	
X_{Fe}	0.51		0.51		0.47		0.62		0.57		0.37		0.53		0.32		0.49	

Biotite

Val Strona di Omegna, metapelite

(number of cations based on 11 O atoms)

Sample	IZ 013		IZ 059		IZ 002		IV 019		IZ 029		IV 058		IZ 034		IV 020		IV 054	
	n=19	sd	n=2	sd	n=11	sd	n=4	sd	n=13	sd	n=4	sd	n=8	sd	n=8	sd	n=9	sd
SiO_2	36.18	0.28	31.65	0.25	34.28	0.24	34.74	0.15	35.86	0.35	36.10	0.52	35.62	0.12	35.62	0.22	34.93	0.50
TiO_2	1.99	0.32	2.26	0.57	2.98	0.27	3.01	0.23	2.61	0.19	2.85	0.28	4.18	0.22	4.30	0.29	4.72	0.42
Al_2O_3	19.98	0.34	19.02	0.91	19.65	0.22	18.93	0.12	19.94	0.43	20.17	0.71	18.74	0.25	18.27	0.29	17.85	0.53
FeO	16.71	0.41	24.00	0.13	21.42	0.38	18.00	0.31	17.73	0.78	17.11	0.97	18.97	0.39	18.94	0.56	18.14	1.04
MnO	0.12	0.03	0.26	0.01	0.19	0.03	0.21	0.05	0.20	0.04	0.15	0.04	0.02	0.02	0.04	0.02	0.05	0.02
MgO	11.69	0.26	8.87	0.03	7.39	0.34	9.63	0.10	10.00	0.14	9.64	0.90	9.23	0.16	9.35	0.29	9.92	0.62
CaO	0.00	0.01	0.35	0.37	0.00	0.01	0.00	0.00	0.02	0.02	0.05	0.04	0.01	0.02	0.01	0.03	0.01	0.03
Na_2O	0.37	0.05	0.04	0.04	0.18	0.02	0.14	0.05	0.23	0.05	0.14	0.03	0.15	0.04	0.11	0.05	0.09	0.04
K_2O	8.41	0.14	5.42	1.56	9.51	0.14	9.35	0.07	9.07	0.12	8.56	0.43	9.06	0.17	9.08	0.21	9.21	0.23
Cr_2O_3	0.06	0.03	0.04	0.00	0.05	0.03	0.04	0.03	0.06	0.04	0.07	0.04	0.05	0.02	0.08	0.02	0.08	0.02
Total	95.51	0.42	91.90	1.24	95.66	0.28	94.05	0.22	95.70	0.47	94.83	1.19	96.01	0.45	95.80	0.52	95.01	0.30
Si	2.690		2.528		2.633		2.668		2.686		2.708		2.679		2.687		2.657	
Al^{tet}	1.310		1.472		1.367		1.332		1.314		1.292		1.321		1.313		1.343	
Al^{oct}	0.441		0.318		0.412		0.382		0.446		0.491		0.339		0.311		0.258	
Ti	0.111		0.135		0.172		0.174		0.147		0.161		0.237		0.244		0.270	
Fe	1.038		1.603		1.376		1.156		1.110		1.073		1.193		1.195		1.154	
Mn	0.007		0.018		0.013		0.014		0.013		0.009		0.001		0.003		0.003	
Mg	1.295		1.056		0.847		1.103		1.117		1.078		1.034		1.051		1.126	
Ca	0.000		0.030		0.000		0.000		0.001		0.004		0.001		0.001		0.001	
Na	0.053		0.006		0.026		0.021		0.033		0.020		0.021		0.016		0.013	
K	0.798		0.552		0.932		0.916		0.866		0.819		0.869		0.874		0.894	
Cr	0.004		0.003		0.003		0.003		0.003		0.004		0.003		0.005		0.005	
X_{Fe}	0.44		0.60		0.62		0.51		0.50		0.50		0.54		0.53		0.51	

Biotite

Val Strona di Omegna, metapelite

metapsammite/metagreywacke

(number of cations based on 11 O atoms)

Sample	IV 052		IZ 066		IZ 085		IZ 156		IZ 005	IZ 070	IZ 120		IZ 129	
	n=12	sd	n=5	sd	n=3	sd	n=8	sd	n=1	n=1	n=3	sd	n=5	sd
SiO_2	35.81	0.23	36.28	0.19	36.99	0.09	36.11	0.77	37.85	37.84	37.08	0.12	36.76	0.27
TiO_2	4.82	0.28	5.03	0.54	5.28	0.76	5.86	0.68	5.41	5.60	6.56	0.25	6.57	0.20
Al_2O_3	17.62	0.29	17.18	0.25	16.20	0.07	15.94	0.60	14.95	14.82	14.46	0.22	13.65	0.13
FeO	18.21	0.51	16.16	0.24	12.93	0.29	13.92	0.70	8.55	9.86	11.78	0.68	12.63	0.31
MnO	0.03	0.03	0.06	0.03	0.03	0.02	0.02	0.02	0.04	0.05	0.04	0.02	0.03	0.02
MgO	10.35	0.36	12.15	0.38	14.87	0.59	13.30	0.46	17.9	17.31	14.86	0.30	14.40	0.20
CaO	0.00	0.00	0.01	0.01	0.01	0.01	0.02	0.02	0.02	0.00	0.01	0.03	0.01	0.02
Na_2O	0.10	0.03	0.09	0.04	0.15	0.06	0.10	0.03	0.17	0.18	0.11	0.04	0.10	0.02
K_2O	9.40	0.13	9.44	0.13	9.15	0.11	9.37	0.16	9.89	9.54	9.36	0.02	9.20	0.17
Cr_2O_3	0.07	0.03	0.09	0.04	0.12	0.03	0.16	0.05	0.21	0.08	0.15	0.07	0.17	0.04
Total	96.41	0.37	96.49	0.34	95.73	0.31	94.80	0.65	94.99	95.28	94.41	0.39	93.52	0.68
Si	2.682		2.689		2.718		2.702		2.760	2.761	2.758		2.774	
Al^{tet}	1.318		1.311		1.282		1.298		1.240	1.239	1.242		1.214	
Al^{oct}	0.237		0.190		0.121		0.108		0.045	0.035	0.026		0.000	
Ti	0.272		0.281		0.292		0.330		0.297	0.307	0.367		0.373	
Fe	1.140		1.001		0.795		0.871		0.521	0.602	0.733		0.797	
Mn	0.002		0.004		0.002		0.001		0.002	0.003	0.002		0.002	
Mg	1.156		1.343		1.629		1.484		1.946	1.883	1.648		1.620	
Ca	0.000		0.000		0.000		0.001		0.002	0.000	0.001		0.001	
Na	0.014		0.012		0.021		0.014		0.024	0.025	0.016		0.015	
K	0.898		0.892		0.858		0.894		0.920	0.888	0.888		0.886	
Cr	0.004		0.006		0.007		0.010		0.012	0.005	0.009		0.010	
X_{Fe}	0.50		0.43		0.33		0.37		0.21	0.24	0.31		0.33	

Biotite

Val Sesia, metapelite

Val Strona di Postua, metapelite

(number of cations based on 11 O atoms)

Sample	IV 034		IZ 114		IZ 168		IV 026		IZ 201		IZ 132		IZ 165		IZ 163
	n=14	sd	n=16	sd	n=10	sd	n=24	sd	n=14	sd	n=12	sd	n=11	sd	n=1
SiO_2	36.19	0.23	34.33	0.45	34.68	0.16	35.58	0.16	35.27	0.26	35.77	0.17	36.33	0.31	35.82
TiO_2	2.70	0.29	2.49	0.36	3.45	0.09	4.36	0.38	4.29	0.31	4.36	0.72	4.76	0.37	3.94
Al_2O_3	19.20	0.39	19.26	0.35	18.84	0.26	18.52	0.34	18.12	0.32	17.41	0.31	16.40	0.24	16.26
FeO	16.02	0.61	20.34	0.68	20.73	0.42	20.27	0.41	17.93	0.51	15.31	0.47	13.94	0.48	11.35
MnO	0.12	0.04	0.12	0.03	0.18	0.03	0.03	0.02	0.05	0.02	0.02	0.02	0.03	0.02	0.00
MgO	11.43	0.35	7.94	0.31	7.55	0.17	8.44	0.29	10.17	0.35	11.70	0.64	13.60	0.48	15.76
CaO	0.01	0.02	0.01	0.01	0.02	0.02	0.01	0.01	0.04	0.07	0.00	0.01	0.02	0.04	0.00
Na_2O	0.34	0.12	0.19	0.08	0.17	0.02	0.11	0.03	0.17	0.11	0.07	0.04	0.07	0.02	0.14
K_2O	9.15	0.18	8.51	0.36	9.08	0.43	9.51	0.11	9.73	0.09	9.45	0.16	9.52	0.11	9.37
Cr_2O_3	0.06	0.03	0.07	0.04	0.05	0.03	0.07	0.03	0.06	0.04	0.14	0.03	0.16	0.04	0.07
Total	95.22	0.34	93.25	0.58	94.75	0.50	96.89	0.31	95.82	0.44	94.24	0.40	94.82	0.38	92.71
Si	2.705		2.676		2.674		2.676		2.663		2.706		2.716		2.708
Al^{tet}	1.295		1.324		1.326		1.324		1.337		1.294		1.284		1.292
Al^{oct}	0.396		0.446		0.386		0.317		0.275		0.258		0.161		0.157
Ti	0.152		0.146		0.200		0.247		0.244		0.248		0.268		0.224
Fe	1.001		1.326		1.337		1.275		1.132		0.968		0.872		0.718
Mn	0.008		0.008		0.012		0.002		0.003		0.001		0.002		0.000
Mg	1.274		0.922		0.868		0.946		1.145		1.319		1.516		1.776
Ca	0.001		0.001		0.001		0.000		0.003		0.000		0.002		0.000
Na	0.049		0.029		0.026		0.016		0.025		0.011		0.010		0.021
K	0.872		0.846		0.893		0.913		0.937		0.912		0.908		0.904
Cr	0.004		0.004		0.003		0.004		0.004		0.009		0.009		0.004
X_{Fe}	0.44		0.59		0.60		0.57		0.50		0.42		0.36		0.29

Muscovite Val Strona di Omegna, metapelite

(number of cations based on 22 O atoms)

Sample	IZ 008		IZ 009		IZ 010		IZ 011		IZ 015		IZ 016		IZ 017		IZ 018		IZ 013	
	n=6	sd	n=6	sd	n=6	sd	n=14	sd	n=8	sd	n=8	sd	n=9	sd	n=6	sd	n=9	sd
SiO_2	45.42	0.24	45.44	0.24	45.25	0.20	45.70	0.23	45.25	0.25	45.59	0.30	45.82	0.15	43.79	0.31	45.65	0.13
TiO_2	0.96	0.16	0.53	0.47	1.15	0.16	0.59	0.35	1.38	0.23	1.46	0.19	1.32	0.21	0.84	0.06	0.79	0.39
Al_2O_3	35.77	0.36	35.63	0.24	35.79	0.24	36.07	0.31	34.78	0.45	35.17	0.44	35.06	0.27	35.06	0.31	36.13	0.37
FeO	0.90	0.09	0.99	0.12	1.01	0.13	0.93	0.07	0.84	0.10	0.95	0.15	0.72	0.06	0.85	0.08	0.82	0.15
MnO	0.01	0.01	0.02	0.02	0.02	0.01	0.02	0.02	0.01	0.01	0.03	0.02	0.01	0.01	0.02	0.02	0.02	0.02
MgO	0.58	0.09	0.73	0.11	0.48	0.04	0.55	0.08	0.90	0.08	0.62	0.10	0.87	0.04	0.64	0.05	0.55	0.09
CaO	0.01	0.01	0.02	0.03	0.00	0.01	0.01	0.01	0.00	0.01	0.01	0.01	0.00	0.01	0.00	0.00	0.00	0.01
Na_2O	0.46	0.03	0.50	0.05	0.58	0.04	1.03	0.08	0.47	0.04	0.36	0.03	0.80	0.04	0.38	0.02	1.49	0.12
K_2O	10.16	0.11	10.07	0.16	10.65	0.10	9.67	0.12	10.22	0.22	10.15	0.13	9.69	0.15	9.72	0.12	8.62	0.40
Cr_2O_3	0.06	0.03	0.04	0.05	0.04	0.03	0.04	0.04	0.08	0.04	0.07	0.03	0.06	0.03	0.04	0.03	0.06	0.04
Total	94.33	0.17	93.98	0.13	94.97	0.29	94.61	0.29	93.93	0.35	94.39	0.25	94.35	0.33	91.33	0.67	94.13	0.25
Si	3.043		3.056		3.026		3.049		3.050		3.054		3.063		3.027		3.045	
Al^{tet}	0.957		0.944		0.974		0.951		0.950		0.946		0.937		0.973		0.955	
Al^{oct}	1.868		1.880		1.847		1.885		1.813		1.831		1.825		1.883		1.886	
Ti	0.048		0.027		0.058		0.029		0.070		0.074		0.066		0.044		0.039	
Fe	0.050		0.056		0.057		0.052		0.047		0.053		0.040		0.049		0.046	
Mn	0.000		0.001		0.001		0.001		0.000		0.001		0.000		0.001		0.001	
Mg	0.058		0.073		0.048		0.054		0.090		0.062		0.087		0.066		0.055	
Ca	0.000		0.001		0.000		0.000		0.000		0.000		0.000		0.000		0.000	
Na	0.060		0.065		0.075		0.134		0.061		0.046		0.104		0.050		0.192	
K	0.869		0.864		0.908		0.823		0.879		0.867		0.826		0.857		0.734	
Cr	0.003		0.002		0.002		0.002		0.005		0.004		0.003		0.002		0.003	
X_{Na}	0.06		0.07		0.08		0.14		0.06		0.05		0.11		0.06		0.21	

Muscovite

Val Strona di Omegna, metapelite

Val Sesia

(number of cations based on 22 O atoms)

Sample	IZ 059		IZ 002		IV 019		IZ 029		IV 058	IV 044	IZ 070	IZ 114	IZ 168		IV 026
	n=7	sd	n=14	sd	n=7	sd	n=7	sd	n=1	n=1	n=1	n=1	n=5	sd	n=1
SiO_2	44.57	0.24	45.05	0.37	44.25	0.29	45.79	0.20	45.89	48.23	48.50	45.32	45.05	0.10	47.21
TiO_2	0.98	0.08	0.63	0.26	1.02	0.15	0.80	0.11	0.13	0.06	0.11	0.25	0.95	0.13	0.10
Al_2O_3	34.49	0.20	35.42	0.54	33.84	0.33	35.19	0.17	35.56	29.69	30.17	35.64	34.75	0.15	35.02
FeO	1.50	0.05	1.26	0.08	1.24	0.26	1.18	0.05	1.07	3.01	1.83	1.08	1.22	0.07	1.22
MnO	0.02	0.01	0.02	0.02	0.01	0.01	0.02	0.01	0.01	0.02	0.00	0.04	0.03	0.02	0.04
MgO	0.75	0.04	0.51	0.07	0.84	0.15	0.76	0.06	0.78	2.70	1.87	0.47	0.49	0.04	0.52
CaO	0.02	0.02	0.01	0.01	0.00	0.01	0.01	0.01	0.01	0.19	0.12	0.00	0.00	0.01	0.00
Na_2O	0.39	0.03	0.55	0.06	0.38	0.04	0.48	0.04	0.40	0.10	0.17	0.83	0.64	0.06	0.32
K_2O	10.85	0.16	10.53	0.28	10.33	0.16	10.22	0.16	10.13	10.01	10.28	9.74	10.04	0.19	9.62
Cr_2O_3	0.02	0.02	0.06	0.03	0.04	0.05	0.06	0.03	0.03	0.02	0.02	0.05	0.04	0.06	0.01
Total	93.58	0.35	94.05	0.55	91.94	0.45	94.52	0.28	94.00	94.03	93.07	93.41	93.21	0.25	94.07
Si	3.039		3.043		3.059		3.067		3.082	3.269	3.299	3.064	3.063		3.152
Al^{tet}	0.961		0.957		0.941		0.933		0.918	0.731	0.701	0.936	0.937		0.848
Al^{oct}	1.811		1.863		1.815		1.845		1.896	1.640	1.718	1.903	1.847		1.907
Ti	0.050		0.032		0.053		0.040		0.007	0.003	0.006	0.013	0.049		0.005
Fe	0.085		0.071		0.072		0.066		0.060	0.171	0.104	0.061	0.069		0.068
Mn	0.001		0.001		0.001		0.001		0.000	0.001	0.000	0.002	0.001		0.002
Mg	0.076		0.051		0.086		0.076		0.078	0.273	0.190	0.047	0.049		0.052
Ca	0.001		0.001		0.000		0.000		0.001	0.014	0.009	0.000	0.000		0.000
Na	0.052		0.072		0.050		0.063		0.052	0.013	0.022	0.108	0.084		0.042
K	0.944		0.907		0.910		0.873		0.868	0.865	0.892	0.840	0.871		0.819
Cr	0.001		0.003		0.002		0.003		0.001	0.001	0.001	0.002	0.002		0.001
X_{Na}	0.05		0.07		0.05		0.07		0.06	0.02	0.02	0.11	0.09		0.05

K-feldspar Val Strona di Omegna, metapelite

(number of cations based on 8 O atoms)

Sample	IZ 009		IZ 018		IZ 059		IV 019		IZ 029		IZ 034		IV 020		IV 052		IZ 066
	n=2	sd	n=5	sd	n=3	sd	n=6	sd	n=6	sd	n=3	sd	n=7	sd	n=4	sd	n=1
SiO_2	63.78	0.34	61.27	0.30	62.32	0.31	63.62	0.30	63.83	0.14	64.08	0.36	64.29	0.18	64.24	0.32	63.43
TiO_2	0.03	0.04	0.00	0.01	0.00	0.00	0.00	0.00	0.02	0.02	0.04	0.04	0.02	0.02	0.02	0.01	0.03
Al_2O_3	18.72	0.01	18.32	0.08	18.40	0.20	18.46	0.11	18.55	0.10	18.95	0.14	18.74	0.13	18.73	0.05	18.56
FeO	0.00	0.00	0.01	0.01	0.04	0.04	0.02	0.01	0.02	0.03	0.04	0.02	0.02	0.02	0.05	0.08	0.05
MnO	0.01	0.02	0.00	0.01	0.01	0.02	0.00	0.00	0.01	0.02	0.03	0.03	0.02	0.01	0.01	0.01	0.01
MgO	0.01	0.01	0.01	0.01	0.00	0.00	0.01	0.01	0.01	0.01	0.00	0.00	0.01	0.01	0.00	0.01	0.00
CaO	0.01	0.01	0.03	0.02	0.03	0.01	0.03	0.01	0.04	0.02	0.03	0.03	0.06	0.03	0.04	0.03	0.08
Na_2O	1.49	0.18	1.37	0.05	0.75	0.32	0.92	0.18	0.91	0.36	1.84	1.11	1.60	0.71	1.21	0.14	1.23
K_2O	13.44	0.14	13.31	0.11	15.44	0.58	14.99	0.27	14.56	0.51	13.27	1.32	13.59	0.88	14.36	0.11	14.46
Cr_2O_3	0.04	0.01	0.03	0.02	0.01	0.01	0.00	0.00	0.02	0.02	0.02	0.04	0.04	0.02	0.03	0.02	0.00
Total	97.53	0.34	94.37	0.36	96.99	0.40	98.52	0.35	97.98	0.31	98.31	0.34	98.38	0.13	98.68	0.27	97.85
Si	2.987		2.973		2.971		2.987		2.990		2.979		2.989		2.987		2.980
Al	0.001		0.000		0.000		0.000		0.001		0.002		0.001		0.001		0.001
Ti	1.033		1.048		1.034		1.022		1.024		1.038		1.026		1.026		1.028
Fe	0.000		0.001		0.002		0.001		0.001		0.001		0.001		0.002		0.002
Mn	0.000		0.000		0.000		0.000		0.001		0.001		0.001		0.000		0.000
Mg	0.001		0.000		0.000		0.001		0.000		0.000		0.001		0.000		0.000
Ca	0.000		0.002		0.001		0.002		0.002		0.002		0.003		0.002		0.004
Na	0.135		0.129		0.069		0.083		0.083		0.166		0.144		0.109		0.112
K	0.803		0.824		0.939		0.898		0.870		0.787		0.806		0.852		0.867
Cr	0.002		0.001		0.000		0.000		0.001		0.001		0.001		0.001		0.000
Ab	14		14		7		8		9		17		15		11		11
An	0		0		0		0		0		0		0		0		0
Or	86		86		93		91		91		83		85		88		88

K-feldspar

Val Strona di Omegna, metapelite | Val Sesia | Val Strona di Postua

(number of cations based on 8 O atoms)

Sample	IZ 085		IV 044		IZ 005		IZ 070		IZ 048		IZ 102	IV 026		IZ 165		IZ 163	
	n=6	sd	n=3	sd	n=6	sd	n=8	sd	n=8	sd	n=1	n=5	sd	n=3	sd	n=4	sd
SiO_2	63.80	0.24	64.14	0.38	63.56	0.22	63.47	0.23	64.14	0.49	62.98	64.27	0.42	63.31	0.16	62.98	0.32
TiO_2	0.04	0.03	0.03	0.01	0.04	0.03	0.03	0.03	0.04	0.02	0.00	0.02	0.02	0.02	0.03	0.02	0.02
Al_2O_3	18.72	0.09	18.49	0.27	18.60	0.13	18.31	0.07	18.75	0.19	17.92	18.83	0.04	18.30	0.16	17.86	0.11
FeO	0.02	0.02	0.03	0.03	0.03	0.03	0.02	0.01	0.03	0.04	0.08	0.03	0.02	0.05	0.04	0.07	0.06
MnO	0.01	0.01	0.00	0.00	0.01	0.02	0.01	0.01	0.01	0.01	0.00	0.01	0.01	0.00	0.00	0.02	0.01
MgO	0.00	0.01	0.00	0.00	0.00	0.01	0.01	0.01	0.01	0.01	0.03	0.01	0.02	0.01	0.01	0.01	0.01
CaO	0.06	0.04	0.15	0.05	0.16	0.07	0.03	0.02	0.18	0.11	0.00	0.03	0.02	0.06	0.02	0.16	0.12
Na_2O	1.03	0.36	1.12	0.29	1.22	0.18	0.83	0.27	1.35	0.40	1.48	0.96	0.11	0.96	0.12	1.03	0.26
K_2O	14.30	0.31	14.92	0.35	14.79	0.23	15.53	0.40	13.95	0.69	13.54	14.90	0.23	14.68	0.06	14.55	0.52
Cr_2O_3	0.03	0.02	0.04	0.03	0.04	0.04	0.03	0.02	0.02	0.02	0.00	0.03	0.02	0.05	0.04	0.02	0.02
Total	97.99	0.38	98.92	0.53	98.45	0.39	98.26	0.16	98.48	0.30	96.02	99.09	0.45	97.44	0.16	96.72	0.36
Si	2.985		2.986		2.975		2.984		2.984		3.002	2.982		2.988		2.997	
Al	0.002		0.001		0.001		0.001		0.001		0.000	0.001		0.001		0.001	
Ti	1.032		1.014		1.026		1.014		1.028		1.007	1.030		1.018		1.002	
Fe	0.001		0.001		0.001		0.001		0.001		0.003	0.001		0.002		0.003	
Mn	0.000		0.000		0.001		0.000		0.000		0.000	0.000		0.000		0.001	
Mg	0.000		0.000		0.000		0.001		0.001		0.002	0.001		0.001		0.000	
Ca	0.003		0.008		0.008		0.001		0.009		0.000	0.002		0.003		0.008	
Na	0.093		0.101		0.111		0.075		0.122		0.137	0.087		0.088		0.095	
K	0.853		0.886		0.883		0.931		0.828		0.823	0.882		0.884		0.883	
Cr	0.001		0.001		0.002		0.001		0.001		0.000	0.001		0.002		0.001	
Ab	10		10		11		7		13		14	9		9		10	
An	0		1		1		0		1		0	0		0		1	
Or	90		89		88		92		86		86	91		91		89	

Plagioclase

Val Strona di Omegna, metapelite

(number of cations based on 8 O atoms)

Sample	IZ 008		IZ 009		IZ 079		IZ 010		IZ 011		IZ 015		IZ 016		IZ 017		IZ 018	
	n=17	sd	n=11	sd	n=5	sd	n=7	sd	n=18	sd	n=5	sd	n=8	sd	n=14	sd	n=6	sd
SiO_2	62.03	0.35	60.24	0.59	58.36	0.29	64.52	0.65	63.36	0.45	61.33	0.25	56.25	0.71	59.48	0.74	58.39	0.42
TiO_2	0.01	0.01	0.00	0.01	0.01	0.01	0.00	0.01	0.01	0.01	0.01	0.02	0.01	0.02	0.01	0.01	0.00	0.01
Al_2O_3	23.68	0.29	24.84	0.33	25.36	0.19	21.90	0.46	22.81	0.25	23.86	0.27	27.60	0.51	25.38	0.55	23.68	0.29
FeO	0.03	0.03	0.03	0.04	0.12	0.07	0.01	0.01	0.02	0.03	0.06	0.07	0.02	0.02	0.02	0.02	0.04	0.05
MnO	0.01	0.02	0.01	0.02	0.01	0.02	0.01	0.01	0.01	0.01	0.03	0.03	0.02	0.02	0.01	0.01	0.02	0.02
MgO	0.00	0.00	0.00	0.01	0.00	0.00	0.00	0.01	0.00	0.01	0.00	0.00	0.00	0.01	0.00	0.01	0.00	0.01
CaO	4.90	0.29	6.38	0.44	7.34	0.17	2.66	0.31	3.76	0.35	5.17	0.26	9.61	0.61	6.90	0.66	5.36	0.34
Na_2O	8.85	0.20	7.99	0.22	7.36	0.19	10.20	0.19	9.56	0.26	8.64	0.13	6.11	0.39	7.71	0.37	8.25	0.25
K_2O	0.17	0.03	0.17	0.02	0.06	0.02	0.13	0.04	0.11	0.03	0.20	0.02	0.12	0.02	0.07	0.03	0.19	0.05
Cr_2O_3	0.03	0.02	0.03	0.02	0.05	0.01	0.02	0.02	0.02	0.02	0.03	0.03	0.01	0.01	0.03	0.02	0.01	0.01
Total	99.72	0.20	99.70	0.19	98.67	0.13	99.45	0.18	99.65	0.30	99.31	0.69	99.75	0.37	99.63	0.27	95.94	0.70
Si	2.758		2.690		2.641		2.858		2.809		2.741		2.533		2.661		2.707	
Al	0.000		0.000		0.000		0.000		0.000		0.000		0.000		0.000		0.000	
Ti	1.241		1.307		1.353		1.143		1.192		1.257		1.465		1.338		1.294	
Fe	0.001		0.001		0.004		0.000		0.001		0.002		0.001		0.001		0.001	
Mn	0.000		0.000		0.000		0.000		0.000		0.001		0.001		0.000		0.001	
Mg	0.000		0.000		0.000		0.000		0.000		0.000		0.000		0.000		0.000	
Ca	0.234		0.305		0.356		0.126		0.179		0.247		0.463		0.331		0.266	
Na	0.763		0.692		0.646		0.876		0.822		0.749		0.533		0.669		0.742	
K	0.010		0.010		0.004		0.007		0.006		0.011		0.007		0.004		0.011	
Cr	0.001		0.001		0.002		0.001		0.001		0.001		0.000		0.001		0.000	
Ab	76		69		64		87		82		74		53		67		73	
An	23		30		35		13		18		25		46		33		26	
Or	1		1		0		1		1		1		1		0		1	

Plagioclase

Val Strona di Omegna, metapelite

(number of cations based on 8 O atoms)

Sample	IZ 013		IV 059		IZ 002		IZ 029	IV 058		IZ 034		IV 020		IV 054		IV 052	
	n=11	sd	n=4	sd	n=11	sd	n=1	n=8	sd	n=5	sd	n=2	sd	n=5	sd	n=5	sd
SiO_2	63.09	0.24	60.04	0.09	62.30	0.74	58.17	60.87	0.43	62.03	0.44	58.09	0.04	55.79	0.37	56.89	0.40
TiO_2	0.01	0.01	0.00	0.01	0.01	0.02	0.04	0.01	0.02	0.01	0.03	0.00	0.00	0.00	0.00	0.00	0.01
Al_2O_3	22.93	0.14	23.81	0.10	22.79	0.35	25.96	24.38	0.25	23.67	0.19	26.08	0.22	26.73	0.34	26.95	0.27
FeO	0.05	0.06	0.03	0.02	0.04	0.04	0.00	0.03	0.03	0.02	0.02	0.03	0.01	0.08	0.06	0.02	0.02
MnO	0.02	0.02	0.02	0.02	0.02	0.01	0.01	0.02	0.01	0.01	0.02	0.00	0.00	0.04	0.01	0.01	0.01
MgO	0.01	0.01	0.01	0.02	0.00	0.01	0.00	0.00	0.01	0.00	0.01	0.00	0.00	0.01	0.01	0.00	0.00
CaO	3.94	0.11	5.26	0.12	3.98	0.43	7.81	5.49	0.26	4.76	0.24	7.50	0.18	8.93	0.34	9.06	0.33
Na_2O	9.46	0.09	8.63	0.14	9.26	0.19	7.21	8.22	0.18	8.76	0.17	7.03	0.02	6.26	0.20	6.45	0.25
K_2O	0.09	0.03	0.24	0.03	0.21	0.06	0.09	0.19	0.03	0.21	0.05	0.27	0.06	0.18	0.02	0.14	0.04
Cr_2O_3	0.02	0.02	0.03	0.02	0.02	0.01	0.03	0.02	0.03	0.03	0.02	0.05	0.00	0.01	0.01	0.03	0.02
Total	99.59	0.26	98.06	0.06	98.65	0.39	99.32	99.24	0.23	99.51	0.25	99.02	0.34	98.02	0.26	99.56	0.29
Si	2.800		2.723		2.794		2.618	2.722		2.761		2.620		2.555		2.563	
Al	0.000		0.000		0.000		0.001	0.000		0.000		0.000		0.000		0.000	
Ti	1.199		1.272		1.205		1.377	1.285		1.242		1.386		1.442		1.431	
Fe	0.002		0.001		0.002		0.000	0.001		0.001		0.001		0.003		0.001	
Mn	0.001		0.001		0.001		0.000	0.001		0.001		0.000		0.001		0.000	
Mg	0.000		0.001		0.000		0.000	0.000		0.000		0.000		0.000		0.000	
Ca	0.187		0.255		0.191		0.377	0.263		0.227		0.362		0.438		0.437	
Na	0.814		0.759		0.806		0.629	0.713		0.756		0.614		0.556		0.564	
K	0.005		0.014		0.012		0.005	0.011		0.012		0.015		0.011		0.008	
Cr	0.001		0.001		0.001		0.001	0.001		0.001		0.002		0.001		0.001	
Ab	81		74		80		62	72		76		62		55		56	
An	19		25		19		37	27		23		37		44		43	
Or	0		1		1		1	1		1		2		1		1	

Plagioclase

Val Strona di Omegna, metapelite

metapsammite/ metagreywacke

(number of cations based on 8 O atoms)

Sample	IZ 066		IZ 085		IZ 156		IV 044		IZ 005	IZ 048		IZ 102		IZ 120		IZ 129	
	n=12	sd	n=8	sd	n=10	sd	n=27	sd	n=1	n=8	sd	n=6	sd	n=21	sd	n=10	sd
SiO_2	54.87	0.52	57.06	0.41	58.86	0.53	58.46	0.28	57.88	60.86	0.38	59.78	0.43	47.70	0.98	54.58	0.65
TiO_2	0.01	0.02	0.02	0.03	0.00	0.01	0.01	0.01	0.00	0.02	0.01	0.00	0.01	0.00	0.01	0.01	0.02
Al_2O_3	28.19	0.29	27.01	0.23	24.77	0.35	26.04	0.21	25.51	24.41	0.36	23.58	0.30	31.78	0.64	27.07	0.48
FeO	0.03	0.03	0.06	0.08	0.07	0.06	0.03	0.02	0.06	0.01	0.02	0.02	0.02	0.13	0.08	0.08	0.02
MnO	0.02	0.03	0.02	0.02	0.01	0.01	0.02	0.02	0.01	0.01	0.02	0.01	0.01	0.01	0.02	0.01	0.01
MgO	0.00	0.01	0.00	0.00	0.01	0.01	0.00	0.00	0.00	0.00	0.01	0.00	0.01	0.01	0.01	0.01	0.01
CaO	10.52	0.34	8.62	0.23	7.00	0.44	8.22	0.22	7.70	5.92	0.34	6.01	0.17	15.95	0.79	10.43	0.42
Na_2O	5.56	0.21	6.40	0.12	7.45	0.17	7.07	0.14	7.07	8.20	0.24	8.07	0.06	2.35	0.45	5.45	0.31
K_2O	0.15	0.04	0.16	0.06	0.19	0.23	0.23	0.05	0.22	0.13	0.07	0.15	0.02	0.06	0.02	0.25	0.04
Cr_2O_3	0.03	0.03	0.02	0.02	0.03	0.03	0.02	0.02	0.02	0.04	0.02	0.02	0.01	0.02	0.03	0.02	0.02
Total	99.38	0.43	99.39	0.13	98.39	0.41	100.09	0.27	98.48	99.61	0.36	97.64	0.49	98.01	0.35	97.91	0.26
Si	2.488		2.571		2.668		2.615		2.628	2.715		2.723		2.230		2.513	
Al	0.000		0.001		0.000		0.000		0.000	0.001		0.000		0.000		0.001	
Ti	1.506		1.434		1.323		1.373		1.365	1.283		1.266		1.751		1.469	
Fe	0.001		0.002		0.003		0.001		0.002	0.001		0.001		0.005		0.003	
Mn	0.001		0.001		0.000		0.001		0.000	0.000		0.000		0.001		0.001	
Mg	0.000		0.000		0.001		0.000		0.000	0.000		0.000		0.000		0.001	
Ca	0.511		0.416		0.340		0.394		0.375	0.283		0.293		0.799		0.514	
Na	0.488		0.559		0.655		0.613		0.622	0.709		0.713		0.213		0.486	
K	0.009		0.009		0.011		0.013		0.013	0.007		0.009		0.003		0.015	
Cr	0.001		0.001		0.001		0.001		0.001	0.001		0.001		0.001		0.001	
Ab	48		57		65		60		62	71		70		21		48	
An	51		42		34		39		37	28		29		79		51	
Or	1		1		1		1		1	1		1		1		1	

Plagioclase

Val Sesia, metapelite

Val Strona di Postua, metapelite

(number of cations based on 8 O atoms)

Sample	IV 034		IZ 114	IZ 168	IV 026		IZ 201		IZ 132		IZ 165		IZ 163	
	n=9	sd	n=1	n=1	n=5	sd	n=26	sd	n=24	sd	n=15	sd	n=13	sd
SiO_2	61.75	0.32	59.22	63.54	61.58	0.31	57.84	1.11	58.32	0.25	57.30	0.36	57.82	0.37
TiO_2	0.00	0.01	0.00	0.00	0.01	0.01	0.01	0.02	0.02	0.02	0.01	0.02	0.01	0.01
Al_2O_3	23.81	0.16	23.04	21.79	24.13	0.21	25.70	0.72	24.82	0.29	25.91	0.22	24.90	0.22
FeO	0.03	0.03	1.40	0.05	0.02	0.02	0.04	0.04	0.03	0.03	0.04	0.03	0.03	0.02
MnO	0.02	0.03	0.06	0.05	0.01	0.01	0.02	0.01	0.01	0.01	0.01	0.02	0.01	0.01
MgO	0.00	0.01	0.02	0.01	0.00	0.01	0.00	0.01	0.00	0.01	0.01	0.01	0.01	0.01
CaO	5.35	0.09	4.25	3.23	5.73	0.08	7.79	0.81	7.37	0.19	8.15	0.18	7.53	0.15
Na_2O	8.81	0.14	7.91	9.97	8.37	0.20	7.16	0.47	7.17	0.18	6.76	0.14	7.02	0.14
K_2O	0.12	0.02	0.38	0.12	0.21	0.02	0.20	0.06	0.28	0.05	0.27	0.07	0.31	0.05
Cr_2O_3	0.02	0.03	0.00	0.00	0.05	0.02	0.02	0.03	0.03	0.03	0.03	0.03	0.03	0.03
Total	99.93	0.34	96.27	98.76	100.12	0.26	98.79	0.45	98.05	0.38	98.48	0.33	97.66	0.41
Si	2.744		2.740	2.841	2.732		2.62		2.656		2.605		2.646	
Al	0.000		0.000	0.000	0.000		0.00		0.001		0.000		0.000	
Ti	1.247		1.257	1.148	1.262		1.37		1.332		1.388		1.343	
Fe	0.001		0.054	0.002	0.001		0.00		0.001		0.001		0.001	
Mn	0.001		0.002	0.002	0.000		0.00		0.000		0.000		0.000	
Mg	0.000		0.001	0.001	0.000		0.00		0.000		0.000		0.000	
Ca	0.255		0.211	0.155	0.273		0.38		0.360		0.397		0.369	
Na	0.759		0.710	0.864	0.720		0.63		0.633		0.596		0.623	
K	0.007		0.022	0.007	0.012		0.01		0.016		0.015		0.018	
Cr	0.001		0.000	0.000	0.002		0.00		0.001		0.001		0.001	
Ab	74		75	84	72		62		63		59		62	
An	25		22	15	27		37		36		39		37	
Or	1		2	1	1		1		2		2		2	

Appendix C

THERMOCALC

- *P–T* pseudosections for IV 058, IZ 114, IZ 168 (high LOI contents)
- Example file ‘tc-IZ 010’ (*P–T* pseudosection)
- Example file ‘dr-IZ 005’ (*P–T* pseudosection)
- Activity-composition models in the system NCKFMASHTO

P–T pseudosections for IV 058, IZ 114, IZ 168 (high LOI contents)

Sample IV 058 is the first sample of the transition zone, located west of Massiola and preserves the assemblage g-sill-bi-pl-q-ilm-*liq*. This sample has an unrealistically high LOI content (14.57 mol%) and does not contain K-feldspar, which would be assumed in the transition zone based on the muscovite-out/K-feldspar-in isograd. Also the amount of 30 % to almost 60 % melt is very unusual at these *P–T* conditions. The solidus is to find at around 650 °C. The assemblage field is present from 710 to 820 °C and 6.1 to 9.2 kbar. Based on the high LOI content a wide field for coexisting H_2O and *liquid* results.

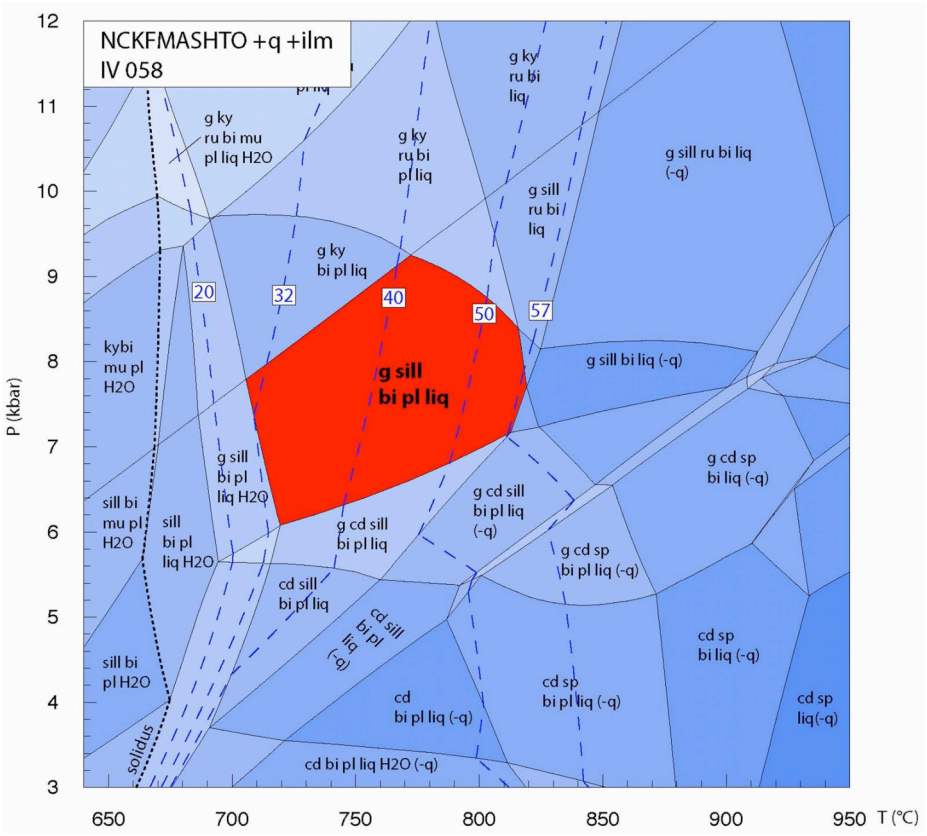

Sample IZ 114 is located southwest of Civiasco and is near the CMB Line. It contains the assemblage g-sill-bi-pl-q-ilm and preserves an unrealistic high LOI content (10.21 mol%), resulting in a wide field for coexisting *liquid* and H_2O. Three assemblage fields are highlighted because it is not clear of this rock contains H_2O, *liquid* or both. The pressures vary between ~ 4.5–8.3 kbar with temperatures from ~ 640 to 760 °C. A rock with this assemblage could be able to produce an amount of > 40 % melt under temperatures more than 850 °C. At around 670 °C the solidus is present.

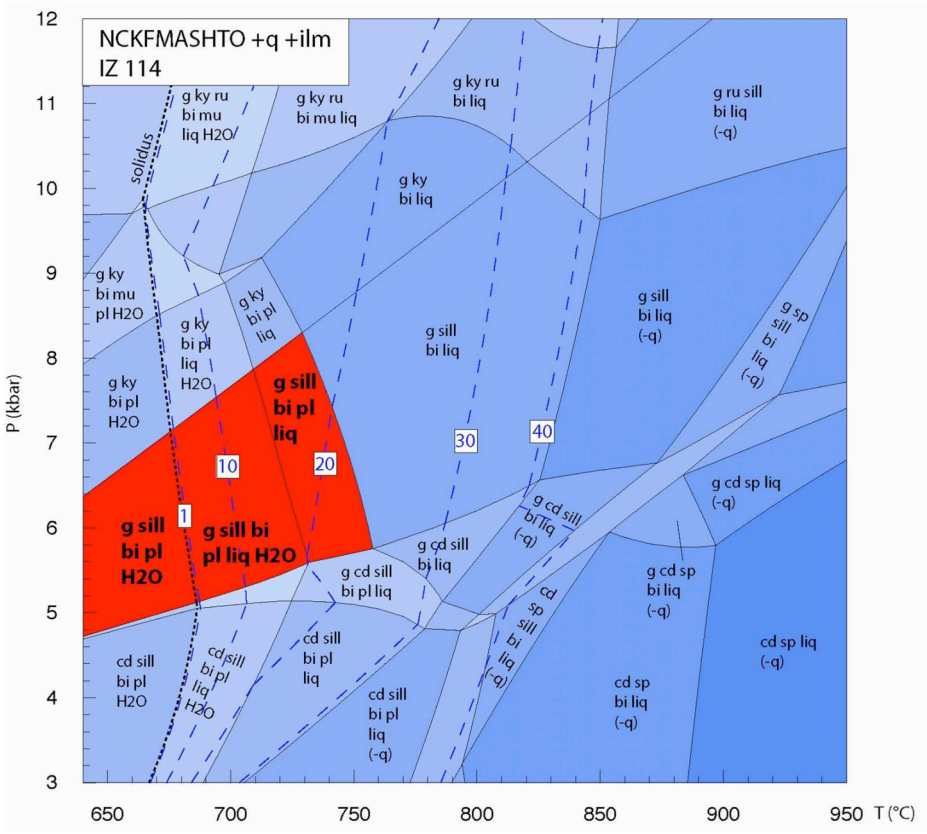

Sample IZ 168 is located in a small valley perpendicular to the main Sesia valley around 3 km north (air-line distance) of Civiasco. The preserved metamorphic assemblage contains g-sill-bi-pl-q-ilm-*liq*. The LOI content is unrealistically high (7.9 mol%), which results in a wide field for coexisting *liquid* and H_2O. Based on the resulted narrow field, temperatures are around 735 °C with pressures from 5.4 to 8.3 kbar. This assemblage contains around 10 % *liquid*. Under higher grade conditions an amount of 30 % *liquid* can resulted from partial melting The solidus occurs at around 650 °C.

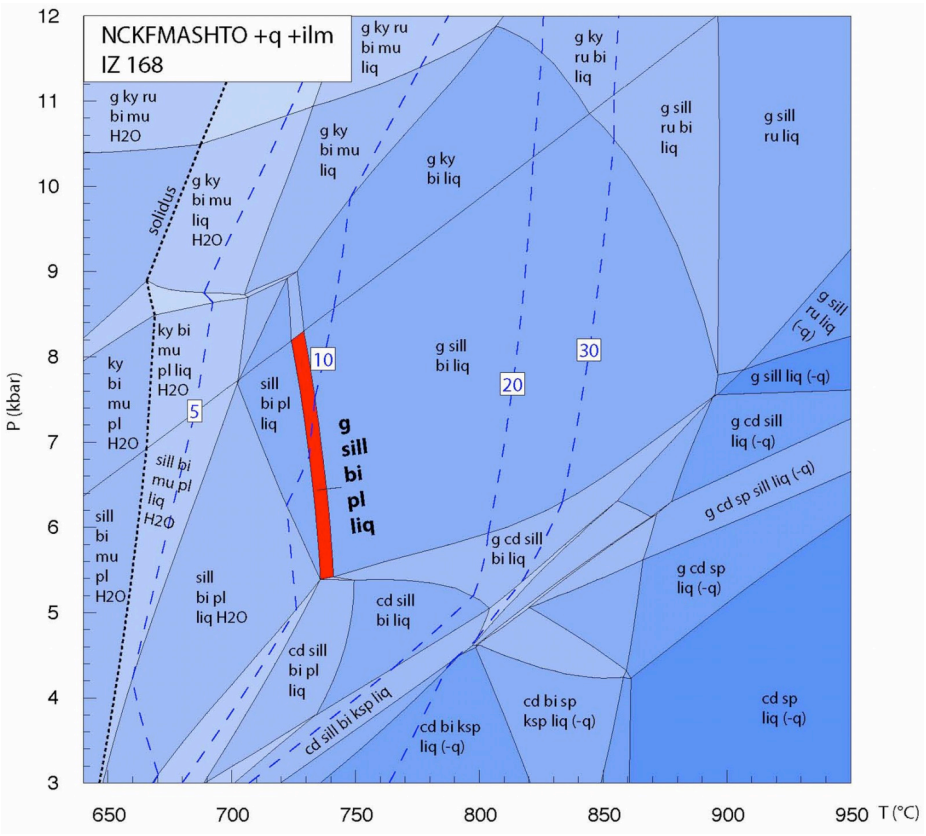

Example file ‘tc-IZ 010’

(*P–T* pseudosection)

```
axfile NCKFMASHTOp                  % this tells THERMOCALC, which a-x file to use

infolevel 1                         % this controls the type of info that is produced

ignore                              % tells THERMOCALC which minerals in the as file
                                    % can be automatically ignored

printxyz yes                        % prints the compositions variables in the tc-log
                                    % file in format where they can be pasted in
                                    % this files and used as starting guesses

printbulkinfo yes                   % outputs the modes and minerals compositions
                                    % into a matrix that can be used as a bulk rock
                                    % composition

incax no                            % whether or not to print the a-x models used in
                                    % the tc-log file

fluidpresent yes                    % whether fluid may be present

fluidexcess no                      % whether fluid is in excess

setexcess                           % allows to set any phases to excess

calctatp ask                        % whether to set P´s and calc T´s or vice versa
                                    % at each run, or always set P´s and T´s

setdefTwindow yes  400.001 1000.001     % default T window, allows just
                                        % to hit return when promoted
                                        % for T window

setdefPwindow yes  2 14                 % default P window, allows just
                                        % to hit return when promoted
                                        % for P window

project no                          % whether to do a compatibility projection

seta no                             % whether to set any activities

setiso no                           % whether to set any composition variables

pseudosection yes                   % whether to calculate a pseudosection
```

```
% ---------------------------------
% Bulk rock from IZ 010 (CaO adjustment for P2O5 -0.23 apatite)
% ---------------------------------
%              H2O   SiO2   Al2O3   CaO   MgO   FeO   K2O   Na2O   TiO2   O
setbulk yes  4.33   74.25   9.37    0.38   2.53   4.54   2.00   1.57    0.65   0.1
% ------------------------------
```

```
setmodeiso yes                  % whether to set any modes for boundaries and
                                % contours

zeromodeiso yes                 % whether to set zero modes for field boundaries

calcsdnle no                    % whether to calc uncertainties on each equilibria

smath no                        % whether to format the output file for
                                % mathematica

drawpd yes                      % whether to format the output file for drawpd
```

Example file ‘dr-IZ 005’

(*P–T* pseudosection)

```
2    % no of variables in each line of data, in this case, P, T and V
6    % 8 (NCKFMASH) - 2 (+q+pl) = 6
2 1  % which columns to be x,y in phase diagram
% _____________________________________________
% POINTS
% ------------------------------
i1   liq g ksp pl ilm sill q  - bi cd
7.29 870.8  % bi = 0cd = 0

% ------------------------------
i2   bi g ksp pl ilm sill q  - liq cd
6.40 823.1  % liq = 0cd = 0

% ------------------------------
i3   cd g ksp pl ilm sill q  - liq bi
5.61 798.9  % liq = 0bi = 0

% ------------------------------
i4   cd g ksp pl ilm q  - liq sill
5.56 804.4  % liq = 0sill = 0

% ------------------------------
i5   cd g ksp pl ilm q  - bi sill
5.44 789.5  % bi = 0sill = 0

          .
          .
          .

% ------------------------------
i17   liq g ksp ilm sill ru q  - pl ky
11.96 893.9  % pl = 0ky = 0

% ------------------------------
i18  bi g ksp pl ilm sill ru q  - liq ky
10.29 819.4  % liq = 0ky = 0

% ------------------------------
i19   bi g ksp pl ilm sill q  - liq ru
9.92 821.8  % liq = 0ru = 0

% ------------------------------
i20   bi g ksp pl ilm sill q  - ru ky
```

```
9.68 791.6  % ru = 0ky = 0


% LINES
% --------------------------------
u1  liq cd g ksp pl ilm sill q  - bi
i3  i14
5.80 806.0  % bi = 0
6.00 813.6  % bi = 0
6.20 821.5  % bi = 0
6.40 829.8  % bi = 0
6.60 838.4  % bi = 0
6.80 847.4  % bi = 0
7.00 856.8  % bi = 0
7.20 866.5  % bi = 0

% --------------------------------
u2  liq bi g ksp pl ilm sill q  - cd
i2  i13
6.60 832.8  % cd = 0
6.80 843.1  % cd = 0
7.00 854.0  % cd = 0
7.20 865.5  % cd = 0

% --------------------------------
u3   bi cd g ksp pl ilm sill q  - liq
i3  i2
5.80 804.8  % liq = 0
6.00 810.9  % liq = 0
6.20 817.0  % liq = 0
6.40 823.0  % liq = 0

% --------------------------------
u4  cd g ksp pl ilm sill q  - liq
i4  i3
5.60 799.6  % liq = 0
5.80 771.0  % liq = 0
6.00 637.2  % liq = 0

% --------------------------------
u5  liq bi g ksp pl ilm sill q  - ru
i13 i14 connect

% --------------------------------
u6   liq cd g ksp pl ilm q  - sill
i4  end
5.59 850.0  % sill = 0
5.60 860.0  % sill = 0
5.60 870.0  % sill = 0
5.61 880.0  % sill = 0
5.61 890.0  % sill = 0
5.62 900.0  % sill = 0
5.64 910.0  % sill = 0
5.66 920.0  % sill = 0
5.68 930.0  % sill = 0
```

```
5.71 940.0  % sill = 0
5.76 950.0  % sill = 0

% ------------------------------
u7  liq bi g ksp pl ilm sill q  - cd
i13 i1 connect
% ------------------------------
u8  bi g ksp pl ilm sill q  - liq
i2  i19
5.00 818.1  % liq = 0
5.50 820.2  % liq = 0
6.00 822.0  % liq = 0
6.50 823.3  % liq = 0
7.00 824.2  % liq = 0
7.50 824.7  % liq = 0
8.00 824.9  % liq = 0
8.50 824.6  % liq = 0
9.00 824.0  % liq = 0
9.50 822.9  % liq = 0
10.00 821.5  % liq = 0

% ------------------------------
u9  bi g ksp pl ilm sill q  - cd
begin  i2
4.34 640.0  % cd = 0
4.43 650.0  % cd = 0
4.52 660.0  % cd = 0
4.61 670.0  % cd = 0
4.71 680.0  % cd = 0
4.80 690.0  % cd = 0
4.90 700.0  % cd = 0
5.00 710.0  % cd = 0
5.11 720.0  % cd = 0
5.21 730.0  % cd = 0
5.33 740.0  % cd = 0
5.44 750.0  % cd = 0
5.56 760.0  % cd = 0
5.68 770.0  % cd = 0
5.81 780.0  % cd = 0
5.94 790.0  % cd = 0
6.07 800.0  % cd = 0
6.21 810.0  % cd = 0
6.36 820.0  % cd = 0
6.51 830.0  % cd = 0
6.66 840.0  % cd = 0
6.82 850.0  % cd = 0

% ------------------------------
u10   cd g ksp pl ilm sill q  - bi
i5 i3
5.45 790.0  % bi = 0
5.63 800.0  % bi = 0
5.80 810.0  % bi = 0
5.98 820.0  % bi = 0
6.15 830.0  % bi = 0
```

```
6.33 840.0  % bi = 0
6.51 850.0  % bi = 0

% --------------------------------
u11   cd g ksp pl ilm q  - sill
i5 i4
5.13 750.0  % sill = 0
5.21 760.0  % sill = 0
5.29 770.0  % sill = 0
5.37 780.0  % sill = 0
5.44 790.0  % sill = 0
5.52 800.0  % sill = 0
5.60 810.0  % sill = 0
5.68 820.0  % sill = 0
5.76 830.0  % sill = 0
5.83 840.0  % sill = 0
5.91 850.0  % sill = 0

% --------------------------------
u12   bi cd g ksp pl ilm q  - sill
begin  i5
3.26 640.0  % sill = 0
3.39 650.0  % sill = 0
3.52 660.0  % sill = 0
3.66 670.0  % sill = 0
3.79 680.0  % sill = 0
3.93 690.0  % sill = 0
4.08 700.0  % sill = 0
4.22 710.0  % sill = 0
4.37 720.0  % sill = 0
4.51 730.0  % sill = 0
4.66 740.0  % sill = 0
4.82 750.0  % sill = 0

          .
          .
          .
          .
          .
          .

% --------------------------------
u46   bi g ksp pl ilm sill q  - ky
begin  i20
6.00 622.9  % ky = 0
6.20 632.2  % ky = 0
6.40 641.5  % ky = 0
6.60 650.7  % ky = 0
6.80 660.0  % ky = 0
7.00 669.2  % ky = 0
7.20 678.4  % ky = 0
7.40 687.7  % ky = 0
7.60 696.8  % ky = 0
7.80 706.0  % ky = 0
8.00 715.2  % ky = 0
```

```
8.20 724.4  % ky = 0
8.40 733.5  % ky = 0
8.60 742.7  % ky = 0
8.80 751.8  % ky = 0
9.00 760.9  % ky = 0
9.20 770.0  % ky = 0
9.40 779.0  % ky = 0
9.60 788.1  % ky = 0
9.80 797.2  % ky = 0
10.00 806.2  % ky = 0

% ------------------------------
u47  liq g ksp pl ilm ru ky q  - bi
i16  end
10.00 863.4  % bi = 0
10.20 863.3  % bi = 0
10.40 863.2  % bi = 0
10.60 863.0  % bi = 0
10.80 862.7  % bi = 0
11.00 862.4  % bi = 0
11.20 862.1  % bi = 0
11.40 861.6  % bi = 0
11.60 861.2  % bi = 0
11.80 860.9  % bi = 0
12.00 860.4  % bi = 0

% ------------------------------
u48  liq g ksp ilm ru ky q  - pl
i17  end
11.80 918.4  % pl = 0
12.00 887.4  % pl = 0

% ------------------------------
u49   bi g ksp pl ilm ru ky q  - liq
i18  end
10.00 820.5  % liq = 0
10.20 819.7  % liq = 0
10.40 819.0  % liq = 0
10.60 818.3  % liq = 0
10.80 817.6  % liq = 0
11.00 816.9  % liq = 0
11.20 816.2  % liq = 0
11.40 815.4  % liq = 0
11.60 814.6  % liq = 0
11.80 813.8  % liq = 0
12.00 813.0  % liq = 0

% ------------------------------
u50   bi g ksp pl ilm ky q  - ru
begin  i20
9.36 640.0  % ru = 0
9.39 660.0  % ru = 0
9.42 680.0  % ru = 0
9.46 700.0  % ru = 0
9.50 720.0  % ru = 0
```

```
9.54 740.0  % ru = 0
9.59 760.0  % ru = 0
9.64 780.0  % ru = 0
9.70 800.0  % ru = 0

*
% _____________________________________________
% areas
% 2:0.8 3:0.7 4:0.6 5:0.5 6:0.4 7:0.3 8:0.2

0.8 u5 u7 u33
0.7 u33 u35 u34
0.7 u49 u42 u47
0.7 u18 u17 u19 u22
0.7 u1 u5 u2 u3
0.7 u43 u42 u38 u7 u32
0.6 u6 u4 u1 u34 u36
0.6 u2 u8 u32
0.6 u44 u43 u45
0.6 u15 u16 u17
0.6 u47 u39 u48
0.6 u50 u44 u49
0.6 u9 u3 u10 u12
0.6 u20 u18 u21
0.6 u23 u22 u24
0.6 u25 u28 u26 u19
0.6 u40 u39 u38 u35 u37
0.5 u37 u36
0.5 u24 u26 u27
0.5 u21 u23
0.5 u12 u13 u15 u20
0.5 u48 u41
0.5 u41 u40
0.5 u50 u46
0.5 u46 u45 u8 u9
0.5 u30 u28 u29
0.5 u10 u11 u4
0.5 u6 u14 u16 u25 u31
0.4 u31 u30
0.4 u27 u29
0.4 u13 u11 u14
*

% _____________________________________________
window  640 950 3 12          % 610 810 2 7.5
                              % T,P window
bigticks  50 650 1 3          % 20 620  1 2
                              % main T ticks at 20° intervals, starting at 640
smallticks 10 0.2             % minor T,P ticks
darkcolour 29 93 242          % red green blue in 0<->255 => Illustrator RGB
                              % this choice gives the diagram in blues
showlineinfo yes              % puts line info into log file
doareas yes                   % uses the area info
numbering yes                 % numbering the lines on the diagram
*
```

Activity-composition models in NCKFMASHTO

%THERMOCALC datafile in NCKFMASHTO for calculations in pelitic and semipelitic rock
% compositions at subsolidus and suprasolidus conditions.
%
%File contains coding for:
% ged, anth, liq, bi, cd, ep, st, g, opx, chl, mu, pa, osm, ksp, pl, sp, mt, ilm, hem
% compiled by RWW, 28/12/07
%
% Amphiboles:
% Diener, JFA, Powell, R, White, RW & Holland, TJB (2007) A new thermo-dynamic
% model for clino- and orthoamphiboles in Na2O-CaO-FeO-MgO-Al2O3-SiO2-H2O-O.
% Journal of Metamorphic Geology, 25, 631-656.
%
% Silicate melt:
% White, RW, Powell, R & Holland, TJB (2007) Progress relating to calculation of partial
% melting equilibria for metapelites. Journal of Metamorphic Geology, 25, 511-527.
%
% Biotite:
% White, RW, Powell, R & Holland, TJB (2007) Progress relating to calculation of partial
% melting equilibria for metapelites. Journal of Metamorphic Geology, 25, 511-527.
%
% Cordierite, Epidote & Staurolite:
% Holland, TJB, & Powell, R (1998) An internally consistent thermodynamic dataset for
% phases of petrological interest. Journal of Metamorphic Geology, 16, 309-343.
%
% Garnet*:
% White, RW, Powell, R & Holland, TJB (2007) Progress relating to calculation of partial
% melting equilibria for metapelites. Journal of Metamorphic Geology, 25, 511-527.
% *Note: model here is more symmetric
%
% Orthopyroxene:
% White RW, Powell R, Clarke GL (2002) The interpretation of reaction textures in Fe-rich
% metapelitic granulites of the Musgrave Block, central Australia: constraints from mineral
% equilibria calculations in the system K2O-FeO-MgO-Al2O3-SiO2-H2O-TiO2-Fe2O3.
% Journal of Metamorphic Geology 20, 41-55.
%
% Chlorite:
% Holland, TJB, Baker, JM & Powell, R (1998) Mixing properties and activity-composition
% relationships of chlorites in the system MgO-FeO-Al2O3-SiO2-H2O. European Journal
% of Mineralogy, 10, 395-406.
%
% Chloritoid:
% White, RW, Powell, R, Holland, TJB & Worley, BA (2000) The effect of TiO2 and
% Fe2O3 on metapelitic assemblages at greenschist and amphibolite facies conditions:

% mineral equilibria calculations in the system K2O-FeO-MgO-Al2O3-SiO2-H2O-TiO2-
% Fe2O3. Journal of Metamorphic Geology, 18, 497-511.
%
% Muscovite & Paragonite:
% Coggon, R & Holland, TJB (2002) Mixing properties of phengitic micas and revised
% garnet- phengite thermobarometers. Journal of Metamorphic Geology, 20, 683-696.
%
% Plagioclase & K-Feldspar:
% Holland, TJB & Powell, R (2003) Activity-composition relations for phases in
% petrological calculations: an asymmetric multicomponent formulation. Contributions to
% Mineralogy and Petrology, 145, 492-501.
%
% Osumilite:
% Holland, TJB, Babu, EVSSK & Waters, DJ (1996) Phase relations of Osumilite
% and dehydration melting in pelitic rocks: a simple thermodynamic model for the
% KFMASH system. Contributions to Mineralogy and Petrology, 124, 383-394.
%
% Spinel & Magnetite:
% White, RW, Powell, R & Clarke, GL (2002) The interpretation of reaction textures in Fe-
% rich metapelitic granulites of the Musgrave Block, central Australia: constraints from
% mineral equilibria calculations in the system K2O-FeO-MgO-Al2O3-SiO2-H2O-TiO2-
% Fe2O3. Journal of Metamorphic Geology, 20, 41-55.
%
% Ilmenite and hematite:
% White, RW, Powell, R, Holland, TJB & Worley, BA (2000) The effect of TiO2 and
% Fe2O3 on metapelitic assemblages at greenschist and amphibolite facies conditions:
% mineral equilibria calculations in the system K2O-FeO-MgO-Al2O3-SiO2-H2O-TiO2-
% Fe2O3. Journal of Metamorphic Geology, 18, 497-511.
%
% Magnetite: alternate model for low grade rocks. *a-x* model at bottom of file below *
% White, RW, Powell, R, Holland, TJB & Worley, BA (2000) The effect of TiO2 and
% Fe2O3 on metapelitic assemblages at greenschist and amphibolite facies conditions:
% mineral equilibria calculations in the system K2O-FeO-MgO-Al2O3-SiO2-H2O-TiO2-
% Fe2O3. Journal of Metamorphic Geology, 18, 497-511.
%
% Clinopyroxene:
% Green, ECR, Holland, TJB & Powell, R (2007) An order-disorder model for omphacitic
% pyroxenes in the system jadeite-diopside-hedenbergite-acmite, with applications to
% eclogite rocks. American Mineralogist, 92, 1181-1189.
%
% ==
% --
% orthoamphibole: NCFMASHO
%

%	A		M4				M13		M2				T1	
%	v	Na	Ca	Na	Mg	Fe	Mg	Fe	Al	Fe3	Mg	Fe	Al	Si
% anth	1	0	0	0	2	0	3	0	0	0	2	0	0	4
% ged	1	0	0	0	2	0	3	0	2	0	0	0	2	2
% ompa	0	1	0	0	2	0	3	0	1	0	1	0	2	2
% omgl	1	0	0	2	0	0	3	0	2	0	0	0	0	4
% otr	1	0	2	0	0	0	3	0	0	0	2	0	0	4
% fanth	1	0	0	0	0	2	0	3	0	0	0	2	0	4
% omrb	1	0	0	2	0	0	3	0	0	2	0	0	0	4
% a	1	0	0	0	0	2	3	0	0	0	0	2	0	4
% b	1	0	0	0	0	2	0	3	0	0	2	0	0	4

```
%
%                    3 xFeM13 + 2 xFeM2 + 2 xFeM4
% x -> ------------------------------------------------------------
%      3 xFeM13 + 2 xFeM2 + 2 xFeM4 + 3 xMgM13 + 2 xMgM2 + 2 xMgM4
%
% y -> xAlM2
%
% z -> xNaM4
%
% a -> xNaA
%
% c -> xCaM4
%
% f -> xFe3M2
%
%              xFeM13
% Q1 -> x - ----------------
%          xFeM13 + xMgM13
%
%              xFeM2
% Q2 -> x - --------------
%          xFeM2 + xMgM2
% ------------------------------------------------
ged  9

 x(ged)          0.3
 y(ged)          0.5
 z(ged)          0.05
 a(ged)          0.4
 c(ged)          0.05
 f(ged)          0.05
 Q1(ged)         0 range -1 1
 Q2(ged)         0 range -1 1
% ------------------------------------------------
p(anth)          5 1   1  7  -1/2  a  -1  c  -1  f  -1  Q2  -1  x  -1  y  -3/2  Q1
                  2   0  1  1  f   0  1  1  Q2
                  2   0  1  1  c   0  1  1  x
                  2   0  1  1  Q2   0  1  1  y
                  2   0  1  1  x   0  1  1  z

p(ged)           1 1   0  4  -1/2  a   1  f   1  y  -1  z

p(ompa)          1 1   0  1  1  a

p(omgl)          1 1   0  2  -1  f   1  z

p(otr)           1 1   0  1  1  c

p(fanth)         7 1   0  3   1  x  -2  Q2  -5/2  Q1
                  2   0  1  2  f   0  1  1  Q2
                  2   0  1  1  c   0  1  1  x
                  2   0  1  -1  f   0  1  1  x
                  2   0  1  2  Q2   0  1  1  y
                  2   0  1  -1  x   0  1  1  y
                  2   0  1  1  x   0  1  1  z
```

```
p(omrb)          1 1   0  1  1  f

p(a)             5 1   0  2   1  Q2  5/2  Q1
                  2   0  1  -1  f   0  1  1  Q2
                  2   0  1  -1  c   0  1  1  x
                  2   0  1  -1  Q2   0  1  1  y
                  2   0  1  -1  x   0  1  1  z

p(b)             7 1   0  2  2  Q2  3/2  Q1
                  2   0  1  -2  f   0  1  1  Q2
                  2   0  1  -1  c   0  1  1  x
                  2   0  1  1  f   0  1  1  x
                  2   0  1  -2  Q2   0  1  1  y
                  2   0  1  1  x   0  1  1  y
                  2   0  1  -1  x   0  1  1  z
% --------------------------------------------------
asf

W(anth,ged)              25    0  0
W(anth,ompa)             25    0  0
W(anth,omgl)             65    0  0
W(anth,otr)              45    0  0
W(anth,fanth)            33    0  0
W(anth,omrb)             65    0  0 %
W(anth,a)                18    0  0
W(anth,b)                23    0  0
W(ged,ompa)             -40    0  0
W(ged,omgl)              25    0  0
W(ged,otr)               70    0  0
W(ged,fanth)             39.5  0  0
W(ged,omrb)              25    0  0 %
W(ged,a)                 29    0  0
W(ged,b)                 34.6  0  0
W(ompa,omgl)             50    0  0
W(ompa,otr)              90    0  0
W(ompa,fanth)            45    0  0
W(ompa,omrb)             50    0  0 %
W(ompa,a)                33.2  0  0
W(ompa,b)                36    0  0
W(omgl,otr)              65    0  0
W(omgl,fanth)            81.2  0  0
W(omgl,omrb)              0    0  0 %
W(omgl,a)                65.5  0  0
W(omgl,b)                78.4  0  0
W(otr,fanth)             75    0  0
W(otr,omrb)              65    0  0 %
W(otr,a)                 57    0  0
W(otr,b)                 63    0  0
W(fanth,omrb)            81.2  0  0 %
W(fanth,a)               12    0  0
W(fanth,b)                8    0  0
W(omrb,a)                65.5  0  0 %
W(omrb,b)                78.4  0  0 %
W(a,b)                   20    0  0
```

```
anth    1    0  0
ged     1.5  0  0
ompa    1.7  0  0
omgl    0.8  0  0
otr     1    0  0
fanth   1    0  0
omrb    0.8  0  0
a       1    0  0
b       1    0  0
% --------------------------------------------------
14

xvA             1 1   1  1  -1  a

xNaA            1 1   0  1  1  a

xCaM4           1 1   0  1  1  c

xNaM4           1 1   0  1  1  z

xMgM4           5 1   1  5  -1  c  -1  Q2  -1  x  -1  z  -3/2  Q1
                2   0  1  1  f   0  1  1  Q2
                2   0  1  1  c   0  1  1  x
                2   0  1  1  Q2   0  1  1  y
                2   0  1  1  x   0  1  1  z

xFeM4           5 1   0  3   1  Q2   1  x  3/2  Q1
                2   0  1  -1  f   0  1  1  Q2
                2   0  1  -1  c   0  1  1  x
                2   0  1  -1  Q2   0  1  1  y
                2   0  1  -1  x   0  1  1  z

xMgM13          1 1   1  2   1  Q1  -1  x

xFeM13          1 1   0  2  -1  Q1   1  x

xAlM2           1 1   0  1  1  y

xFe3M2          1 1   0  1  1  f

xMgM2           5 1   1  4  -1  f   1  Q2  -1  x  -1  y
                2   0  1  -1  f   0  1  1  Q2
                2   0  1  1  f   0  1  1  x
                2   0  1  -1  Q2   0  1  1  y
                2   0  1  1  x   0  1  1  y

xFeM2           5 1   0  2  -1  Q2   1  x
                2   0  1  1  f   0  1  1  Q2
                2   0  1  -1  f   0  1  1  x
                2   0  1  1  Q2   0  1  1  y
                2   0  1  -1  x   0  1  1  y

xAlT1           1 1   0  4  1/2  f  1/2  y  -1/2  z  1/4  a

xSiT1           1 1   1  4  -1/2  f  -1/2  y  1/2  z  -1/4  a
```

```
% ---------------------------------------------------
anth     1    5  xvA 1  xMgM4 2  xMgM13 3  xMgM2 2  xSiT1 1
 check 0  0  0  0  0  0  0  0

ged      2    6  xvA 1  xMgM4 2  xMgM13 3  xAlM2 2  xAlT1 1/2  xSiT1 1/2
 check 0  1  0  0  0  0  0  0
 DQF  22 0 0

ompa    8   7  xNaA 1  xMgM4 2  xMgM13 3  xAlM2 1  xMgM2 1  xAlT1 1/2 xSiT1 1/2
 check 0  1/2  0  1  0  0  0  0
 make  3 parg 1 tr -1 anth 1
 DQF  27 0 0

omgl    1    5  xvA 1  xNaM4 2  xMgM13 3  xAlM2 2  xSiT1 1
 check 0  1  1  0  0  0  0  0
 make  1 gl 1
 DQF 15 0 0

otr       1    5  xvA 1  xCaM4 2  xMgM13 3  xMgM2 2  xSiT1 1
 check 0  0  0  0  1  0  0  0
 make 1 tr 1
 DQF 0 0 0

fanth   1    5  xvA 1  xFeM4 2  xFeM13 3  xFeM2 2  xSiT1 1
 check 1  0  0  0  0  0  0  0
 DQF   7  0  0

omrb    1    5  xvA 1  xNaM4 2  xMgM13 3  xFe3M2 2  xSiT1 1
 check 0  0  1  0  0  1  0  0
 make 3 gl 1 jd -2 acm 2
 DQF   33 0 0

a       1    5  xvA 1  xFeM4 2  xMgM13 3  xFeM2 2  xSiT1 1
 check 4/7  0  0  0  0  0  4/7  -3/7
 make  2  anth 3/7 fanth 4/7
 DQF   -5.5  0  0

b       1    5  xvA 1  xFeM4 2  xFeM13 3  xMgM2 2  xSiT1 1
 check 5/7  0  0  0  0  0  -2/7  5/7
 make  2  anth 2/7 fanth 5/7
 DQF   -6.7  0  0

% ===================================================
% ---------------------------------------------------
% orthoamphibole: NCFMASHO
%
%                A        M4                 M13       M2                T1
%                v  Na    Ca  Na  Mg  Fe     Mg  Fe    Al  Fe3 Mg  Fe    Al  Si
% anth           1  0     0   0   2   0      3   0     0   0   2   0     0   4
% ged            1  0     0   0   2   0      3   0     2   0   0   0     2   2
% ompa           0  1     0   0   2   0      3   0     1   0   1   0     2   2
% omgl           1  0     0   2   0   0      3   0     2   0   0   0     0   4
% otr            1  0     2   0   0   0      3   0     0   0   2   0     0   4
% fanth          1  0     0   0   0   2      0   3     0   0   0   2     0   4
% omrb           1  0     0   2   0   0      3   0     0   2   0   0     0   4
```

```
% a               1  0     0  0  0    2    3   0    0  0    0   2    0  4
% b               1  0     0  0  0    2    0   3    0  0    2   0    0  4
%
%                  3 xFeM13 + 2 xFeM2 + 2 xFeM4
% x -> ------------------------------------------------------------
%     3 xFeM13 + 2 xFeM2 + 2 xFeM4 + 3 xMgM13 + 2 xMgM2 + 2 xMgM4
%
% y -> xAlM2
%
% z -> xNaM4
%
% a -> xNaA
%
% c -> xCaM4
%
% f -> xFe3M2
%
%             xFeM13
% Q1 -> x - ---------------
%          xFeM13 + xMgM13
5
%             xFeM2
% Q2 -> x - -------------
%          xFeM2 + xMgM2
% -------------------------------------------------
anth  9

 x(anth)          0.28
 y(anth)          0.11
 z(anth)          0.05
 a(anth)          0.09
 c(anth)          0.05
 f(anth)          0.05
 Q1(anth)         0 range -1 1
 Q2(anth)         0 range -1 1
% -------------------------------------------------
p(anth)           5 1   1  7  -1/2  a  -1  c  -1  f  -1  Q2  -1  x  -1  y  -3/2  Q1
                   2   0  1  1  f   0  1  1  Q2
                   2   0  1  1  c   0  1  1  x
                   2   0  1  1  Q2   0  1  1  y
                   2   0  1  1  x   0  1  1  z

p(ged)            1 1   0  4  -1/2  a   1  f   1  y  -1  z

p(ompa)           1 1   0  1  1  a

p(omgl)           1 1   0  2  -1  f   1  z

p(otr)            1 1   0  1  1  c

p(fanth)          7 1   0  3   1  x  -2  Q2  -5/2  Q1
                   2   0  1  2  f   0  1  1  Q2
                   2   0  1  1  c   0  1  1  x
                   2   0  1  -1  f   0  1  1  x
                   2   0  1  2  Q2   0  1  1  y
```

```
                2   0  1  -1  x    0  1  1  y
                2   0  1  1  x    0  1  1  z

p(omrb)         1 1    0  1  1  f

p(a)            5 1    0  2   1  Q2  5/2  Q1
                2   0  1  -1  f    0  1  1  Q2
                2   0  1  -1  c    0  1  1  x
                2   0  1  -1  Q2    0  1  1  y
                2   0  1  -1  x    0  1  1  z

p(b)            7 1    0  2  2  Q2  3/2  Q1
                2   0  1  -2  f    0  1  1  Q2
                2   0  1  -1  c    0  1  1  x
                2   0  1  1  f    0  1  1  x
                2   0  1  -2  Q2    0  1  1  y
                2   0  1  1  x    0  1  1  y
                2   0  1  -1  x    0  1  1  z
% ---------------------------------------------------
asf

W(anth,ged)             25     0  0
W(anth,ompa)            25     0  0
W(anth,omgl)            65     0  0
W(anth,otr)             45     0  0
W(anth,fanth)           33     0  0
W(anth,omrb)            65     0  0 %
W(anth,a)               18     0  0
W(anth,b)               23     0  0
W(ged,ompa)            -40     0  0
W(ged,omgl)             25     0  0
W(ged,otr)              70     0  0
W(ged,fanth)            39.5   0  0
W(ged,omrb)             25     0  0 %
W(ged,a)                29     0  0
W(ged,b)                34.6   0  0
W(ompa,omgl)            50     0  0
W(ompa,otr)             90     0  0
W(ompa,fanth)           45     0  0
W(ompa,omrb)            50     0  0 %
W(ompa,a)               33.2   0  0
W(ompa,b)               36     0  0
W(omgl,otr)             65     0  0
W(omgl,fanth)           81.2   0  0
W(omgl,omrb)             0     0  0 %
W(omgl,a)               65.5   0  0
W(omgl,b)               78.4   0  0
W(otr,fanth)            75     0  0
W(otr,omrb)             65     0  0 %
W(otr,a)                57     0  0
W(otr,b)                63     0  0
W(fanth,omrb)           81.2   0  0 %
W(fanth,a)              12     0  0
W(fanth,b)               8     0  0
W(omrb,a)               65.5   0  0 %
```

```
W(omrb,b)               78.4  0  0 %
W(a,b)                  20    0  0

anth    1    0  0
ged     1.5  0  0
ompa    1.7  0  0
omgl    0.8  0  0
otr     1    0  0
fanth   1    0  0
omrb    0.8  0  0
a       1    0  0
b       1    0  0
% ---------------------------------------------------
14

xvA             1 1   1  1  -1  a

xNaA            1 1   0  1  1  a

xCaM4           1 1   0  1  1  c

xNaM4           1 1   0  1  1  z

xMgM4           5 1   1  5  -1  c  -1  Q2  -1  x  -1  z  -3/2  Q1
                2   0  1  1  f   0  1  1  Q2
                2   0  1  1  c   0  1  1  x
                2   0  1  1  Q2   0  1  1  y
                2   0  1  1  x   0  1  1  z

xFeM4           5 1   0  3   1  Q2   1  x  3/2  Q1
                2   0  1  -1  f   0  1  1  Q2
                2   0  1  -1  c   0  1  1  x
                2   0  1  -1  Q2   0  1  1  y
                2   0  1  -1  x   0  1  1  z

xMgM13          1 1   1  2   1  Q1  -1  x

xFeM13          1 1   0  2  -1  Q1   1  x

xAlM2           1 1   0  1  1  y

xFe3M2          1 1   0  1  1  f

xMgM2           5 1   1  4  -1  f   1  Q2  -1  x  -1  y
                2   0  1  -1  f   0  1  1  Q2
                2   0  1  1  f   0  1  1  x
                2   0  1  -1  Q2   0  1  1  y
                2   0  1  1  x   0  1  1  y

xFeM2           5 1   0  2  -1  Q2   1  x
                2   0  1  1  f   0  1  1  Q2
                2   0  1  -1  f   0  1  1  x
                2   0  1  1  Q2   0  1  1  y
                2   0  1  -1  x   0  1  1  y
```

```
xAlT1              1 1    0  4  1/2  f  1/2  y  -1/2  z  1/4  a

xSiT1              1 1    1  4  -1/2  f  -1/2  y  1/2  z  -1/4  a
% ---------------------------------------------------
anth      1    5  xvA 1  xMgM4 2  xMgM13 3  xMgM2 2  xSiT1 1
 check 0  0  0  0  0  0  0  0

ged       2    6  xvA 1  xMgM4 2  xMgM13 3  xAlM2 2  xAlT1 1/2  xSiT1 1/2
 check 0  1  0  0  0  0  0  0
 DQF  22 0 0

ompa    8   7  xNaA 1  xMgM4 2  xMgM13 3  xAlM2 1  xMgM2 1  xAlT1 1/2 xSiT1 1/2
 check 0  1/2  0  1  0  0  0  0
 make  3 parg 1 tr -1 anth 1
 DQF  27 0 0

omgl     1    5  xvA 1  xNaM4 2  xMgM13 3  xAlM2 2  xSiT1 1
 check 0  1  1  0  0  0  0  0
 make  1 gl 1
 DQF 15 0 0

otr        1    5  xvA 1  xCaM4 2  xMgM13 3  xMgM2 2  xSiT1 1
 check 0  0  0  0  1  0  0  0
 make 1 tr 1
 DQF 0 0 0

fanth     1    5  xvA 1  xFeM4 2  xFeM13 3  xFeM2 2  xSiT1 1
 check 1  0  0  0  0  0  0  0
 DQF   7  0  0

omrb     1    5  xvA 1  xNaM4 2  xMgM13 3  xFe3M2 2  xSiT1 1
 check 0  0  1  0  0  1  0  0
 make 3 gl 1 jd -2 acm 2
 DQF   33 0 0

a          1    5  xvA 1  xFeM4 2  xMgM13 3  xFeM2 2  xSiT1 1
 check 4/7  0  0  0  0  0  4/7  -3/7
 make  2  anth 3/7 fanth 4/7
 DQF   -5.5  0  0

b          1    5  xvA 1  xFeM4 2  xFeM13 3  xMgM2 2  xSiT1 1
 check 5/7  0  0  0  0  0  -2/7  5/7
 make  2  anth 2/7 fanth 5/7
 DQF   -6.7  0  0

% ================================================================
% ---------------------------------------------------
% Melt: NCKFMASH

liq 8

q(L)               0.1915
fsp(L)             0.3272
na(L)              0.3570
an(L)              0.01849
```

```
ol(L)              0.007373
x(L)               0.6686
h2o(L)             0.4406
% ---------------------------------------------------
p(qL)              1 1     0  1  1  q

p(abL)             1 2     0  1  1  fsp    0  1  1  na

p(kspL)            1 2     0  1  1  fsp    1  1 -1  na

p(anL)             1 1     0  1  1  an

p(silL)            1 1     1  5 -1 q -1 fsp -1 an -1 ol -1 h2o

p(foL)             1 2     0  1  1  ol   1  1 -1  x

p(faL)             1 2     0  1  1  ol   0  1  1  x

p(h2oL)            1 1     0  1  1  h2o
% ---------------------------------------------------
sf

W(qLabL)          12  0  -0.4
W(qLkspL)         -2  0  -0.5
W(qLanL)         -10  0   0
W(qLsilL)         12  0   0
W(qLfoL)          12  0  -0.4
W(qLfaL)          14  0   0
W(qLh2oL)         15  0   0
W(abLkspL)         6  0   3.0
W(abLanL)          0  0   0
W(abLsilL)        12  0   0
W(abLfoL)         10  0   0
W(abLfaL)          2  0   0
W(abLh2oL)         1  0  -0.2
W(kspLanL)         0  0  -1.0
W(kspLsilL)       12  0   0
W(kspLfoL)        12  0   0
W(kspLfaL)        12  0   0
W(kspLh2oL)       11  0  -0.45
W(anLsilL)         0  0   0
W(anLfoL)          0  0   0
W(anLfaL)          0  0   0
W(anLh2oL)         9  0  -0.85
W(silLfoL)        12  0   0
W(silLfaL)        12  0   0
W(silLh2oL)       16  0   0
W(foLfaL)         18  0   0
W(foLh2oL)        11  0  -0.5
W(faLh2oL)        12  0   0
% ---------------------------------------------------
10

fac        1 1      1  1 -1  h2o
```

```
pq       1 1     0  1  1  q

xab      1 2     0  1  1  fsp    0  1  1  na

xksp     1 2     0  1  1  fsp    1  1 -1  na

pan      1 1     0  1  1  an

psil     1 1     1  5 -1 q -1 fsp -1 an -1 ol -1 h2o

pol      1 1     0  1  1  ol

xFe      1 1     0  1  1  x

xMg       1 1    1  1 -1  x

ph2o     1 1      0  1  1  h2o
% ---------------------------------------------------
% ideal mixing activities

qL       1  2     fac 1 pq 1
 make   1  qL 4

abL      1  2     fac 1 xab 1

kspL     1  2     fac 1 xksp 1

anL      1  2     fac 1 pan 1

sill       1  2     fac 1  psil 1
 make   1  silL  8/5
 DQF  -10 0 0

foL      1  3     fac 1  pol 1  xMg  5
 make   1  foL 2
 DQF  -10 0 0

faL      1  3     fac 1  pol 1  xFe  5
 make  1  faL 2
 DQF  -9 0 -1.3

h2oL     1  1     ph2o 2

% ============================================================
% ----------------------------------------------
% Biotite: KFMASHTO
%
% x(bi)  = Fe/(Fe + Mg)
% y(bi)  = x(Al,M1)
% Q(bi) = 3(x - x(Fe,M2))
% f(bi)  = x(Fe3+,M1)
% t(bi)  = x(Ti,M1)

bi  6
```

```
x(bi)     0.6372
y(bi)     0.4761
f(bi)     0.02182
t(bi)     0.1184
Q(bi)     0.1160
% --------------------------------------------------
p(phl)   2 1    1  5  -1  f  -1  t  -1  x  -1  y  -2/3  Q
          2    0  1  1  x    0  3  1  f  1  t  1  y

p(ann)   1 1    0  2  -1/3  Q   1  x

p(obi)   2 1    0  1   1  Q
          2    0  1  -1  x    0  3  1  f  1  t  1  y

p(east)  1 1    0  1  1  y

p(tbi)    1 1    0  1  1  t

p(fbi)    1 1    0  1  1  f
% --------------------------------------------------
sf

W(phl,ann)        9  0  0
W(phl,obi)        3  0  0
W(phl,east)      10  0  0
W(phl,tbi)        0  0  0
W(phl,fbi)        0  0  0
W(ann,obi)        6  0  0
W(ann,east)      -1  0  0
W(ann,tbi)       10  0  0
W(ann,fbi)        8  0  0
W(obi,east)      10  0  0
W(obi,tbi)        0  0  0
W(obi,fbi)        0  0  0
W(east,tbi)       0  0  0
W(east,fbi)       0  0  0
W(tbi,fbi)        0  0  0
% --------------------------------------------------
11

xMgM1           2 1    1  5  -1  f  -1  t  -1  x  -1  y  -2/3  Q
                 2    0  1  1  x    0  3  1  f  1  t  1  y

xFeM1           2 1    0  2   1  x  2/3  Q
                 2    0  1  -1  x    0  3  1  f  1  t  1  y

xAlM1           1 1    0  1  1  y

xFe3M1          1 1    0  1  1  f

xTiM1           1 1    0  1  1  t

xMgM2           1 1    1  2  1/3  Q  -1  x

xFeM2           1 1    0  2  -1/3  Q   1  x
```

```
xSiT              1 1    1/2  2  -1/2  f  -1/2  y

xAlT              1 1    1/2  2  1/2  f  1/2  y

xOHV              1 1    1  1  -1  t

xOV               1 1    0  1  1  t
% ---------------------------------------------------
phl       4    5  xMgM1 1  xMgM2 2  xSiT 1  xAlT 1  xOHV 2
 check 0  0  0  0  0

ann       4    5  xFeM1 1  xFeM2 2  xSiT 1  xAlT 1  xOHV 2
 check 1  0  0  0  0
 DQF      -3  0  0

obi       4    5  xFeM1 1  xMgM2 2  xSiT 1  xAlT 1  xOHV 2
 check 1/3  0  0  0  1
 make       2   phl 2/3 ann 1/3
 DQF      -10.73  0  0

east      1    4  xAlM1 1  xMgM2 2  xAlT 2  xOHV 2
 check 0  1  0  0  0

tbi       4    5  xTiM1 1  xMgM2 2  xSiT 1  xAlT 1  xOV 2
 check 0  0  0  1  0
 make 3 phl 1 br -1 ru 1
 DQF      78  0  0     % 60 with +/- at least 30

fbi       1    4  xFe3M1 1  xMgM2 2  xAlT 2  xOHV 2
 check 0  0  1  0  0
 make 3 east 1 cor -1/2  hem 1/2
 DQF      13 0  0     % 13 with +/- at least 10

% ===========================================================
% ---------------------------------------------------
% Cordierite: FMASH
%
% x(cd) = Fe/(Fe + Mg)
% h(cd) = H2O pfu

cd 3
x(cd)    0.4703
h(cd)    0.5285
% ---------------------------------------------------
p(crd)            1 1      1  2 -1  x -1  h

p(fcrd)           1 1      0  1  1  x

p(hcrd)           1 1      0  1  1  h
% ---------------------------------------------------
ideal
% ---------------------------------------------------
4

x(Mg)   1 1      1  1 -1  x
```

```
x(Fe)    1 1      0  1  1  x

h        1 1      0  1  1  h

noth     1 1      1  1 -1  h
% ----------------------------------------------------
crd      1    2     x(Mg)  2    noth  1

fcrd     1    2     x(Fe)  2    noth  1

hcrd     1    2     x(Mg)  2      h  1

% ============================================================
% ----------------------------------------------
% Epidote: CASHO
%
% Fe3+ - Al mixing on M1 & M3.  M2-all Al
%
%  f(ep)   = Fe3+(m13)/(Fe3+(m13) + Al(m13))
%  Q(ep) = 1/2(Fe3+(m3) - Fe3+(m1))

ep 3

f(ep)     0.117
Q(ep)   0.116  range 0 0.5
%-------------------------------------------------------------------
p(cz)    1  1    1  2 -1  f  -1  Q

p(ep)    1  1    0  1  2  Q

p(fep)   1  1    0  2  1  f  -1  Q
% ----------------------------------------------
sf

W(cz,ep)            0     0  0
W(cz,fep)         15.4  0  0
W(ep,fep)           3     0  0
% ----------------------------------------------
4
% 4 "site fractions"

xFeM1             1  1    0  2  1  f  -1  Q

xAlM1             1  1    1  2 -1  f   1  Q

xFeM3             1  1    0  2  1  f   1  Q

xAlM3             1  1    1  2 -1  f  -1  Q
% ----------------------------------------------
% ideal mixing activities

cz        1  2     xAlM1  1  xAlM3   1

ep        1  2     xAlM1  1  xFeM3   1
```

```
fep       1  2      xFeM1  1  xFeM3   1

% ============================================================
% ------------------------------------------------
% Staurolite: FMASH
%
% x(st) = Fe/(Fe + Mg)

st 2

x(st)     0.89
% ------------------------------------------------
p(mst)              1 1      1  1 -1  x

p(fst)              1 1      0  1  1  x
% ------------------------------------------------
sf

w(st)     -8 0 0
% ------------------------------------------------
  2
x(Mg)               1 1      1  1 -1  x

x(Fe)               1 1      0  1  1  x
% ------------------------------------------------
mst       1  1      x(Mg)  4

fst       1  1      x(Fe)  4

% ============================================================
% ------------------------------------------------
% Garnet: CFMASO
%
% this model is somewhat less asymmetric than used in the calculations of the white et al
2007
% paper, but this is our currently preferred model
%
% x = Fe2/(Fe2 + Mg)
% z = Ca/(Fe2 + Mg + Ca)
% f = Fe3/2

g 4      % garnet with ferric (and van Laar)

x(g)      0.8399
z(g)      0.01441
f(g)      0.001
% ------------------------------------------------
p(alm)              1  2    1  1 -1  z    0  1  1  x

p(py)               1  2    1  1 -1  z    1  1 -1  x

p(gr)               1 1    0  2  1  z -1  f

p(andr)             1 1    0  1  1  f
% ------------------------------------------------
```

```
asf

W(alm,py)        2.5  0  0
W(alm,gr)        10   0  0
W(alm,andr)      75   0  0
W(py,gr)         45   0  0
W(py,andr)       90   0  0
W(gr,andr)        0   0  0

alm      1 0 0
py       1 0 0
gr       3 0 0
andr     3 0 0
% ----------------------------------------------------
5     % no of site fractions

xFeX             1  2    1  1 -1  z    0  1  1  x

xMgX             1  2    1  1 -1  z    1  1 -1  x

xCaX             1  1    0  1  1  z

xAlY             1 1     1  1 -1  f

xFe3Y            1 1     0  1  1  f
% ----------------------------------------------------
alm      1  2     xFeX  3   xAlY 2

py       1  2     xMgX  3   xAlY 2

gr       1  2     xCaX  3   xAlY 2

andr     1  2     xCaX  3   xFe3Y 2

%=================================================
% ---------------------------------------------------
% Orthopyroxene: FMASO

% x(opx)  = Fe2/(Fe2 + Mg)
% y(opx)  = x(Al,M1)
% Q(opx) = 2(x(Fe,M2) - x)
% f(opx)   = x(Fe3+,m1)

opx 5   % no tet terms model

x(opx)           0.5156
y(opx)           0.1519
Q(opx)           0.3927
f(opx)           0.006407
% ----------------------------------------------------
p(en)            1 1   1  4 -1  x -1  y -1/2 Q  -1  f

p(fs)            2 1   0  1      -1/2 Q
                  2   0  1  1  x    1  2 -1  y  -1  f
```

```
p(mgts)          1 1   0  1  1  y

p(fm)            2 1   0  1  1  Q
                  2   0  1  1 x     0  2  1  y 1  f

p(mots)          1 1   0  1  1  f
% -----------------------------------------------------
sf

W(en,fs)           6.8  0  0
W(en,mgts)         0    0  0
W(en,fm)           4.5  0  0
W(en,mots)       -14    0  0
W(fs,mgts)         -1   0  0
W(fs,fm)           4.5  0  0
W(fs,mots)         6    0  0
W(mgts,fm)         1.2  0  0
W(mgts,mots)       0    0  0
W(fm,mots)         6    0  0
% -----------------------------------------------------
6

x(Al,M1)         1 1   0  1  1  y

x(Fe3,M1)        1 1   0  1  1  f

x(Mg,M1)         2 1   1  3 -1  y  -1  f  1/2 Q
                  2   0  1 -1  x    1  2 -1  y  -1  f

x(Fe,M1)         2 1   0  1       -1/2 Q
                  2   0  1  1 x    1  2 -1  y -1  f

x(Mg,M2)         1 1   1  2 -1  x -1/2 Q

x(Fe,M2)         1 1   0  2  1  x  1/2 Q
% -----------------------------------------------------
en       1  2      x(Mg,M1)  1    x(Mg,M2) 1
 check 0 0 0 0

fs       1  2      x(Fe,M1) 1    x(Fe,M2) 1
 check 1 0 0 0

mgts     1  2      x(Al,M1) 1    x(Mg,M2) 1
 check 0 1 0 0

fm       1  2      x(Mg,M1)  1    x(Fe,M2) 1
 check 1/2 0 1 0
 make       2       en 1/2    fs 1/2
 DQF    -6.95  0  0

mots     1  2      x(Fe3,M1)  1    x(Mg,M2) 1
 check 0 0 0 1
 make       3       mgts 1    cor -1/2   hem 1/2
 DQF    22  0  0
```

```
% ================================================================
% ----------------------------------------------
% Chlorite: FMASH
%
% x(chl)  = Fe/(Fe + Mg)
% y(chl)  = x(Al,T2)
% Q(chl) = y - x(Al,M1)

chl 4

x(chl)          0.4508
y(chl)          0.532
Q(chl)          0.4676
% ----------------------------------------------
p(afchl)        1  1    1  2 -1  y -1  Q

p(clin)         2  1    0  1  2  Q
                 2    0  1 -2/5  x    3  1 -1  y

p(daph)         1  2    0  1  2/5  x    3  1 -1  y

p(ames)         1  1    0  2  1  y -1  Q
% ----------------------------------------------
sf

W(afchl,clin)           18    0  0
W(afchl,daph)           14.5  0  0
W(afchl,ames)           20    0  0
W(clin,daph)             2.5  0  0
W(clin,ames)            18    0  0
W(daph,ames)            13.5  0  0
 % ----------------------------------------------
10

x(Fe,M23)       1  1    0  1  1  x

x(Mg,M23)       1  1    1  1 -1  x

x(Al,M1)        1  1    0  2  1  y -1  Q

x(Fe,M1)        1  2    0  1  1  x    1  2 -1  y  1  Q

x(Mg,M1)        1  2    1  1 -1  x    1  2 -1  y  1  Q

x(Al,M4)        1  1    0  2  1  y  1  Q

x(Fe,M4)        1  2    0  1  1  x    1  2 -1  y -1  Q

x(Mg,M4)        1  2    1  1 -1  x    1  2 -1  y -1  Q

x(Al,T2)        1  1    0  1  1  y

x(Si,T2)        1  1    1  1 -1  y
% ----------------------------------------------
afchl    1  4    x(Mg,M23) 4   x(Mg,M1) 1   x(Mg,M4) 1   x(Si,T2) 2
```

```
 check 0 0 0

clin       4  5    x(Mg,M23) 4   x(Mg,M1) 1   x(Al,M4) 1   x(Al,T2) 1  x(Si,T2) 1
 check 0 1/2 1/2

daph     4  5    x(Fe,M23) 4   x(Fe,M1) 1   x(Al,M4) 1   x(Al,T2) 1  x(Si,T2) 1
 check 1 1/2 1/2

ames    1  4    x(Mg,M23) 4   x(Al,M1) 1   x(Al,M4) 1   x(Al,T2) 2
 check 0 1 0

% ============================================================
% ----------------------------------------------------
% Chloritoid: FMASHO
%
% x(ctd) = Fe/(Fe + Mg)
% y(ctd) = x(Fe3+,Y)

ctd 3

x(ctd)    0.7411
f(ctd)    0.01701
% ----------------------------------------------------
p(mctd)             1 1    1  2 -1  x  -1  f

p(fctd)             1 1    0  1  1  x

p(ctdo)             1 1    0  1  1  f
% ----------------------------------------------------
sf

W(mctd,fctd)     1  0  0
W(mctd,ctdo)    0  0  0
W(fctd,ctdo)     0  0  0
% ----------------------------------------------------
4     % no of site fractions
x(Al,Y)             1 1    1  1  -1   f

x(Fe3,Y)           1 1    0  1  1    f

x(Fe,X)             1 1    0  1  1    x

x(Mg,X)            1 1    1  1  -1   x
% ----------------------------------------------------
mctd     1  2    x(Mg,X) 1   x(Al,Y) 2
 check 0 0

fctd       1  2    x(Fe,X) 1   x(Al,Y) 2
 check 1 0

ctdo      1  2    x(Mg,X) 1   x(Fe3,Y) 2
 make    3 mctd 1 cor -1  hem 1
 DQF      53  0  0
 check 0 1
```

```
% ================================================================
% ----------------------------------------------
% Muscovite: NKFMASH
%
% fe(mu)  = Fe/(Fe+Mg)
% y(mu)   = X(Al,M2A)
% na(mu) = X(Na,A)

mu  4

fe(mu)              0.45  % Fe/(Fe+Mg)
y(mu)               0.96  % XAl,M2A
na(mu)              0.11  % XNa,A
% ----------------------------------------------------
p(mu)               1 1   0  2  1 y -1  na

p(pa)               1 1   0  1  1 na

p(cel)              1 2   1  1 -1 fe     1  1 -1  y

p(fcel)             1 2   0  1  1 fe     1  1 -1  y
% ----------------------------------------------------
asf

W(mu,pa)          10.12   0.0034   0.353
W(mu,cel)           0.00   0.0000   0.200
W(mu,fcel)          0.00   0.0000   0.200
W(pa,cel)          52.00   0.0000   0.000
W(pa,fcel)         52.00   0.0000   0.000
W(cel,fcel)         0.00   0.0000   0.000

Mu        0.63   0.0   0.0
pa        0.37   0.0   0.0
cel       0.63   0.0   0.0
fcel      0.63   0.0   0.0
% ----------------------------------------------------
x(K,A)              1  1   1  1 -1  na

x(Na,A)             1  1   0  1  1  na

x(Al,M2A)           1  1   0  1  1  y

x(Fe,M2A)           1  2   0  1  1  fe    1  1 -1  y

x(Mg,M2A)           1  2   1  1 -1  fe    1  1 -1  y

x(Si,T1)            1  1   1  1 -1/2  y

x(Al,T1)            1  1   0  1  1/2  y
% ----------------------------------------------------
mu        4  4  x(K,A) 1    x(Al,M2A) 1 x(Al,T1) 1  x(Si,T1) 1
 check 0  1  0

pa        4  4  x(Na,A) 1   x(Al,M2A) 1 x(Al,T1) 1  x(Si,T1) 1
 check 0  1  1
```

```
cel       1  3       x(K,A) 1    x(Mg,M2A) 1 x(Si,T1) 2
 check 0  0  0

fcel      1  3       x(K,A) 1    x(Fe,M2A) 1 x(Si,T1) 2
 check 1  0  0

% ============================================================
% ------------------------------------------------
% Paragonite: NKFMASH

% fe(mu)  = Fe/(Fe+Mg)
% y(mu)   = X(Al,M2A)
% na(mu) = X(Na,A)

pa  4

fe(pa)   0.45  % Fe/(Fe+Mg)
y(pa)    0.96  % XAl,M2A
na(pa)  0.89  % XNa,A
% ------------------------------------------------
p(mu)              1 1   0  2  1 y -1  na

p(pa)              1 1   0  1  1 na

p(cel)             1 2   1  1 -1 fe     1  1 -1  y

p(fcel)            1 2   0  1  1 fe     1  1 -1  y
% ------------------------------------------------
asf

W(mu,pa)         10.12   0.0034   0.353
W(mu,cel)          0.00   0.0000   0.200
W(mu,fcel)         0.00   0.0000   0.200
W(pa,cel)         52.00   0.0000   0.000
W(pa,fcel)        52.00   0.0000   0.000
W(cel,fcel)        0.00   0.0000   0.000

mu       0.63   0.0   0.0
pa       0.37   0.0   0.0
cel      0.63   0.0   0.0
fcel     0.63   0.0   0.0
% ------------------------------------------------
7

x(K,A)             1  1   1  1 -1  na

x(Na,A)            1  1   0  1  1  na

x(Al,M2A)          1  1   0  1  1  y

x(Fe,M2A)          1  2   0  1  1  fe    1  1 -1  y

x(Mg,M2A)          1  2   1  1 -1  fe    1  1 -1  y

x(Si,T1)           1  1   1  1 -1/2  y
```

```
x(Al,T1)            1  1   0  1  1/2  y
% ---------------------------------------------------
mu       4  4  x(K,A) 1    x(Al,M2A) 1 x(Al,T1) 1  x(Si,T1) 1
 check 0  1  0

pa       4  4  x(Na,A) 1   x(Al,M2A) 1 x(Al,T1) 1  x(Si,T1) 1
 check 0  1  1

cel      1  3      x(K,A) 1    x(Mg,M2A) 1 x(Si,T1) 2
 check 0  0  0

fcel     1  3      x(K,A) 1    x(Fe,M2A) 1 x(Si,T1) 2
 check 1  0  0

% ===================================================================
% ---------------------------------------------------
% K-Feldspar: NCKAS  Cbar1 ASF

% na(ksp) = Na/(Na + Ca + K)
% ca(ksp) = Ca/(Na + Ca + K)

ksp   3

na(ksp)             0.1
ca(ksp)             0.004
% ---------------------------------------------------
 p(san)             1 1    1 2 -1 na -1 ca

p(abh)              1 1    0 1  1 na

p(an)               1 1    0 1  1 ca
% ---------------------------------------------------
asf

w(sanabh)        25.1  -0.0108  0.338
w(sanan)         40      0          0
w(abhan)          3.1   0          0

san      1.0      0  0
abh      0.643  0  0
an       1.0      0  0
% ---------------------------------------------------
3

x(K)     1 1    1 2 -1 na -1 ca

x(Na)    1 1    0 1  1 na

x(Ca)    1 1    0 1  1 ca
% ---------------------------------------------------
san      1 1     x(K) 1

abh      1 1     x(Na) 1

an       1 1     x(Ca) 1
```

```
 DQF   7.03  -0.00466   0

% ============================================================
% ----------------------------------------------------
% Plagioclase:  NCKAS  Cbar1 ASF

% ca(pl) = Ca/(Na + Ca + K)
% k(pl)   = K/(Na + Ca + K)

pl 3

ca(pl)    0.5562
k(pl)     0.003681
% ----------------------------------------------------
p(abh)              1 1    1 2 -1 k -1 ca

p(an)               1 1    0 1  1 ca

p(san)              1 1    0 1  1 k
% ----------------------------------------------------
asf

w(abhan)            3.1   0          0
w(sanabh)          25.1  -0.0108  0.338
w(sanan)           40     0          0

abh       0.643  0  0
an        1.0    0  0
san       1.0    0  0
% ----------------------------------------------------
3

x(K)      1 1    0 1  1 k

x(Na)     1 1    1 2 -1 k -1 ca

x(Ca)     1 1    0 1  1 ca
% ----------------------------------------------------
abh       1 1     x(Na) 1

an        1 1     x(Ca) 1
 DQF   7.03  -0.00466   0

san       1 1     x(K) 1

% ============================================================
% ----------------------------------------------------
% Osumilite: KFMAS

osm 3

x(os)     0.58
y(os)     0.18
% ----------------------------------------------------
p(osm1)           2 1        1  1 -1  y
```

```
                  2       0  1 -1  x  1  1  1/2  y

p(osm2)           1       1        0  1  1  y

p(fosm)           1 2     0  1  1  x  1  1  1/2  y
% ----------------------------------------------------
ideal
% ----------------------------------------------------
7

X(Fe,T1)          1 2     0  1  1  x     0  1  1/3  y

X(Mg,T1)          1 2     1  1 -1  x     0  1  1/3  y

X(Al,T1)          1 1     1  1 -1/3 y

X(Al,T2)          1 1     1  1 -1/2 y

X(Si,T2)          1 1     0  1  1/2 y

X(Fe,M1)          1 1     0  1  1  x

X(Mg,M1)          1 1     1  1 -1  x
% ----------------------------------------------------
osm1    1         3       X(Mg,M1) 2     X(Al,T1) 3       X(Al,T2) 2

osm2    27        5       X(Mg,M1) 2     X(Al,T1) 2       X(Mg,T1)  1            X(Al,T2)  1
X(Si,T2) 1

fosm    1         3       X(Fe,M1) 2     X(Al,T1) 3       X(Al,T2) 2

% ================================================================
% ----------------------------------------------
% Spinel: FMATO

% x(he) = Fe2/(Mg + Fe2)
% y(he) = Al/(Al + Fe3 + 2Ti)
% z(he) = 2Ti/(Al + Fe3 + 2Ti)

sp 4

x(sp)   0.93   % Fe2/(Mg + Fe2)
y(sp)   0.80   % Al/(Al + Fe3 + 2Ti)
z(sp)   0.01   % 2Ti/(Al + Fe3 + 2Ti)
% ----------------------------------------------------
p(herc)           2 1   0  1   1  y
                   2   -1  1   1 x   1  1   1  z

p(sp)             1 2   1  1  -1  x   1  1   1  z

p(mt)             1 1   1  2  -1  y -1  z

p(usp)            1 1   0  1   1  z
% ----------------------------------------------------
sf
```

```
W(herc,sp)        0     0  0
W(herc,mt)       18.5   0  0
W(herc,usp)      27     0  0
W(sp,mt)         40     0  0
W(sp,usp)        30     0  0    % * free
W(mt,usp)         0     0  0
% ----------------------------------------------------
5     % site fractions

x(Al)              1 1    0  1  1  y

x(Fe3)             1 1    1  2 -1  y -1  z

x(Ti)              1 1    0  1  1  z

x(Mg)              1 1    1  1 -1  x

x(Fe2)             1 1    0  1  1  x
% ----------------------------------------------------
herc     1  2    x(Al)  1    x(Fe2)  1

sp       1  2    x(Al)  1    x(Mg)   1

mt       1  2    x(Fe3) 1    x(Fe2)  1

usp      1  2    x(Ti)  1    x(Fe2)  1

% ============================================================
% Magnetite: FMATO
%
% x(he) = Fe2/(Mg + Fe2)
% y(he) = Al/(Al + Fe3 + 2Ti)
% z(he) = 2Ti/(Al + Fe3 + 2Ti)

mt 4

x(mt)    0.98    % Fe2/(Mg + Fe2)
y(mt)    0.12    % Al/(Al + Fe3 + 2Ti)
z(mt)    0.14    % 2Ti/(Al + Fe3 + 2Ti)
% ----------------------------------------------------
p(herc)            2 1    0  1   1  y
                    2   -1  1   1  x    1  1   1  z

p(sp)              1 2    1  1  -1  x    1  1   1  z

p(mt)              1 1    1  2  -1  y -1  z

p(usp)             1 1    0  1   1  z
% ----------------------------------------------------
sf

W(herc,sp)        0     0  0
W(herc,mt)       18.5   0  0
W(herc,usp)      27     0  0
W(sp,mt)         40     0  0
```

```
W(sp,usp)        30    0  0 % * free
W(mt,usp)         0    0  0
% --------------------------------------------------
5    % site fractions

x(Al)            1 1   0  1  1  y

x(Fe3)           1 1   1  2 -1  y -1  z

x(Ti)            1 1   0  1  1  z

x(Mg)            1 1   1  1 -1  x

x(Fe2)           1 1   0  1  1  x
% --------------------------------------------------
herc     1  2   x(Al)  1   x(Fe2)  1

sp       1  2   x(Al)  1   x(Mg)   1

mt       1  2   x(Fe3) 1   x(Fe2)  1

usp      1  2   x(Ti)  1   x(Fe2)  1

% ============================================================
% --------------------------------------------------
% Ilmenite: FTO
%
% x(ilm)   = prop ilm
% Q(ilm) =  x(Fe2,A) - x(Fe2,B)
% NOTE: Q(ilm) must have a range of -x to +x

ilm 3

x(ilm)   0.920
Q(ilm)   0.8      range -0.920 0.920
% --------------------------------------------------
% psub = {ph -> 1 - x, po -> Q, pd -> x - Q};

p(oilm)          1 1   0  1  1  Q

p(dilm)          1 1   0  2  1  x -1  Q

p(hem)           1 1   1  1 -1  x
% --------------------------------------------------
sf

W(oilm,dilm)     15.6  0  0
W(oilm,hem)      26.6  0  0
W(dilm,hem)      11    0  0
% --------------------------------------------------
6    % site fractions

% sfsub = {xFe2A -> (x + Q)/2, xTiA -> (x - Q)/2, xFe3A -> 1 - x,
%          xFe2B -> (x - Q)/2, xTiB -> (x + Q)/2, xFe3B -> 1 - x};
```

```
x(Fe2,A)          1 1    0  2  1/2  x  1/2  Q

x(Ti,A)           1 1    0  2  1/2  x -1/2  Q

x(Fe3,A)          1 1    1  1 -1  x

x(Fe2,B)          1 1    0  2  1/2  x -1/2  Q

x(Ti,B)           1 1    0  2  1/2  x  1/2  Q

x(Fe3,B)          1 1    1  1 -1  x
% ---------------------------------------------------
oilm      1  2    x(Fe2,A)  1  x(Ti,B)  1
 make  1  ilm  1
 DQF    -13.6075 0.009426 0  % DQF - dH + R Log[4]; dH = 15.6
 check 1 1

dilm      4  4    x(Fe2,A)  1/2   x(Ti,A)  1/2   x(Fe2,B)  1/2   x(Ti,B)  1/2
 make  1  ilm  1
 DQF     1.9928 -0.0021 0    % DQF = G(equil,Landau) - G(equil,SF)
 check 1 0

hem      1  2    x(Fe3,A)  1  x(Fe3,B)  1
 check 0 0
 make 1 hem 1

% ===========================================================
% ---------------------------------------------------
% hematite: FTO
#5
% x(hem)  = prop ilm
% Q(hem) =  x(Fe2,A) - x(Fe2,B)
% NOTE: Q(hem) must have a range of -x to +x

hem 3

x(hem)            0.05
Q(hem)            0.0002 range -0.05 0.05
% ---------------------------------------------------
% psub = {ph -> 1 - x, po -> Q, pd -> x - Q};

p(oilm)           1 1    0  1  1  Q

p(dilm)           1 1    0  2  1  x -1  Q

p(hem)            1 1    1  1 -1  x
% ---------------------------------------------------
sf

W(oilm,dilm)      15.6  0  0
W(oilm,hem)       26.6  0  0
W(dilm,hem)       11    0  0
% ---------------------------------------------------
6     % site fractions
```

```
% sfsub = {xFe2A -> (x + Q)/2, xTiA -> (x - Q)/2, xFe3A -> 1 - x,
%         xFe2B -> (x - Q)/2, xTiB -> (x + Q)/2, xFe3B -> 1 - x};

x(Fe2,A)          1 1    0  2  1/2  x  1/2  Q

x(Ti,A)           1 1    0  2  1/2  x -1/2  Q

x(Fe3,A)          1 1    1  1 -1  x

x(Fe2,B)          1 1    0  2  1/2  x -1/2  Q

x(Ti,B)           1 1    0  2  1/2  x  1/2  Q

x(Fe3,B)          1 1    1  1 -1  x
% ---------------------------------------------------
oilm      1  2    x(Fe2,A)  1  x(Ti,B)  1
 make  1  ilm  1
 DQF    -13.6075 0.009426 0  % DQF - dH + R Log[4]; dH = 15.6
 check 1 1

dilm      4  4    x(Fe2,A)  1/2   x(Ti,A)  1/2   x(Fe2,B)  1/2   x(Ti,B)  1/2
 make  1  ilm  1
 DQF     1.9928 -0.0021 0    % DQF = G(equil,Landau) - G(equil,SF)
 check 1 0

hem      1  2    x(Fe3,A)  1  x(Fe3,B)  1
 check 0 0
 make 1 hem 1

% ============================================================
% ---------------------------------------------------
% Hornblende:
% clinoamphibole: NCFMASH: OD
%
%                  A          M4                  M13       M2            T1
%                  v   Na   Ca  Na  Mg  Fe   Mg  Fe   Al  Mg  Fe   Al  Si
% tr               1   0    2   0   0   0    3   0    0   2   0    0   4
% ts               1   0    2   0   0   0    3   0    2   0   0    2   2
% parg             0   1    2   0   0   0    3   0    1   1   0    2   2
% gl               1   0    0   2   0   0    3   0    2   0   0    0   4
% cumm             1   0    0   0   2   0    3   0    0   2   0    0   4
% grun             1   0    0   0   0   2    0   3    0   0   2    0   4
% a                1   0    0   0   0   2    3   0    0   0   2    0   4
% b                1   0    0   0   0   2    0   3    0   2   0    0   4
%
%                  3 xFeM13 + 2 xFeM2 + 2 xFeM4
% x -> ------------------------------------------------------------
%      3 xFeM13 + 2 xFeM2 + 2 xFeM4 + 3 xMgM13 + 2 xMgM2 + 2 xMgM4
%
% y -> xAlM2
%
% z -> xNaM4
%
% a -> xNaA
%
```

```
% c -> xCaM4

%              xFeM13
% Q1 -> x - ----------------
%          xFeM13 + xMgM13

%              xFeM2
% Q2 -> x - -------------
%          xFeM2 + xMgM2
% ---------------------------------------------------
hb  8

x(hb)              0.3925
y(hb)              0.8456
z(hb)              0.2544
a(hb)              0.6056
c(hb)              0.5917
Q1(hb)             0.03215 range -1 1
Q2(hb)             0.1781 range  -1 1
% ---------------------------------------------------
p(tr)              1 1   0  4  -1/2  a   1  c  -1  y   1  z

p(ts)              1 1   0  3  -1/2  a   1  y  -1  z

p(parg)            1 1   0  1  1  a

p(gl)              1 1   0  1  1  z

p(cumm)            4 1    1  5  -1  c  -1  Q2  -1  x  -1  z  -3/2  Q1
                   2    0  1  1  c    0  1  1  x
                   2    0  1  1  Q2    0  1  1  y
                   2    0  1  1  x    0  1  1  z

p(grun)            5 1    0  3   1  x  -2  Q2  -5/2  Q1
                   2    0  1  1  c    0  1  1  x
                   2    0  1  2  Q2    0  1  1  y
                   2    0  1  -1  x    0  1  1  y
                   2    0  1  1  x    0  1  1  z

p(a)               4 1    0  2   1  Q2  5/2  Q1
                   2    0  1  -1  c    0  1  1  x
                   2    0  1  -1  Q2    0  1  1  y
                   2    0  1  -1  x    0  1  1  z

p(b)               5 1    0  2  2  Q2  3/2  Q1
                   2    0  1  -1  c    0  1  1  x
                   2    0  1  -2  Q2    0  1  1  y
                   2    0  1  1  x    0  1  1  y
                   2    0  1  -1  x    0  1  1  z
% ---------------------------------------------------
asf

W(tr,ts)                    20     0  0
W(tr,parg)                  25     0  0
W(tr,gl)                    65     0  0
```

```
W(tr,cumm)              45    0  0
W(tr,grun)              75    0  0
W(tr,a)                 57    0  0
W(tr,b)                 63    0  0
W(ts,parg)             -40    0  0
W(ts,gl)                25    0  0
W(ts,cumm)              70    0  0
W(ts,grun)              80    0  0
W(ts,a)                 70    0  0
W(ts,b)                 72.5  0  0
W(parg,gl)              50    0  0
W(parg,cumm)            90    0  0
W(parg,grun)           106.7  0  0
W(parg,a)               94.8  0  0
W(parg,b)               94.8  0  0
W(gl,cumm)             100    0  0
W(gl,grun)             113.5  0  0
W(gl,a)                100    0  0
W(gl,b)                111.2  0  0
W(cumm,grun)            33    0  0
W(cumm,a)               18    0  0
W(cumm,b)               23    0  0
W(grun,a)               12    0  0
W(grun,b)                8    0  0
W(a,b)  20  0  0

tr              1    0  0
ts              1.5  0  0
parg            1.7  0  0
gl              0.8  0  0
cumm            1    0  0
grun            1    0  0
a               1    0  0
b               1    0  0
% ------------------------------------------------
13

xvA             1 1   1  1  -1  a

xNaA            1 1   0  1  1  a

xCaM4           1 1   0  1  1  c

xNaM4           1 1   0  1  1  z

xMgM4           4 1   1  5  -1  c  -1  Q2  -1  x  -1  z  -3/2  Q1
                 2   0  1  1  c   0  1  1  x
                 2   0  1  1  Q2   0  1  1  y
                 2   0  1  1  x   0  1  1  z

xFeM4           4 1   0  3   1  Q2   1  x  3/2  Q1
                 2   0  1  -1  c   0  1  1  x
                 2   0  1  -1  Q2   0  1  1  y
                 2   0  1  -1  x   0  1  1  z
```

```
xMgM13          1 1    1  2   1  Q1  -1  x

xFeM13          1 1    0  2  -1  Q1   1  x

xAlM2           1 1    0  1  1  y

xMgM2           3 1    1  3   1  Q2  -1  x  -1  y
                 2    0  1  -1  Q2    0  1  1  y
                 2    0  1  1  x    0  1  1  y

xFeM2           3 1    0  2  -1  Q2   1  x
                 2    0  1  1  Q2    0  1  1  y
                 2    0  1  -1  x    0  1  1  y

xAlT1           1 1    0  3  1/2  y  -1/2  z  1/4  a

xSiT1           1 1    1  3  -1/2  y  1/2  z  -1/4  a
% ------------------------------------------------
tr          1    5  xvA 1  xCaM4 2  xMgM13 3  xMgM2 2  xSiT1 1
 check 0  0  0  0  1  0  0

ts          2    6  xvA 1  xCaM4 2  xMgM13 3  xAlM2 2  xAlT1 1/2  xSiT1 1/2
 check 0  1  0  0  1  0  0
 DQF   10  0 0

parg     8    7  xNaA 1  xCaM4 2  xMgM13 3  xAlM2 1  xMgM2 1  xAlT1 1/2  xSiT1 1/2
 check 0  1/2  0  1  1  0  0
 DQF   15  0 0

gl          1    5  xvA 1  xNaM4 2  xMgM13 3  xAlM2 2  xSiT1 1
 check 0  1  1  0  0  0  0
 DQF   3  0 0

cumm   1    5  xvA 1  xMgM4 2  xMgM13 3  xMgM2 2  xSiT1 1
 check 0  0  0  0  0  0  0
 DQF  -6.4 0 0

grun     1    5  xvA 1  xFeM4 2  xFeM13 3  xFeM2 2  xSiT1 1
 check 1  0  0  0  0  0  0
 DQF  -5 0 0

a           1    5  xvA 1  xFeM4 2  xMgM13 3  xFeM2 2  xSiT1 1
 check 4/7  0  0  0  0  4/7  -3/7
 make   2  cumm 3/7  grun 4/7
 DQF    -15.1  0  0

b           1    5  xvA 1  xFeM4 2  xFeM13 3  xMgM2 2  xSiT1 1
 check 5/7  0  0  0  0  -2/7  5/7
 make   2  cumm 2/7  grun 5/7
 DQF    -17.1  0  0

% ================================================
% ------------------------------------------------
% cpx: NCFF3MAS
%
```

```
%                M1m                M1a                M2c     M2n
%                Mg  Fe  Fe3  Al    Mg  Fe  Fe3  Al    Na  Ca  Na  Ca
% jd             0   0   0    1/2   0   0   0    1/2   1/2 0   1/2 0
% di             1/2 0   0    0     1/2 0   0    0     0   1/2 0   1/2
% hed            0   1/2 0    0     0   1/2 0    0     0   1/2 0   1/2
% acm            0   0   1/2  0     0   0   1/2  0     1/2 0   1/2 0
% om             1/2 0   0    0     0   0   0    1/2   0   1/2 1/2 0
% cfm            0   1/2 0    0     1/2 0   0    0     0   1/2 0   1/2
% jac            0   0   0    1/2   0   0   1/2  0     1/2 0   1/2 0
%
%              xFe3M1a + xFe3M1m
% f -> ------------------------------------
%      xAlM1a + xAlM1m + xFe3M1a + xFe3M1m
%
%              xFeM1a + xFeM1m
% x -> --------------------------------
%      xFeM1a + xFeM1m + xMgM1a + xMgM1m
%
%      xNaM2c + xNaM2n
% j -> ---------------
%             2
%
%      -xNaM2c + xNaM2n
% Q -> -----------------
%             2
%
%        xFe3M1a - xFe3M1m
% Qaf -> ------------------
%               2
%
%                xFeM1a
% Qfm -> -x + ---------------
%             xFeM1a + xMgM1a
% ------------------------------------------------
di  7   % Qaf < f j

x(di)              0.3481
j(di)              0.1747
f(di)              0.3345
Q(di)              0.02126
Qaf(di)            0.009286 range -0.5 0.5
Qfm(di)            -0.1135  range -0.5 0.5
% ------------------------------------------------
p(jd)              2 1   0  3   1  j  -1  Q  -1  Qaf
                   2   0  1  -1  f   0  1  1  j

p(di)              5 1   1  4  -1  j  -1  Q   1  Qfm  -1  x
                   2   0  1  -1  j   0  1  1  Qfm
                   2   0  1  -1  Q   0  1  1  Qfm
                   2   0  1  1   j   0  1  1  x
                   2   0  1  -1  Q   0  1  1  x

p(hed)             5 1   0  2   1  Qfm   1  x
                   2   0  1  -1  j   0  1  1  Qfm
                   2   0  1  -1  Q   0  1  1  Qfm
```

```
                2   0  1  -1  j    0  1  1  x
                2   0  1  -1  Q    0  1  1  x

p(acm)          2 1    0  1  -1  Qaf
                2   0  1  1  f    0  1  1  j

p(om)           1 1    0  1  2  Q

p(cfm)          4 1    0  1  -2  Qfm
                2   0  1  2  j    0  1  1  Qfm
                2   0  1  2  Q    0  1  1  Qfm
                2   0  1  2  Q    0  1  1  x

p(jac)          1 1    0  1  2  Qaf
% ------------------------------------------------
sf

W(jd,di)        26       0  0
W(jd,hed)       24       0  0
W(jd,acm)        5       0  0
W(jd,om)        15.5     0  0
W(jd,cfm)       25.2     0  0      % 14.8 + Wjdfom - y
W(jd,jac)        3       0  0
W(di,hed)        4       0  0
W(di,acm)       15       0  0
W(di,om)        15.75    0  0
W(di,cfm)        2       0  0
W(di,jac)       21.05    0  0
W(hed,acm)      14       0  0
W(hed,om)       17.2     0  0      % 6.3 + Whedfom - y
W(hed,cfm)       2       0  0
W(hed,jac)      20.1     0  0
W(acm,om)       12.8     0  0
W(acm,cfm)      15.5     0  0
W(acm,jac)       3       0  0
W(om,cfm)       18.45    0  0
W(om,jac)       19.3     0  0
W(cfm,jac)      21.05    0  0
% ------------------------------------------------
12

xMgM1m          5 1    1  4  -1  j   1  Q   1  Qfm  -1  x
                2   0  1  -1  j    0  1  1  Qfm
                2   0  1  -1  Q    0  1  1  Qfm
                2   0  1  1  j    0  1  1  x
                2   0  1  -1  Q    0  1  1  x

xFeM1m          5 1    0  2  -1  Qfm   1  x
                2   0  1  1  j    0  1  1  Qfm
                2   0  1  1  Q    0  1  1  Qfm
                2   0  1  -1  j    0  1  1  x
                2   0  1  1  Q    0  1  1  x

xFe3M1m         2 1    0  1  -1  Qaf
                2   0  1  1  f    0  1  1  j
```

```
xAlM1m          2 1   0  3   1  j  -1  Q   1  Qaf
                 2   0  1  -1  f   0  1  1  j

xMgM1a          5 1   1  4  -1  j  -1  Q  -1  Qfm  -1  x
                 2   0  1  1  j   0  1  1  Qfm
                 2   0  1  1  Q   0  1  1  Qfm
                 2   0  1  1  j   0  1  1  x
                 2   0  1  1  Q   0  1  1  x

xFeM1a          5 1   0  2   1  Qfm   1  x
                 2   0  1  -1  j   0  1  1  Qfm
                 2   0  1  -1  Q   0  1  1  Qfm
                 2   0  1  -1  j   0  1  1  x
                 2   0  1  -1  Q   0  1  1  x

xFe3M1a         2 1   0  1   1  Qaf
                 2   0  1  1  f   0  1  1  j

xAlM1a          2 1   0  3   1  j   1  Q  -1  Qaf
                 2   0  1  -1  f   0  1  1  j

xNaM2c          1 1   0  2   1  j  -1  Q

xCaM2c          1 1   1  2  -1  j   1  Q

xNaM2n          1 1   0  2   1  j   1  Q

xCaM2n          1 1   1  2  -1  j  -1  Q
% ---------------------------------------------------
jd        1   4  xAlM1m 1/2  xAlM1a 1/2  xNaM2c 1/2  xNaM2n 1/2

di        1   4  xMgM1m 1/2  xMgM1a 1/2  xCaM2c 1/2  xCaM2n 1/2

hed       1   4  xFeM1m 1/2  xFeM1a 1/2  xCaM2c 1/2  xCaM2n 1/2

acm       1   4  xFe3M1m 1/2  xFe3M1a 1/2  xNaM2c 1/2  xNaM2n 1/2

om        1   4  xMgM1m 1/2  xAlM1a 1/2  xCaM2c 1/2  xNaM2n 1/2
 make  2  jd 1/2  di 1/2
 DQF  -2.9  0  0

cfm       1   4  xFeM1m 1/2  xMgM1a 1/2  xCaM2c 1/2  xCaM2n 1/2
 make  2  di 1/2  hed 1/2
 DQF  -1.5  0  0

jac       1   4  xAlM1m 1/2  xFe3M1a 1/2  xNaM2c 1/2  xNaM2n 1/2
 make  2  jd 1/2  acm 1/2
 DQF  -1.0  0  0

% ===========================================================
 and sill ru ky q H2O
*
```

```
% This is an alternative magnetite that should be used at greenschist up to amphibolite
% grade ie if you are only looking at sub solidus equilibria use this model if you are
% looking at suprasolidus equilibria use the model  in the file above
% You can activate this model by replacing the model in the above file.
% ============================================================
% Magnetite: FTO
% White, RW, Powell, R, Holland, TJB & Worley, BA (2000) The effect of TiO2 and
% Fe2O3 on metapelitic assemblages at greenschist and amphibolite facies conditions:
% mineral equilibria calculations in the system K2O-FeO-MgO-Al2O3-SiO2-H2O-TiO2-
% Fe2O3. Journal of Metamorphic Geology, 18, 497-511.

% no Al, but proper od

mt 3

 x(mt) 0.9704    % prop "mt"
 Q(mt) 0.7472   % x(Fe3,tet)
% ---------------------------------------------------
% psub = {pi -> 3Q - 2x, pd -> 3x - 3Q, pu -> 1 - x};

p(imt)   1 1       0  2 -2  x  3  Q

p(dmt)  1 1       0  2  3  x -3  Q

p(usp)  1 1       1  1 -1  x
% ---------------------------------------------------
sf

 W(imt,dmt)       2.4  0  0
 W(imt,usp)        1     0  0
 W(dmt,usp)      -5     0  0
% ---------------------------------------------------
 5

% sfsub = {xFe3oct -> x - Q/2, xFe2oct -> 1/2 + Q/2 - x/2, xTioct -> 1/2 - 1/2 x,
% xFe3tet -> Q, xFe2tet -> 1 - Q};

 x(Ti,oct)          1 1   1/2   1 -1/2  x

 x(Fe3,oct)        1 1    0    2   1   x -1/2 Q

 x(Fe2,oct)        1 1   1/2   2 -1/2  x  1/2 Q

 x(Fe3,tet)        1 1    0    1   1   Q

 x(Fe2,tet)        1 1    1    1  -1   Q
% ---------------------------------------------------
% magnetic landau NOT included

imt      4  3    x(Fe3,oct)  1  x(Fe2,oct)  1  x(Fe3,tet)  1
 make  1  mt  1
 DQF      -1.8595  0.003166 0   % from dmt, - dHid - RT Log[16/27]
   check 1 1                    %      dHid = 3.19

dmt   27/4  4    x(Fe3,oct) 4/3 x(Fe2,oct) 2/3 x(Fe3,tet)  2/3 x(Fe2,tet) 1/3
```

```
 make  1  mt  1
 DQF   1.3305  -0.0011845  0    % taking off config dqf
   check 1 2/3

usp      4  3    x(Ti,oct)  1  x(Fe2,oct)  1  x(Fe2,tet)  1
 check 0 0
% ============================================================
```